UNIVERSITY OF CALIFORNIA, SAN DIEGO

Spectral Properties of Gamma-Ray Bursts Observed by the Burst and Transient Source Experiment

A dissertation submitted in partial satisfaction of the
requirements for the degree Doctor of Philosophy
in Physics

by

Lyle A. Ford

Committee in charge:

Laurence E. Peterson, Chair
David L. Band
Kim Griest
Devendra Lal
D. Asoka Mendis
Sally K. Ride

1996

The dissertation of Lyle A. Ford is approved, and it is acceptable in quality and form for publication on microfilm:

_____

_____

_____

_____

_____

_____

Chair

University of California, San Diego

1996

For my folks

TABLE OF CONTENTS

Signature Page iii

Dedication Page iv

Table of Contents v

List of Figures vii

List of Tables ix

Acknowledgements x

Vita xii

Publications xiii

Fields of Study xvii

Abstract xviii

I Introduction 1
A. Objectives 1
B. General Burst Properties 2
C. Pre-BATSE Missions 4
D. The BATSE Era 12
E. Post-BATSE Models 23
F. Summary 24

II BATSE 26
A. CGRO 26
B. The BATSE Large Area Detectors 31
C. The BATSE Spectroscopy Detectors 36
D. The Spectroscopy Detector Calibration 38
1. The Detector Model 39
2. Implementation 46
3. Results 52

III Spectral Features 56
A. Analysis Techniques 56
B. Pre-BATSE Observations 59
1. Absorption Features 59
2. Emission Features 61
C. Physical Interpretations 62

D. BATSE Observations 64
1. The Search 64
2. Complications 65
3. GRB 3B930506 68
4. Consistency and Future Prospects 74

IV Spectral Evolution 76
A. Introduction 76
B. Analysis 79
C. Results 89
D. Discussion 112
1. Phenomenological Implications 113
2. Implications for Burst Models 115
E. Summary 117

V Extrapolations to the Optical–UV 118
A. Introduction 118
B. Analysis 120
C. Instrumentation 125
D. Discussion 127

VI Short Time Scale Emission 131
A. Introduction 131
B. Statistical Background 134
1. The Problem with Traditional Analysis 134
2. Bayesian Probability Theory 135
3. Application to Count Data 139
C. Pair Correlations 142
1. Comparing Counts 142
2. Significance 146
3. Black Body Characteristics and Upper Limits 149
D. Tests 153
E. Results 161
F. Discussion 175

VII Conclusion 177

Appendix A Model Weights for χ^2 181

References 184

LIST OF FIGURES

I.1 Sample GRB Time Histories 5
I.2 Integral Log N-Log P for GRBs from the BATSE 3B Catalog 13
I.3 Locations of GRBs from the BATSE 3B Catalog 15
I.4 A GRB Photon Spectrum Observed by BATSE 18
I.5 Duration Distribution of Bursts from the BATSE 3B Catalog 20

II.1 The *Compton Gamma-Ray Observatory* 28
II.2 SD Spectrum with SLED 39
II.3 Schematic Diagram of SD Electronics 42
II.4 Schematic Explanation of the SLED 43
II.5 Energy-Loss to Light-Output Curve for the SDs 47
II.6 Comparison Between Calibrated and Uncalibrated Spectra 53

III.1 Energy-Loss Distribution for Incident Photons for the BATSE SDs . . 58
III.2 A Rebinned SHERB Spectrum 66
III.3 Time History of 3B930506 69
III.4 Count Spectrum of 3B930506 (SD2) 70
III.5 SD7 Background for GRB 3B930506 72
III.6 Count Spectrum of 3B930506 (SD7) 73

IV.1 E_P as a Function of Time Resolution 82
IV.2 E_P as a Function of Binning 85
IV.3 E_P from Two SDs Viewing GRB 3B910503 87
IV.4 E_P from Two SDs Viewing 3B921207 88
IV.5 Spectral Evolution of 37 GRBs 92
IV.6 Comparison of Peak of E_P Between Pulses 109
IV.7 E_P as a function of Time of Emission 111

V.1 The Number of GRBs at a Given Fluence-Based Magnitude 123
V.2 The Number of Bursts at a Given Flux Based Magnitude 128

VI.1 Comparison of Black Body and GRB Spectra 132
VI.2 Black Body Detection Significance as a Function of Peak Flux Fraction 145
VI.3 Distribution of Residuals for Test Data 147
VI.4 The Ratio of Calculated Variance to Mean Number of Pairs 148
VI.5 Black Body Self-Correlation as a Function of Temperature 152
VI.6 Spectrum from the First Test 154
VI.7 $A(\Delta t)$ for the First Test 155
VI.8 $A(\Delta t)$ for the Second Test 156
VI.9 $A(\Delta t)$ for the Third Test 157
VI.10 $A(\Delta t)$ for the Fourth Test 158
VI.11 $A(\Delta t)$ for the Fifth Test 159
VI.12 Time Histories and Correlation Curves for STTE Sample 163

VI.13 Spectral Evolution of GRB 3B930131 173
VI.14 $A(\Delta t)$ for a Randomly Evolving GRB 174

LIST OF TABLES

I.1 Energy requirements for GRBs 3
I.2 GRB Dipole and Quadrupole Moments from BATSE 17

II.1 LAD Data Types 35
II.2 SD Data Types 37
II.3 Pre-Flight SD Calibration Data 49
II.4 Calibration Parameters 52
II.5 Background Line Fits to Recalibrated Spectra 55

III.1 Detector Viewing Angles to 3B930506 68

IV.1 Contiuum Fits to Spectra with Different Binning 81
IV.2 Bursts Studied for Spectral Evolution 90
IV.3 Summary of GRB Spectral Evolution 107
IV.4 Unbiased Burst Separation 110
IV.5 E_P as a Function of Relative Emission Time 112

V.1 Fluence Based Extrapolated Brightness 122
V.2 Summary of Optical Counterpart Search Experiments 126
V.3 Flux Based Extrapolated Brightness of GRBs 127

VI.1 Summary of Test Data 154
VI.2 Statistics for Test Data 160
VI.3 Characteristics of STTE sample 162
VI.4 Results of Correlation Analysis 172

ACKNOWLEDGEMENTS

This thesis represents the culmination of six years of graduate study which amounts to nearly a quarter of my life. Clearly, I cannot sufficiently express the debts I owe in a few short paragraphs and hope no offense is taken by those whose contributions I have inadvertently omitted.

The person primarily responsible for ensuring the existence of this work is my advisor, David Band. His patience and persistence is greatly appreciated and I could not have asked for a better mentor. Also significantly assisting in my scientific development were the other researchers in the High-Energy Astrophysics group, in particular, Duane Gruber, Richard Lingenfelter, Jim Matteson, and Rick Rothschild. In addition to enormous contributions to my education, I wish to thank Larry Peterson for maintaining a professionally outstanding and exceedingly personable research group.

Many fellow graduate students have helped me along the way but I am particularly grateful to have shared an office with David Marsden and Wayne Coburn. I have had many interesting and helpful discussions with these two which made my time here much more enjoyable. I owe a particular debt to Dave for helping me through some rough times.

The research described in this thesis would not have been possible without the computers maintained by Pete James, who has always been available to discuss concerns great and small. I also thank Tom Gasaway and George Huszar for answering all my pesky programming questions.

Cheryl Matson and Shirley Roy have been invaluable in helping with administrative matters and ensuring that my many travel arrangements and accommodations were more than adequate.

This thesis is a study of BATSE data and I would be remiss if I did not acknowledge the excellent work of the BATSE team at Marshall Space Flight Center. Led by Jerry Fishman, this group has ensured that BATSE has operated well and

provided quality data. I would like to thank Michael Briggs, Bill Paciesas, Geoff Pendleton, and Rob Preece for being great partners in our continual collaborations.

Some of the debts I owe for this thesis are personal. I must thank Erick Burns and Cheryl McGrath for timely road trips and Robert Ford for being the best role model I could have had. Finally, I want to thank my parents, Alan and Janet Ford, for their unflagging support. They may not have always understood what I was doing, but never stopped encouraging be in my pursuits.

VITA

November 12, 1967	Born, Cedar Falls, Iowa
1990	B.S. in Physics and Astronomy, University of Iowa
1990-1991, 1993	Teaching Assistant, Department of Physics, University of California, San Diego
1991	M.S. in Physics, University of California, San Diego
1991-1996	Research Assistant, University of California, San Diego
1994	C.Phil. in Physics, University of California, San Diego
1996	Doctor of Philosophy in Physics, University of California, San Diego

PUBLICATIONS

"Spectral Evolution of Gamma-Ray Bursts", D. Band, J. Matteson, L. Ford, B. Schaefer, B. J. Teegarden, T. Cline, W. Paciesas, G. Pendleton, G. Fishman, C. Meegan, R. Wilson, & P. Lestrade, *Gamma Ray Bursts, AIP Conference Proceedings 256*, ed. W. Paciesas & G. Fishman (AIP: New York), p. 169, 1991.

"Spectral Evolution During a Complex Gamma-Ray Burst Observed With BATSE", D. E. Gruber, D. L. Band, L. Ford, J. L. Matteson, C. L. Meegan, R. B. Wilson, *ESA ISY-3, European 'International Space Year' Conference*, p. 161, 1992.

"BATSE Spectroscopy Detector Calibration", D. Band, L. Ford, J. Matteson, J. P. Lestrade, B. Teegarden, B. Schaefer, T. Cline, M. Briggs, W. Paciesas, G. Pendleton, R. Austin, G. Fishman, C. Meegan, & R. Wilson, *Experimental Astronomy*, **2**, 307, 1992.

"Observability of Line Features in BATSE Spectroscopy Detector Observations of Gamma-Ray Bursts", L. A. Ford, D. L. Band, J. L. Matteson, D. M. Palmer, B. E. Schaefer, B. J. Teegarden, T. L. Cline, R. D. Preece, G. J. Fishman, C. A. Meegan, R. B. Wilson, M. S. Briggs, W. S. Paciesas, & G. N. Pendleton, *Compton Gamma-Ray Observatory, AIP Conference Proceedings 280*, eds. M. Friedlander, N. Gehrels, & D.J. Macomb (AIP: New York), p. 887, 1993.

"BATSE Observations of Gamma-Ray Burst Spectral Diversity", D. Band, J. Matteson, L. Ford, B. Schaefer, D. Palmer, B. Teegarden, T. Cline, G. Fishman, C. Meegan, R. Wilson, W. Paciesas, G. Pendleton, & P. Lestrade, *Compton Gamma-Ray Observatory, AIP Conference Proceedings 280*, eds. M. Friedlander, N. Gehrels, & D.J. Macomb (AIP: New York), p. 872, 1993.

"Search for Gamma-Ray Burst Spectral Features in the Compton GRO BATSE Data", B. J. Teegarden, T. L. Cline, D. Palmer, B. E. Schaefer, G. J. Fishman, C. Meegan, R. B. Wilson, M. S. Briggs, W. S. Paciesas, G. N. Pendleton, P. Lestrade, D. L. Band, L. Ford, & J. L. Matteson, *Compton Gamma-Ray Observatory, AIP Conference Proceedings 280*, eds. M. Friedlander, N. Gehrels, & D.J. Macomb (AIP: New York), p. 860, 1993.

"Cyclotron Line Searches in Gamma-Ray Bursts Using the BATSE Spectroscopy Detectors", D. M. Palmer, B. Teegarden, B. Schaefer, T. Cline, G. Fishman, C. Meegan, R. Wilson, M. Briggs, W. Paciesas, G. Pendleton, D. Band, L. Ford, J. Matteson, & P. Lestrade, *Compton Gamma-Ray Observatory, AIP Conference Proceedings 280*, eds. M. Friedlander, N. Gehrels, & D.J. Macomb (AIP: New York), p. 892, 1993.

"BATSE Observations of Gamma-Ray Burst Spectra: I. Spectral Diversity", D. Band, J. Matteson, L. Ford, B. Schaefer, D. Palmer, B. Teegarden, T. Cline, M. Briggs, W. Paciesas, G. Pendleton, G. Fishman, C. Kouveliotou, C. Meegan, R. Wilson, & P. Lestrade, *The Astrophysical Journal*, **413**, 281, 1993.

"BATSE Observations of Gamma Ray Burst Continua", D. Band, L. Ford, B. Schaefer, J. Matteson, M. Briggs, D. Palmer, B. Teegarden, W. Paciesas, & G. Pendleton, *Proceedings of the 23rd International Cosmic Ray Conference (Calgary)*, p. 1:101, 1993.

"Search for Absorption Lines in BATSE Observations of Gamma Ray Burst Spectra", D. Band, D. Palmer, B. Teegarden, L. Ford, M. Briggs, J. Matteson, B. Schaefer, W. Paciesas, & G. Pendleton, *Proceedings of the 23rd International Cosmic Ray Conference (Calgary)*, p. 1:105, 1993.

"Consistency between BATSE and Ginga Detections of Absorption Lines in Gamma Ray Burst Continua", D. Band, L. Ford, D. Palmer, B. Teegarden, M. Briggs, J. Matteson, B. Schaefer, W. Paciesas, & G. Pendleton, *Proceedings of the 23rd International Cosmic Ray Conference (Calgary)*, p. 1:120, 1993.

"The BATSE Spectroscopy Catalog", B. E. Schaefer, B. J. Teegarden, S. F. Fantasia, D. Palmer, T. L. Cline, J. L. Matteson, D. L. Band, L. A. Ford, G. J. Fishman, C. A. Meegan, R. B. Wilson, W. S. Paciesas, G. N. Pendleton, M. S. Briggs, & J. P. Lestrade, *The Astrophysical Journal Supplement*, **92**, 285, 1994.

"BATSE Gamma-Ray Burst Line Search. I. Search for Narrow Lines in Spectroscopy Detector Data", David M. Palmer, Bonnard J. Teegarden, Bradley E. Schaefer, Thomas L. Cline, David L. Band, Lyle A. Ford, James L. Matteson, William S. Paciesas, Geoffrey N. Pendleton, Michael S. Briggs, Robert D. Preece, Gerald J. Fishman, Charles A. Meegan, Robert B. Wilson, & J. Patrick Lestrade, *The Astrophysical Journal*, **433**, L77, 1994.

"Continuum Evolution of Bright Gamma Ray Bursts Observed by BATSE", L. Ford, D. Band, J. Matteson, B. Teegarden, & W. Paciesas, *Gamma-Ray Bursts, Second Workshop—AIP Conference Proceedings 307*, eds. G. J. Fishman, J. J. Brainerd, & K. Hurley (New York:AIP), p. 298, 1994.

"A Candidate Absorption Feature from a Gamma Ray Burst Observed by BATSE", L. Ford, D. Band, J. Matteson, D. Palmer, B. Teegarden, B. Schaefer, R. Preece, M. Briggs, W. Paciesas, & G. Pendleton, *Gamma-Ray Bursts, Second Workshop—AIP Conference Proceedings 307*, eds. G. J. Fishman, J. J. Brainerd, & K. Hurley (New York:AIP), p. 261, 1994.

"Cyclotron Line Search: BATSE-Ginga Consistency", D. Band, L. Ford, J. Matteson, D. Palmer, B. Teegarden, B. Schaefer, M. Briggs, W. Paciesas, G. Pendleton, & R. Preece, *Gamma-Ray Bursts, Second Workshop—AIP Conference Proceedings 307*, eds. G. J. Fishman, J. J. Brainerd, & K. Hurley (New York:AIP), p. 256, 1994.

"The Search for Gamma-Ray Burst Spectral Features in the Compton GRO BATSE Data", D. M. Palmer, B. J. Teegarden, B. E. Schaefer, T. L. Cline, D. L. Band, L. A. Ford, J. L. Matteson, G. J. Fishman, C. A. Meegan, R. B. Wilson, R. D. Preece,

W. S. Paciesas, G. N. Pendleton, M. S. Briggs, & J. P. Lestrade, *Gamma-Ray Bursts, Second Workshop—AIP Conference Proceedings 307*, eds. G. J. Fishman, J. J. Brainerd, & K. Hurley (New York:AIP), p. 247, 1994.

"Consistency Analysis of the GRB930506 56 keV Candidate Line Feature in the BATSE LADs", R. Preece, M. Briggs, W. Paciesas, G. Pendleton, L. Ford, D. Band, J. Matteson, D. Palmer, B. Teegarden, B. Schaefer, M. Brock, *Gamma-Ray Bursts, Second Workshop—AIP Conference Proceedings 307*, eds. G. J. Fishman, J. J. Brainerd, & K. Hurley (New York:AIP), p. 266, 1994.

"BATSE Cyclotron Line Search Protocol", B. E. Schaefer, B. J. Teegarden, D. M. Palmer, T. L. Cline, S. Mitruka, L. A. Ford, D. L. Band, J. L. Matteson, M. S. Briggs, W. S. Paciesas, G. N. Pendleton, R. D. Preece, *Gamma-Ray Bursts, Second Workshop—AIP Conference Proceedings 307*, eds. G. J. Fishman, J. J. Brainerd, & K. Hurley (New York:AIP), p. 271, 1994.

"BATSE Gamma-Ray Burst Line Search: II. Bayesian Consistency Methodology", D. L. Band, L. A. Ford, J. L. Matteson, M. Briggs, W. Paciesas, G. Pendleton, R. Preece, D. Palmer, B. Teegarden, & B. Schaefer, *The Astrophysical Journal*, **434**, 560, 1994.

"Extended High Energy Emission from a Gamma-Ray Burst", K. Hurley, B. L. Dingus, R. Mukherjee, P. Sreckumar, C. Kouveliotou, C. Meegan, G. J. Fishman, D. Band, L. Ford, D. Bertsch, T. Cline, C. Fictel, R. Hartman, S. Hunter, D. J. Thompson, G. Kanbach, H. Mayer-Hasselwander, C. von Montigny, M. Sommer, Y. Lin, P. Nolan, P. Michelson, D. Kniffen, J. Mattox, E. Schneid, M. Boer, & M. Niel, *Nature*, **372**, 652, 1994.

"BATSE Observations of Gamma-Ray Burst Spectra II. Peak Energy Evolution in Bright, Long Bursts", L. A. Ford, D. L. Band, J. L. Matteson, M. S. Briggs, G. N. Pendleton, R. D. Preece, W. S. Paciesas, B. J. Teegarden, D. M. Palmer, B. E. Schaefer, T. L. Cline, G. J. Fishman, C. Kouveliotou, C. Meegan, R. B. Wilson, & J. P. Lestrade, *The Astrophysical Journal*, **439**, 307, 1995.

"BATSE Gamma-Ray Burst Line Search: III. Line Detectability", D. L. Band, L. A. Ford, J. L. Matteson, M. S. Briggs, W. S. Paciesas, G. N. Pendleton, R. D. Preece, D. Palmer, B. Teegarden, B. Schaefer, *The Astrophysical Journal*, **447**, 289, 1995.

"The Evaluation of BATSE Line Candidates", D. Band, S. Ryder, L. Ford, J. Matteson, D. Palmer, B. Teegarden, M. Briggs, W. Paciesas, G. Pendleton, & R. Preece, *Proceedings of the 29th ESLAB Symposium: Towards the Source of Gamma Ray Bursts*, *Astrophysics & Space Science*, **231**, 203, 1995.

"Extrapolating BATSE Burst Spectra to the Optical-UV Band", D. Band & L. Ford, *Proceedings of the 29th ESLAB Symposium: Towards the Source of Gamma Ray Bursts*, *Astrophysics & Space Science*, **231**, 247, 1995.

"BATSE Time-Resolved Observations of GRBs: the Burst 'Topographic' Map" R. Preece, M. Briggs, G. Pendleton, W. Paciesas, D. Band, & L. Ford, *Proceedings of the 29th ESLAB Symposium: Towards the Source of Gamma Ray Bursts*, *Astrophysics & Space Science*, **231**, 149, 1995.

"GRBs in the 5-10 keV Regime as Seen by BATSE", R. Preece, M. Briggs, G. Pendleton, W. Paciesas, D. Band, & L. Ford, *Proceedings of the 29th ESLAB Symposium: Towards the Source of Gamma Ray Bursts*, *Astrophysics & Space Science*, **231**, 210, 1995.

"BATSE Gamma-Ray Burst Line Search. IV. Line Candidates from the Visual Search", Band, D. L., Ryder, S., Ford, L. A., Matteson, J. L., Palmer, D. M., Teegarden, B. J., Briggs, M. S., Paciesas, W. S., Pendleton, G. N., & Preece, R. D., 1996, *The Astrophysical Journal*, **458**, 746.

"Extrapolations of BATSE Gamma-Ray Burst Spectra to the Optical-UV Band", L. Ford & D. Band, *Gamma-Ray Bursts, 3rd Huntsville Symposium*, eds. C. Kouveliotou, M. S. Briggs, & G. J. Fishman, in press, 1996.

"Short Time Scale Characteristics of Gamma-Ray Burst Continua", L. Ford, D. Band, & J. Matteson, *Gamma-Ray Bursts, 3rd Huntsville Symposium*, eds. C. Kouveliotou, M. S. Briggs, & G. J. Fishman, in press, 1996.

"The Statistics of the Search for Absorption Lines in Burst Spectra", D. Band, L. Ford, J. Matteson, M. Briggs, W. Paciesas, G. Pendleton, R. Preece, D. Palmer, & B. Teegarden, *Gamma-Ray Bursts, 3rd Huntsville Symposium*, eds. C. Kouveliotou, M. S. Briggs, & G. J. Fishman, in press.

"A Comprehensive Search for Low-Energy Lines in BATSE GRBs", M. S. Briggs, R. D. Preece, G. N. Pendleton, W. S. Paciesas, D. L. Band, L. Ford, & J. L. Matteson, *Gamma-Ray Bursts, 3rd Huntsville Symposium*, eds. C. Kouveliotou, M. S. Briggs, & G. J. Fishman, in press, 1996.

"Time-resolved Spectroscopy with the BATSE LADs: High-Energy Behavior", R. D. Preece, M. S. Briggs, G. N. Pendleton, W. S. Paciesas, D. L. Band, & L. A. Ford, *Gamma-Ray Bursts, 3rd Huntsville Symposium*, eds. C. Kouveliotou, M. S. Briggs, & G. J. Fishman, in press, 1996.

"Extrapolations of BATSE Gamma-Ray Burst Spectra to the Optical-UV Band", Lyle A. Ford & David L. Band, *The Astrophysical Journal*, in press, 1996.

FIELDS OF STUDY

Major Field: Physics

Studies in Classical Mechanics
Professors Thomas M. O'Neil and Marshall N. Rosenbluth

Studies in Classical Electrodynamics
Professor Norman M. Kroll

Studies in Quantum Mechanics
Professors Herbert Levine and Roger F. Daschen

Studies in Mathematical Methods
Professor Marshall N. Rosenbluth

Studies in Statistical Mechanics
Professor Daniel H. Dubin

Studies in Astrophysics
Professors George M. Fuller, Robert J. Gould, and Arthur M. Wolfe

Studies in Atomic Physics
Professor Robert J. Gould

Studies in General Relativity and Cosmology
Professor George M. Fuller

Studies in Nuclear Physics
Professor Robert J. Gould

Studies in Field Theory
Professor Aneesh V. Manohar

Studies in Particle Physics
Professor Hans P. Paar

ABSTRACT OF THE DISSERTATION

Spectral Properties of Gamma-Ray Bursts
Observed by the Burst and Transient
Source Experiment

by

Lyle A. Ford
Doctor of Philosophy in Physics
University of California, San Diego, 1996
Professor Laurence E. Peterson, Chair

This thesis studies Gamma-Ray Burst (GRB) continuum spectra as a way to understand the physical processes which occur in these events. The continuum analyses in this work concern evolution of spectra within a GRB, the likelihood that optical counterparts can be observed if the optical spectrum can be extrapolated from the gamma-ray spectrum, and a search for short-lived black body spectra within a GRB. Spectral features are discussed, but their rarity prevents direct physical interpretation.

The spectral evolution study confirmed previous claims that GRB spectra tend to evolve from hard to soft though there does appear to be a complicated dependence on intensity. These results might imply that the emitting region is being continuously flooded with radiating particles which reduce the average energy of the observed radiation or it could suggest an efficient cooling process. In either case, electron-positron pair processes are not directly observable.

By extrapolating GRB spectra to optical wavelengths, it is possible to determine whether telescopes designed to detect flaring optical emission from GRBs are likely to discover anything. It is found that unless there is more emission at lower energies than is implied by a simple extrapolation of GRB spectra, flaring counterparts will be difficult to observe.

Finally, a new statistical method is used to determine whether short duration black bodies compose a significant fraction of GRB spectra. This is an important question because thermal emission appears to be a natural consequence of GRB models from distant sources. The method determines the likelihood that a given pair of counts came from photons of similar energies. If short-lived black body emission is important in GRBs, then pairs of counts separated by small times should be more correlated. In most bursts, no evidence for this type of emission is found though there are a few exceptions which are likely a consequence of extremely complex spectral evolution. Therefore, short time scale thermal emission appears incompatible with GRBs.

Chapter I

Introduction

I.A Objectives

Of all the phenomena studied by astrophysicists, perhaps none is as strange as Gamma-Ray Bursts (GRBs). Discovered in the late 1960's by the Vela satellites (Klebesadel, Strong, & Olson 1973), GRBs are intense, transient outbursts from unknown cosmic sources. They have been observed to last from milliseconds to over an hour and can outshine all other objects in the gamma-ray sky by several orders of magnitude. Although the radiation from these events between 10 keV and 1 GeV can be quite intense, GRBs have not been observed below 1 keV and no convincing quiescent counterparts at any wavelength have been discovered suggesting incredibly efficient emission of gamma-rays. Observations from several experiments devoted to the study of these events in the 1970's and 1980's led to a consensus that GRBs arose from nearby ($\sim$100 pc) neutron stars. However, data from the most sensitive experiment to date, the Burst and Transient Source Experiment (BATSE), show that such a population of GRB sources cannot exist. The BATSE results were completely unexpected and most now believe that GRBs arise from sources located at either extreme Galactic Halo ($\sim$150 kpc) or cosmological ($\sim$1 Gpc) distances. Many new GRB source models have been proposed in response to the BATSE observations but none have garnered anything near universal acceptance. The uncertainty in the type

and distance to the source is a problem that must be resolved since aside from being truly amazing events in themselves, GRBs offer an excellent opportunity to probe the structure of the Galactic Halo or the entire universe depending on where these events take place.

The purpose of this thesis is to use BATSE observations of GRB spectra to discover common properties which can help resolve the mystery of these events. Burst spectroscopy is an area which has received a great deal of attention, mostly focused on the search for absorption and emission features. The bias toward lines is easy to understand since an enormous amount of information can be derived from these features. For example, within the old paradigm of a local neutron star origin for GRBs, spectral features were used to determine the magnetic field strength, the temperature of the absorbing region, and gravitational potential of the putative neutron star. While this thesis does discuss spectral features, the continuum is considered in greater detail. This is for two reasons. The first is that spectral features appear to be quite rare (if they exist at all) and it is dangerous to assume properties specific to a handfull of events are typical for a phenomenon as diverse as gamma-ray bursts. Second, a detailed description of continuum emission is vital for judging the validity of GRB theories. For a given GRB model, the continuum can reveal source temperatures, the distribution of radiating particles, or bulk relativistic motion of the source region. Since continuum spectra evolve significantly during a burst (Ford *et al.* 1995 and Chapter IV), an understanding of the temporal characteristics of continua can specify spectral behavior that all GRB models must reproduce. Therefore, the goal of this thesis is to determine quantitative properties of the continuum which constrain burst models and suggest promising directions for future research.

I.B General Burst Properties

From the time of the first observations, GRBs were recognized as exceptional events. GRBs have peak fluxes as high as 100 photons/cm^2-s in the 50–300

Distance	Flux (ergs/s)	Energy Density (ergs/cm^3-s)
100 pc	$10^{35} - 10^{38}$	$10^{16} - 10^{19}$
150 kpc	$10^{41} - 10^{42}$	$10^{22} - 10^{25}$
1 Gpc	$10^{49} - 10^{52}$	$10^{30} - 10^{33}$

Table I.1: Energy required to produce GRBs observed by BATSE assuming isotropic emission. Energy density is calculated for bursts in a 10 km volume (neutron star dimensions).

keV band (Meegan *et al.* 1996), much brighter than the Crab pulsar (the brightest persistent source of astrophysical gamma rays) which has a phase averaged flux of 0.01 photons/cm^2-s in the same band (Ulmer *et al.* 1994). Such large burst fluxes require an enormous energy release though the exact luminosity of GRBs is uncertain because the distance to the sources is unknown. Energy requirements for several source distances are given in Table I.1 where isotropic emission from a neutron star has been assumed. It is clear from this table that GRBs are events of extreme violence regardless of the distance scale adopted.

One way to appreciate the difficulty of explaining GRBs is to look at their temporal properties. In fact, explaining burst emission time scales and energetics is the focus of most burst models with only cursory attention given to spectral issues. GRBs have been observed to last anywhere between 0.03 s to 90 m (Meegan *et al.* 1996; Hurley *et al.* 1994a) and their intensity fluctuates rapidly with rise times are as short as milliseconds (see Figure I.1). This fact can be used to make a simple argument that GRBs must come from a small source region. Assuming an outburst must spread from the triggering point across a finite source region, then the source region cannot be larger than $\sim$ 100 km without violating causality. This argument has confined most speculation about burst sources to neutron stars and black holes, objects which are not only small, but have potential energy reservoirs sufficient to power a GRB.

While the problems of explaining duration and variability may appear surmountable at first glance, the difficulty of modeling GRBs rapidly increases when the

diversity of GRB time profiles is included, regardless of the assumed source. There is large variation in time profiles, so much so that there are no obvious groups of bursts on which meaningful morphology-based classification schemes can be constructed to simplify the problem (see Bhat *et al.* 1994b and Lestrade 1994 for recent attempts at numerical classification). Several time histories are shown in Figure I.1, displaying the wide variety of behaviors. Examining the figure, one finds bursts which are simple and others much more complex. There are bursts with a suggestion of periodic pulses and others which are completely chaotic. Some GRBs have smoothly varying profiles while others are quite rough. Essentially, each burst appears distinct, complicating efforts to understand them.

I.C Pre-BATSE Missions

Beginning in the late 1970's, experiments dedicated to GRB studies were launched aboard several spacecraft. The most important of these were the various KONUS experiments on *Venera* 11–14, SIGNE on *Venera* 11-12, the Gamma-Ray Burst Spectrometer on the *International Comet Explorer* (*ICE*), the Gamma Burst Detector on the *Pioneer Venus Orbiter* (*PVO*), and the Gamma Ray Burst Detector on the *Ginga* satellite. In addition to these dedicated instruments, experiments on the first *High Energy Astronomical Observatory* (*HEAO-1*) and the *Solar Maximum Mission* (*SMM*) satellites made important observations of GRBs. Data from these missions were primarily responsible for the predominant view that GRBs arose on neutron stars in the Galactic plane (see reviews by Harding [1991] and Higdon & Lingenfelter [1990]).

Figure I.1: A sample of GRB time histories of bursts observed by BATSE in the $30 - 500$ keV band.

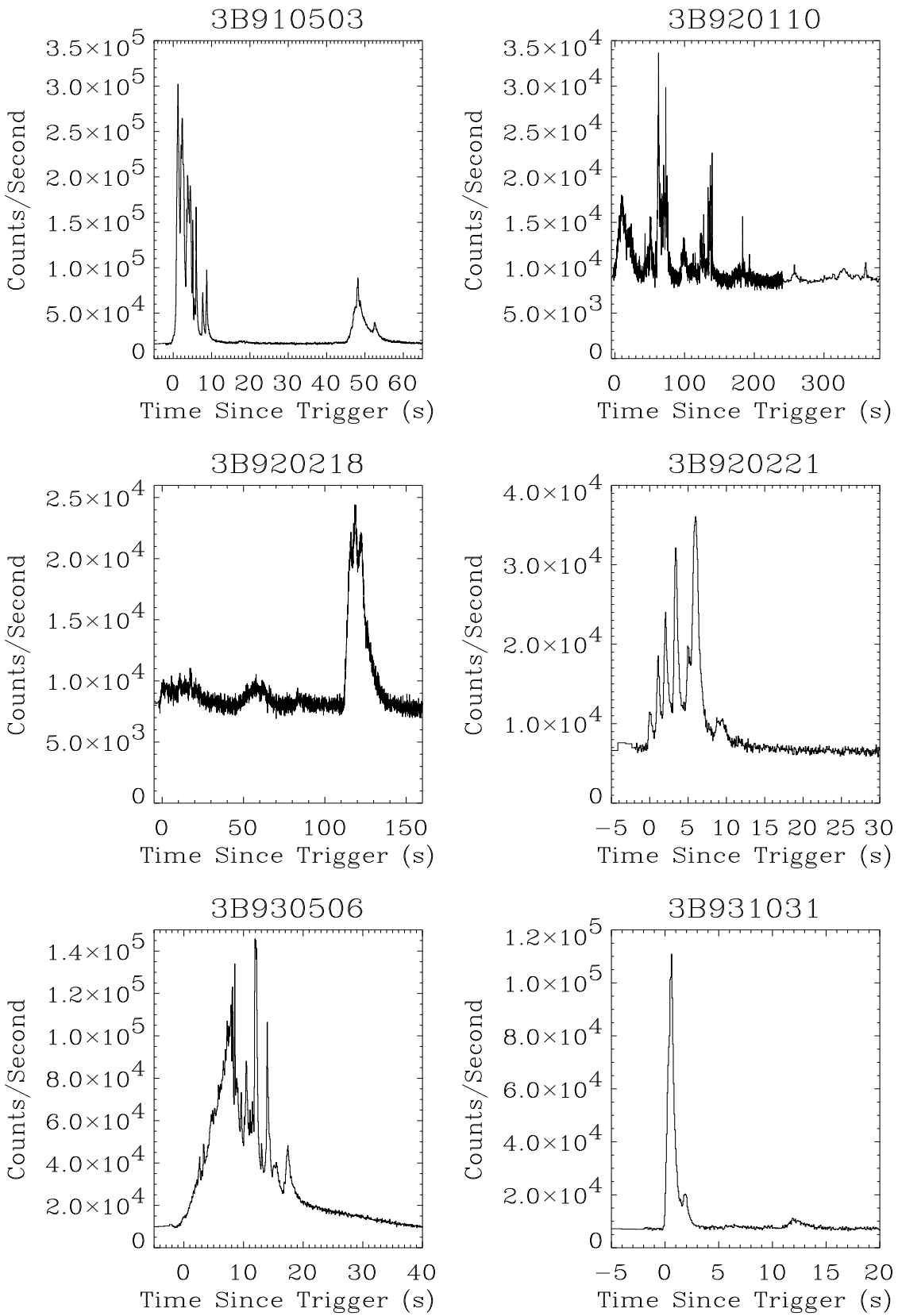
3B910503
Counts/Second
Time Since Trigger (s)
3B920110
Counts/Second
Time Since Trigger (s)
3B920218
Counts/Second
Time Since Trigger (s)
3B920221
Counts/Second
Time Since Trigger (s)
3B930506
Counts/Second
Time Since Trigger (s)
3B931031
Counts/Second
Time Since Trigger (s)

Initially, evidence for local neutron star sources was highly circumstantial. Aside from the causality argument limiting the size of the source region, the observation of MeV photons was used by Schmidt (1978) to place an upper limit on the distance scale because at large energy densities, opacity from $\gamma\gamma \rightarrow e^+e^-$ becomes large. The argument is as follows. The threshold energy of a test photon for pair production interacting with a photon of energy E is

$$\epsilon_T = \frac{2(mc^2)^2}{E(1-\cos\theta)}, \tag{I.1}$$

where m is the electron mass, c is the speed of light, and θ is the angle between the momentum vectors of the photons. For a source radius r and ambient photon density $n(\epsilon)$, the optical depth for the test photon is

$$\tau(E) = r\int_{\epsilon_T}^{\infty} n(\epsilon)\sigma_{\gamma\gamma}(E,\epsilon)d\epsilon, \tag{I.2}$$

where $\sigma_{\gamma\gamma}(E,\epsilon)$ is the cross-section for photon-photon interaction. For an observed photon flux $F(\epsilon)$, the density of photons on the surface of the source is

$$n(\epsilon) = \frac{F(\epsilon)}{c}\frac{D^2}{r^2}, \tag{I.3}$$

where D is the distance to the source. Substituting equation I.3 into equation I.2 and solving for D yields

$$D(E) = \left[\frac{\tau/c}{\int_{\epsilon_T}^{\infty} F(\epsilon)\sigma_{\gamma\gamma}(E,\epsilon)d\epsilon}\right]. \tag{I.4}$$

Assuming an optical density of unity was sufficient to render the source region optically thick to photons of a given energy and that the photons were not relativistically beamed, Schmidt found that the observation of MeV photons implied GRB sources must not be farther than $\sim$1 kpc from the Earth.

Much more powerful evidence in support of the neutron star hypothesis came from the observation of both absorption and emission lines in burst spectra. Mazets *et al.* (1981) first reported a paucity of counts in the 20-70 keV range when an optically thin thermal bremsstrahlung model was used to fit spectra from several bursts. In many cases, the deviation occurred over a narrow energy range implying

line-like absorption of gamma-rays. Such absorption could occur if radiation from these GRBs passed through a layer of electrons trapped in a strong magnetic field. In such a field, the electron orbits around the field lines are quantized and harmonically spaced in energy. The energy of the fundamental (the cyclotron energy) and spacing between all energy levels (known as Landau levels) is given by

$$E_c = 2\pi h \left(\frac{eB}{mc}\right), \tag{I.5}$$

where h is Planck's constant, c is the speed of light, B is the magnetic field strength, and e and m are the charge and mass of the electron respectively (Mészáros 1992, p. 31). Spectral features are produced when gamma-rays of energy E_c are absorbed and the electron moves to the next higher Landau level. For absorption to occur in the $20 - 70$ keV range, the magnetic field must be of the order 10^{12} G. The only known fields of this strength are associated with neutron stars. Absorption features were also reported in two bursts observed by *HEAO-1* (Hueter 1987) and most convincingly by *Ginga* (Murakami *et al.* 1988; Fenimore *et al.* 1988; Yoshida *et al.* 1991; Graziani *et al.* 1992), strengthening faith in the existence of lines.

In addition to absorption lines, emission lines observed between 350–500 keV (Teegarden & Cline 1980; Mazets *et al.* 1981; Barat *et al.* 1984; Hueter 1987) solidified the neutron star hypothesis. These features were interpreted as electron-positron annihilation in a hot plasma where the characteristic 511 keV signature of this radiation was redshifted by the strong gravitational potential near the surface of the neutron star.

If GRBs do indeed come from sources predominantly residing in the Galactic plane, then the distribution of bursts on the sky should show a preference for the plane. The 175 GRBs located by KONUS (Golenetskii 1988) show an isotropic distribution on the sky as do 54 bursts located by the second interplanetary network (Atteia *et al.* 1987). Therefore, if GRBs do come from a local disk distribution of sources, these instruments must not have been sensitive enough to sample beyond the scale height of the distribution. This can be tested quantitatively by examining the size-frequency distribution, commonly known as $\log N$-$\log S$. The size-frequency

distribution gives the number of bursts (N) which are brighter than a specified intensity level. The size-frequency distribution's utility as a diagnostic of uniformity can be understood as follows. The observed peak brightness of a burst varies as the inverse square of the distance to the burst. If bursts are distributed uniformly in space, then the total number of bursts (seen and unseen) is proportional to the cube of the distance. Therefore, the number of observed bursts greater than a given intensity should vary as the –3/2 power of the brightness. However, Higdon & Lingenfelter (1986) showed that instrument biases can make these distributions meaningless for weaker bursts if threshold effects are not accounted for. This was responsible for contradictory interpretations of the KONUS data (Yamagami & Nishimura 1986; Golenetskii 1988; Jennings 1988; Paczyński & Long 1988b). Originally, intensity was quantified by the fluence (S) of the GRB. However, the measured fluence depends on the way the detector works and how the threshold varies. Therefore the instrument independent peak flux (P) or peak count rate above the trigger threshold (C_{min}) is used instead. Balloon borne experiments which were more sensitive than KONUS (and thus, lower intensity at which instrument effects are important) found far fewer bursts than expected assuming the number of weak bursts followed a power law of index -3/2 for weaker bursts (Beurle *et al.* 1981; Meegan *et al.* 1985). In particular, the instrument used by Meegan *et al.* was a BATSE prototype which indicated that when launched, BATSE would see the expected concentration of bursts in the Galactic plane.

A second way to test the spatial uniformity of GRBs in three dimensional Euclidean space which is free of instrument bias is the V/V_{max} test (Schmidt 1968; Schmidt, Higdon, & Hueter 1988). The value of V/V_{max} for a burst is the ratio of the spherical volumes defined by the distance to the burst and the maximum distance at which the burst could have been detected. Thus, a very bright burst would have $V/V_{max} \sim 0$ and a very dim one would have $V/V_{max} \sim 1$. Because the maximum distance at which a GRB depends on conditions at the time of detection, such as background level and the angle between the detector and the source, instrument effects are

included in the V/V_{max} statistic and do not have to be accounted for independently. If GRBs are uniformly distributed in Euclidean space, then the average value of V/V_{max} should be 0.5 and have smaller values if the instrument is sensitive to events beyond a uniformly distributed Euclidean core. For 123 KONUS GRBs, Higdon & Schmidt (1990) found $< V/V_{max} >= 0.45 \pm 0.03$, consistent with the size-frequency result of spatial uniformity.

Along with observations that deepened understanding of GRBs, the instruments of the late 1970's and 1980's also discovered a new type of source, the Soft Gamma-ray Repeater (SGR). These sources differ from classical GRBs in that they tend to be short (< 1s), have simple time profiles, soft energy spectra (a larger fraction of low energy photons) which do not evolve in time, and repeat (Kouveliotou *et al.* 1987; Rothschild 1996). Three SGRs were identified prior to BATSE's launch (see Higdon & Lingenfelter [1990] for details), one of which was coincident with the supernova remnant N49 in the Large Magellanic Cloud (Evans *et al.* 1980). Whether the SGR events observed were actually from N49 was a matter of some controversy since a luminosity of 10^{44} ergs/s is required to account for the brightest observed outburst at the distance of N49 (assuming isotropic emission). This energy was much larger than most were willing to acknowledge as possible from an SGR or GRB source.

Although the common view was that GRBs arose from nearby neutron stars, a number of different burst models had been proposed. Most of these models suggested that gamma-rays were generated during the disturbance of the strong magnetic field of the neutron star initiated by some epsisodic event. Harwit & Salpeter (1973) postulated that this event could be the impact of a comet with the neutron star, causing magnetic reconnection or inducing large magnetic fields which accelerate non-thermal particles (Sturrock *et al.* 1989). Another idea was that material slowly accreted by the neutron star undergoes a thermonuclear runaway which could induce instabalities in the magnetic field leading to Alfvén waves (Hameury *et al.* 1982; Woosley & Wallace 1982). Neutron star crustquakes provide an excellent way to shake the magnetic field (Pacini & Ruderman 1974). Finally, Ruderman & Cheng (1988) suggested that

energy extracted from rotation of the neutron star could sustain an electron-positron pair cascade which is responsible for gamma-ray emission. An excellent discussion of these models and a summary of the relevant physics can be found in Harding (1991).

While most of the astrophysical community believed GRBs originated on Galactic neutron stars, some suggested cosmological models of burst origin. The most significant work in this direction before 1990 was by Goodman (1986) and Paczyński (1986). As discussed above, the observation of MeV gamma-rays was used to rule out such large distances. However, if the emission region moves with a large bulk velocity, then even though the region may remain optically thick to its own radiation, the resulting black body spectrum will be blue-shifted relative to the observer at Earth, accounting for the high energy photons. The resulting spectrum will be morphologically similar to a black body (though of higher temperature), which is inconsistent with the non-thermal spectra measured by SMM (Matz *et al.* 1985). Paczyński suggested that if the temperature varied rapidly, then a succession of black bodies might appear non-thermal on long time scales. These cosmological models did not explain absorption features however since the enormous energy requirements to generate the burst ($\sim 10^{51}$ ergs) would appear to destroy any absorption layer near the source.

The close of the 1980's was a time of optimism in the field of GRB research. The previous decade had brought substantial advances in understanding the phenomenon and although it could not be proven that the sources of these events were Galactic neutron stars, it was felt that when BATSE was launched, its improved sensitivity would find the expected concentration of bursts in the Galactic plane. This combined with the enormous number of detailed observations of GRBs led most to expect that the final solution to GRBs was at hand. BATSE did revolutionize the field, although in a way few would have predicted.

I.D The BATSE Era

On April 5, 1991, the *Compton Gamma-Ray Observatory* (*CGRO*) was carried into low-Earth orbit by the space shuttle Atlantis. It contains four experiments, each designed to study cosmic gamma-rays, although the BATSE instrument was built specifically for GRB detection and measurement (both *CGRO* and BATSE are discussed in Chapter II). BATSE detected 260 GRBs in its first year of operation (Fishman *et al.* 1994), nearly equaling the total number observed before BATSE was launched (Higdon & Lingenfelter 1990), a clear indication of the sensitivity of the experiment. These BATSE bursts proved a Galactic disk population of sources cannot account for all GRBs, causing an upheaval in the field.

The primary problem for local ($\sim$ 1 kpc) models is the observed distribution of GRBs is inconsistent with a disk population. Figure I.2 shows the log N-log P distribution for 772 BATSE GRBs from the BATSE 3B catalog[1] (Meegan *et al.* 1996). The distribution clearly deviates from a –3/2 power law at low fluxes, indicating that BATSE sees beyond the edge of a core homogeneous distribution. This is consistent with $< V/V_{max} >= 0.33 \pm 0.01$ for these bursts. However, burst locations (Figure I.3) show an isotropic distribution, not a preference for the Galactic disk. The isotropy of the BATSE sky distribution can be quantified by measuring the Galactic dipole and quadrupole moments which test whether there is a concentration of bursts toward the Galactic center or Galactic plane, respectively. In addition, the Bingham and Rayleigh-Watson statistics (Briggs 1993) measure dipole and quadrupole moments independent of coordinate system and would find an anisotropy in any direction. These statistics must be compared with values of what BATSE would have seen if GRBs were distributed isotropically on the sky taking into account the fact

[1]BATSE has produced three catalogs of GRBs, the latest known as the 3B catalog. Throughout this thesis, individual bursts observed by BATSE are designated 3BYYMMDD, where 3B is the catalog name, YY is the last two digits of the year the burst was observed, MM is the number of the month, and DD is the day of the month the burst was observed. Bursts which do not appear in the 3B catalog are identified by date only. For example GRB 3B930131 is the burst observed by BATSE on January 31, 1993 and GRB 880205 is a burst which occurred on February 5, 1988 and not observed by BATSE.

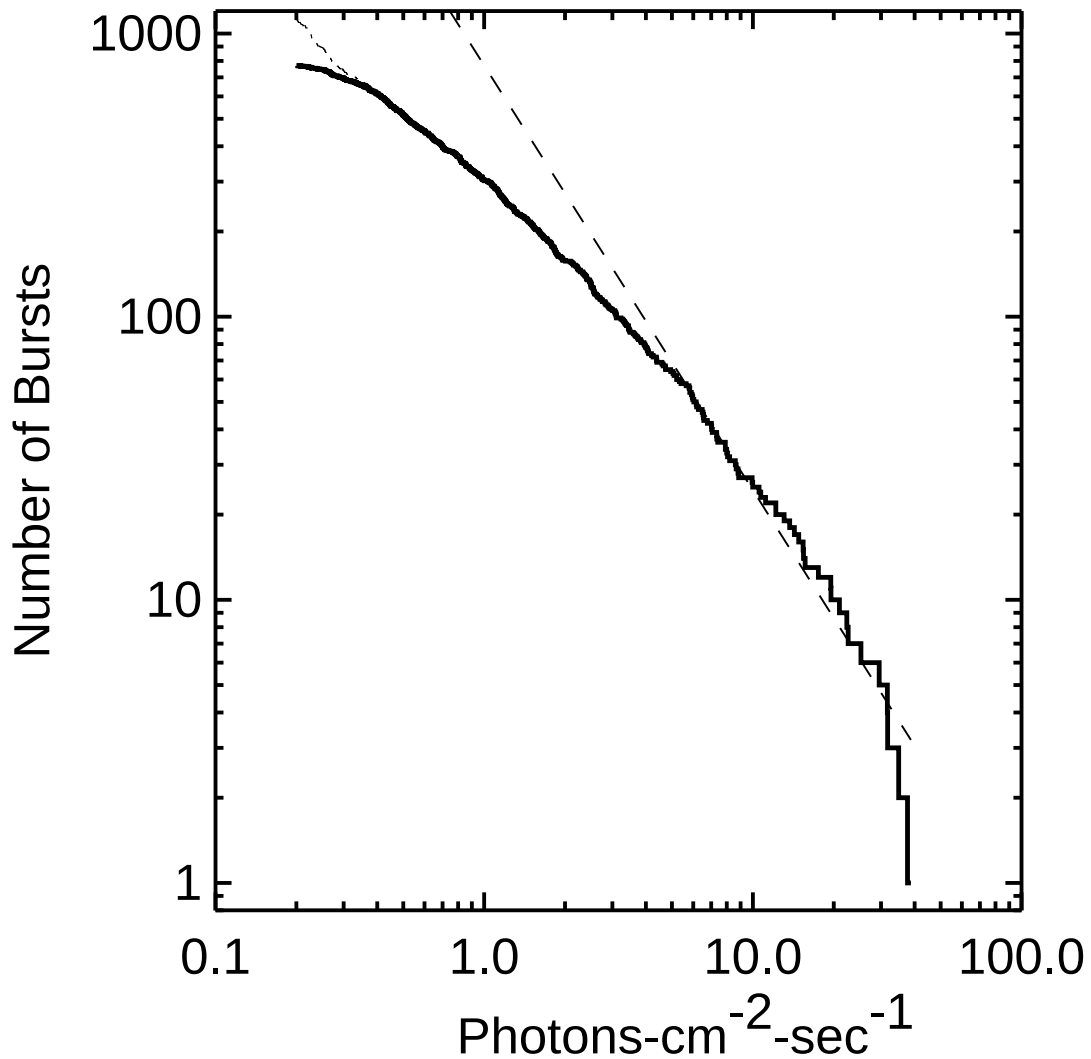

Figure I.2: The integral log N-log P distribution for GRBs from the BATSE 3B catalog (taken from Meegan *et al.* 1996). The dashed line is a –3/2 power law and the uncertainty at low photon flux (the dot-dashed line) is caused by the variable instrument threshold.

that BATSE cannot observe the entire sky at once, primarily because *CGRO*'s low-Earth, low inclination orbit allows better coverage of the celestial poles than the celestial equator. Table I.2 gives the measured and expected values of these statistics, all of which are consistent with isotropy. These results prove that BATSE sees an isotropic distribution of sources on the sky and is sensitive beyond the homogenous core distribution of GRB sources which means that if GRBs arise from a single source distribution, they must reside in an extended Galactic Halo ($\sim$ 150 kpc) or are at cosmological distances ($\sim$ 1 Gpc). If bursts are associated with the Galaxy, then a large constant density Halo is needed to mask the anisotropy caused by the 8.5 kpc offset of the Earth from the center of the Galaxy. Outside this core, the source density decreases with radius which would explain the observed inhomgeneity of GRBs in space. If bursts are extragalactic, then they must be cosmological since GRBs are not observed to be concentrated around nearby clusters or superclusters of galaxies. In this case, inhomogeneity can be explained by the curvature of space which produces an apparent smaller source density at large redshifts. The fact that sources of GRBs are at either distance is interesting. If bursts come from the Halo, then a new and fascinating galactic population can be studied. If bursts arise from cosmological sources, GRBs could be used to probe the geometry and dynamics of the universe (*e.g.,* Trimble 1994).

Figure I.3: The locations in Galactic coordinates of 1122 GRBs from the BATSE 3B Catalog (Meegan *et al.* 1996).

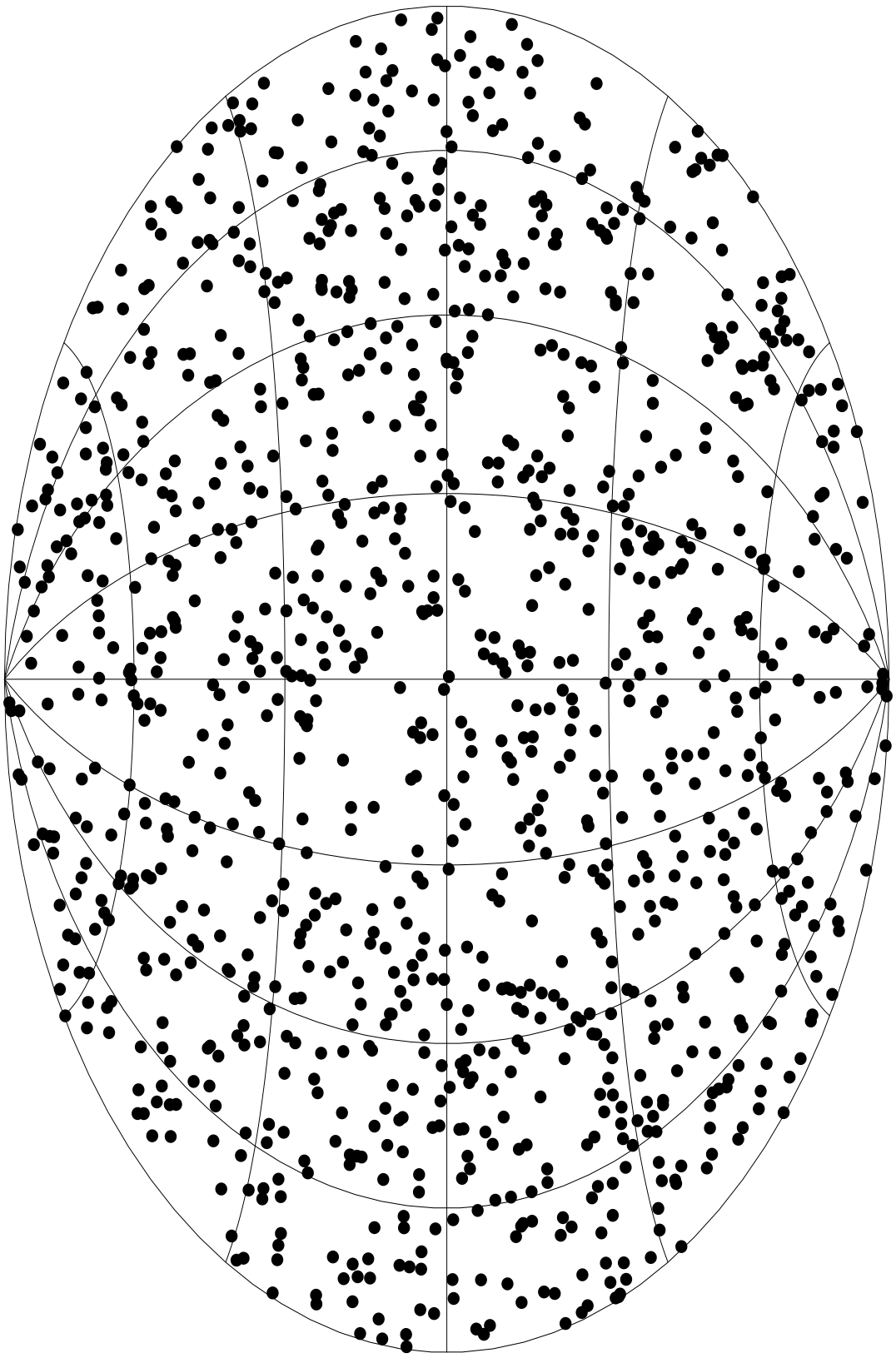

Moment	Type	Coordinates	Observed	Expected	Deviation (σ)
$\cos\theta$	dipole	galactic	-0.002	-0.013	0.6
$sin^2 b - 1/3$	quadrupole	galactic	-0.003	-0.005	0.3
Watson	dipole	independent	0.5	5.2	-1.2
Bingham	quadrupole	independent	5.8	13.6	-1.2

Table I.2: The dipole and quadrupole moments for 1122 BATSE GRBs (taken from Meegan *et al.* 1996). θ is the galactic latitude of a GRB and b is the Galactic latitude. The expected value for isotropy is based on BATSE's non-uniform sky coverage.

In addition to showing GRB sources do not have a spatial distribution consistent with a Galactic plane population, BATSE's results on spectral features are surprising. BATSE was expected to detect absorption and emission lines in a significant fraction of bursts. Thus far, it has not produced a firm detection although there have been many candidates (Palmer *et al.* 1994; Ford *et al.* 1994; Preece *et al.* 1994; Band *et al.* 1996). Statistical analysis (Band *et al.* 1994b) shows that the BATSE results are unlikely if such features do exist in GRB spectra and BATSE operates as expected but does not indicate a compelling inconsistency with previous detections. The consistency analysis has done little to settle the issue of the existence of spectral features in bursts and it will likely require a BATSE detection, a demonstration that the previously claimed detections were spurious, or proof that BATSE is insensitive to lines before a consensus is achieved on the existence of spectral features (these issues are discussed in detail in Chapter III).

Several BATSE results have not been as controversial as those discussed above. For example, studies of spectral shape and evolution have proved quite useful. Prior to BATSE, exponential or thermal bremsstrahlung spectra seemed to fit low energies well (Cline *et al.* 1973, Mazets *et al.* 1982), while at higher energies ($\gtrsim$ 1 MeV), power laws were required (Matz *et al.* 1985). Band *et al.* (1993) showed that burst spectra in the 10 keV–10 MeV region are well described by a function of the

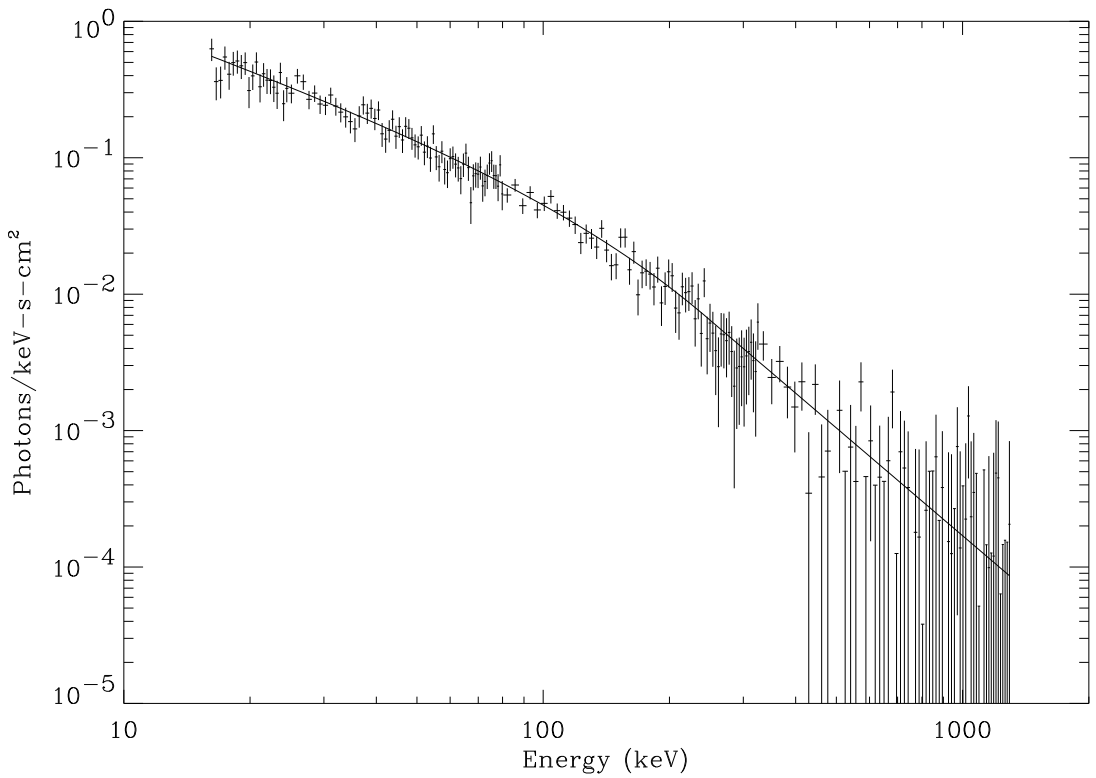

Figure I.4: A photon spectrum from GRB 3B930119 observed with BATSE spectroscopy detector 0. The data were taken between 73.0–76.3 seconds after the trigger. Equation I.6 was fit to the data with best fit parameters $A = 0.084$ photons/keV-s-cm^2, $\alpha = -1.09$, $\beta = -2.62$, and $E_0 = 159$ keV.

form

$$N_E(E)\left(\frac{\text{photons}}{\text{keV-s-cm}^2}\right) = \begin{cases} A\left(\frac{E}{100\ \text{keV}}\right)^{\alpha} e^{-E/E_0}, & E \leq (\alpha-\beta)E_0 \\ A'\left(\frac{E}{100\ \text{keV}}\right)^{\beta}, & E > (\alpha-\beta)E_0 \end{cases} \tag{I.6}$$

where A, α, β, and E_0 are parameters and A' is chosen so that the function is continuously differentiable everywhere (a GRB spectrum is shown in Figure I.4). These parameters are typically $-1.5 < \alpha < 0$, $-5 < \beta < -1.5$, and 100 keV $< E_0 <$ 1000 keV and vary substantially both between and within bursts (Band *et al.* 1993; Ford *et al.* 1995). The key to the success of this empirical spectral form in describing GRB spectra is its flexibility. Among the physical models this spectral form can accommodate are optically thin thermal bremsstrahlung without Gaunt factor ($\alpha = -1$, $\beta = -\infty$), single power laws, smoothly broken power laws and power laws with an exponential cutoff. Although the form is not based on a physical model of GRBs, its superiority to spectral forms rooted in physical theory has led to its adoption as the standard form for describing burst spectra, an indication of the lack of compelling theoretical spectral models. This flexibility also explains why previous spectral models gave reasonable fits since these models are limiting forms of equation I.6.

Another important BATSE result is the confirmation of a bimodality in the GRB duration distribution (Kouveliotou *et al.* 1993b; Lamb, Graziani, & Smith 1993). Previous studies (Mazets *et al.* 1981; Norris *et al.* 1984; Hurley 1991; Klebesadel 1992) had suggested such a bimodality but were unable to prove the effect conclusively because of various biases against detecting short duration events (Kouveliotou *et al.* 1993b). Durations for BATSE GRBs are shown in Figure I.5, clearly demonstrating the dual-peak form. Many properties of bursts have been compared between long and short bursts, but have not shown much promise for forming a useful classification system based on duration. The only significant difference between the two sets of GRBs is that short bursts have harder time averaged spectra than long bursts (Kouveliotou *et al.* 1993b; Lamb, Graziani, & Smith 1993).

BATSE has also aided studies of SGRs. As mentioned above, one SGR

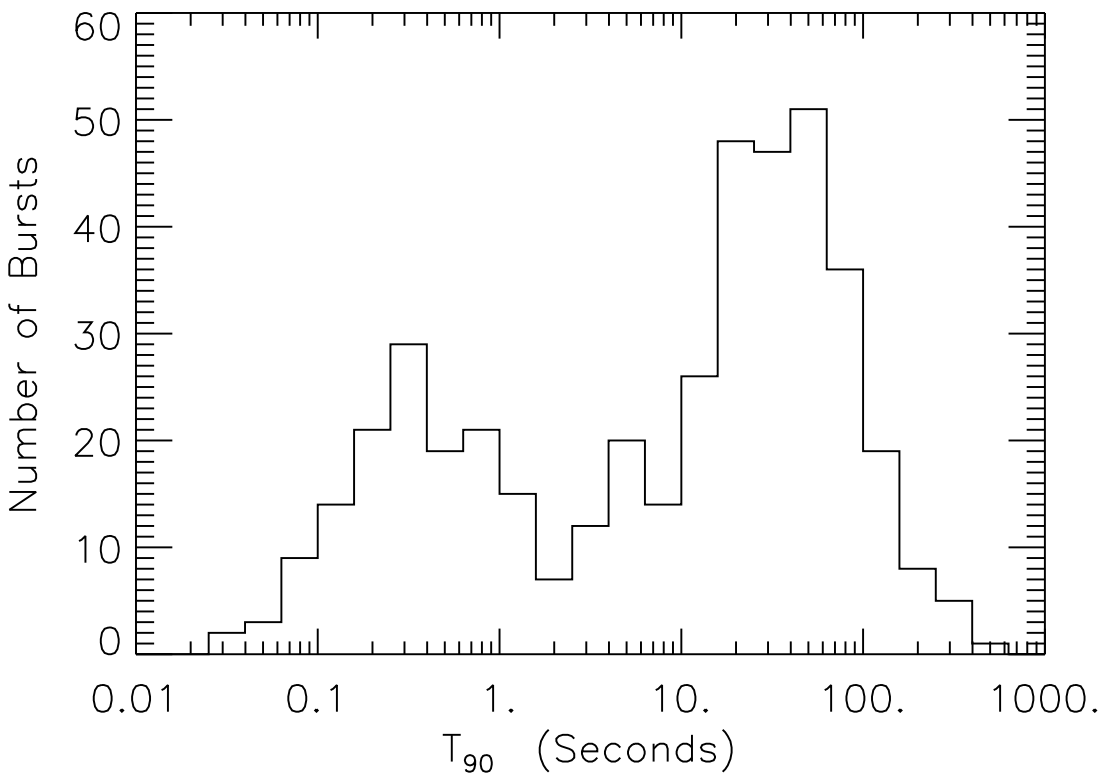

Figure I.5: The distribution of durations of GRBs in the BATSE 3B catalog (Meegan *et al.* 1996). Duration is defined as the time in which 90% of the total burst flux is observed.

(SGR0526–66) was known to be spatially coincident with the supernova remnant N49 in the Large Magellanic Cloud. Further analysis (Rothschild, Kulkarni, & Lingenfelter 1994) found point-like emission in the nebula consistent with the small SGR error box (0.09 arcmin^2). This source is far from the center of the remnant (6.6 pc if the remnant is in the Large Magellanic Cloud) and implies a high transverse velocity ($\sim$ 1200 km/s) if it is a neutron star which was created at the center of the remnant during a supernova 5400 years ago. BATSE observed events which are spatially and spectrally consistent with the remaining two SGRs (SGR1900+14, Kouveliotou *et al.* 1993a and SGR1806–20, Kouveliotou *et al.* 1994). These observations, along with the observation of some of the same outbursts and quiescent emission by instruments with excellent imaging capabilities (in particular, the ASCA satellite), find these SGRs are associated with Galactic supernova remnants which have young, high velocity neutron stars (Hurley *et al.* 1994b; Kulkarni *et al.* 1994; Murakami *et al.* 1994; Vasisht *et al.* 1994). It appears then that the source of SGRs is known. However, most regard SGRs as a separate phenomenon from classical gamma-ray bursts and therefore the source of GRBs remains elusive. However, it is important to note that the opinion that GRBs and SGRs are distinct phenomena is not universal and some work has been done attempting to find a connection between these types of events (see Rothschild & Lingenfelter 1996).

Observationally, the most recent attempts to connect SGRs to GRBs involve the controversial issue of burst repetition. If more than one GRB is observed from the same source, then the most significant difference between SGRs and GRBs is no longer a factor. Wang & Lingenfelter (1993; 1995) noticed five GRBs in the first BATSE GRB catalog (Fishman *et al.* 1994) were clustered in both time and space, a statistically rare event if bursts are distributed randomly (probability less than 2×10^{-5}). However, Brainerd *et al.* (1995) concluded this clustering was not significant in the second catalog, which included more GRBs. Quashnock & Lamb (1993) found clustering on angular scales less than 4° (the minimum uncertainty in BATSE GRB positions at the time) which had a probability of chance occurrence of

only 8×10^{-5}. The clustering statistic used was the nearest neighbor statistic which describes the average separation between a burst and its nearest neighbor. Using the two point angular correlation function, Narayan & Piran (1993) found this clustering was much less significant (a probability of chance occurrence of 0.01). Yet another statistical analysis performed by Petrosian & Efron (1995) found marginal but not compelling evidence for repetition.

Clearly, attempts to show GRB repetition using BATSE data rely on statistical arguments. This is because of the large positional uncertainties in bursts observed by BATSE. BATSE GRB localizations (known as error boxes) are a function of the strength of the bursts. Bright bursts can be positioned within 2° (the size of BATSE's systematic location error) on the sky but weak bursts can have uncertainties as large as 30° because small count rates have large statistical uncertainties (Meegan *et al.* 1996, nearly all bursts in the 3B catalog are localized to within 10°). This makes studies of clustering difficult because the large number of bursts observed by BATSE makes overlapping error boxes very common. Therefore, GRB repetition is likely to remain a controversial issue until more accurate GRB positions are determined for a large number of bursts.

The success of SGR counterpart searches in determining the apparent sources of these events inspires many GRB counterpart searches. Lack of knowledge about the source of GRBs is the largest impediment to progress in the field and identification of a counterpart would be one of the most significant steps taken since the BATSE observation of GRB isotropy and inhomogeneity. A number of counterpart searches have been conducted in all regions of the electromagnetic spectrum (see Schaefer 1994a for a review) but no clear counterparts have been found in quiescence, flaring with the burst, or fading afterward. Given the difficulty of such searches, however, the lack of success cannot be taken to mean that GRBs do not significantly radiate at energies other than gamma-rays or that some object associated with GRBs (*e.g.,* a distant galaxy) is inherently unobservable. For example, Larson, McLean, & Becklin (1996) have found luminous infrared galaxies near arcminute-size error boxes from six

GRBs. Although the result is not statistically significant at present, the association of more GRBs with luminous galaxies would suggest a cosmological origin for GRBs.

I.E Post-BATSE Models

BATSE has ushered in a new era in GRB studies. The shift in source location from the Galactic Disk to the Halo or the far reaches of the universe was so unexpected that only recently have tests designed to reveal cosmological source distances been applied. Unfortunately, these studies have not been as successful as hoped. Norris *et al.* (1993) claimed a cosmological signature, but their results could be caused by correlations intrinsic to GRBs (Band 1994a; Brainerd 1994). Mitrofanov *et al.* (1994; 1996) performed a test similar to one by Norris *et al.* but found no cosmological signature. Proponents of Halo models have had a difficult time as well. If GRB sources were a simple extended Halo distribution, it would have a radius of at least 100 kpc (Hakkila *et al.* 1994). Studies of galaxies similar to the Milky Way suggest the mass distribution in halos can be as large as 200 kpc (Zaritsky *et al.* 1993) and part of that mass could be in GRB sources. However, if GRB sources populate such a large halo, an excess of bursts from the direction of M31 is eventually expected and missions have been proposed to search for such a signal. Ideas assuming non-spherical Halos (Podsiadlowski, Rees, & Ruderman 1995) or two-population distributions (Smith & Lamb 1993; Higdon & Lingenfelter 1994) can provide the observed isotropy, but in the former case can be quite contrived or in the latter, seem to imply two distinct classes of GRB, something not yet generally accepted.

Lack of even an approximate distance measure for GRBs has not stood in the way of healthy speculation about the sources themselves. Indeed, the dearth of observational constraints has led to a wide range of suggestions about burst origins. A small sample of the multitude of ideas are models of merging neutron star binaries (Eichler *et al.* 1989), failed supernovae (Woosley 1993), comets impacting neutron stars (Colgate & Leonard 1994), tidal disruption of normal stars by black

holes (Carter 1992), and evaporating primordial black holes (Cline & Hong 1992). In many recent models, a primary aim is to reproduce the observed GRB distribution and most succeed (the exception being some early Halo models, see Briggs *et al.* 1996a). However, few attempt to describe the wide range of temporal and spectral properties that bursts exhibit. A notable exception is the blast wave model of Rees & Mészáros (1992; also Mészáros & Rees 1993a, and Mészáros, Laguna, & Rees 1993b) in which highly relativistic ejecta from collapse of a compact object or coalescence of a compact binary system runs into the interstellar medium. In this model, a shock forms and gamma-rays are produced by synchrotron and inverse Compton processes. Although this model and others similar to it are currently popular, the community remains divided regarding the most likely explanation of GRBs, an indication of the enormous complexity of the phenomenon.

I.F Summary

Gamma-ray bursts have been a perplexing mystery since they were discovered 30 years ago. BATSE was expected to confirm hypotheses about the phenomenon developed over 20 years but has instead shown those ideas to be irreconcilable with observations. This caught the community studying GRBs by surprise and as a result, there are many notions about bursts but little consensus. Because of this confusion, this thesis does not develop or analyze a single detailed model for GRBs which can be tested and likely fail. Instead, it is more valuable to examine aspects of burst phenomenology which can be used to narrow the vast realm of what is currently thought possible to a restricted area of what physical processes are likely to be occurring in these events . To do this, GRB spectra are examined with the intention of striking down entire classes of models. To start, the BATSE detectors are described (Chapter II) to familiarize one with its spectral capabilities and describe the recalibration I performed which allowed BATSE spectral analysis to be performed. In Chapter III, the issue of absorption and emission features in GRBs is discussed, focusing on the

current controversy of the existence of these features. In particular, I demonstrate the difficulty of spectral observations using a candidate absorption feature I found in the BATSE data. Chapter IV is devoted to continuum evolution within bursts. In this chapter (which is taken from Ford *et al.* 1995), I show that GRB spectra usually evolve from hard to soft with an interesting intensity dependence which has important implications for the source environment. Chapter V (taken from Ford & Band 1996) considers the expected brightness of counterpart emission from simple extrapolations of observed GRB spectra, providing a useful guide for expectations regarding optical counterpart searches and for interpretation of the results. Chapter VI discusses and applies a statistical technique I developed which can detect short time scale, narrow energy band emission in GRBs, providing a stringent constraint on a popular class of GRB models. The entire thesis is summarized in Chapter VII, in which the significance of this work is discussed.

Chapter II

BATSE

II.A CGRO

The Burst and Transient Source Experiment (BATSE) is one of four instruments on the *Compton Gamma-Ray Observatory* (*CGRO*, Figure II.1), a satellite devoted to the study of high energy radiation from astrophysical sources. The second in NASA's 'Great Observatories' program (the *Hubble Space Telescope* was the first), *CGRO* is playing a major role in shaping current thought about many types of energetic cosmic phenomena. In this chapter, the spacecraft and instruments on *CGRO* are briefly described. The BATSE detectors are then discussed in detail with special attention paid to my recalibration of the spectroscopy detectors.

CGRO was carried into space by the Space Shuttle Atlantis on April 5, 1991 where it was released into low-Earth orbit. The nominal altitude of *CGRO*'s orbit is 450 km but the true altitude slowly falls because of drag in the Earth's tenuous upper atmosphere. *CGRO* has been reboosted twice since launch after its altitude had fallen to roughly 300 km. The inclination of the orbit is 28.5° with respect to the Earth's equator and has a period of 90 minutes. A disadvantage of *CGRO*'s orbit is that it passes through the South Atlantic Anomaly (SAA), a region where the Earth's magnetosphere is weak, allowing charged particles which are ordinarily trapped at high altitudes to fall to lower altitudes. The large charged particle flux in

the SAA causes dangerously high counting rates in *CGRO*'s instruments. As a safety measure the instruments are turned off for the $5-10$ minutes it takes to traverse the region. Because three of the instruments on *CGRO* have limited fields-of-view, the spacecraft is reoriented for each observation.

BATSE (Figure II.1) is a set of eight detector modules located on the corners of the *CGRO* spacecraft (Fishman *et al.* 1989). Each detector module contains a Large Area Detector (LAD) and a Spectroscopy Detector (SD). The LADs use a cylindrical $20''$ diameter by $0.5''$ thick NaI(Tl) scintillating crystal to detect gamma rays. Gamma-rays lose energy in the crystal via photoelectric, Compton scatter, and pair-production processes which cause ionization in the crystal. As the crystal settles back to its ground state, optical light pulses are produced. The amount of light produced is proportional to the energy lost in the crystal by the gamma-ray. The LADs are optimized for burst detection and timing. The planes of the LADs are oriented parallel to the faces of a regular octahedron so nearly all bursts illuminate four detectors and GRBs are localized by comparing the relative fluxes observed by several detectors. The SDs also use a cylindrical NaI(Tl) scintillator though of different dimension than the LAD crystals ($5''$ diameter by $3''$ thick). The thickness of the SD crystals make it much more likely that an incident gamma-ray will lose all its energy in the crystal, giving the SDs better energy resolution though their smaller area makes them less sensitive to weak bursts than the LADs. The LADs are sensitive to gamma-rays from 25 keV to about 2 MeV. The energy range covered by the SDs depends on a commandable gain setting which specifies a two decade range between 10 keV and 30 MeV. Both detectors are uncollimated and the full BATSE field-of-view is 4π sr, 39% of which is blocked by the Earth because of *CGRO*'s low altitude orbit (Brock *et al.* 1992).

Figure II.1: The *Compton Gamma-Ray Observatory* and a BATSE detector module.

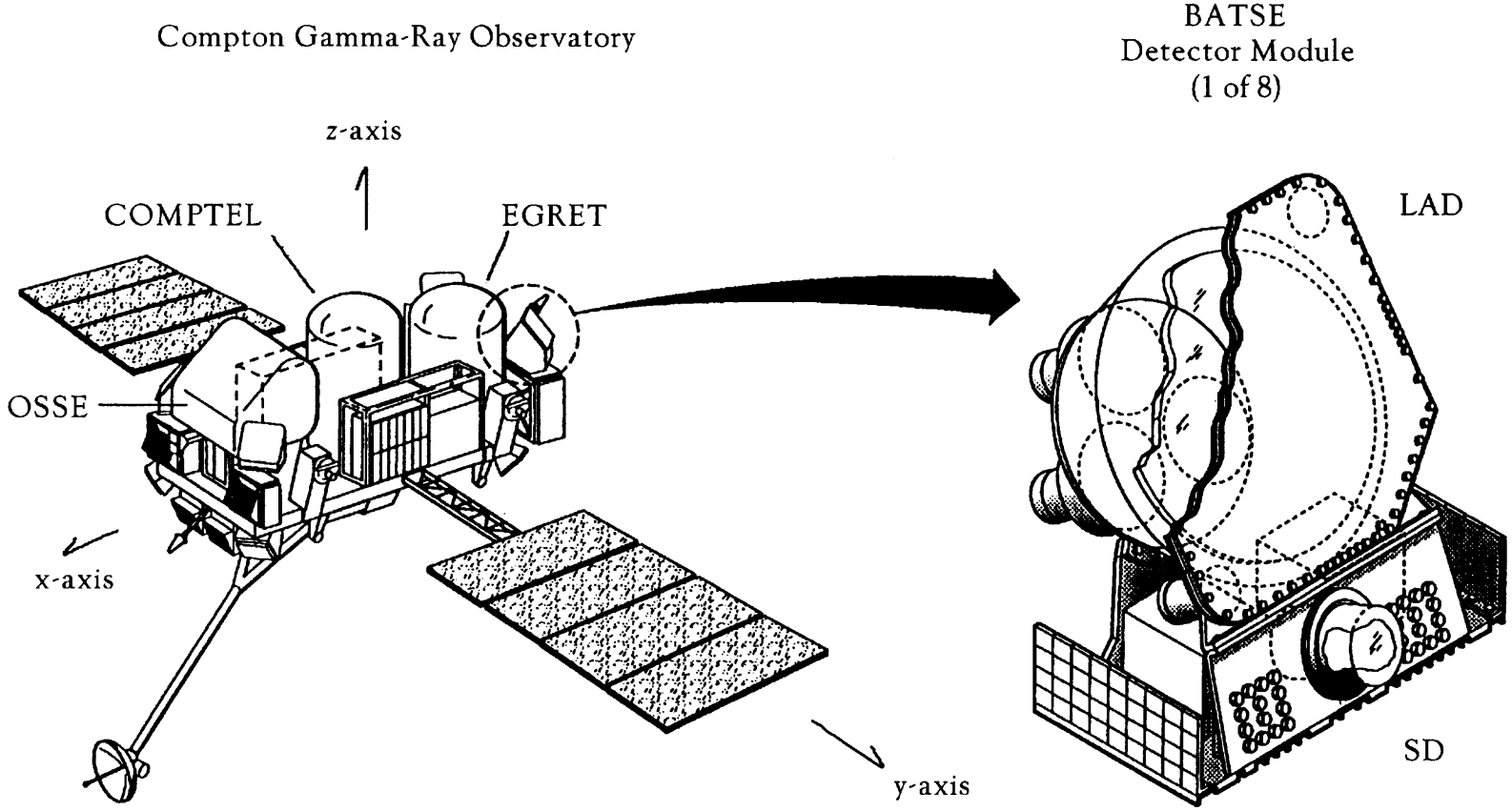
Compton Gamma-Ray Observatory
z-axis
COMPTEL
EGRET
OSSE
x-axis
y-axis
BATSE
Detector Module
(1 of 8)
LAD
SD

The Oriented Scintillation Spectrometer Experiment (OSSE, Johnson *et al.* 1993) is a spectrometer designed to operate in the $0.05 - 10$ MeV range. OSSE is composed of four 'phoswich' detectors, an arrangement in which a 13-inch diameter by 4-inch thick NaI(Tl) scintillating crystal is shielded in the rear by an optically coupled 3-inch thick CsI(Na) scintillator. Both crystals are surrounded by an annular NaI(Tl) shield. This complicated arrangement uses anti-coincidence to ensure that all recorded events come from the forward direction. Particles which enter from the side will activate the shield and will be rejected. Events from the rear of the detector are rejected by examining the shape of the light pulse produced in the scintillator. Since NaI(Tl) and CsI(Na) have distinctly different pulse shapes, events caused by particles entering from the rear are easily rejected. Because there is no anti-coincidence electronics between the NaI(Tl) and CsI(Na) crystals, any event which deposits energy in the CsI(Tl) is rejected. OSSE has a $3.8° \times 11.4°$ field-of-view but no positional sensitivity (*i.e.,* sources in the field-of-view are indistinguishable). To find the background rate (which is subtracted from the source observation to find the source signal), background observations are performed on alternate sides of the source, typically 5° away.

The Imaging Compton Telescope (COMPTEL, Schönfelder *et al.* 1993) is used for imaging and spectroscopy in the $1 - 30$ MeV range. COMPTEL consists of two well-spaced detector arrays. The upper array uses a liquid scintillator (NE 213A) and the lower uses a NaI(Tl) scintillator to detect gamma-rays. Gamma-rays are Compton-scattered in the upper detector array and then interact in the lower array. The energy loss of the photon in both arrays is measured from which the Compton scattering angle in the upper array is deduced. This confines the possible arrival direction of the incident photon to an annulus on the sky. After a sufficient number of events have been recorded, complex but effective techniques can be used to construct an image (Strong & Diehl 1989). COMPTEL has a 1 sr field-of-view and an angular resolution between $1° - 2°$ depending on source location with respect to the instrument axis and energy of the gamma-rays.

The Energetic Gamma-Ray Experiment Telescope (EGRET, Thompson *et*

al. 1993) observes the highest energy gamma-rays, photons from 20 MeV−30 GeV. EGRET is a spark chamber. Gamma-rays which enter the front of the detector trigger electron-positron pair production in a layer of tantalum foils in the upper spark chamber. This triggers coincidence electronics which record the path of the gamma-ray using two 4×4 arrays of scintillator tiles, one in the middle of the chamber and the other at the bottom. Behind the second tile array is a thick slab of NaI(Tl) which records the energy of the gamma-ray. EGRET has a 0.6 sr field-of-view and angular resolution of 10 arcmin.

Except for BATSE, the instruments on *CGRO* are pointed, that is, an object of interest is selected and the spacecraft oriented so that the object is in the center of the the instruments' field-of-view. COMPTEL and EGRET point parallel to the spacecraft's z-axis (see II.1) but OSSE can rotate 192° about the spacecraft y-axis. Although OSSE is normally co-aligned with COMPTEL and EGRET, OSSE's rotational freedom allows it to be used independently of the other two instruments. Among the objects studied with *CGRO* are active galaxies (including quasars and blazars), pulsars, supernova remnants, and black hole candidates. Because the fields-of-view of all the instruments is large, GRBs have occasionally been observed by all the experiments and substantially advanced understanding of the very high energy behavior of GRBs. In particular, the imaging capabilities of COMPTEL and EGRET allow better localizations of GRBs than BATSE and provide good spectral information at energies above the BATSE SD's operating range.

II.B The BATSE Large Area Detectors

The LADs are BATSE's primary detectors. They are used to detect and locate GRBs as well as provide precise information about time profiles of these events. Gamma-rays are detected by the LADs when they interact with atoms in the NaI(Tl) crystal, raising electrons into the conduction band via photoionization, Compton scattering, or (if above 1 MeV) electron-positron pair production. The electrons then

fall back to the valence band via 'activation sites', locations in the crystal lattice containing Tl atoms which alter the band structure of pure NaI (Knoll 1989, p. 225). These sites allow a much more efficient way for electrons to return to the valence band than in a pure crystal. During de-excitation, photons with energies of a few eV (optical light) are emitted. These photons reflect around a light collection cone until they enter one of three photomultiplier tubes (PMTs) at the bottom of the cone. The signal from the PMTs is a charge which is proportional to the amount of light observed. Thus, gamma-rays which lose more energy in the crystal will cause more charge to leave the PMTs. This charge is converted to a voltage pulse which is used to assign the event to a spectral channel with a monolithic charge-to-time converter chip (MQT). The channel which is assigned to a given photon energy loss is kept constant by means of an automatic gain control system which adjusts the voltage of the phototube (gain) to ensure that a test pulse from a light emitting diode remains in a fixed channel.

High energy photons are not the only particles which can cause scintillations in the crystal. Electrons, protons, and neutrons are common in *CGRO*'s low Earth orbit and can produce events which would be recorded by the LADs. To eliminate background caused by the former two particles, a charged particle detector sits in front of the NaI(Tl) crystal. If this detector notes an event, the LAD ignores events in the NaI(Tl) which are in time coincidence with it. In addition to this active shielding, an aluminum window on the face of the detector attenuates photons below $\sim$ 20 keV. A combination of tin and lead shielding on the sides of the focusing cone shield the rear of the detector to photons up to an energy of 400 keV.

BATSE operates in burst and non-burst modes, the difference being the amount and type of data recorded. Each LAD accumulates counts on time scales of 64, 256, and 1024 ms and compares the results to the number of counts expected based on the number of counts measured in the previous 17 s. When the number of counts in two LADs exceeds the expected number in a given energy band on any of the three time scales, the burst mode is triggered. The threshold level and energy

range are commandable parameters. For most of the mission, a 5.5 σ deviation from the background counting rate in the $50 - 300$ keV band was required to trigger the burst mode (unless a burst is stored in memory, see below). Recently however, the energy band has been varied to facilitate studies of soft gamma-ray repeaters and hard transients believed to be caused by terrestrial lightning. The threshold has also been raised at times in response to bright active periods from objects such the black hole candidate Cygnus X-1. While these events are interesting in themselves, they are a nuisance for GRB studies. Triggers are stored until they can be telemetered to a ground station which can be up to 90 minutes after a trigger. Only a burst which is brighter than a stored event will retrigger BATSE so the sensitivity to weak GRBs is reduced when there are many triggers.

As implied above, BATSE triggers on events which are not GRBs. As of May 1, 1996, BATSE triggered on 1518 GRBs out of 5347 triggers. The most common non-GRB triggers are solar flares and electron precipitation events in the Earth's magnetosphere. Other non-GRB triggers have been caused by soft gamma-ray repeaters, the rise of bright sources over the Earth's limb, bright transients from non-GRB sources, and terrestrial lightning. Fortunately, most of these events can be clearly distinguished from GRBs. For example, solar flares are typically very soft, come from the direction of the Sun, and are often observed at other wavelengths by other instruments. Electron precipitation events have very smooth time profiles and often illuminate all eight LADs. While the origin of most events can be reliably determined, some cases are particularly problematic. The number of misclassifications is believed to be small, however, and the BATSE team estimates that only one or two non-GRB events are included among the 1122 GRBs in the 3B catalog.

LAD data are available in several formats, each serving a different purpose. The different types are defined in Table II.1 along with a brief description of their use. Signals from the NaI(Tl) crystal are analyzed by a set of four energy discriminators, which produce four channel spectra, and a pulse height analyzer (MQT) which produces 16 and 128 channel data. Generally speaking, there is a trade-off between the

number of energy channels and the time resolution of the data (*e.g.,* four channel data types have excellent time resolution but little energy information). Most burst data types begin at the trigger time and continue until the end of the pre-programmed trigger length (4 m early in the mission, 10 m later on). If a GRB rose slowly or had some sub-threshold precursor activity, the pre-trigger information would not be recorded in these types. Fortunately, the PREB and TTE data types include some pre-trigger information with excellent time resolution. The amount of HERB and TTE data collected depends on the strength of the burst. The time resolution of the HERB spectra is determined using a time-to-spill criterion. A spectrum is accumulated until the total number of counts observed reaches a given level. At this point, the current accumulation ends and the next begins. HERB data is hierarchical in the sense that the most brightly illuminated (first rank) detector has the finest time resolution. For every four spectra recorded by the first rank detector, two are saved from the second and one each from the third and fourth detectors. The remaining four detectors have no HERB spectra. Spectra are accumulated until either a total of 128 have been recorded or the burst mode ends. TTE data records the arrival times of individual photons as opposed to the other data types which assign all events in a given time interval to a spectral energy bin. TTE data is count limited and is only collected for detectors which had exceeded the trigger threshold. A maximum of 16,384 counts can be recorded using four memory buffers. When not in burst mode, TTE data is collected in one buffer for all eight detectors. When a trigger occurs, the data in the buffer is not overwritten and further TTE data is collected only for those detectors which exceeded the trigger threshold.

BATSE's all-sky monitor capability has allowed it to make important observations of many high-energy phenomena. BATSE has been used to monitor previously known isolated pulsars and disk fed binaries (PSR1509–58 and Her X-1, Wilson *et al.* 1993), discovered previously unknown high-energy pulsars (GROJ 1948+32, Chakrabarty *et al.* 1995), observed black hole candidates (GX 339–4, Harmon *et al.* 1994), discovered new transients (GROJ 1744-28, Kouveliotou *et al.* 1996) performed

Name	Acronym	Burst Mode	Energy Channels	Time Resolution	Uses
Continuous	CONT	Both	16	2 s	Strong source monitoring, weak burst detection
Discriminator	DISCLA	No	4	1 s	Source monitoring, burst detection
	DISCSC	Yes	4	64 ms	Burst temporal structure
High Energy Resolution (Burst)	HER	No	128	>49 s	Background for HERB
	HERB	Yes	128	> 0.128 s	Burst spectroscopy
Medium Energy Resolution	MER	Yes	16	$16 - 64$ ms	Burst spectral evolution
Pre-Burst	PREB	Yes	4	64 ms	Burst precursor emission
Time Tagged Events	TTE	Yes	4	2 μs	Burst temporal properties

Table II.1: Data types from the LADs (adapted from Horack 1991). The Burst Mode column refers to whether or not the data is taken during a trigger. CONT data is taken at all times.

imaging with an Earth occultation technique (Zhang *et al.* 1993), and discovered intense gamma-ray emission from lightning in the Earth's atmosphere (Fishman *et al.* 1994). These secondary functions show that BATSE has not only been important for understanding GRBs, but is a valuable resource in other areas of high-energy astrophysics.

II.C The BATSE Spectroscopy Detectors

Although the LADs do have spectral capabilities, the higher energy resolution data from the Spectroscopy Detectors (SDs) are better suited to many types of spectral observations. For example, the energy resolution of the SDs at 40 keV (a typical energy for previously reported absorption features) is about 23% while the LADs have a resolution of only 32% at this energy (Fishman *et al.* 1989). This improved resolution is a consequence of the thickness of the SDs' NaI(Tl) crystals. Gamma-rays are more likely to leave only a fraction of their total energy in the thin LAD crystals leading to uncertainty in the energy the particle had before it struck the detector.

Photon detection and event processing in the SDs and LADs are very similar. Since the SDs have smaller area than the LADs, a single 5″ PMT optically coupled to the crystal is all that is necessary to detect scintillation photons. The output PMT charge is converted to 4 channel discriminator and 256 channel spectra in the same way as in the LADs (the process is described in detail in the next section). The SDs do not have a charged particle detector so all events which leave any energy in the crystal are recorded, leading to a larger background than would be expected based on what is observed in the LADs. The only shielding the SDs have is the aluminum housing which holds the crystal and PMT. The SDs also lack automatic gain control and the gain can drift over time as well as be commanded to change from the ground. Therefore, all energy-loss spectra must be individually calibrated. Gain drifts are annoying, but it is a small effect and occurs slowly compared to GRB time scales.

Name	Acronym	Burst Mode	Energy Channels	Time Resolution	Uses
Spectroscopy Discriminator	SDISC	Both	4	2 s (non-burst) 64 ms (burst)	High & low energy counts
Spectroscopy High Energy Resolution (Burst)	SHER	No	256	> 49 s	Background for SHERB
	SHERB	Yes	256	> 0.128 s	Burst spectroscopy
Spectroscopy Time Tagged Events	STTE	Yes	256	128 μs	Fine time resolution spectra

Table II.2: Data types from the SDs (adapted from Horack 1991). The Burst Mode column refers to whether or not the data is taken during a trigger.

The SDs provide spectra covering two decades in energy in the 10 keV to 30 MeV range, the exact range being determined by a commandable gain setting. For example, at the nominal gain setting, the energy range covered is $\sim 40 - 4000$ keV while at '4X' gain (the high voltage in the phototube is four times the nominal setting) the energy range covered is $\sim 20 - 2000$ keV. Because of the desire to reach low energies, the front of the aluminum case containing the NaI(Tl) crystal has a 3-inch diameter hole filled with a 0.68 mm beryllium window. This window allows low energy measurements for face-on bursts since attenuation of photons in beryllium is only important below about 10 keV.

The SDs are primarily burst-mode instruments and the data types returned are listed in Table II.2. The data types which are most often used are the two Spectroscopy High Energy Resolution (SHER) types. These are 256 channel data and are analogous to the 128 channel HER and HERB types. The four SDs for which SHERB data are accumulated in burst mode are selected and ranked according to the intensity observed by the associated LAD. Thus, the first rank SD will be the SD in the detector module with the first rank LAD. The accumulation scheme for SHERB data is identical to that used to gather HERB data except that 64 additional spectra are recorded by the SDs after the HERB accumulations end. Thus, there are

128 HERB and SHERB spectra covering identical intervals and 64 SHERB spectra accumulated at later times. Engineering constraints forced the SDs to be mounted so that the angle between the LAD and SD detector normals is 18.5° with the SD normal lying closer to the $x-y$ plane of *CGRO* (see Figure II.1). Therefore, the SD ranks often do not reflect the actual distribution of intensities observed by the SDs. Another problem caused by the offset normals is that on many occasions, the GRB is not in the field-of-view of the SDs associated with the least brightly lit of the four LADs. These problems are unavoidable however, since triggering is based entirely on LAD observations.

The SDs return two additional data types useful for GRB studies. Spectroscopy Discriminator (SDISC) data provides extremely low ($\sim 5-10$ keV depending on gain) and extremely high (>50 MeV) energy information in four channels. SDISC data is accumulated on a 64 ms time scale in burst mode and in 2 s intervals otherwise. Spectroscopy Time Tagged Event (STTE) data is analogous to the TTE data from the LADs. STTE data have a time resolution of 128 μs, use 256 energy channels, and are recorded for SDs whose associated LADs exceeded the trigger threshold. Events are recorded until a total of 65,536 counts have been stored or the burst mode ends. Like TTE data, STTE data can provide some pre-trigger information.

II.D The Spectroscopy Detector Calibration

Shortly after GRB data became available from the SDs, it was realized that the channel-to-energy calibration was inadequate. Background lines of known energy appeared at different energies in different detectors and shifted in time within the same detector when the gain changed. In addition, an alarming artifact appeared at the low end of spectra. This artifact (the Spectroscopy detector Low Energy Distortion, or SLED) is caused by a noise pulse generated in the detector electronics which alters the apparent energy-loss by a photon in the NaI(Tl) crystal. Figure II.2 shows the effect of the SLED. The dramatic gap just above 100 keV should be a continuation of

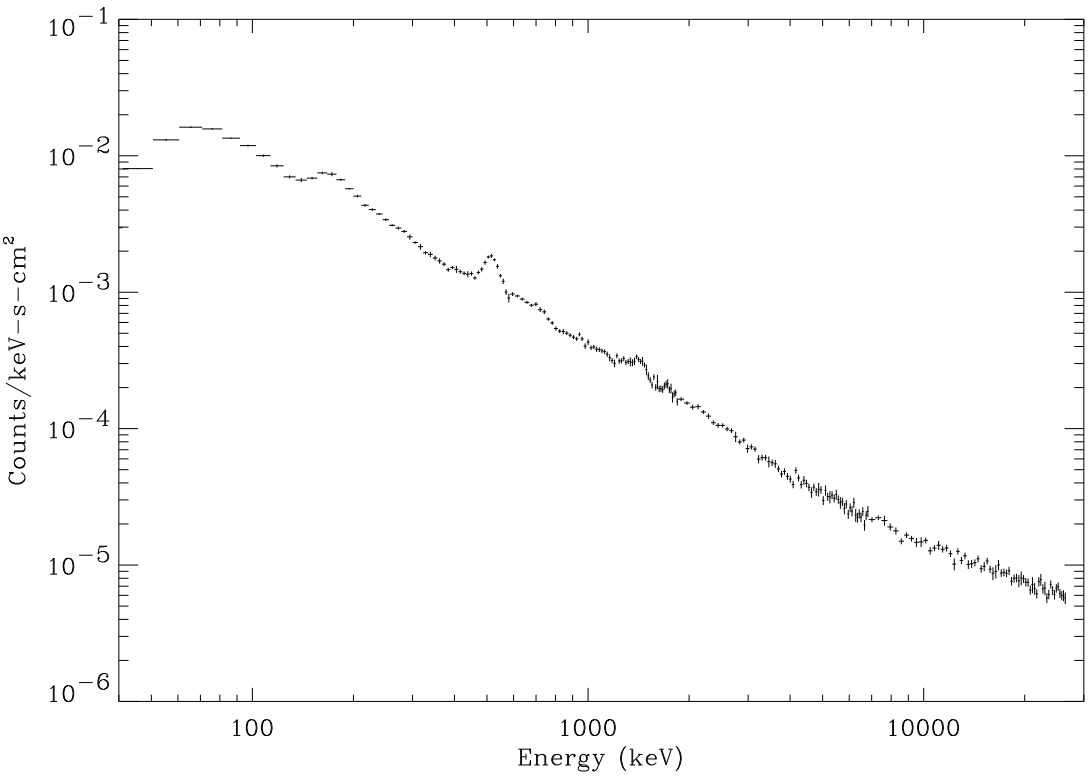

Figure II.2: A typical background spectrum with the SLED. The severe dip above 100 keV should be a continuation of the power law observed between 200 and 300 keV. The rollover below 70 keV is the LLD cutoff. The large emission feature at 511 keV is caused by gamma-rays from electron-positron annihilation, mainly from the Earth's atmosphere.

the power law seen at higher energies. For detectors which are used to make detailed spectral observations, these flaws are serious problems which must be remedied before definitive spectral analysis can be performed. Fortunately, a better calibration of the energy-loss spectrum can alleviate the problem.

II.D.1 The Detector Model

The initial calibration was empirical and based on a calibration for the LADs (Lestrade 1991). To make substantial improvements, a physical model of the photon

energy-loss to channel assignment process which allows a quantitative understanding of the detector is the best way to proceed. Such a method has been developed (Band *et al.* 1992a) which I was able to successfully implement.

The detector model traces an event from the energy lost by a gamma-ray in the NaI(Tl) crystal to the assignment of the event to an energy-loss channel (see Figure II.3 for a schematic diagram of the SDs). The model is not an attempt to describe the entire detection process but merely determines the amount of energy left in the crystal by an incident gamma-ray. In other words, the detection process is broken into two parts, calibration and detector response. The latter includes efficiency factors, incomplete absorption of gamma-rays, photon scattering outside the crystal, *etc.*, which are not considered here (see Pendleton *et al.* 1995 for a discussion of the BATSE response function). When a gamma-ray passes through the NaI(Tl) crystal, energetic electrons are produced via photoionization, Compton scattering, and pair production. These electrons excite other electrons in the crystal into the conduction band. When the the secondary electrons settle back to the valence band, optical scintillations are produced. The energy of the light emitted is nearly a linear function of the energy lost in the crystal but there are variations of order 15% so the relation between the energy lost by the photon and light emitted by the crystal is represented as

$$L = g_c(E)E, \tag{II.1}$$

where L is the light emitted by the crystal, E is the energy lost by the photon in the crystal, and $g_c(E)$ contains the nonlinearities of the crystal response. The light is converted to a charge by the PMT and then to a voltage pulse by a preamp. The PMT and preamp are assumed to be operated in their linear regimes so the height of the voltage pulse out of the preamp is

$$V_P = Gg_c(E)E, \tag{II.2}$$

where G is a function of detector gain. The detector gain is proportional to the voltage applied to the PMT. If the voltage is high, then the PMT is more sensitive to less

intense optical signals and therefore, lower energy events. Conversely, at low voltage, more scintillations are required to produce appreciable charge from the PMT. The fact that gain is proportional to voltage is why high gain settings return low energy spectra and *vice versa*, a somewhat confusing convention.

The voltage pulse out of the preamp travels down two paths. The first path leads to a set of four discriminators, one of which is a Low-Level Discriminator (LLD), and the second path goes to the pulse height analyzer (a monolithic charge-to-time converter or MQT) via a delay line (Figure II.3). The LLD is used to select events which have a higher voltage than a threshold value which keeps pulses caused by very low energy events from saturating the MQT. If a voltage pulse is large enough to trigger the LLD, the MQT gate is opened and the pulse arriving via the delay line is analyzed.

If the electronics operated ideally, then the voltage into the MQT would be V_P plus a constant pedestal voltage V_a which ensures the electronics operate linearly when V_P is small. Unfortunately, when the LLD triggers, a noise pulse is generated which travels along the delay line path and can be included in the signal voltage. This noise would not be a problem if the amount of noise added to the signal was the same for all V_P which would be the case if the LLD triggered at the same time for every pulse. However, the LLD triggers at the time when the integrated value of V_P exceeds the threshold. For large pulses, this is at the beginning of the pulse while for pulses near threshold, the LLD fires later in the pulse (Figure II.4). In the former case, the entire noise pulse enters the MQT whereas in the latter, the MQT gate closes before the noise pulse arrives. In between, a varying amount of noise is added to the signal because the noise pulse is part in, part out of the gate. When dealing with spectra, the quantity of interest is the number of counts per unit energy which depends on the energy width of the bin. In the regions where the noise pulse is either entirely included or excluded from the signal, the noise pulse does not affect the width of the bin. In the regions of partial inclusion, the energy bins are narrower than expected because the voltage into the MQT is not simply proportional to V_P.

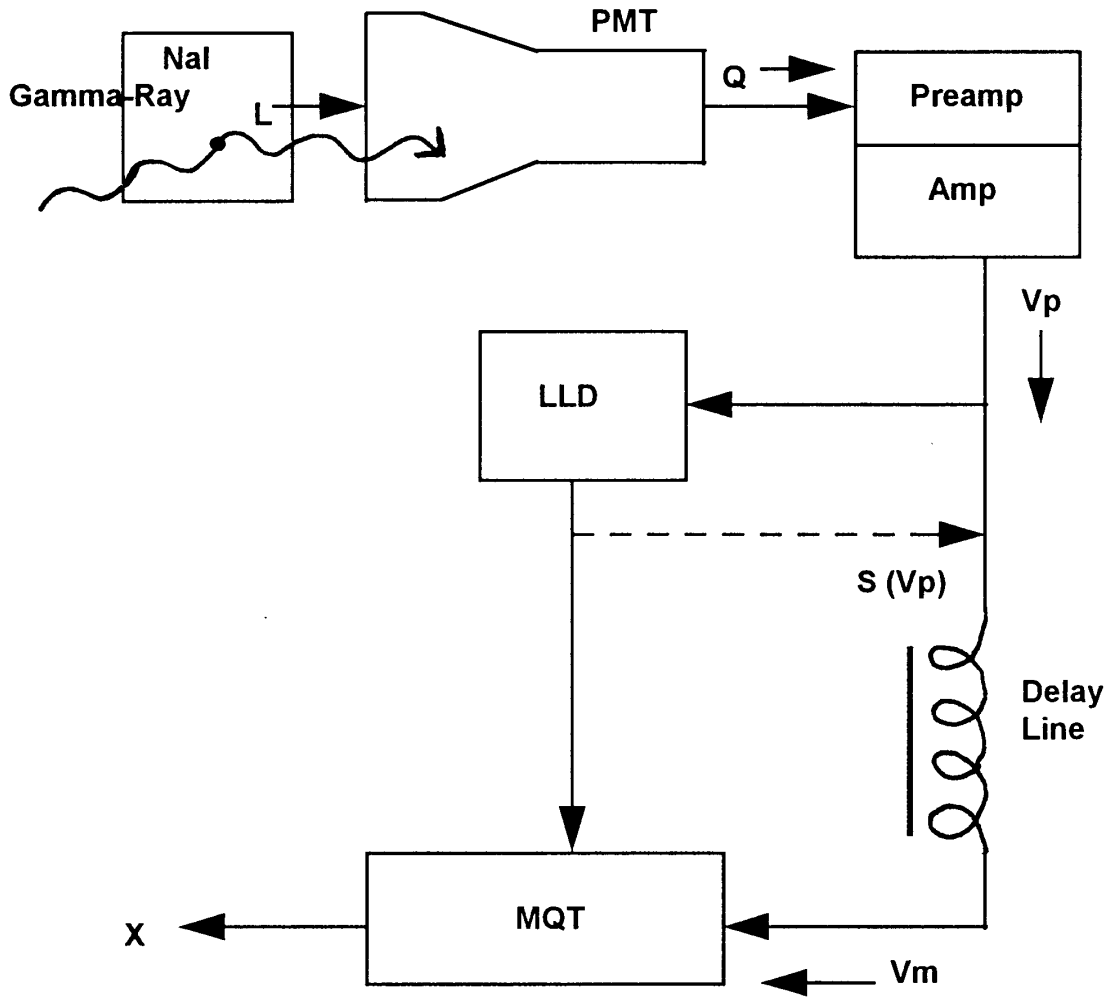

Figure II.3: A schematic diagram of the SD electronics. Gamma-rays lose energy in the NaI(Tl) crystal which produce optical scintillations. These scintillations are converted to a charge by the PMT and then to a voltage pulse by a preamp. If the pulse is strong enough to trigger the LLD, the event is assigned to a channel by the MQT.

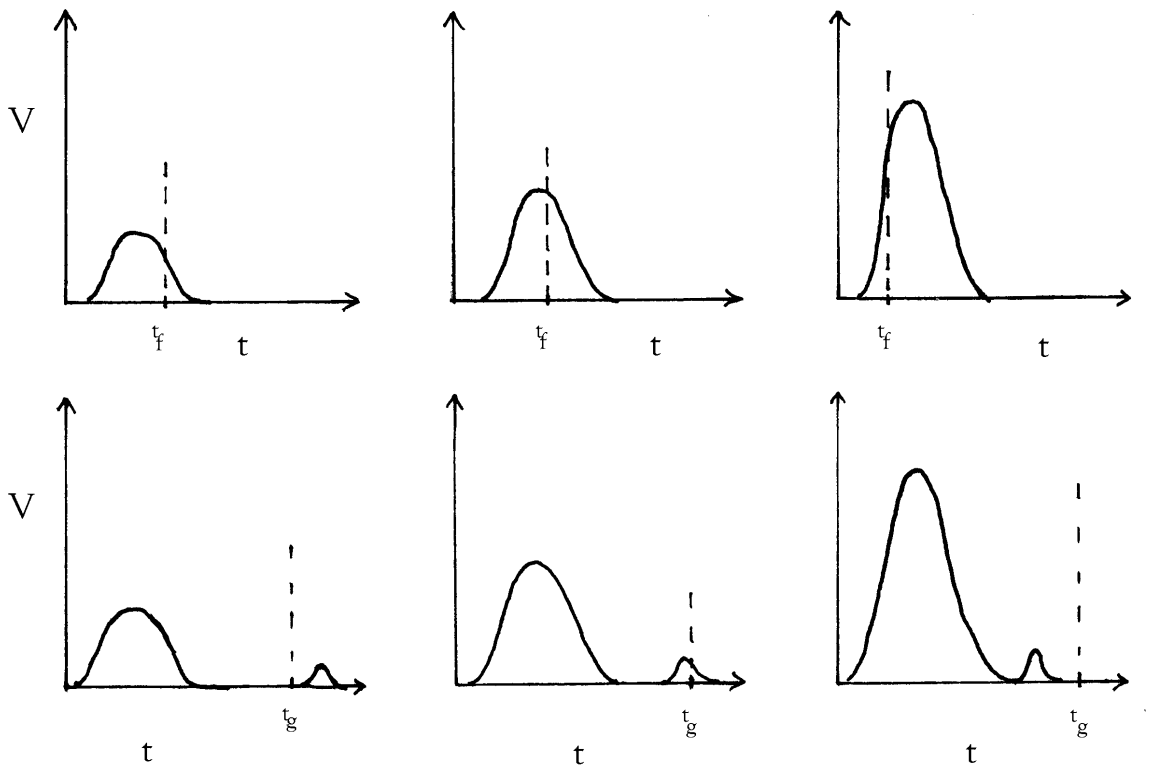

Figure II.4: A graphic explanation of the SLED. In this figure, the top row indicates the point at which the LLD fires during a voltage pulse (t_f). This sends a noise pulse to the MQT which can be included in the signal pulse into the MQT if the gate is open when the pulse arrives (bottom row, the gate closes at time t_g). The left column is for an event which is just above the LLD threshold (MQT gate closes before noise arrives), the right column for an event well above threshold (noise pulse entirely included in signal), and the middle column for an event in between (noise pulse partially included in signal).

Therefore, in the transition region, the number of counts per bin is underestimated because the signal is being divided by bins which are too wide which causes the dip in Figure II.2. Including the noise pulse in equation II.2, the voltage into the MQT becomes

$$V_M = Gg_c(E)E + V_a + s(V_P), \tag{II.3}$$

where $s(V_P)$ is the SLED noise pulse.

The MQT converts this voltage to a channel number but since the quantity of interest is the energy lost in the crystal, it is more useful to consider the inverse relation, that is,

$$V_M = F(x) \tag{II.4}$$

where x is the channel number. While the MQT was designed to be linear, tests with a sliding voltage pulser have shown that the count rate (which is proportional to dV_M/dx) increases with decreasing channel number in the lowest channels with apparently constant slope. This can be used to form an empirical derivative

$$\frac{dF(x)}{dx} = b - c(x - x_0)\Theta(x_0 - x), \tag{II.5}$$

where $\Theta(x - x_0)$ is the Heaviside function

$$\Theta(y) = \begin{cases} 0, & x - x_0 < 0; \\ 1, & x - x_0 \geq 0. \end{cases} \tag{II.6}$$

Equation II.5 can be integrated to give the MQT response,

$$F(x) = a + bx - \frac{c}{2}(x - x_0)^2\Theta(x_0 - x). \tag{II.7}$$

Before explicitly writing the energy-loss to channel relation, it is useful to note that equations II.3 and II.4 define a unique mapping between V_P and x for a given gain, LLD setting, and detector. Therefore, it is possible to restate the SLED correction as a function of channel number. Using this fact and solving equations II.3, II.4, and II.7 yields

$$Gg_c(E)E + V_a = a + bx - \frac{c}{2}(x - x_0)^2 + s'(x), \tag{II.8}$$

where $s'(x)$ is the SLED correction parameterized in channel space. Solving this equation for $g_c(E)E$ gives

$$g_c(E)E = \frac{a - v_a - s'(\infty)}{G} + \frac{bx + s'(\infty) - s'(x)}{G} - \frac{c(x - x_0)^2\Theta(x_0 - x)}{2G}, \qquad \text{(II.9)}$$

where the $s'(\infty)$ terms have been added to make the SLED correction a translation in the linear term in x below the SLED. The translation is

$$x' = x + \delta(x), \qquad \text{(II.10)}$$

where $\delta(x)$ is the change in channel number. Comparing equations II.9 and II.10, $\delta(x)$ is found to be

$$\delta(x) = \frac{s'(\infty) - s'(x)}{b}. \qquad \text{(II.11)}$$

The SLED is modeled as a function which adds to the channel number at the low end of the spectrum and leaves the upper end unchanged. Such a function is a step with rounded edges where the larger value is used for low channel number and nothing is added at the high end. Expressing this as an equation to show the free parameters gives

$$\delta(x) = s_d(H(x; s_b, s_c)), \qquad \text{(II.12)}$$

where $1/s_b$ is the width of the step, s_c is the center of the step, and s_d is the size of the step. The noise pulse is created by the firing of the LLD which should generate a pulse of constant amplitude regardless of LLD setting. Therefore, the parameter s_d should be independent of the location of the LLD. The center of the SLED and its width should vary linearly with LLD setting. This is because the signal voltages are self-similar (*i.e.,* change only in height, not shape) and since the SLED is essentially a timing effect, the width and center should be directly proportional to the size of the input pulse. Therefore, specifying the values of s_b, s_c, and s_d for at least two LLD settings will allow the SLED to be specified for any LLD setting.

To establish calibration parameters, equation II.9 is more useful when recast as

$$g_c(E)E = A(G) + B(G)x + C(G)(x - x_0)^2\Theta(x_0 - x) \qquad \text{(II.13)}$$

where $B(G)$ includes the SLED correction and all the coefficients are proportional to $1/G$. This relation is desirable for once a set of coefficients A, B, and C has been obtained for a given spectrum, it can be used as fiducial parameters to calibrate any other spectrum by a simple scaling,

$$A = \xi A_f, \quad B = \xi B_f, \quad C = \xi C_f,$$
$$\xi = \frac{E_l g_c(E_l)}{A_f + B_f x_l + C_f (x_l - x_0)^2 \Theta(x_0 - x_l)} \tag{II.14}$$

where E_l is the energy of a suitable calibration line and x_l is the location of the line in channel space. Once the parameters have been scaled, the energy for a channel can be found by inverting equation II.13. Therefore, in light of equations II.12 and II.14, the implementation of this model requires only one set of fiducial coefficients for each detector and SLED parameterizations for two LLD settings.

II.D.2 Implementation

The various terms in the calibration equation were determined using pre-flight calibration data and in-orbit background spectra. The crystal response was measured for energies below 100 keV with the synchrotron source at the Stanford Linear Accelerator and using radioactive sources for larger energies. The results are presented in Figure II.5, the solid line being a spline curve characterizing the general trend of the data. The curve is slowly varying everywhere except at the iodine K-edge (33.17 keV). To find the energy loss, equation II.13 requires an inversion of $g_c(E)E$ which will fail at the K-edge because $g_c(E)$ is not monotonic there. With this in mind, the spline which is used for $g_c(E)$ smooths the K-edge into a monotonic function and the difference is left for detector response models to handle. This situation is not ideal and some work remains to be done to eliminate all problems at the K-edge.

There is also an ambiguity in the form of the curve above about 1 MeV. There is a significant amount of scatter in the laboratory data, but it does seem to have an upward trend. Very little experimental work has been done with the properties of NaI at high energies but in one of the few works that does take NaI to MeV energies,

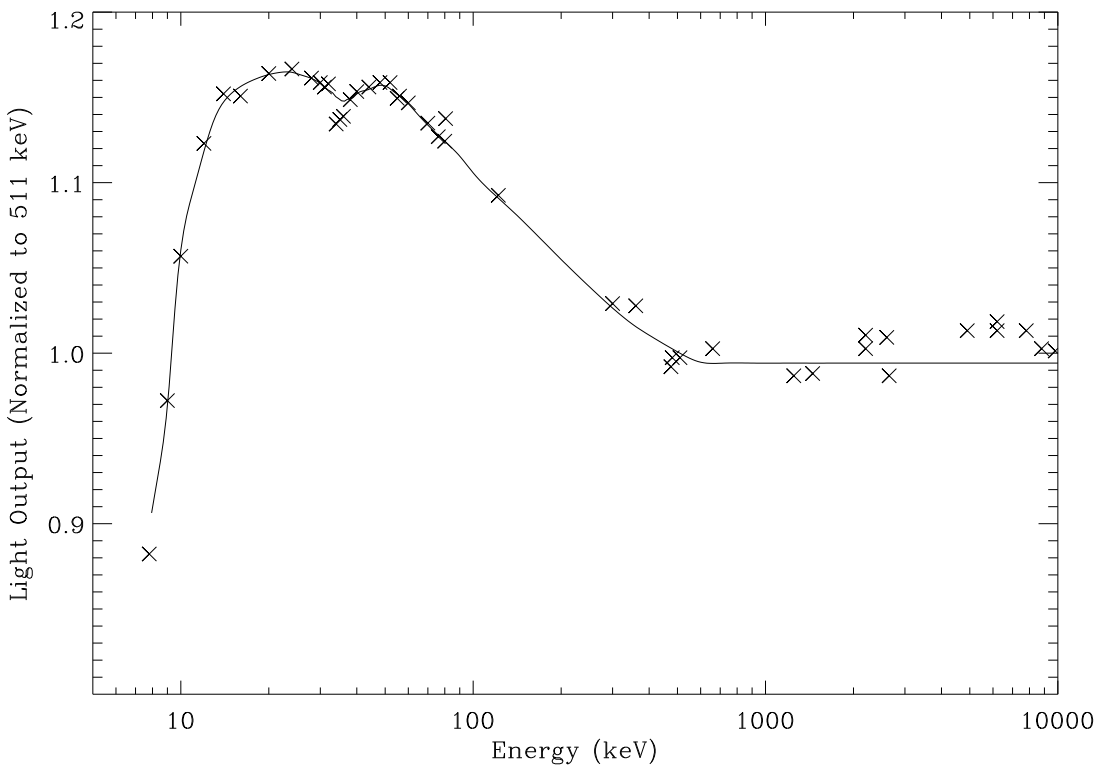

Figure II.5: The light output as a function of energy lost in the NaI(Tl) crystal by an incident photon. The crosses are measured data points and the solid curve is a spline characterizing the general trend.

an upward trend also appears but is not discussed (Zerby, Meyer, & Murray 1961). Theoretically, such an upturn can be explained by considering pair-production, since two electrons with energy $m_e c^2$ energy produce more light than a single electron with energy $2m_e c^2$ as produced by Compton scatter. A fit to the $g_c(E)$ data was performed using an analytic function which took into account Compton scattering and pair-production, giving a good description above about 300 keV. Unfortunately, when this function was used on pre-launch test data, the results were unsatisfactory with the data indicating a linear or slightly negative trend. Taking a conservative approach, a linear approximation was used for higher energies.

The linear MQT response coefficients (A_f and B_f) were determined from pre-flight calibration data (Lestrade 1991). This data set consists of spectra from radioactive sources taken at four different gains. While there is a wealth of information available, very high standards were set for data used in the sample which rendered much of the data unusable. These criteria were based on four concerns. First, we found that the gain drifted from the nominal value between spectra taken from different sources at supposedly the same gain so that only data from the same spectrum could be considered at the same gain. Second, to avoid problems associated with the way contamination of the peaks by Compton edges from other lines was handled, only strong lines were used. The third concern was inadequate knowledge of the crystal response (*i.e.,* $g_c(E)$) at high energies, which eliminated lines above 720 keV. Finally, lines which appeared below the upper end of the SLED were eliminated since a reasonable correction was unavailable. This left a short list (Table II.3) of data points to work with. To obtain significant results, the entire set for a given SD was combined while performing fits, introducing a relative gain correction parameter for each test which scaled the points to a common gain. Only the linear terms A_f and B_f were found using pre-flight data since there were not enough data to reliably determine the quadratic terms which appear only at low channel number.

The fit was performed in the following way. As can be seen from equation II.13, the light output from the crystal is a function of channel number. The

		SD0	SD1	SD2	SD3
Nuclide	Energy (keV)	Channel	Channel	Channel	Channel
^{212}Pb(Th)	239	64.9	65.9	52.3	59.2
^{214}Bi(Ra)	609	156.0	151.9	146.4	147.4
^{212}Pb(Th)	239	230.6	237.7	227.8	229.6
^{214}Bi(Ra)	609	571.0	575.6	573.4	569.0
^{212}Pb(Th)	239	249.3	251.2	244.5	246.0
^{214}Bi(Ra)	609	608.1	610.1	613.2	610.2
^{212}Pb(Th)	239	125.5	124.4	114.3	120.5
^{214}Bi(Ra)	609	299.1	294.8	291.6	290.2
^{133}Ba	81.0	47.6	48.3	34.1	43.1
^{133}Ba	303	156.0	152.1	143.4	148.7
^{133}Ba	356	181.6	181.8	172.1	178.6
^{133}Ba	30.8	39.5	41.3	26.3	35.4
^{133}Ba	81.0	93.4	95.4	82.7	90.6
^{133}Ba	303	314.0	310.7	304.8	312.8
^{133}Ba	356	373.0	370.9	366.6	372.2
		SD4	SD5	SD6	SD7
Nuclide	Energy (keV)	Channel	Channel	Channel	Channel
^{212}Pb(Th)	239	62.0	64.5	68.4	66.1
^{214}Bi(Ra)	609	152.0	152.2	158.6	159.9
^{212}Pb(Th)	239	222.2	229.4	228.9	231.2
^{214}Bi(Ra)	609	545.7	560.3	547.1	567.4
^{212}Pb(Th)	239	232.5	247.5	242.6	244.3
^{214}Bi(Ra)	609	581.8	604.9	584.4	600.0
^{212}Pb(Th)	239	124.1	122.8	127.1	123.1
^{214}Bi(Ra)	609	295.6	285.9	297.6	295.9
^{133}Ba	81.0	...	47.2	52.0	46.8
^{133}Ba	303	...	147.2	158.7	152.6
^{133}Ba	356	...	177.7	188.7	181.7
^{133}Ba	30.8	39.8	41.3	43.7	38.8
^{133}Ba	81.0	96.3	96.7	98.8	91.6
^{133}Ba	303	310.9	321.6	314.2	306.6
^{133}Ba	356	376.5	377.5	375.1	370.2

Table II.3: Pre-flight calibration data used to find the linear terms in the MQT response. The data were accumulated at different times, the horizontal rules in the table indicating data taken at different times. The data were taken from Lestrade (1991).

energies of the calibration lines were converted to light output (using the spline for $g_c(E)$ from Figure II.5) and the fits were of channel number, light output pairs. The parameters to be fit were the linear MQT response coefficients and the relative gains from each test. The fit was performed with a Levenberg-Marquardt χ^2 minimization algorithm (Bevington 1969, p. 237, Press *et al.* 1992 p. 675).

The quadratic terms in the response function (C_f and x_0) as well as the SLED parameters were found using data obtained during two periods when the SDs were cycled through a number of different gain settings while BATSE was in orbit. A hyperbolic tangent function was used to parameterize the SLED,

$$\delta = s_d \left[1 - \tanh\left(s_b(j - s_c)\right)\right], \tag{II.15}$$

where δ is the shift in channel number and j is the linear channel number. In this analysis, SHER spectra covering the second orbit after a passage through the South Atlantic Anomaly (SAA) were summed. The large charged particle flux in the SAA activates nuclear lines in the crystal. The two orbit wait minimized time dependent effects in the background by allowing time for the short-lived lines to die out. Aside from this activation, the spectral structure of the background integrated over one orbit was assumed to be constant during each gain cycling so that for a given energy range, spectral shapes should be similar.

To find the quadratic parameters, two measurements of the background at different gains (and hence energy range) were compared. If spectral shapes are identical, then the spectra taken at different gains should look the same in the energy region where they overlap. Since the calibration terms in question are only important for the lower channels regardless of gain, then the high gain (low energy coverage) calibrated spectrum should be essentially correct in its high channels. This region of the high gain spectrum specifies the flux in the low channels in a low gain spectrum (the ones which overlap the high gain spectrum). Thus, the task was to adjust the unknown parameters until the spectra being compared were consistent in the region of energy overlap.

Optimization of the calibration parameters was performed using a modified

version of the χ^2 minimization algorithm. This algorithm compares a set of data values to a modeling equation and finds the best values for the parameters of the function. In this case, one spectrum was fit to another by changing the coefficients of the calibration equation. The 'data' were the ratio of the counts/keV of a low gain spectrum to the same quantity in the high gain spectrum for each low gain energy bin. Since the bins for each spectrum were not centered on the same energy, a spline was used to interpolate the high gain bins to the center of the low gain. The values of the SLED and quadratic terms were assumed not to affect the ratio of the spectra at high energies so the 'model' value of the ratio was set to the average of the ratio in the highest 20 overlapping channels. If the spectra were identical, then this 'model' ratio would be unity. However, it was found that the background intensity varied slightly from day to day, which caused a slight offset (always less than 10%). The range of energies used was from the location of the LLD of the low gain spectrum to around 720 keV, the higher limit due to the uncertainty of the crystal response.

The fits were performed simultaneously for all suitable pairs within a gain cycling set. Since both spectra were allowed to change as the parameters were varied, the quadratic parameters had a tendency to wander off to large values of x_0 if the initial conditions were not correctly chosen. Analysis of the final values of the fitting ratios showed that excellent agreement between the fit and the 'true' ratio was obtained at the high end, but was very poor at the low end. To remedy this situation, spectra were weighted by the number of counts per energy interval (the numerator in the ratio defined as 'data' above), increasing the importance of the low end of the spectrum.

A more important difficulty concerned gain independent noise spikes. Before this recalibration, noise spikes which appeared in a particular channel regardless of gain setting had been observed in SDs 1, 4, and 5. Other, smaller noise problems were found in SDs 2, 3, and 7 during the recalibration process. The cause of this noise is thought to be improper restoration of the baseline voltage in the electronics after cosmic ray events in the crystal. For the calibration spectra, only a few channels

Detector	LLD (HEX)	A_f	B_f	C_f	x_0	s_b	s_c	s_d
0	24	−8.99	3.951	-3.85×10^{-4}	181.2	0.30	27.3	1.33
1	20	−20.32	4.111	-8.58×10^{-4}	167.8	0.34	31.5	0.82
2	20	45.00	3.848	0.0	0.0	0.23	10.4	1.86
3	1C	7.29	4.066	5.98×10^{-3}	43.7	0.46	18.3	0.73
3	24	7.29	4.066	5.98×10^{-3}	43.7	0.35	22.4	0.73
4	14	−6.43	4.054	-2.30×10^{-3}	127.3	0.42	25.3	0.59
4	24	−6.43	4.054	-2.30×10^{-3}	127.3	0.33	34.1	0.59
5	1C	−16.79	4.099	-3.37×10^{-3}	80.9	0.30	25.4	1.07
6	24	−27.28	4.005	-2.04×10^{-4}	167.2	0.38	32.0	0.9
7	2C	−6.58	3.840	5.00×10^{-3}	57.0	0.40	30.5	0.87
7	24	−6.58	3.840	5.00×10^{-3}	57.0	0.35	26.0	0.87

Table II.4: The best fit SD calibration parameters. The LLD column refers to the LLD setting of the SDs.

were affected by this channel-dependent noise. Therefore, the channels in question were masked out. This worked well for all detectors except SD 5, which had a broad ridge accompanying the spike and caused fits for that detector to be rather poor.

II.D.3 Results

The best fit calibration parameters are given in Table II.4 and a representative spectral pair is shown in Figure II.6. This figure shows the results of the recalibration are generally good though not perfect. While the new calibration provides spectra which are much more consistent between gains settings than the previous calibration, in several cases the SLED remains visible at a small level. Subsequent efforts to remove the SLED completely have failed and it appears the SLED may depend on temperature or gain, something which is presently unmodeled. Despite this deficiency, the calibration discussed here is the most successful to date for the SDs.

The results of the fits should look reasonable since the fitting scheme was designed to make each pair look similar. A more revealing test is to examine the effect of this calibration on some generic background spectra. This has been done for SHER spectra which accompanied several GRBs by fitting background lines for

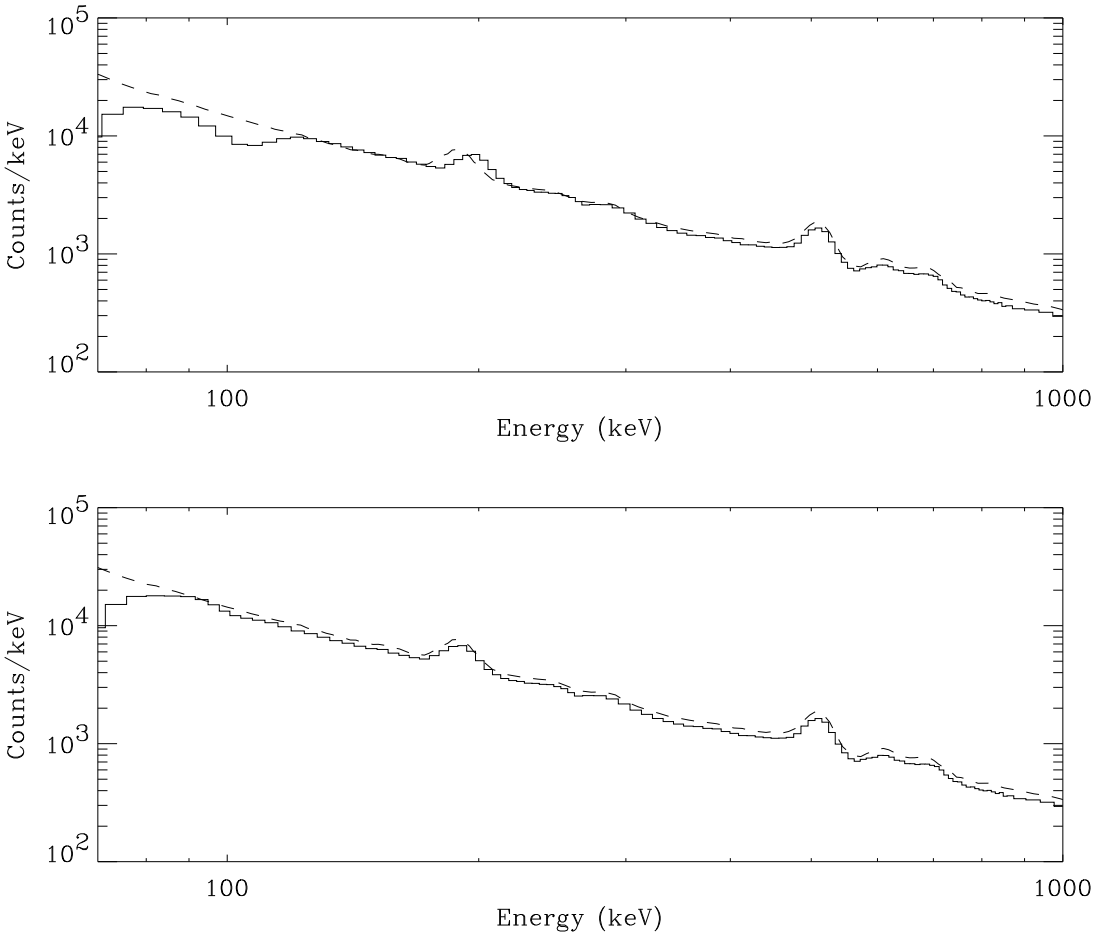

Figure II.6: A comparison of calibrated and uncalibrated background spectra for SD 0. The dashed histograms are the high gain spectrum which is assumed to be correct and the solid histogram is the spectrum being calibrated. The top frame shows spectra uncorrected for the MQT nonlinearity and SLED while the bottom frame shows fully corrected spectra. The rollover in the low gain spectrum below 80 keV is caused by the LLD cutoff.

detectors at various gains. A Gaussian profile was used to describe the lines and the centroids are given in Table II.5. These fits show that the calibration assigns the correct energy to background lines, ensuring consistency between detectors.

The energy-loss to channel number calibration outlined here is superior to the empirical method used for the SDs at launch. Most significantly it places background lines of known energy in the right places and makes spectra from different detectors consistent with each other. This stability in the calibration allows valuable inter-detector and inter-burst measurements which were not possible with the previous calibration scheme. These improvements succeeded because a physical model of the SDs was used to create a calibration algorithm. While the SLED could not be completely removed, this calibration does allow spectral studies to proceed without concerns about gross detector dependent effects.

Trunc. JD	Detector	67 keV	193 keV	511 keV
8437	2	···	193.1 ± 0.3	512.2 ± 0.8
8437	3	···	···	512.4 ± 1.0
8437	6	68.1 ± 0.3	191.3 ± 0.1	511.6 ± 0.6
8437	7	66.1 ± 0.5	188.5 ± 0.2	511.4 ± 0.7
8454	0	67.9 ± 0.1	191.5 ± 0.3	512.0 ± 0.5
8454	4	···	···	512.8 ± 1.0
8454	5	···	188.5 ± 0.2	512.5 ± 0.6
8454	6	68.5 ± 0.1	192.9 ± 0.2	512.1 ± 0.5
8477	0	67.3 ± 0.3	192.6 ± 0.3	511.4 ± 0.6
8477	1	70.0 ± 0.3	196.0 ± 0.5	511.3 ± 0.6
8477	2	···	197.3 ± 0.4	511.9 ± 0.7
8477	5	···	189.1 ± 0.4	512.0 ± 0.7
8554	0	67.3 ± 0.1	192.3 ± 0.3	510.9 ± 1.1
8554	3	66.1 ± 0.1	···	513.2 ± 1.1
8554	4	69.8 ± 0.1	193.7 ± 0.3	512.5 ± 1.1
8554	7	66.5 ± 0.1	192.2 ± 0.3	511.7 ± 1.0
8564	0	67.0 ± 0.1	192.2 ± 0.4	510.7 ± 1.1
8564	2	···	194.0 ± 0.4	512.0 ± 0.8
8564	3	66.2 ± 0.2	185.2 ± 0.5	512.7 ± 1.2
8564	6	69.0 ± 0.1	193.9 ± 0.2	512.5 ± 0.8
8566	0	67.3 ± 0.1	192.5 ± 0.7	512.0 ± 1.2
8566	3	66.7 ± 0.2	···	512.7 ± 1.3
8566	4	68.7 ± 0.1	193.5 ± 0.6	510.3 ± 1.9
8566	6	69.0 ± 0.2	194.0 ± 0.4	512.1 ± 0.8
8583	3	66.9 ± 0.2	198.0 ± 0.6	513.5 ± 1.2
8583	4	70.7 ± 0.2	190.1 ± 0.5	511.3 ± 0.7
8583	5	···	186.0 ± 0.7	512.9 ± 0.8
8583	7	66.9 ± 0.1	193.7 ± 0.8	511.7 ± 1.1
8587	1	69.4 ± 0.3	195.3 ± 0.2	511.7 ± 0.7
8587	3	66.9 ± 0.3	196.7 ± 0.4	513.3 ± 1.3
8587	5	···	188.6 ± 0.5	512.8 ± 0.8
8587	7	67.1 ± 0.1	196.2 ± 0.7	513.3 ± 1.1

Table II.5: Fits to background lines from SHER spectra from various days early in the BATSE mission. The 67 keV line is caused by gamma-ray emission during electron capture in I^{125} (Gruber *et al.* 1987). The 193 keV line is caused by a similar process in I^{123}.

Chapter III

Spectral Features

III.A Analysis Techniques

The existence of line-like absorption and emission features in GRB spectra is an extremely important and unresolved issue. As discussed below, early observations of these features were used to support the view that GRBs originated on highly magnetized ($B \sim 10^{12}$ G) neutron stars. While neutron stars remain a popular component of GRB models with or without spectral features, establishing the reality of these features is vital since they can provide important diagnostics of the GRB environment.

To appreciate the difficulty of establishing the existence of spectral features, it is important to understand the subtleties involved in the analysis of gamma-ray data. Gamma-ray detectors do not record the energy of an incident photon (Chapter II). Instead, they measure the amount of energy lost by the photon in the detector element (*e.g.,* a scintillating crystal) which is not necessarily equal to the energy of the incident photon. The incident energy itself can be different from the energy the photon had at the source since it can scatter off of structures in the neighborhood of the detector and the Earth's atmosphere. Furthermore, the entire energy lost in the NaI(Tl) crystal may not be recorded by the instrument. For example, if the incident gamma-ray knocks an iodine K-shell electron loose, the electron can escape the de-

tector which is an important loss mechanism. In short, a count in a given energy-loss bin could have come from a broad range of photon energies.

Spectral analysis involves fitting models to observed spectra. In this case, the detector has a significant effect on the observations and either the model must be folded through a model of the detector response or the incident spectrum must be directly deconvolved from detector processes. In either case, a complete model of the detector response is required. These models are generally constructed from Monte Carlo simulations of source photons with varying incidence angles and energies impinging on the detectors (Pendleton *et al.* 1995). The result for a given photon is the probability that it will end up in a certain energy-loss bin. Probability distributions for a typical BATSE response model are shown in Figure III.1, displaying the complex structure which makes spectral analysis difficult.

Once a detector model has been obtained, spectra can be analyzed by folding a model spectrum through the model response and comparing to the observed spectrum (a method known as 'forward folding deconvolution') or attempting to directly deconvolve the observed spectrum. Both methods have serious difficulties stemming from the fact that finding the incident spectrum is an ill-posed problem (Craig & Brown 1986). Because the detector acts to distort the spectrum, smoothing out fine structures, the solutions found through any deconvolution are not unique in the sense that a number of possible models can adequately describe the data. Incident photon spectra found using forward folding deconvolution are very model dependent and obliging in the sense that models tend to fit reasonably well even when the model itself is incorrect (Fenimore, Klebesadel, & Laros 1984), a consequence of the smoothing effect of detector processes. Direct deconvolution methods (c.f. Blissett & Cruise 1979; Loredo & Epstein 1989) require enormous computational resources and can either amplify or smooth narrow structures depending on whether one is attempting to reconstruct the broad spectral behavior or is looking for small scale structure. For reasons of practicality, the time-consuming direct deconvolution methods are rarely employed in spectral analysis.

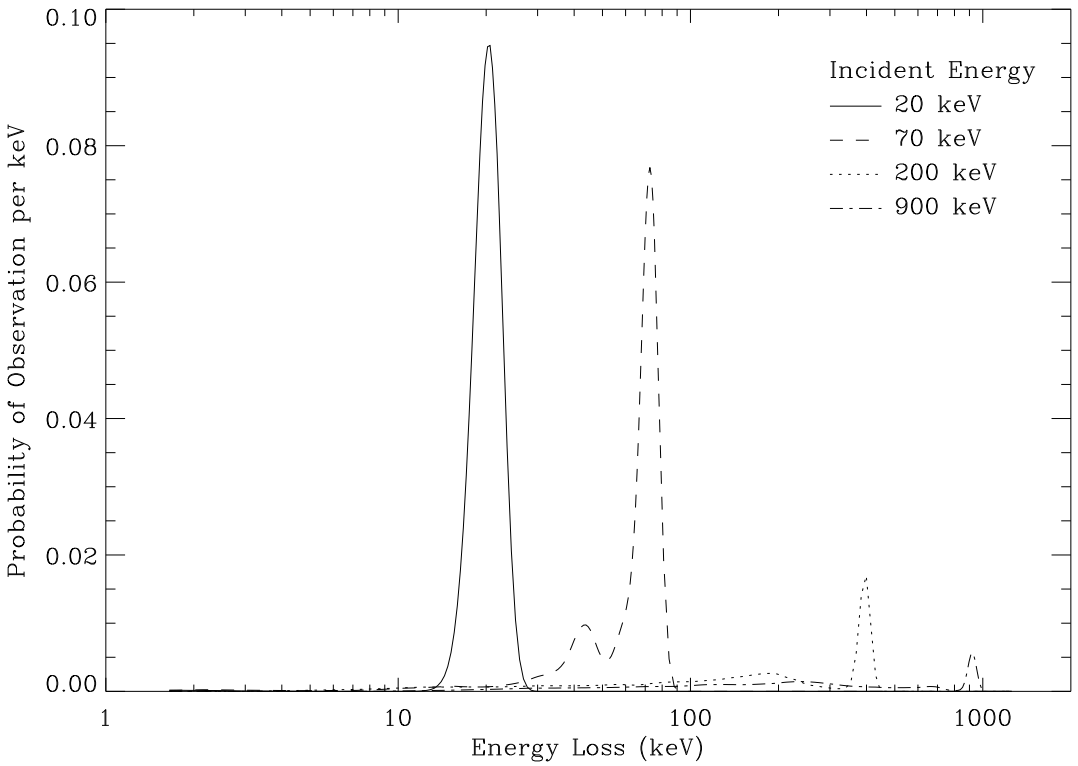

Figure III.1: Probability distributions for the BATSE SD energy-loss channel to which a photon of a given incident energy is assigned. These response curves model SD 6 during GRB 3B920227 which had an angle of 8° to the detector normal. The SDs are assumed identical, i.e., if two detectors were in identical gain states and had identical geometries with respect to the earth and burst, their response curves would be the same.

Regardless of how a photon spectrum is found, if a spectral feature is observed, it must be determined whether the feature is real or a statistical fluctuation. Traditionally, the statistical significance of a feature is found by comparing the χ^2 statistics for fitted models with and without the feature using the F-test (Martin 1971, p. 66). The results are quoted as the probability that the feature is a statistical fluctuation so that the smaller the number, the more likely the feature is real. It has recently been suggested that model comparison be carried out using a Bayesian formalism (Loredo 1990). The debate between these formalisms is mainly philosophical and since the Bayesian and traditional methods have not produced conflicting results, the debate is largely academic at this time.

III.B Pre-BATSE Observations

III.B.1 Absorption Features

Line-like features in GRB spectra were first reported in spectra observed by the KONUS experiment (Mazets *et al.* 1981). The continuum was assumed to be produced by bremsstrahlung from thermal electrons in a hot, optically thin plasma which produces a spectrum of the form

$$N_E(E)\left(\frac{\text{photons}}{\text{keV}-\text{cm}^2-\text{s}}\right) \propto E^{-1}\exp(-E/kT), \qquad \text{(III.1)}$$

where T is the temperature of the plasma (Rybicki & Lightman 1979, p. 162, note that the Gaunt factor is ignored). Deviations from the continuum at energies between $30-70$ keV were found to be quite common, occurring in roughly 20% of GRBs. These deviations were assumed to result from absorption of continuum radiation at the cyclotron frequency of electrons trapped in the cold outer region of the magnetosphere of a neutron star. However, these low energy deviations may in many cases be caused by a poor continuum model. Band *et al.* (1993) found GRB spectra tend to have a variety of spectral indices below 100 keV, most flatter than the -1 index of the bremsstrahlung model. Another difficulty with interpreting the KONUS results is

that a formal statistical analysis was not presented so it is impossible to judge the significance of these features.

The next experiment to detect absorption features was the *HEAO-1* A-4 experiment (Hueter 1987). Twenty one GRBs were observed and absorption features between $50 - 80$ keV found in two of them. An analysis to determine the reality of these features showed that the probability that the events were statistical fluctuations was 1% and 0.1% respectively. Even though the significance of these features is low (roughly 3σ), the lines were regarded as real based on the KONUS precedent. As with the KONUS results however, the lines may result from a poor continuum choice. Continuum models used in the *HEAO-1* analysis were a simple power law and a power law with an exponential, and use of a more flexible model such as equation I.6 may significantly change the significance of these results. In addition, the detector response model has been improved which will also affect the analysis. Therefore the *HEAO-1* results are not definitive though a reanalysis may show them to be significant.

The best documented and most significant absorption features observed to date are from *Ginga* observations (Murakami *et al.* 1988; Fenimore *et al.* 1988; Yoshida *et al.* 1991; Graziani *et al.* 1992). *Ginga* not only detected line-like absorption features, but because it could detect photons to much lower energies than either the KONUS or *HEAO-1* A-4 detectors, found harmonically spaced pairs of absorption lines in three bursts. The lower energy lines fell in the $20 - 25$ keV range while the higher energy features were found at twice the energy of the lower line. Rigorous statistical analysis was performed using a wide range of continuum shapes and two of these candidates proved too weak to be definitive detections (GRBs 870303 with $E_1 = 21.4 \pm 0.7$ keV and $E_2 = 2E_1$ and 890929 with $E_1 = 26.3 \pm 1.5$ keV and $E_2 = 46.6 \pm 1.7$ keV) though GRB 870303 did show a significant single line at 21.1 ± 1.0 keV (probability of statistical fluctuation 1.2×10^{-5}, Graziani *et al.* 1992) in a time segment different from the less significant pair of lines. The third burst (GRB 880205) proved very significant, the probability that the lines observed at 19.7 ± 0.7 and 38.0 ± 1.6 keV were statistical fluctuations was 6×10^{-5} (Fenimore *et al.* 1988).

A concern involving these observations is that the directions to the GRBs were not known so the direction-dependant model of the detector response could be in error. However, analysis of the most significant detection (GRB 880205) showed that the results were not dependent on the incident angle (Fenimore *et al.* 1988). The single, apparently significant line in GRB 870303 is somewhat problematic because the final fit was improbably good which might indicate a systematic problem with the data. Detailed studies have not found other irregularites with the data which would indicate an instrumental effect (Graziani *et al.* 1992) but a consensus on the reality of this feature has yet to be formed. On the other hand, the lines in GRB 880205 cannot be dismissed easily. Thus, excellent evidence exists that at least some GRBs have spectral features.

III.B.2 Emission Features

Emission features in GRBs have been reported in spectra recorded by *ISEE-3* (Teegarden & Cline 1980), KONUS (Mazets *et al.* 1981), SIGNE (Barat *et al.* 1984), and *HEAO-1* (Hueter 1987). These features lie in the $400 - 500$ keV range and have been interpreted as radiation from electron-positron annihilation deep in the potential well of a neutron star. Statistical evidence for the reality of these lines is much weaker than for absorption lines. The line seen by *ISEE-3* had a 6.7% chance of being a statistical fluctuation, *HEAO-1*'s most significant feature had a 15% chance of being a fluctuation, and SIGNE's line had a 0.1% probability of being a chance event. KONUS did not report a statistical analysis. Since definite detections are typically claimed at the 3σ level (*i.e.,* there is a 0.3% probability that the feature is a chance occurrence), only the SIGNE result can be considered a positive result and it is marginal. Therefore, the existence of emission lines in pre-BATSE GRB spectra is questionable.

III.C Physical Interpretations

The common interpretation of absorption features has involved a layer of cool electrons trapped in a magnetic field of order 10^{12} G. The electrons must be cool because the absorption features are narrow indicating little thermal broadening. The most complete model of line formation was developed by Wang *et al.* (1989) who assumed the first harmonic absorption feature in GRB 880205 was caused by cyclotron resonant scattering and the second harmonic a product of Raman scattering. In this model, gamma-rays generated near the surface of a neutron star pass through the strong magnetic field of the neutron star which has trapped electrons. In magnetic fields of order 10^{12} G, the orbits of electrons perpendicular to the magnetic field lines are quantized and the electron cyclotron energy is

$$E_n = \frac{nh}{2\pi}\left(\frac{eB}{mc}\right) = 11.6\ nB_{12}\ \text{keV}, \tag{III.2}$$

where h is Planck's constant, c is the speed of light, B is the magnetic field strength, B_{12} is the magnetic field strength in units of 10^{12} G, n is the quantization level, and e and m are the charge and mass of the electron respectively (Mészáros 1992, p. 31). These quantization states are known as Landau levels with Landau level 0 referring to the fundamental. In the theory, the line at 19.7 keV is produced by resonant scattering in which electrons undergo radiative $0 \rightarrow 1 \rightarrow 0$ Landau transitions caused by photons of energy E_0 (the energy of the fundamental is the same as the energy separation between levels). The 38.0 keV line is produced by Raman scattering in which the electrons undergo $0 \rightarrow 2 \rightarrow 1 \rightarrow 0$ Landau transitions initiated by photons of energy $2E_0$.

The temperature of the scattering layer was found by assuming that there was no net energy input into the region from the incident flux, that is, all energy absorbed by the electrons was radiated away. This requirement along with the width of the line fixed the temperature of the electrons to be 5.3 keV by self consistency. The magnetic field in the scattering layer was determined to be $B = (1.71 \pm 0.07) \times 10^{12}$ G and the column depth of electrons was $N_e = (1.2 \pm 0.6) \times 10^{21}$ cm^{-2}. These results

were consistent with the widely held belief that GRBs arose from nearby neutron stars since the larger energy flux through the scattering region implied by distances greater that ~ 1 kpc would destroy the absorbing layer by radiation pressure. When the BATSE observation of isotropy was announced and no features were found in BATSE spectra, work on modeling absorption features as cyclotron lines virtually ceased.

In the wake of the BATSE results, a great deal of effort has gone into creating cosmological models of GRBs. These sources tend to be extremely energetic and are not consistent with the cyclotron resonant scattering model of absorption feature formation because the scattering layer would not survive the event. While most cosmological models do not incorporate the possibility of absorption features yet, two attempts have been made to explain lines in cosmological scenarios. Mészáros & Rees (1993) speculate that Lyman α lines from H I (10.2 eV) and He I (21.2 eV) Doppler boosted to a Lorentz factor of ~ 1000 in their blast wave model could produce absorption features at 10's of keV. Stanek, Paczyński, & Goodman (1993) propose a scheme in which any source of cosmological GRBs can appear to have lines. The idea is that if there are a significant number of objects with mass $\sim 10^{17} - 10^{20}$ g in the universe (perhaps accounting for the dark matter), gravitational lensing could introduce a complicated interference pattern resembling absorption or emission lines.

Although evidence for the existence of emission lines is questionable, at least one attempt has been made to derive information about neutron stars from GRB emission line observations. Liang (1986) examined low significance emission lines from KONUS and found they tended to cluster around a neutron star gravitational redshift of $0.25 - 0.35$ for the 511 keV lines, similar to redshifts observed for the Crab pulsar (Leventhal, MacCallum, & Watts 1977) and X-ray burster X1636-536 (Fujimoto 1985). Combining the neutron star radius upper limits implied by these redshifts with mass data from pulsars, a preference for soft equations of state for nuclear matter was found. While this analysis was based on data of poor quality, it does illustrate what can be learned from emission lines should they be seen.

III.D BATSE Observations

III.D.1 The Search

Unambiguously real spectral features have not been detected in the BATSE data in spite of great efforts to find them. Many candidates do exist but since the number of trials in the BATSE data is ~ 3000 (Band *et al.* 1996), a high statistical significance is required to ensure any observed candidate features are not statistical fluctuations. For BATSE to declare a positive detection, a feature must have an F-test probability of less than 10^{-4} of being a statistical fluctuation and all BATSE detectors which could have seen the feature must have spectra which are consistent with each other. Detectors are said to be consistent if the observed spectra in all detectors can be explained with a single incident spectrum. For example, if a significant feature appears in one detector and is evident in another (though not necessarily significant), the detectors are consistent. While the F-test threshold may appear to allow a significant likelihood for a false positive, consistency between detectors is a powerful constraint.

To date, the most complete search for spectral features has been a visual search of 192 bright BATSE GRBs (Palmer *et al.* 1994; Band *et al.* 1996). SHERB spectra were combined to form a spectrum of the entire burst and a series of spectra accumulated on the same time scale as the third-rank detector (Chapter II). This was done to allow comparisons between detectors but does not probe the smallest available time scales. A background interpolated from SHER data taken before and after the burst was subtracted from these spectra and the data rebinned to approximately half the full-width, half-maximum energy resolution of the SDs. Rebinning spectra in this way reduces statistical uncertainty in the data points without compromising sensitivity to line features. The visual effect of rebinning data is graphically demonstrated in Figure III.2. The sensitivity of the eye to line features has been tested with simulated data which showed that features at 20 and 40 keV became obvious when their F-test probabilities were less than 10^{-2}. Simulations also show any statistical

analysis is independent of the binning of data as long as the rebinning results in energy bins which are smaller than the energy resolution of the SDs. This is expected since the energy resolution, not the number of channels, defines the sensitivity of the detector. Therefore, lines should not be missed based on the way spectra are binned in energy.

When a candidate feature was found, the number of SHERB spectra combined was varied to maximize the significance of the feature. This was done because the feature could be marginal in many individual SHERB spectra but stand out in a summed spectrum through improvement in the signal-to-noise ratio. If the F-test probability exceeded the threshold, then consistency between detectors was checked. To date, no candidate has passed both tests but if one does in the future and there is no clear evidence of a systematic problem with the data, then the candidate will be declared a real line.

The apparent lack of lines in the BATSE could be caused by a number of factors. The most obvious is that the SDs simply lack the sensitivity to see lines similar to those observed by past detectors. This is not expected to be the case for several reasons. First, background lines are quite clear in BATSE SHER spectra with the expected energy resolution. Simulations of *Ginga*-like bursts show lines would appear clearly in the BATSE data if they were there (Palmer *et al.* 1993; Band *et al.* 1995). Finally, BATSE sees the cyclotron absorption feature in the spectrum of Her X-1 (Freeman *et al.* 1996), a system in which a highly magnetized neutron star is accreting material from a main sequence companion star. These facts prove that the SDs are sensitive enough to see lines similar to those reported by *Ginga* in GRBs.

III.D.2 Complications

Despite the large number of spectra searched thus far, it is possible that lines exist in the data which were not discovered with the search technique described above for a number of reasons. Therefore, concurrent with the search described above, I searched spectra from several strong GRBs in a comprehensive fashion. For

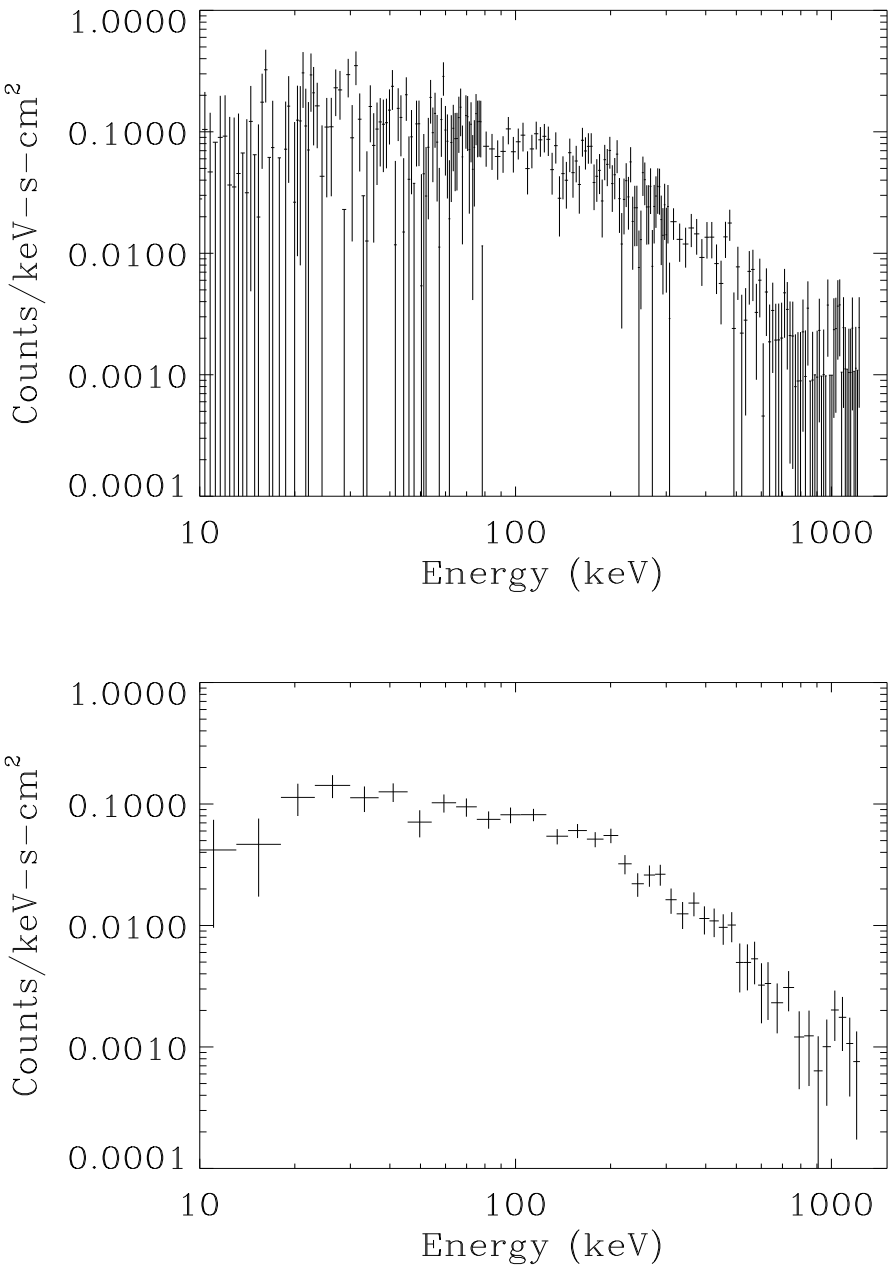

Figure III.2: An example of the effect of rebinning on SHERB spectra. The spectrum is a taken from GRB 3B920311 and has had the background removed. The top frame shows the spectrum with the 256 channel spacecraft binning while the bottom frame is the same spectrum rebinned to roughly the full-width at half-maximum energy resolution of the SDs.

these bursts, individual SHERB spectra were searched, then all contiguous pairs, triplets, quadruplets, and so on until 10−12 individual SHERB spectra were combined providing opportunities to discover lines which may only appear significant on time scales much shorter or longer than the time scale on which the previous search was conducted. This exhaustive search revealed one of the most significant line candidates in the BATSE data (Ford *et al.* 1994). This candidate was missed by the global search since many SHERB spectra had to be combined before the feature became visually obvious.

Another complicating factor when dealing with the reality of spectral features is the energy range for which data is available and the exact form of the continuum. The energy range affects the ability to find spectral features in two ways. First, the SLED occupies several channels near the low energy cut-off. Many times, the SLED (see Chapter II) lies at or near 20 kev, an interesting energy because of the *Ginga* detections. Even if the SLED does not affect a line directly, it can lead to difficulties during the fitting process since it cripples low energy observations when pinning down the continuum below the line is critical to establishing the correct overall continuum. Without knowledge of the low energy continuum, it is impossible to determine whether low energy deficits are narrow features or just a change in the continuum.

The form used for the continuum is vital to the fitting procedure. If a poorly chosen continuum model is used, lines will be assigned a much higher significance than they really have since inclusion of the line can compensate for a poor continuum fit. A correct continuum is also important for modeling high energy emission. Although higher energies would appear to have little to do with a fit at low energies, photons can lose significant energy when scattering off the spacecraft or the Earth and fill in the line. If too little high energy flux is included, the line can have reduced significance. If too much, the significance of the line will be overestimated.

Detector	Viewing Angle
LAD3	28.8°
LAD7	42.8°
SD3	43.7°
SD7	56.2°
SD2	73.7°

Table III.1: The detector viewing angles to GRB 3B930506. The angle measured between the detector normal and the direction to the source.

III.D.3 GRB 3B930506

An excellent example of all the pitfalls involved in candidate analysis is the 55 keV feature which I found in GRB 3B930506 (Ford *et al.* 1994). This feature was missed by the global visual search but found when I performed a comprehensive visual search. Five BATSE detectors (three SDs and two LADs) had favorable viewing angles (Table III.1) but only SD2 saw a clear absorption feature. Of the others, SD3 was in a gain state with a low energy cutoff of around 200 keV and the rest had channel-to-energy conversion uncertainties.

A time history of the burst as seen by SD2 is given in Figure III.3 and the count spectrum in which the feature is strongest is in Figure III.4, showing a clear feature at about 55 keV. Initially, only the $30 - 100$ keV energy range was used in the fits and the continuum model used was a power law,

$$N_E(E)\left(\frac{\text{photons}}{\text{keV} - \text{s} - \text{cm}^2}\right) = A\left(\frac{E}{100\text{ keV}}\right)^{\alpha}, \tag{III.3}$$

where A and α were fitted parameters. A model which allowed continuum curvature was tried but no curvature was required. The continuum-plus-line model included a multiplicative absorption feature,

$$N_E(E) = A\left(\frac{E}{100\text{ keV}}\right)^{\alpha}\exp\left[-\tau\exp\left(-\frac{(E-E_0)^2}{\Delta E^2}\right)\right], \tag{III.4}$$

where A, α, τ, E_0, and ΔE were fit. The best fit line parameters were $\tau = 60$ (τ was constrained to be ≤ 60), $E_0 = 55.8 \pm 1.4$ keV, and $\Delta E = 0.94^{+2.45}_{-0.29}$ keV. The equivalent width of the feature was 4 keV, much less than the detector resolution at

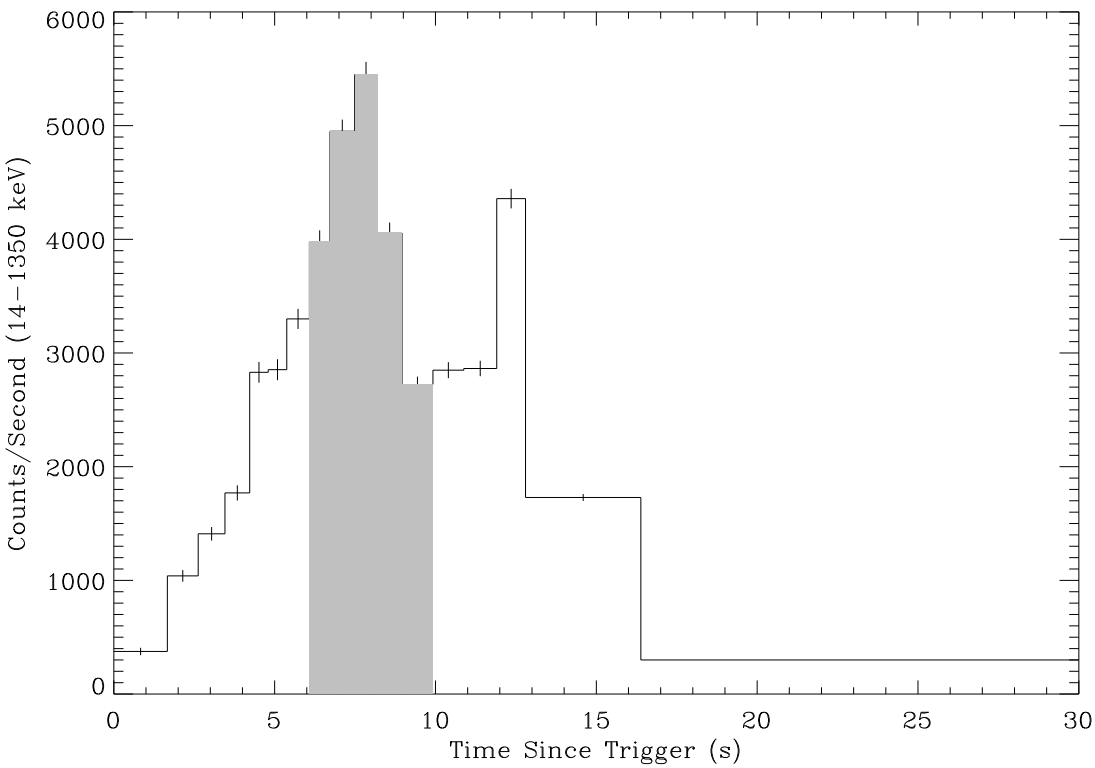

Figure III.3: A time history of GRB 3B930506 as seen by SD2. The period during which the candidate line feature is most prominent is shaded.

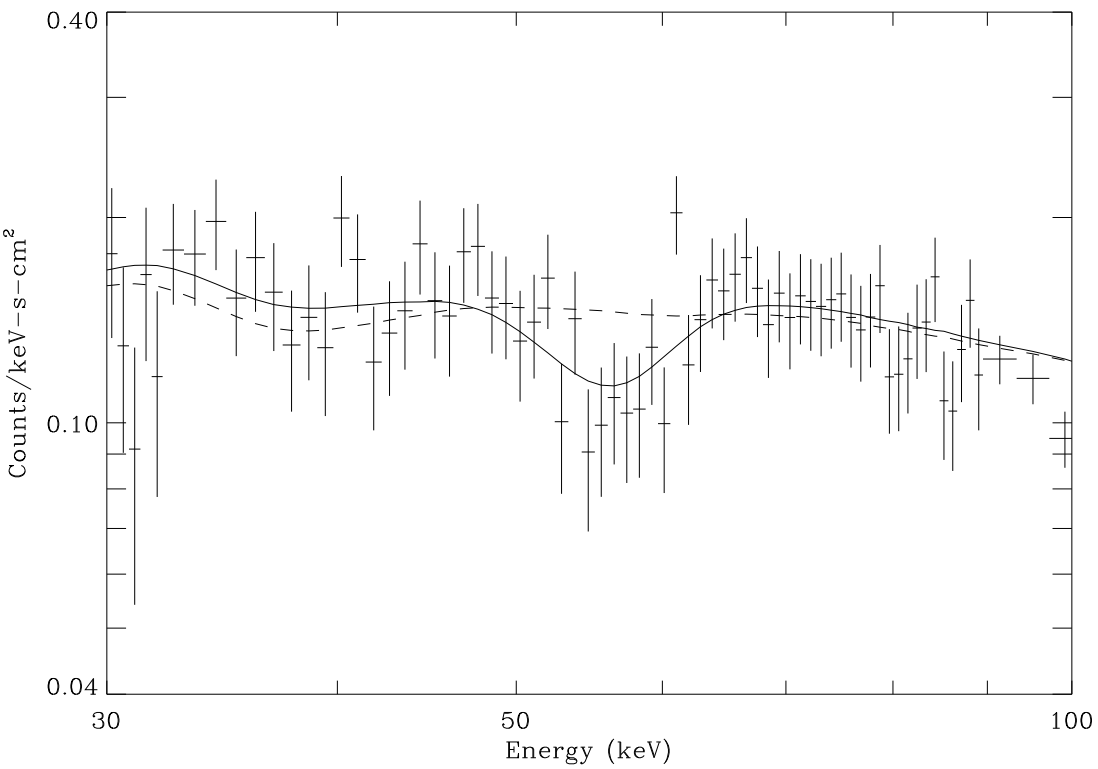

Figure III.4: A count spectrum from SD2 of GRB 3B930506 in which the line candidate is most significant ($6.08 - 9.92$ s after the trigger). The solid curve is a fit to the data which includes a Gaussian line while the dashed curve is a continuum-only fit.

this energy (about 11 keV). A Voigt profile (a line profile which arises from thermal processes and quantum uncertainty) was also tried but the fit went to the Gaussian limit.

The fitted count spectrum appears in Figure III.4. Since the best fit line is black (*i.e.,* has no flux at the centroid energy of the line) and the width is much less than the detector resolution, the true profile of the line cannot be determined and the fitted profile degenerates to a nearly rectangular form. Therefore, a fit of centroid and equivalent width is all that is required and only two additional parameters are added by the line. For two additional parameters, the probability that the line is a statistical fluctuation is 3.8×10^{-5}. The F-test for three additional parameters gives a significance of 1.5×10^{-4}.

At the time of discovery, checking consistency between detectors was problematic. The only other SD which could have detected the line (SD7) had a SLED which was centered at 50 keV which would obscure the line at 56 keV and the LADs had unresolved channel-to-energy calibration issues. Taken at face value, the candidate would have to be accepted as real since the detectors could not be proven inconsistent. Fortunately, additional work on SD7's SLED correction and the LADs allowed a judgement to be made based on firmer information.

The revised *ad hoc* SLED correction for SD7 was made using the same algorithm discussed in Chapter II. In place of gain-cycled spectra, the background from $40-60$ kev was assumed to a power law continuation of the background observed by SD7 between $60-65$ keV. The assumption was based on the fact that the SD background has been featureless in this energy range throughout the mission. For the revised calibration, the quadratic terms in the MQT response were held constant while the three SLED parameters were allowed to vary. Figure III.5 shows the background before and after the revised SLED correction. The SLED has been almost entirely removed with only a slight ripple remaining. Considering the strength of the feature in SD2 and the fact that SD7 had a better viewing angle, the line should be clearly visible in the corrected SD7 spectra as can be shown quantitatively.

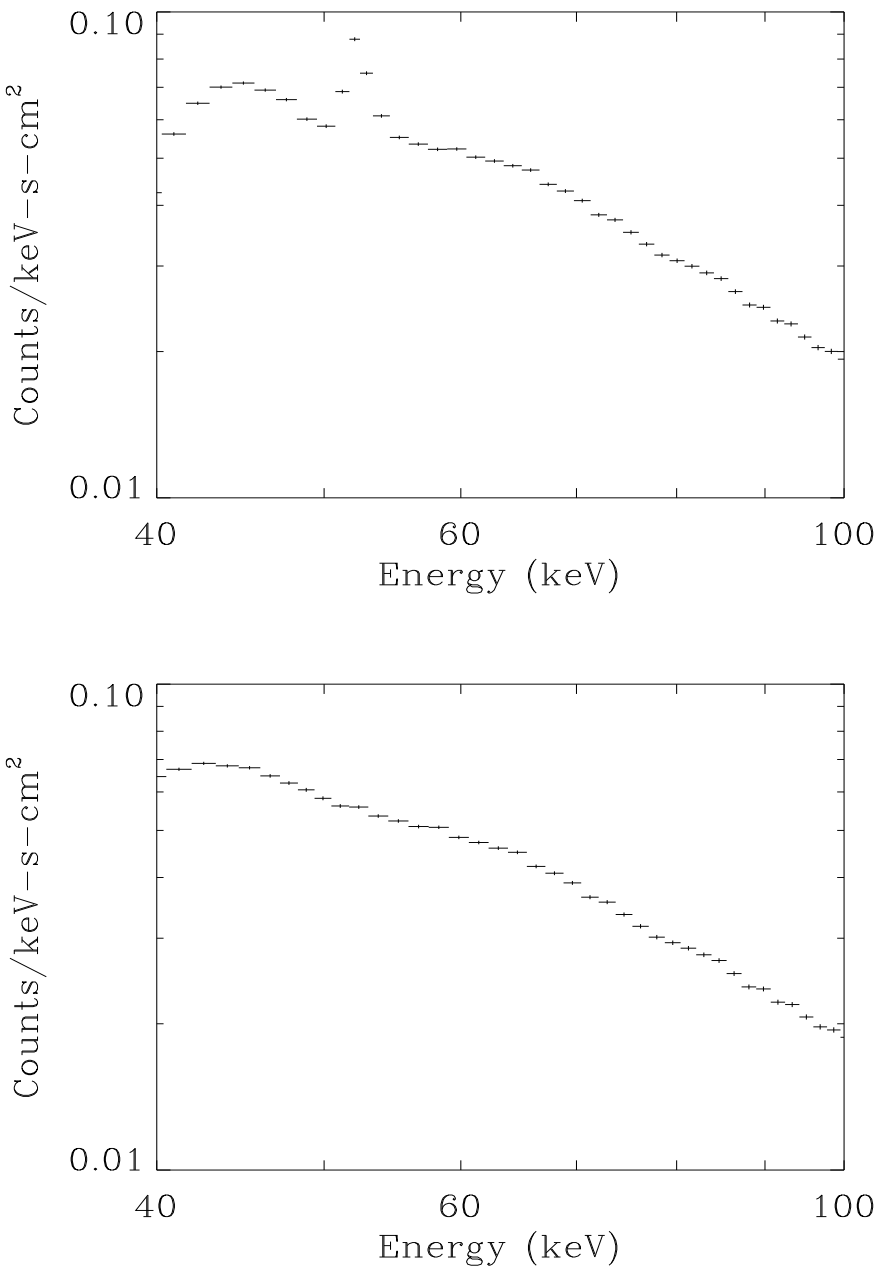

Figure III.5: The background observed by SD7 for 3B930506. The top frame shows a spectrum with a poor SLED correction and the bottom frame has a revised SLED correction.

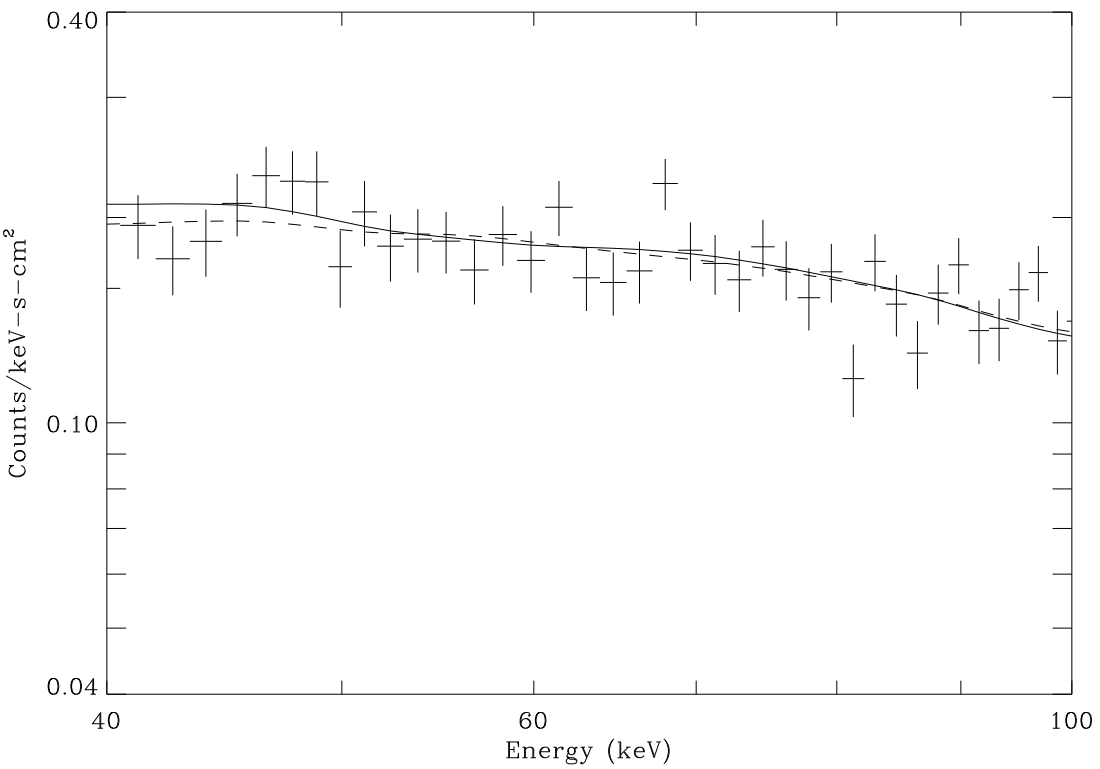

Figure III.6: A count spectrum from SD7 of GRB 3B930506 in which the line candidate is most significant ($6.08 - 9.92$ s after the trigger). The solid curve is a fit to the data which includes a Gaussian line while the dashed curve is a continuum-only fit.

No feature stands out in SD7's corrected count spectrum (Figure III.6). Using the same models as for SD2 (but fitting from 45 to 100 keV), a very weak line was found at 55.9 keV with probability of being a statistical fluctuation of 0.73. This is less significant than an average statistical fluctuation. To determine the likelihood that a line would be seen in SD2 but not SD7, a Monte Carlo simulation of 200 spectra containing a line with SD2's fitted parameters was run for SD7. These simulations showed that if the line in SD2 was real, then the probability of seeing the line in SD7 with an F-test probability of 0.73 or larger is less than one percent. Therefore, there is a serious inconsistency between SD7 and SD2. Since the LADs did not see a feature either once their calibration difficulties were corrected (Preece *et al.* 1994), the feature seen in SD2 cannot be considered real given BATSE's detection criteria.

While the line candidate in GRB 3B930506 could be rejected based on a consistency argument, the F-test significance is uncomfortably high given that it is supposedly a statistical fluctuation. If BATSE has $\sim$ 3000 trials, then there is a $\sim$ 10% likelihood that a statistical fluctuation of this magnitude could occur. This is non-negligible but worrisome. These concerns were removed when a more thorough analysis was performed by Band *et al.* (1996) who demonstrated that when a continuum model which fit all the available data above 100 keV is used, the F-test significance of the feature drops to 1.87×10^{-4} for the two extra parameters introduced by the line in the most significant case. Therefore, despite the excitement generated by intial analysis of the 3B930506, the candidate fails both the significance and consistency requirements.

III.D.4 Consistency and Future Prospects

The lack of BATSE line detections and apparent reality of the *Ginga* lines has left most astrophysicists thinking the instruments contradict each other. This thinking is rooted in the sheer number of GRBs BATSE has observed compared to the number seen by *Ginga* (BATSE has seen over an order of magnitude more). However, a majority of the BATSE bursts are too dim to examine for significant line

features. While BATSE has observed more strong bursts than *Ginga*, the results thus far do not imply an inconsistency. Band *et al.* (1994b) have shown that the observations are consistent and will remain so even if BATSE does not detect lines for several years. Despite this quantitative analysis, many still feel uneasy about accepting the idea that spectral features do exist and BATSE was just unfortunate in not observing any. Therefore, it will likely be some time before this issue is resolved.

The easiest way to settle the question would be to find line features in BATSE data. An effort to make an exhaustive search of the BATSE data for spectral features has been carefully developed and is beginning to be applied to BATSE data (Schaefer *et al.* 1994; Briggs *et al.* 1996). This search is performed in two parts. First, all meaningful combinations of spectra are fitted by models with and without lines at fixed energies by computer and significances calculated. The energies used are separated by one-third of an instrument resolution element. If the significance of a feature in a particular spectrum or group of spectra exceeds a threshold value, further analysis is performed seeking to find the time interval in which the candidate is most significant and determine the true line energy and width. Using an automatic computer search is superior to a visual search since the latter is independent of the subjectivity and stamina of the individual performing the search. The computer search also provides data on the completeness of the search. The major drawback is that it is extremely time consuming both in computer and analyst time.

Despite the time involved in the computer search, it is worthwhile since it will eventually provide a definite answer to the question of whether spectral features exist in BATSE data. If such features exist, then they will provide an important constraint on all GRB models. If features are not found, then they are likely a rare phenomenon, not present in 20% of the bursts as implied by earlier experiments. In either case, the statement BATSE can make on this subject will be one of the most important results from the BATSE SDs.

Chapter IV

Spectral Evolution

IV.A Introduction

Gamma-ray burst continuum spectra provide the most direct information about the emission processes involved in these violent events. Unfortunately, the continuum generating process is unknown, making physical interpretation of spectral observations difficult. A striking feature of gamma-ray bursts is the temporal variability of spectra both between and within bursts. Therefore, an empirical study of the dynamics of burst spectra may provide vital clues for resolving the mystery surrounding these puzzling events.

Bursts have only been observed above $\gtrsim$2 keV and no emission has been seen in quiescence (Schaefer 1994a). Spectral properties of time integrated spectra from 54 bright bursts were studied by Band *et al.* (1993, hereafter B93). While spectra were shown to be quite diverse, a simple and flexible empirical model successfully described all spectra. This model is used this chapter to describe burst spectra and monitor the evolution of the energy at which the energy flux per logarithmic energy band peaks (E_P, energy of the peak of νF_ν).

The study of burst spectral evolution has a long history. Golenetskii *et al.* (1983, hereafter G83) examined two-channel data covering $\sim$ 40-700 keV with $\sim$0.5 s time resolution from five bursts observed by the KONUS experiment on *Venera* 13

and 14. Spectra were described by an optically thin thermal bremsstrahlung (OTTB) model, $N_E(E) \propto E^{-1} \exp(-E/kT)$ ph-keV^{-1}-s^{-1}-cm^{-2}. A correlation between intensity and temperature parameter T was discovered ($I \propto T^{\gamma}$, $\gamma \approx$1.5-1.7), implying spectral hardness at a given time is related to the intensity of the burst in a simple way. Laros *et al.* (1985) performed a similar analysis using five bursts observed by the *Pioneer Venus Orbiter* ($\sim$ 0.1-2 MeV, $\sim$0.2 s time resolution) but found no correlation and speculated that the G83 results were an artifact of the way temperature was inferred.

Norris *et al.* (1986, hereafter N86) investigated ten bursts seen by instruments on the *Solar Maximum Mission* satellite using hardness ratios (the ratio of observed flux in two energy bands). The energy bands used in the hardness ratio were 52-182 keV and 300-350 keV and the time resolution ranged over 0.128-1s, depending on the data available. They found that individual intensity pulses evolved from hard-to-soft with the hardness peaking before intensity. This implies a more complex relationship between hardness and intensity than proposed by G83.

Recent studies of spectral evolution have tended to follow the lead of G83 or N86, obtaining similar results. Kargatis *et al.* (1994, hereafter K94) fit OTTB and thermal synchrotron models ($N_E(E) \propto \exp[-(E/E_c)^{1/3}]$ ph-keV^{-1}-s^{-1}-cm^{-2}) to sixteen bursts from the SIGNE experiment, covering $\sim$50-700 keV with 0.5 second resolution. An intensity-temperature correlation was found in seven of the bursts ($\gamma \approx$ 1.4-3.0) but two clearly did not show this correlation (the remainder were questionable) indicating that while many bursts may have a intensity-temperature correlation, the trend is not universal. On the other hand, Band *et al.* (1992b) analyzed nine bursts observed by the BATSE SDs ($\sim$25-1000 keV, $\geq$0.128s) using models of the form $N_E(E) \propto E^{\alpha} \exp[-(E/kT)]$ ph-keV^{-1}-s^{-1}-cm^{-2}, confirming the results of N86 including T leading the intensity when fine time resolution was available. Bhat *et al.* (1994a) used hardness ratios with BATSE LAD data to study single pulse bursts which had a fast rise followed by a gradual decay. The energy bands used for the ratio were E=25-100 keV and E >100 keV. The time resolution of the sample was

64 ms. Hard-to-soft spectral evolution was found with hardness leading the intensity. The time lag between the peak hardness ratio and peak count rate was found to be directly correlated with the rise time of the counting rate.

Although the analyses exemplified by G83 and N86 give apparently inconsistent results, they can be reconciled by considering the time resolution of the data. The analysis of G83 and K94 had a time resolution of ~ 0.5 s while the resolution of N86 was as small as ~ 0.128 s and Bhat *et al.* (1994a) had 64 ms resolution. Therefore, slightly asynchronous behavior could be masked by the poor time resolution in the G83 and K94 samples. This conclusion is supported by the results of Band *et al.* (1992a), who performed an analysis similar to that of G83 and K94, but found that the spectral hardness (parameterized by T) led the intensity on short time scales. The need for fine time resolution is emphasized by Kouveliotou *et al.* (1992), who examined 22 bursts observed with the LADs and performed Fourier transforms on intensity profiles in different energy bands. The hard band was found to lead the soft by $\sim$0.1 second. In addition, Kouveliotou *et al.* (1994b) reported significant variations in the hardness ratio at the 2 ms level in an extremely intense burst observed with BATSE.

The spectral analyses of G83 and N86 characterize the spectrum in very different ways. Both G83 and K94 use spectral models which are assumed to describe the gamma-ray burst continuum and whose parameters are interpreted as physically meaningful. Most often, the model chosen is one which cuts off rapidly at high energies (e.g., OTTB). It was demonstrated by B93 that such models do not reproduce spectra observed by the BATSE SDs and conflict with the observation of high energy emission by other experiments (Matz *et al.* 1985; Schneid *et al.* 1992; Hanlon *et al.* 1994). Consequently, these models cannot be physically correct and though the parameters are certainly physically linked to the emission process, one must realize that the parameters do not necessarily have their apparent meaning (e.g., the OTTB cutoff energy may not be temperature). On the other hand, hardness ratios (such as used by N86) do not assume any knowledge of the source physics but do depend

on instrumental properties which are accounted for in spectral fitting. While this characterization tracks changes in the shape and slope of a spectrum, the numerical values do not have a quantitative physical meaning and do not lend themselves to additional insights as a characteristic temperature or spectral shape can. Therefore it is helpful to use an empirical model which describes the photon spectrum but does not depend strongly on preconceived notions of spectrum formation in bursts.

In this work, a description of the photon spectrum independent of physical models is achieved by fitting the empirical spectral model from B93 to BATSE SD data. This model was shown to adequately describe spectra in the BATSE energy range and incorporates many simple physical models as special cases, accommodating uncertainty about the actual continuum emission process. Although the model is phenomenological, physically meaningful parameters can be derived from it. In this work, E_P (the energy of the peak of νF_ν) is used to quantify fitted spectra, a parameter which indicates the energy of maximum radiated power. This allows a study of spectral evolution in gamma-ray bursts based on a well-defined physical measure of spectral hardness which does not depend strongly on assumed emission processes.

In this work, the word hardness is used to describe the energy of E_P. Spectra in which E_P is at high energies are called hard and soft spectra have small E_P.

IV.B Analysis

It was shown by B93 that the following empirical model is sufficient to describe burst spectra:

$$N_E(E)\ \left(\frac{\text{photons}}{\text{keV-s-cm}^2}\right) = \begin{cases} A\left(\frac{E}{100\ \text{keV}}\right)^{\alpha} e^{-E/E_0}, & E \le (\alpha-\beta)E_0 \\ A'\left(\frac{E}{100\ \text{keV}}\right)^{\beta}, & E > (\alpha-\beta)E_0 \end{cases} \qquad \text{(IV.1)}$$

where A, α, β, and E_0 are fit to observed spectra and A' is chosen so that the function is continuously differentiable everywhere. The success of this model can be traced to its flexibility. Included in equation IV.1 as special cases are a power law, photon exponential, OTTB, and a broken power law with continuous transition. Since

the emission process is unknown, equation IV.1 is a logical choice for determining physically meaningful parameters. The quantity of interest in this study is the energy of the peak of νF_ν (E_P) and since $N_E(E)E^2 \propto \nu F_\nu$, $E_P = (2+\alpha)E_0$ (assuming $\beta < -2$).

Burst data were selected from detectors in high gain states, most covering ~15-1500 keV with about a third extending to higher energies. This choice was motivated by the results of B93 which demonstrated that for most bursts the spectral slope changes at energies less than 1 MeV and that the observed signal is greatest around 100 keV (a detector dependent property, not necessarily true for the incident spectrum).

Bursts which had many high quality spectra were required so that E_P could be reliably determined and meaningful trends discovered. However, most bursts were not sufficiently long or intense to provide enough spectra to resolve the evolution. To understand the necessary signal strength, a Monte Carlo simulation of a typical spectrum was performed to investigate the reliability of the determination of E_P as a function of the signal-to-noise ratio (S/N, the number of source counts divided by the uncertainty in the number of source counts) in the 60-200 keV energy band. The results of this simulation are given in Table IV.1 which shows that a large S/N level is required to reduce the variance in E_P to reasonable values.

Even for many strong bursts, most individual SHERB spectra do not have large S/N levels. However, the quality of the signal can be improved by averaging spectra together weighted by livetime. An explicit demonstration of this process for burst 3B910807 is given in Figure IV.1. In this figure, E_P as determined from spectra at the finest time resolution available and from averaged pairs of spectra are plotted together. S/N in the 60-200 keV band ranged from 7.0-17.0 with a median of 11.7 for the fine time resolution data and 9.7-23.1 with median 16.3 for the averaged spectra. It is apparent that not only do the estimated errors in the determination of E_P get smaller as spectra are accumulated, but that the fitted value converges to the average of E_P determined from the fine resolution spectra.

Binning[1]	t(s)[2]	Med(C)[3]	Max(C)[4]	Med(E_P)[5]	Var(E_P)[6]	S/N[7]
nobin	0.1	0.23	4.66	259	286	10.0
	0.25	0.99	7.78	285	77	15.6
	0.5	2.11	16.48	265	50	21.6
	1.0	4.41	30.31	251	36	29.6
	2.0	9.70	43.72	250	21	39.5
half	0.1	1.18	9.52	271	176	10.0
	0.25	2.78	26.85	259	85	15.6
	0.5	4.66	45.71	256	56	21.6
	1.0	9.05	86.85	252	39	29.6
	2.0	21.50	219.33	251	22	39.5
full	0.1	2.46	15.47	252	153	10.0
	0.25	4.95	36.03	244	68	15.6
	0.5	8.55	72.05	253	50	21.6
	1.0	19.30	141.77	251	35	29.6
	2.0	45.47	321.04	250	21	39.5
eight	0.1	3.29	10.52	220	86	10.0
	0.25	8.54	24.35	240	63	15.6
	0.5	17.67	46.76	247	46	21.6
	1.0	34.85	102.28	250	40	29.6
	2.0	73.27	195.23	248	25	39.5

[1]–The binning scheme used for spectra:

nobin — Data in native format.
half — Binned to one half of the detector energy resolution.
full — Binned to the detector energy resolution.
eight — Eight broad energy bins.

[2]–The livetime used to create spectra.
[3]–Median number of counts per channel in the binned spectrum.
[4]–Maximum number of counts per channel in the binned spectrum.
[5]–Median value of E_P (keV).
[6]–Variance of E_P about the median (keV).
[7]–Median S/N in the 60-200 keV energy band.

Table IV.1: 200 spectra were created using the model spectrum of eqn. IV.1 with A=0.1 ph-keV^{-1}-s^{-1}-cm^{-2}, $\alpha = -1$, $\beta = -3$, $E_0 = 250$ keV (E_P=250 keV). Non-integral counts result from subtraction of fractional background counts.

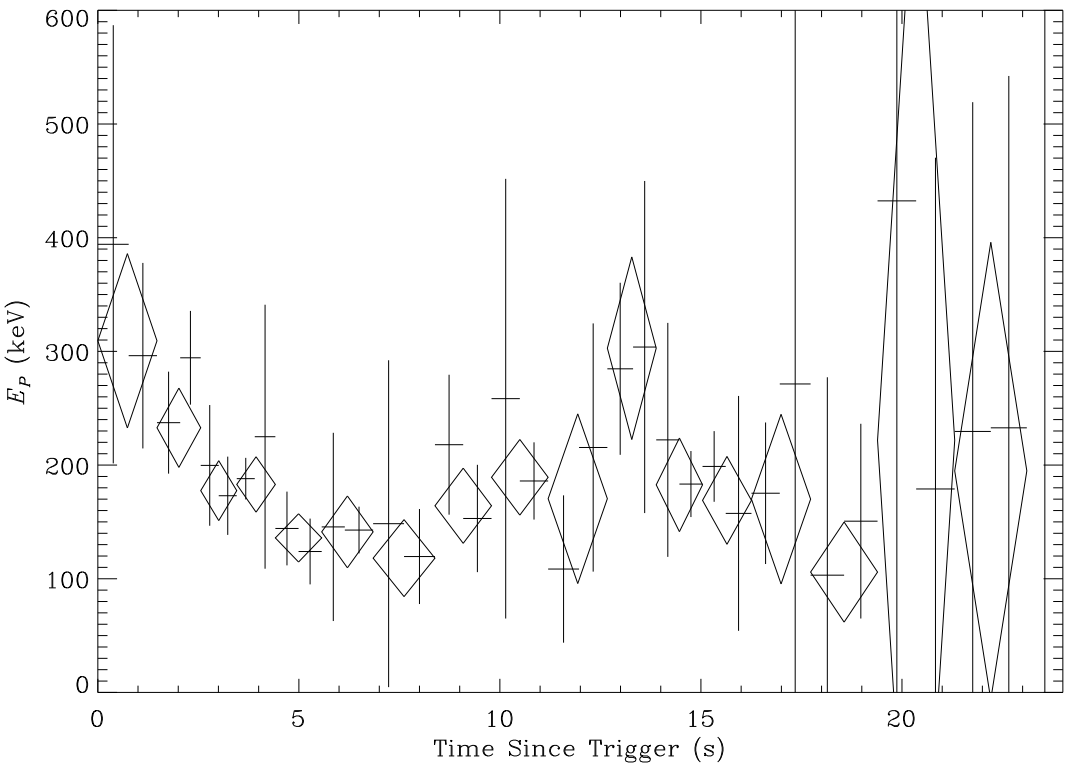

Figure IV.1: E_P as determined from spectra at the finest available time resolution (crosses) and from pairs of spectra averaged together (diamonds). The data are from burst 3B910807 and the size of the symbols represents the time intervals over which spectra were accumulated and the error in E_P.

After selecting candidate bursts, background models were created using a channel-by-channel fit of a time dependent polynomial to data before and after the burst. The order of the polynomial varied from burst to burst; typically the lowest order which gave an acceptable fit was used (never higher than fourth order). After subtracting the background, consecutive spectra were averaged together until S/N$\geq$15 in the 60-200 keV energy band. Although Table IV.1 shows that this choice will result in a sizable dispersion in E_P, a larger S/N level would have essentially destroyed the time resolution in most of the sample. Therefore, some certainty in E_P was sacrificed for time resolution. Exceptions to this S/N criterion were made for a few bursts in which a long period of low activity was bounded by interesting pulse structure. In those cases, all data in between the intense periods were averaged despite a low S/N value. An exception was also made for burst 3B910813 in which the data did not extend below 100 keV. The S/N criterion for this burst was S/N$\geq$12 in the 100-200 keV band.

A burst was included in the sample if it survived the process outlined above with at least six spectra. Since most bursts do not have many spectra with large S/N, only $\sim$4% of all bursts observed by BATSE and 17 of the 54 bursts from B93 were contained in the sample (this sample includes bursts which occurred after those in B93. The empirical model (eqn. IV.1) was fitted to data using forward folding deconvolution (Loredo & Epstein 1989). This method determines the incident photon spectrum by folding an assumed photon spectrum through a model of the detector response and comparing the result to observed data. The best fit was found using a modified version of the Levenberg-Marquardt iterative χ^2 minimization algorithm (Bevington 1969, p. 237; Press *et al.* 1992, p. 678). The modifications were the use of model variances instead of data variances in χ^2 (see Appendix for details) and stopping criteria based on χ^2, χ^2 per degree of freedom in the fit (χ^2_ν), and a test for false minima. The detector response model included the direct component along with scatter off the spacecraft (Pendleton *et al.* 1989) and the Earth's atmosphere (Pendleton *et al.* 1992). The error in E_P was determined through standard

error propagation using the error in α and E_0 and the correlation between these two parameters (Bevington 1969, p. 61).

Each spectrum was fit over the entire energy range above the SLED. The data were not rebinned from the telemetered format so that in most cases the average number of counts per bin in the high energy channels was less than a few. In these channels, the Poisson statistical distribution is not well approximated by a normal distribution and the χ^2 statistic is therefore not strictly applicable. This is a common difficulty in high energy astrophysics which can be avoided by binning the data until the Gaussian limit is reached. To determine the importance of this problem, a set of Monte Carlo simulations was performed for several types of binning. The results for four different binning modes in Table IV.1 show that the fits are not improved by rebinning the data even if most high energy bins have only a few counts. There are two reasons for this. First, the data at higher energies are so sparse that when the Gaussian limit is achieved, the bins are so wide that the upper power law in eqn. IV.1 cannot be accurately determined. Second, the fit is largely determined by the signal below a few hundred keV where the number of counts per channel is largest (Max(C) in Table IV.1). The Gaussian limit can also be achieved if there are a large number of background counts, which can be important at low energies.

These simulations demonstrate that for the SHERB data type used in this sample, any binning is valid. To ensure that this was the case for real data, fits using the telemetered binning and eight broad energy bins were made to spectra from burst 3B930916. The comparison of the values of E_P is presented in Figure IV.2. E_P is consistent between the two fits and determined with roughly equal accuracy. Since the choice of data binning is unimportant, the telemetered channels were not rebinned because the analysis software was optimized for this scheme.

One difficulty with using high gain detectors (where the spectrum extends to low energy) was that occasionally the upper spectral index β was larger than -2 which implies that E_P was beyond the upper end of the fit range, that the spectrum has more gradual curvature than the empirical model could accommodate, or that

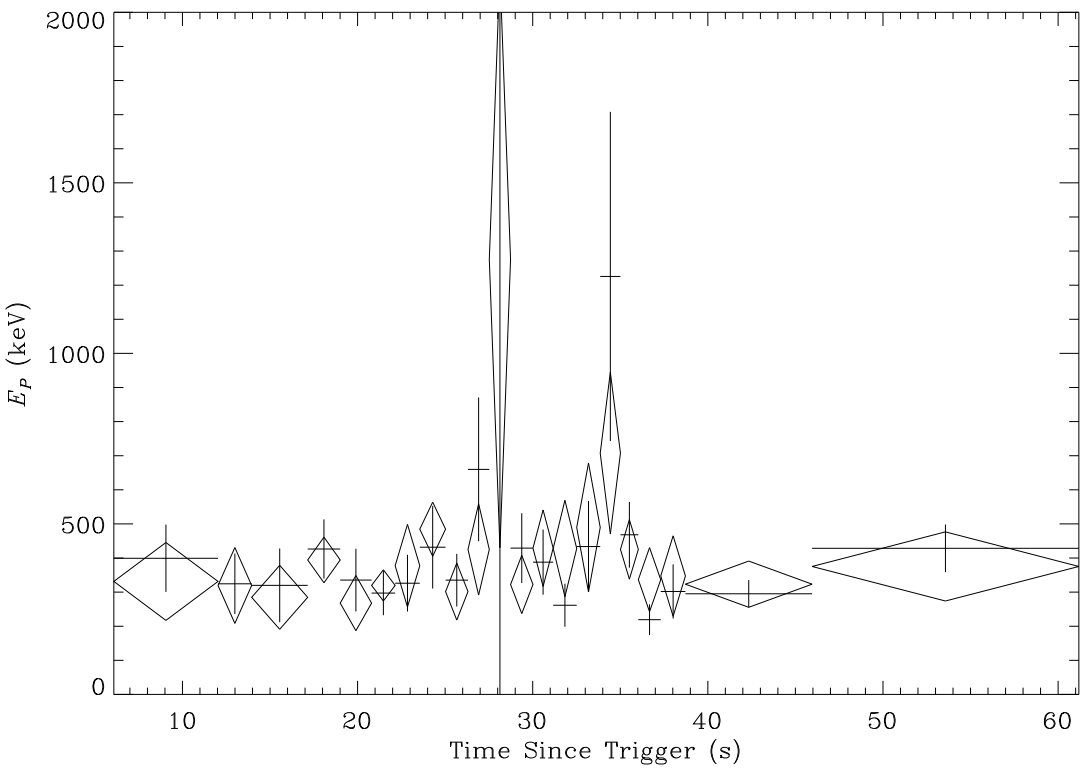

Figure IV.2: E_P as determined from fits to the same spectra with different binnings for burst 3B930916. The crosses represent values from the unrebinned data while the diamonds correspond to the values from spectra which have been rebinned into eight broad energy bins.

the high energy signal was insufficient to fix β. For this work, β was constrained to be less than -2 for all fits. In bursts for which this constraint was important (implying a flatter spectrum), it was found that either β tended to shift rapidly from the upper constraint to the lower ($\beta = -5$) or that it remained at the upper constraint (-2.01) consistently. In the former case, the high energy spectrum was probably not well-determined and should be ignored when calculating E_P. For the latter, E_P should reflect changes in the shape (i.e. hardness) of the spectrum since E_0 will move to higher energies to compensate for the inability of β to adequately describe this region. No bursts were observed to show convincing evidence for evolution of β from above -2 to lower values. Therefore, variations in the fitted value of E_P should be consistent with the true variations in spectral hardness if quantitatively inaccurate (with systematically smaller values of E_P) since E_0 will rise and fall proportionally to the amount of excess power at high energies (i.e., the spectral hardness). Omitting the upper power law would force E_P to higher energies as the model accounts for power at the high end. However, this simpler model may overestimate E_P, placing it far above the detector's energy range where the model is not as sensitive to changes in E_P. As a subset of the empirical four parameter model of equation IV.1, the model without β is not a more accurate description of the true photon spectrum. Since evolution of E_P is the primary focus of this study, equation IV.1 with β constrained is used to model all spectra since it remains sensitive to hardness variations over a broader energy range than a model which cuts off at high energies.

To test whether changes in the fitted values E_P were indeed consistent with real variations in E_P for cases where $\beta > -2$, detectors at lower gain were used to determine E_P for bursts in which the constraint was important. Unfortunately, in all but one case the high energy signal was too weak to reliably fit E_P with any time resolution. Figure IV.3 shows a comparison of the high and low gain detectors for the exception (3B910503). It is apparent from this figure that not only do the two detectors have similar time histories, but that E_P determined by the high gain detector is not far from the value of E_P measured by the low gain detector (for

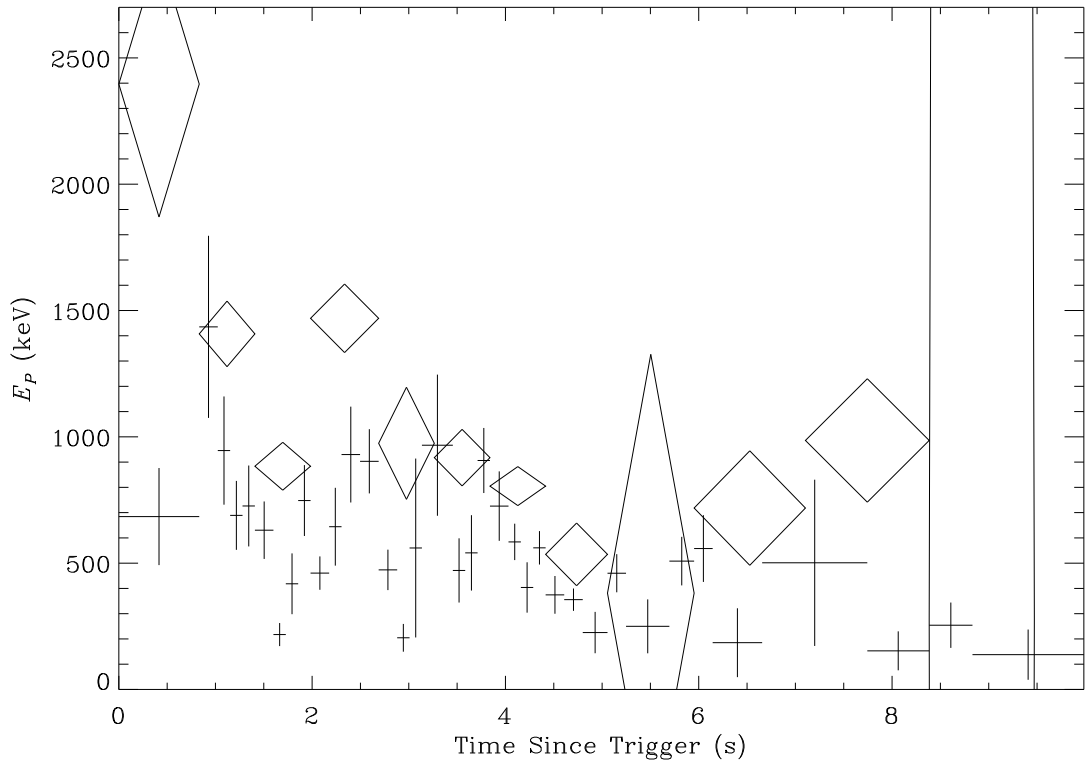

Figure IV.3: E_P as measured by detectors at different gains for burst 3B910503. The high gain detector (crosses) was fit from 25.7-2977 keV and the low gain detector (diamonds) covers 308-26,214 keV. The high gain detector has better time resolution since it had a stronger signal.

which $\beta < -2$). Therefore, it is not expected that qualitative statements about the evolution of E_P depend strongly on the accuracy with which β is determined.

That the low gain detector measures a consistently larger value of E_P than the high gain detector in the previous example suggests the calculated value of E_P may depend on gain setting even though E_P is well defined in all detectors. To ensure that this was not the case, the value of E_P from two detectors at different gains viewing burst 3B921207 were compared ($\beta < -2$ for both detectors). In this case, spectra accumulated by the high gain detector were averaged so that the time intervals covered by both sets of spectra were identical. The comparison in Figure IV.4 shows

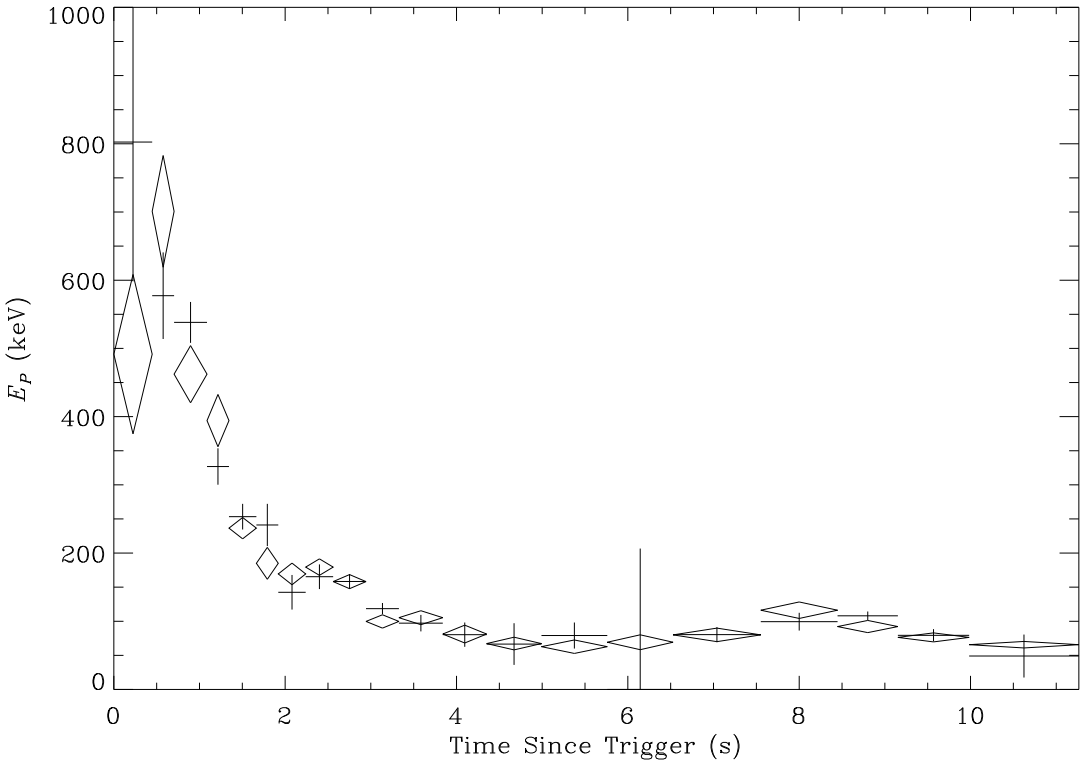

Figure IV.4: E_P as determined from two detectors viewing the burst 3B921207. The high gain detector (crosses) covered the energy range from 20.2-1283 keV and the low gain detector (diamonds) ranged from 43.1-3300 keV.

that the determination of E_P was consistent.

The tests outlined above cover the obvious difficulties involved in the analysis. Although solutions to the S/N and $\beta > -2$ problems are not ideal, they do allow the analysis to proceed so that useful information about burst continua can be derived. Also, the inter-detector test indicates that SD observations are consistent with each other and the results should not depend on the variable energy range covered by the SDs.

IV.C Results

Of the 862 gamma-ray bursts detected by BATSE until the end of 1993, only the 37 bursts listed in Table IV.2 met the criteria outlined above. As expected, equation (1) fit the data well, $\chi^2_\nu \lesssim 1$ for nearly all spectra. For these bursts, E_P was compared to the count rate (see Figure IV.5). Two bursts which clearly demonstrate the general trends observed in the sample as a whole are 3B921207 and 3B920525. In 3B921207, it is apparent that E_P softens over the whole burst except for the increase along with the intensity 8 seconds after the trigger. 3B920525 is a burst in which two strong intensity pulses were resolved. E_P softens after intial hardening within both spikes and the second spike is softer than the first.

	Characteristic				Med(E_P)	ΔE_P
Burst	1	2	3	4	(keV)	(keV)
3B910503*†	+	+	+	+	540	1350
3B910601†	+	0	···	···	700	950
3B910807	+	0	+	0	170	175
3B910814C	···	···	···	···	490	900
3B910814†	···	+	···	···	1400	1300
3B911031*	···	+	···	···	400	850
3B911106	···	0	···	···	165	120
3B911118†	+	+	+	+	180	440
3B911126*	+	+	+	0	250	900
3B911127	···	···	···	···	190	250
3B911202*	0	+	0	···	350	1300
3B911209*	+	+	+	+	270	400
3B920218*	···	+	···	···	220	150
3B920311	+	+	+	+	440	1150
3B920406*	+	0	+	0	240	300
3B920513*	+	···	+	···	220	200
3B920517*	+	···	+	···	230	150
3B920525*	+	+	+	+	380	2075
3B920617	···	+	···	···	145	175
3B920622	+	0	+	···	440	1550
3B920627*	···	···	···	···	210	325
3B920711	+	0	···	0	510	650
3B920720	+	−	−	−	270	525
3B920902*	···	+	+	···	550	1500
3B921009	+	0	···	···	300	225
3B921123	+	+	···	···	250	350
3B921207	+	+	+	+	140	650
3B921209	+	+	+	+	180	375
3B930120	···	···	···	···	125	80

Table IV.2: Characterization of the spectral evolution observed in the GRB sample (continued on next page).

Burst	Characteristic 1	2	3	4	Med(E_P) (keV)	ΔE_P (keV)
3B930405	...	–	...	...	280	300
3B930425	...	...	...	...	250	225
3B930506	+	+	0	...	1030	1750
3B930916*	0	0	0	0	390	350
3B930922	+	+	+	0	110	130
3B931103	+	+	+	+	380	1300
3B931126	+	+	+	+	240	300
3B931204	+	+	+	0	380	775

*–$\beta = -2.01$ throughout the burst.
†–Observed by COMPTEL (Hanlon *et al.* 1994)
Burst Characteristics:

1 — E_P-intensity association.
2 — Overall softening within a burst.
3 — Softening within pulse structures.
4 — Later spikes softer than earlier spikes.

The symbols denote:

+ — Trait observed.
– — Opposite behavior observed.
0 — Neither trait nor opposite observed.
... — Could not be determined.

(Table IV.2 continued)

Figure IV.5: The evolution of E_P and the count rate for all bursts in the sample. The histogram is the count rate for individual SHERB spectra and the diamonds are E_P. The height of the diamonds represent 1-σ error bars and their width indicates the accumulation time of the SHERB spectra averaged together to achieve the S/N criterion outlined above. Note: 3B931204 extends over two frames.

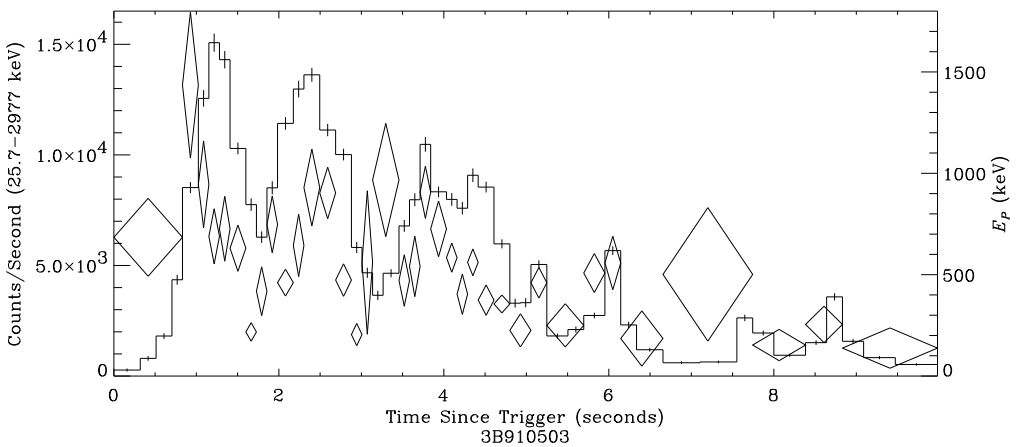

3B910503

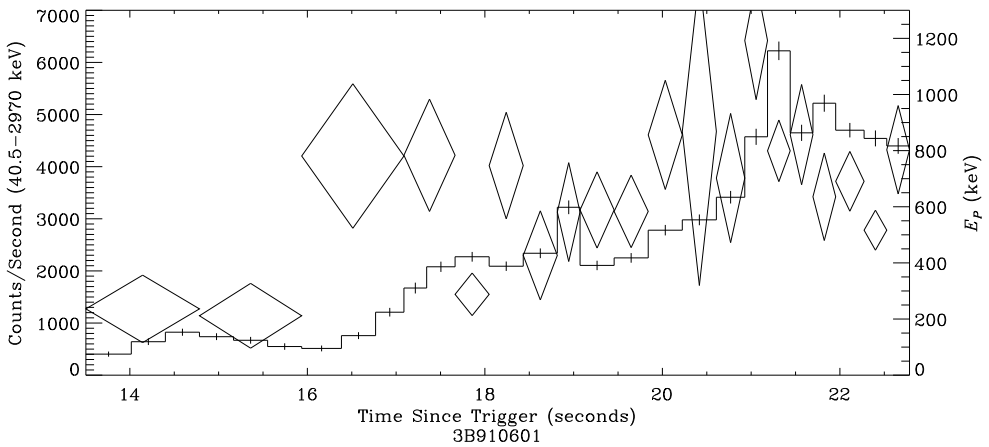

3B910601

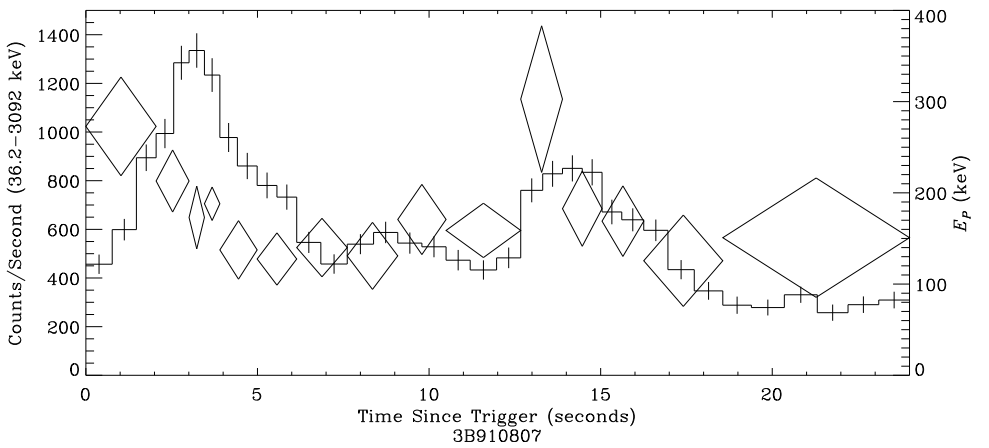

3B910807

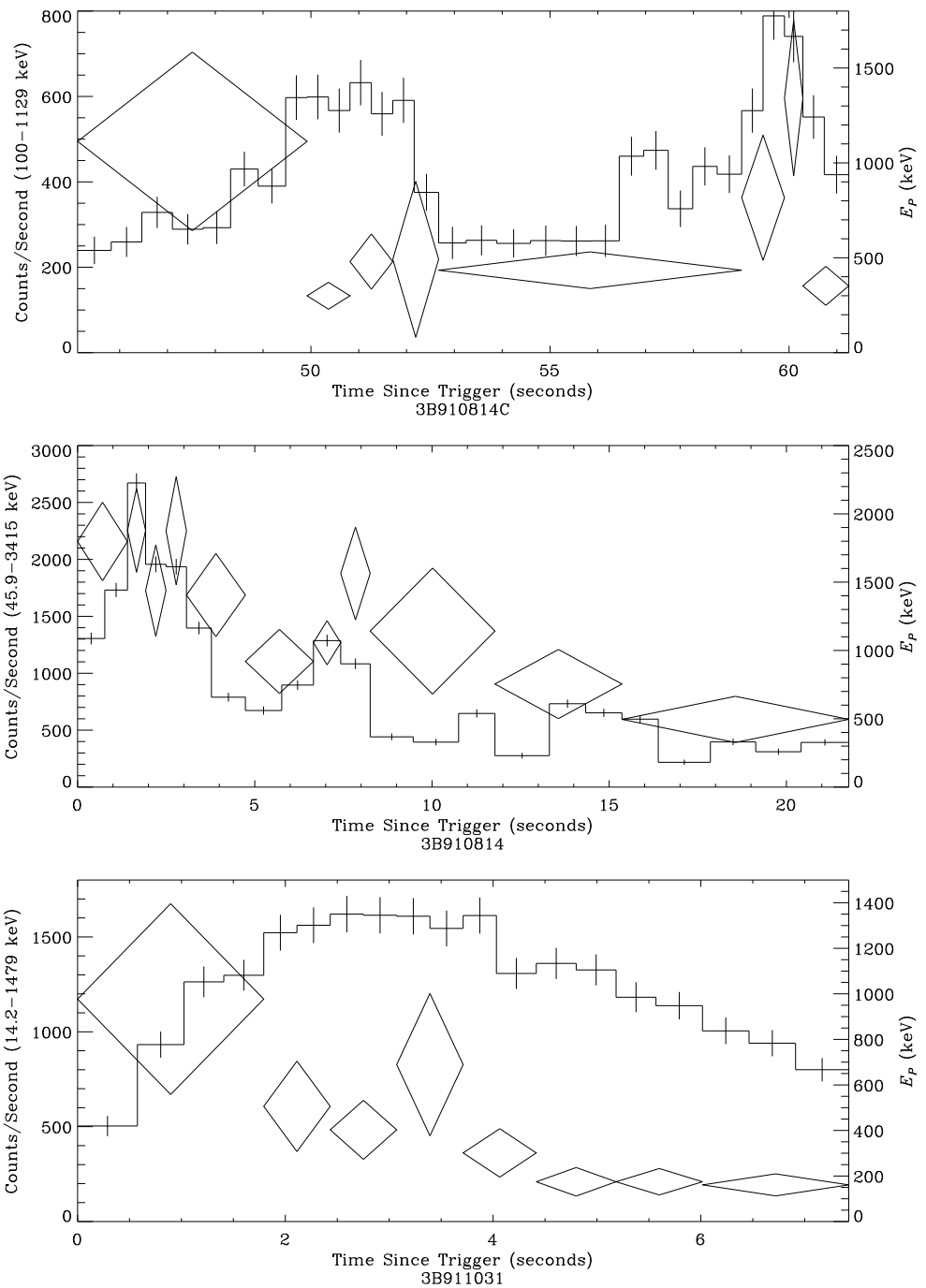

(Figure IV.5 continued)

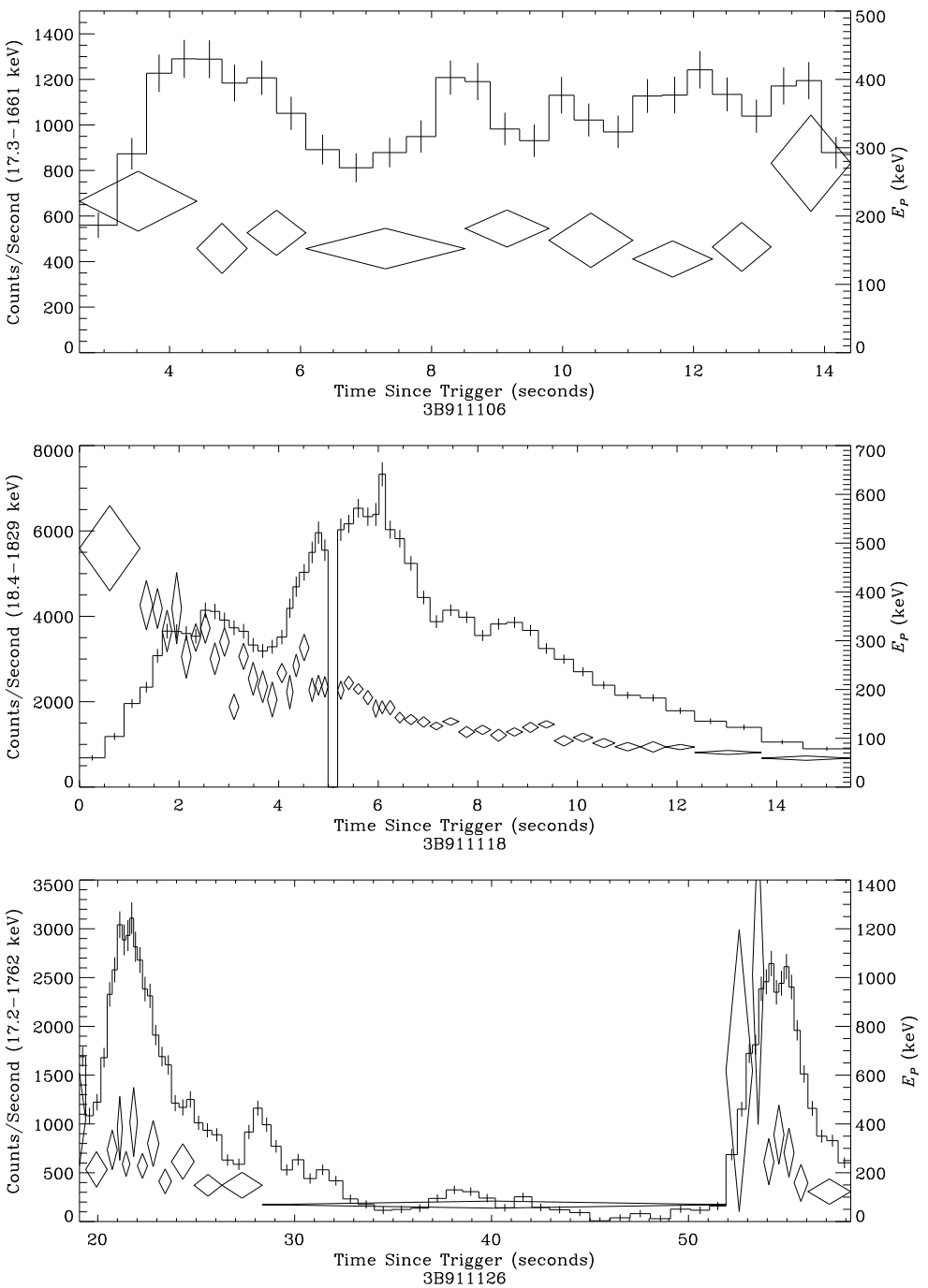

(Figure IV.5 continued)

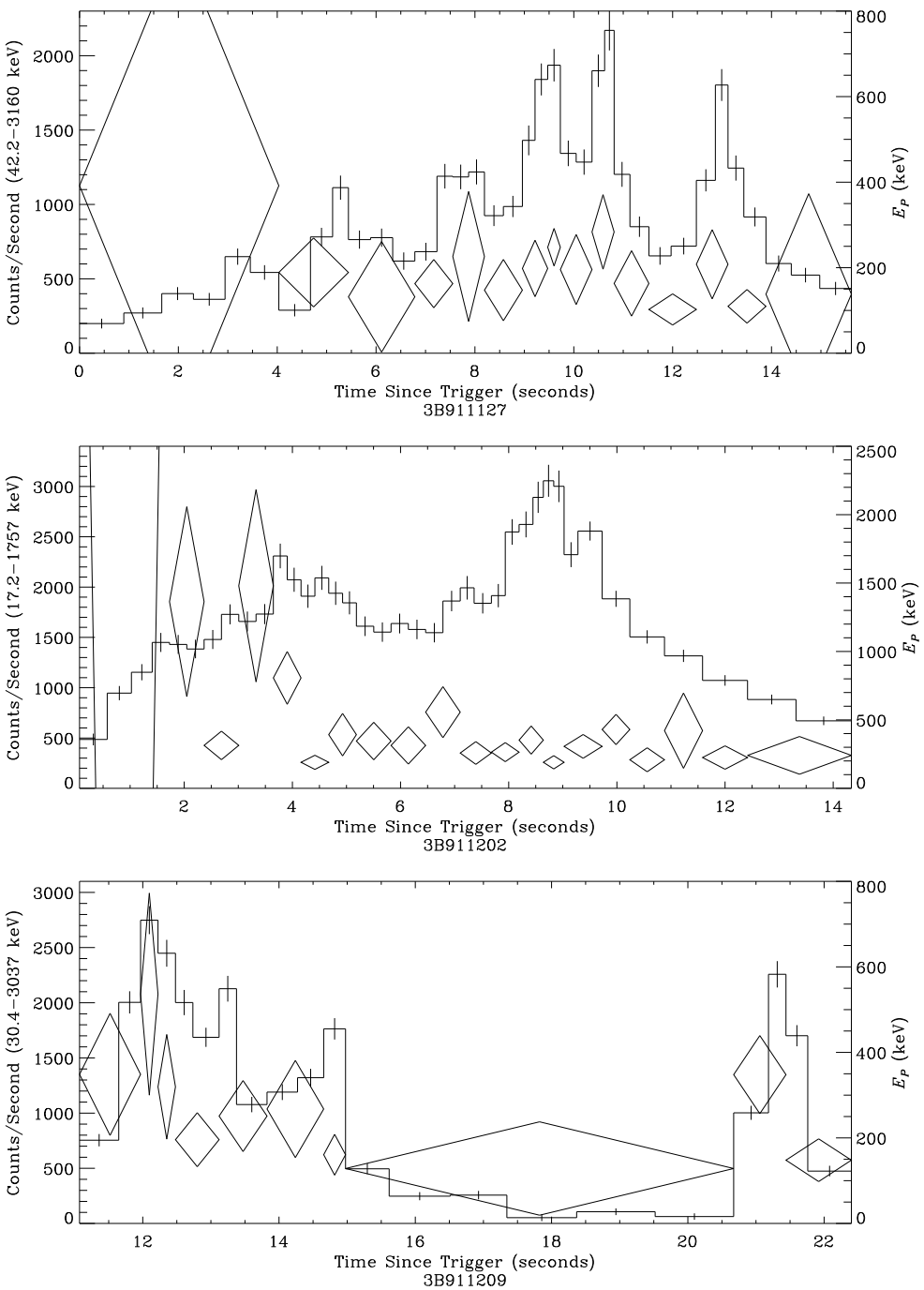

(Figure IV.5 continued)

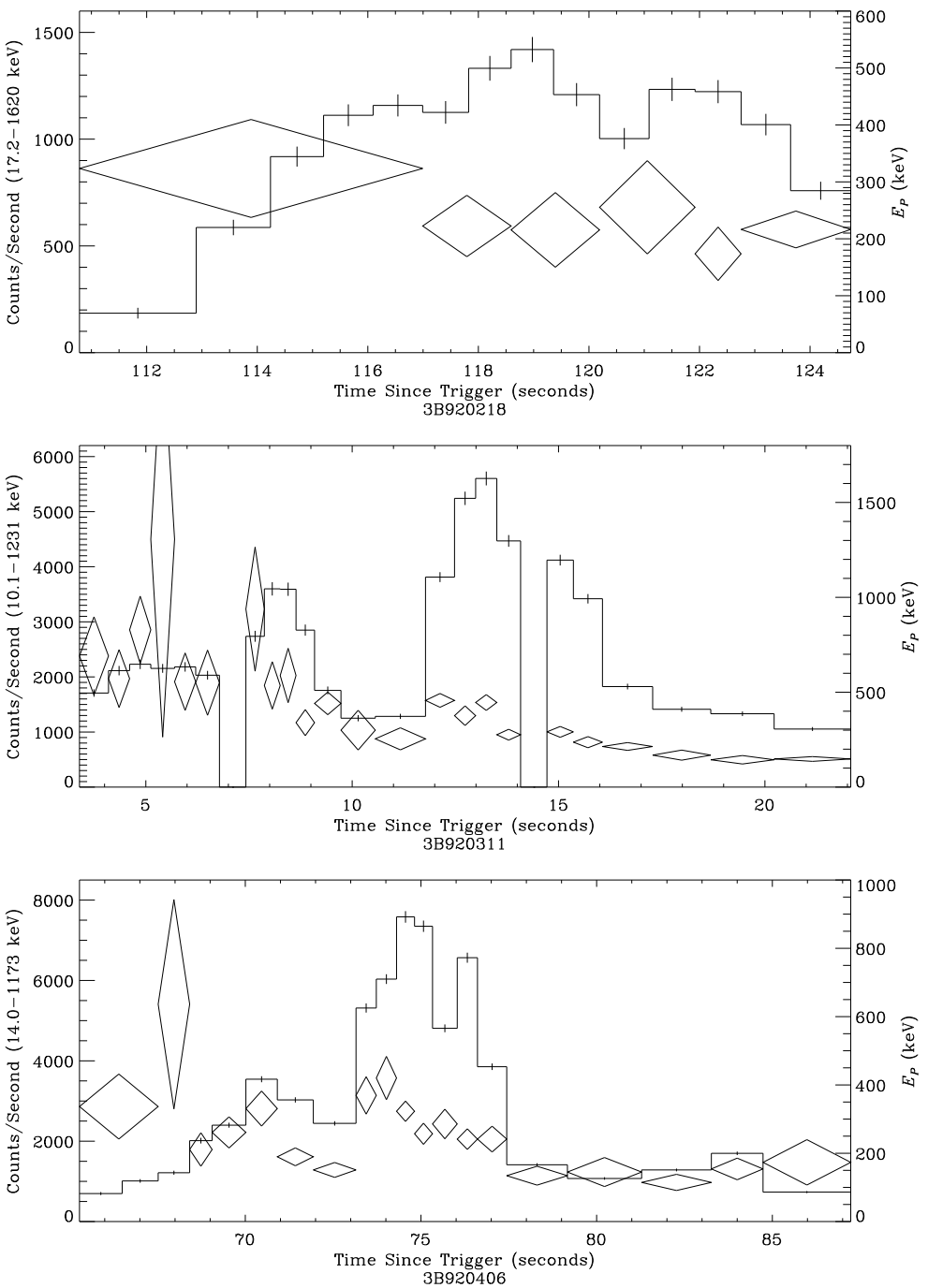

(Figure IV.5 continued)

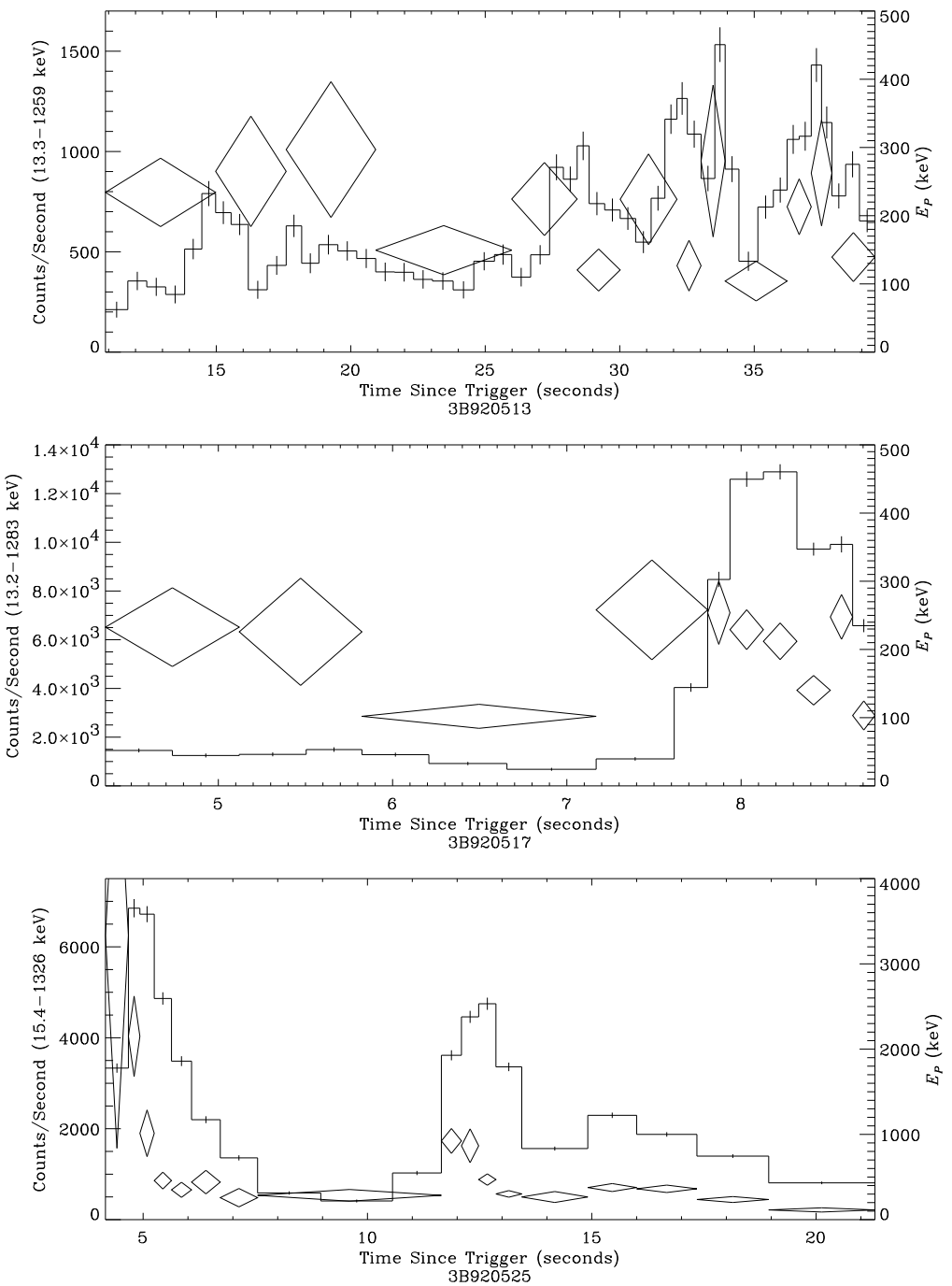

(Figure IV.5 continued)

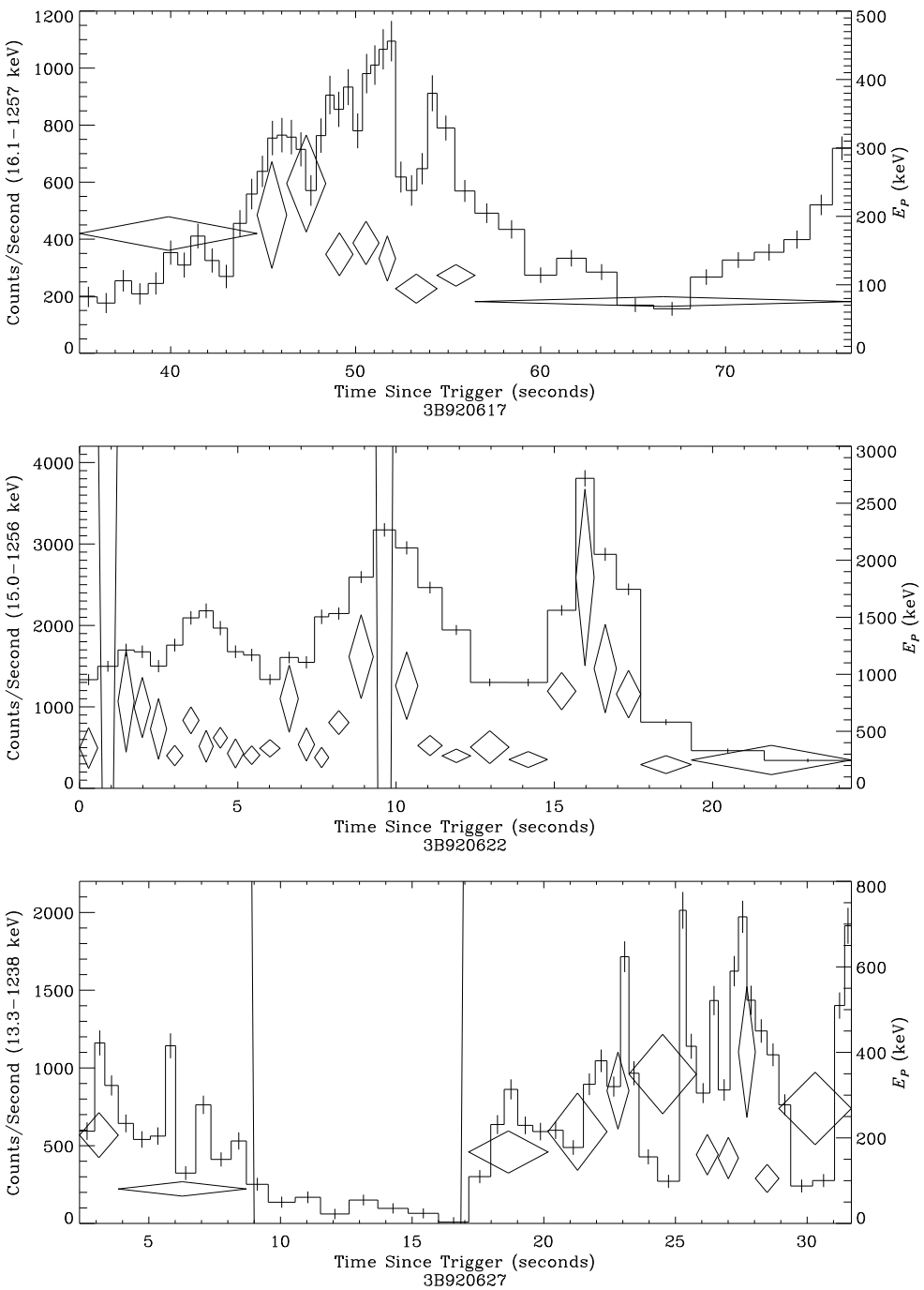

(Figure IV.5 continued)

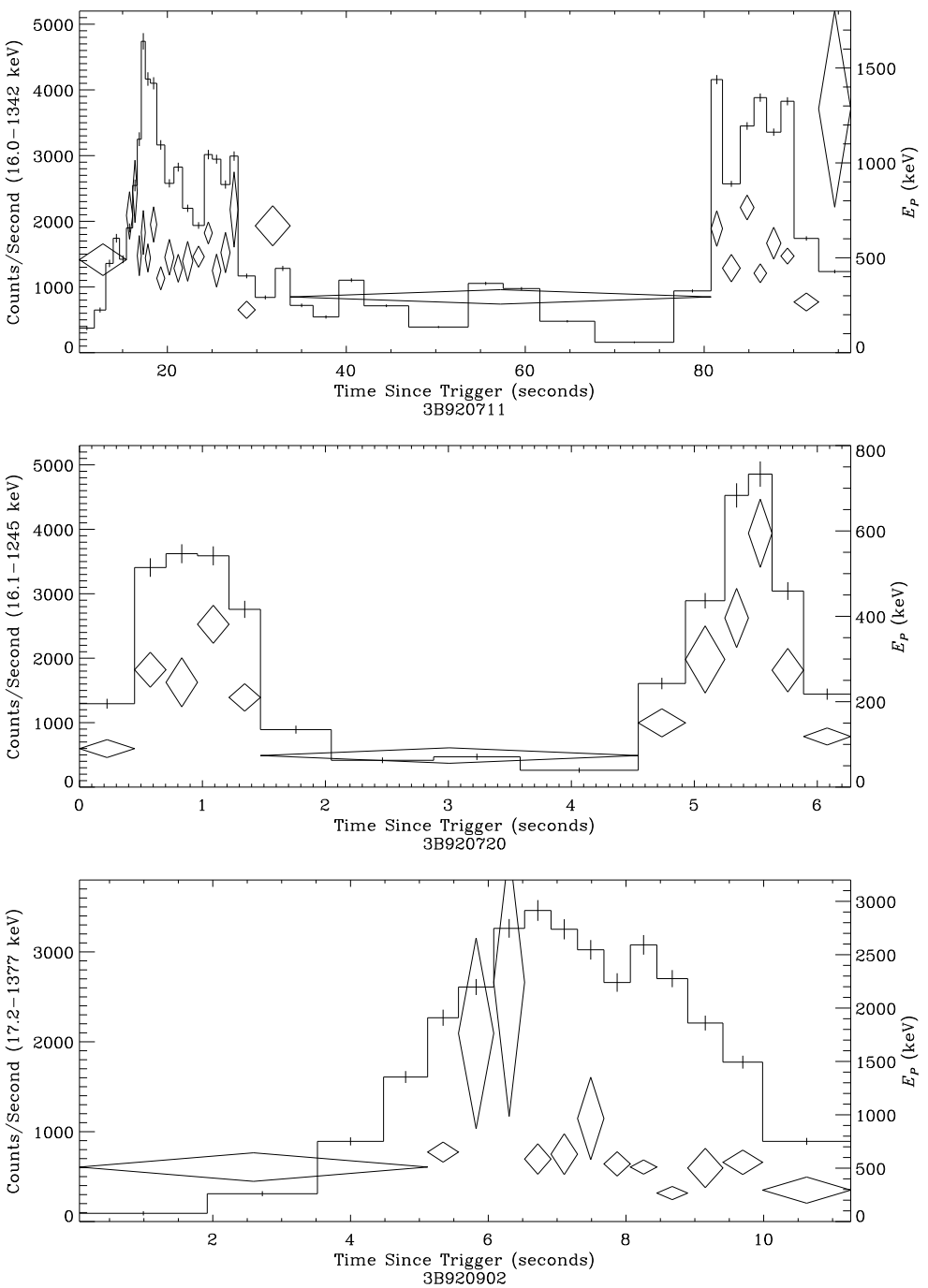

(Figure IV.5 continued)

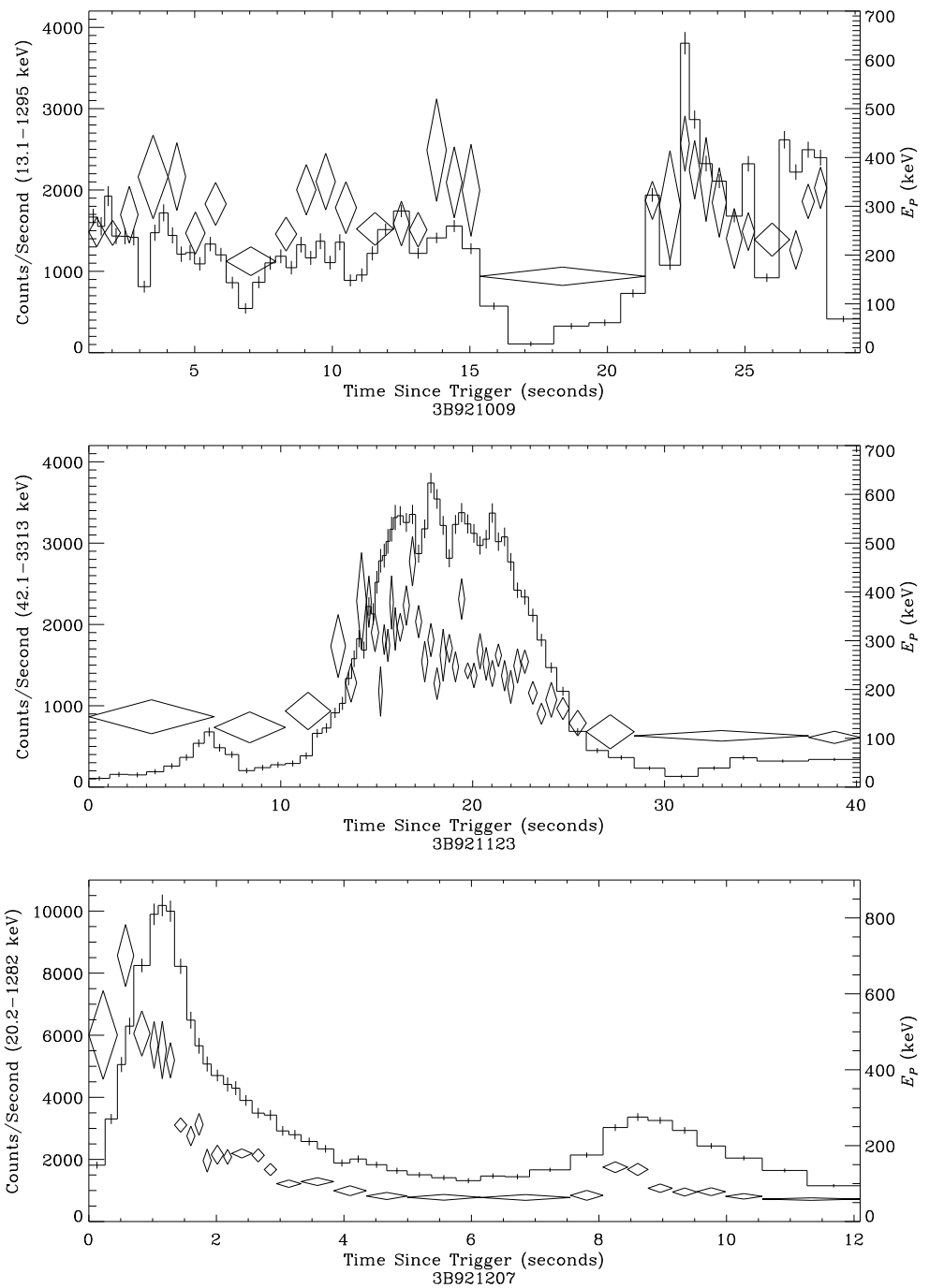

(Figure IV.5 continued)

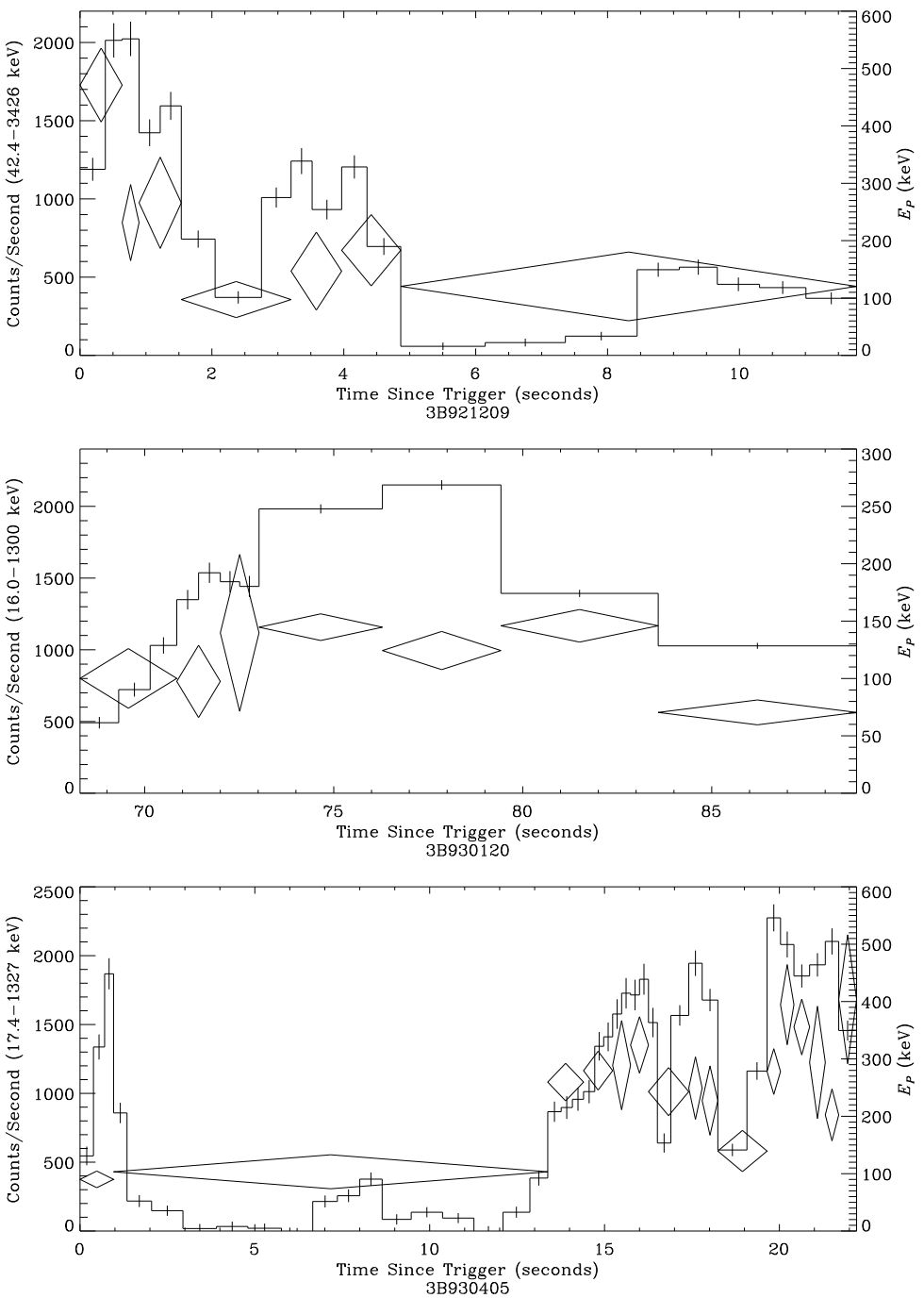

(Figure IV.5 continued)

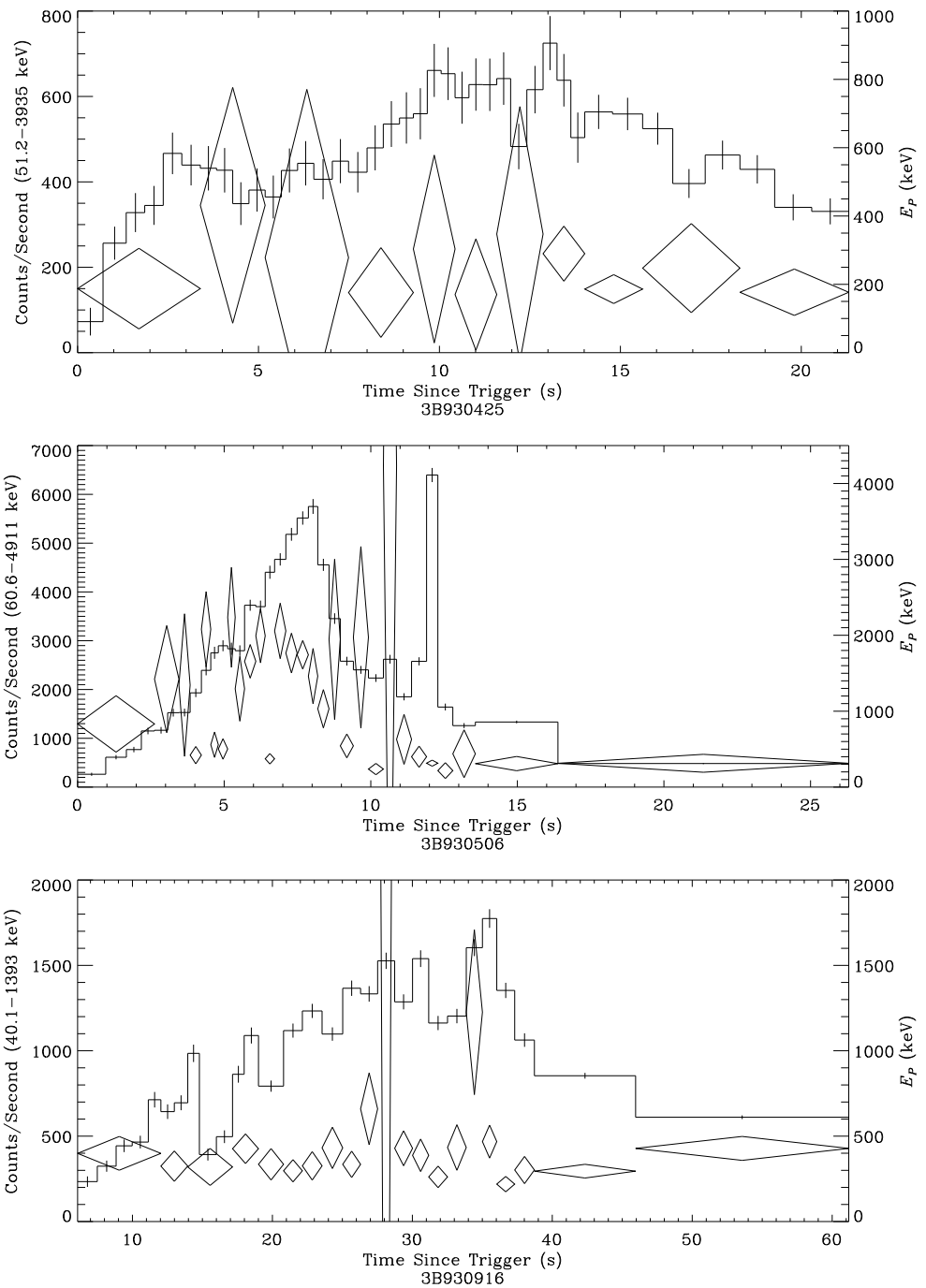

(Figure IV.5 continued)

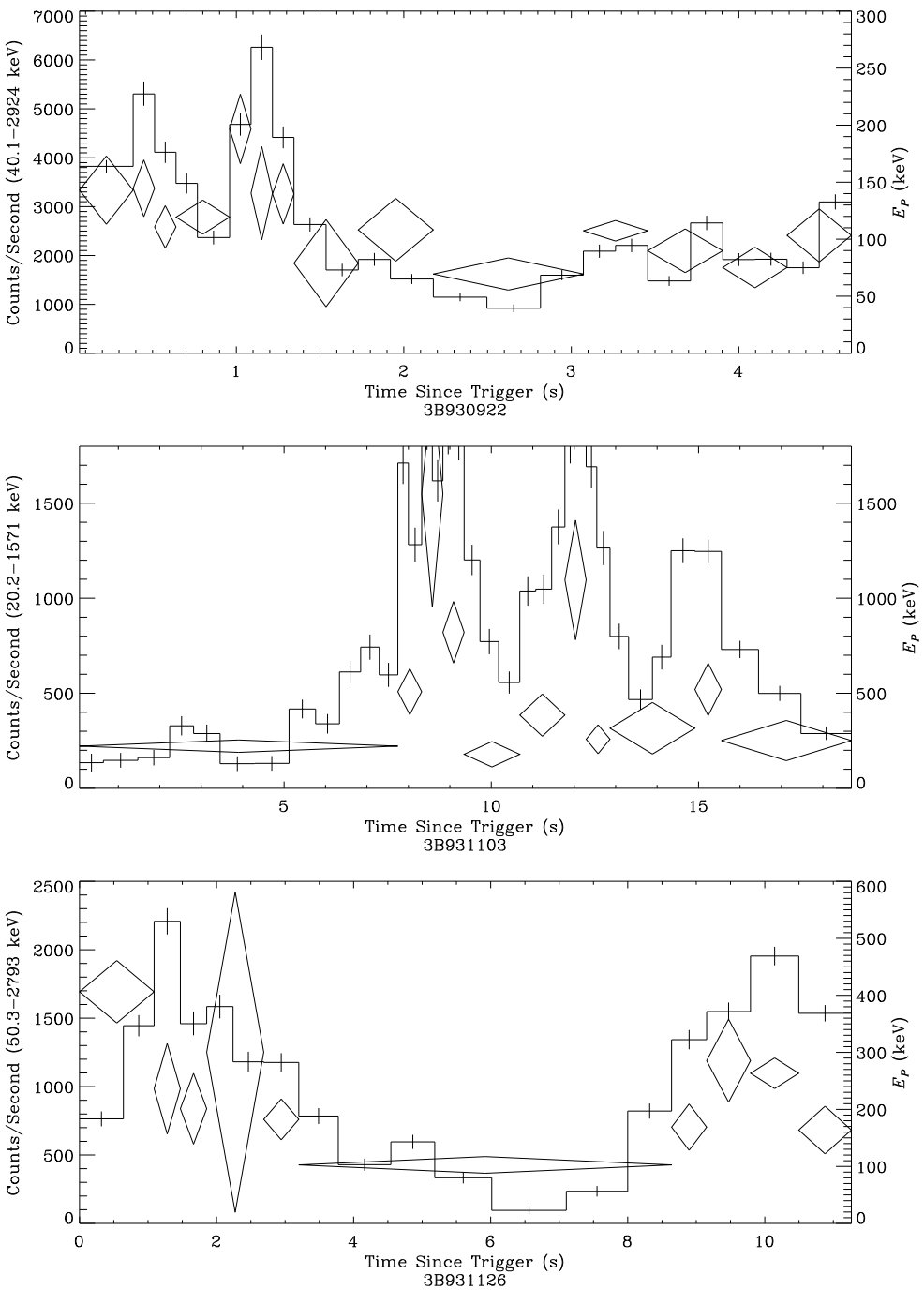

(Figure IV.5 continued)

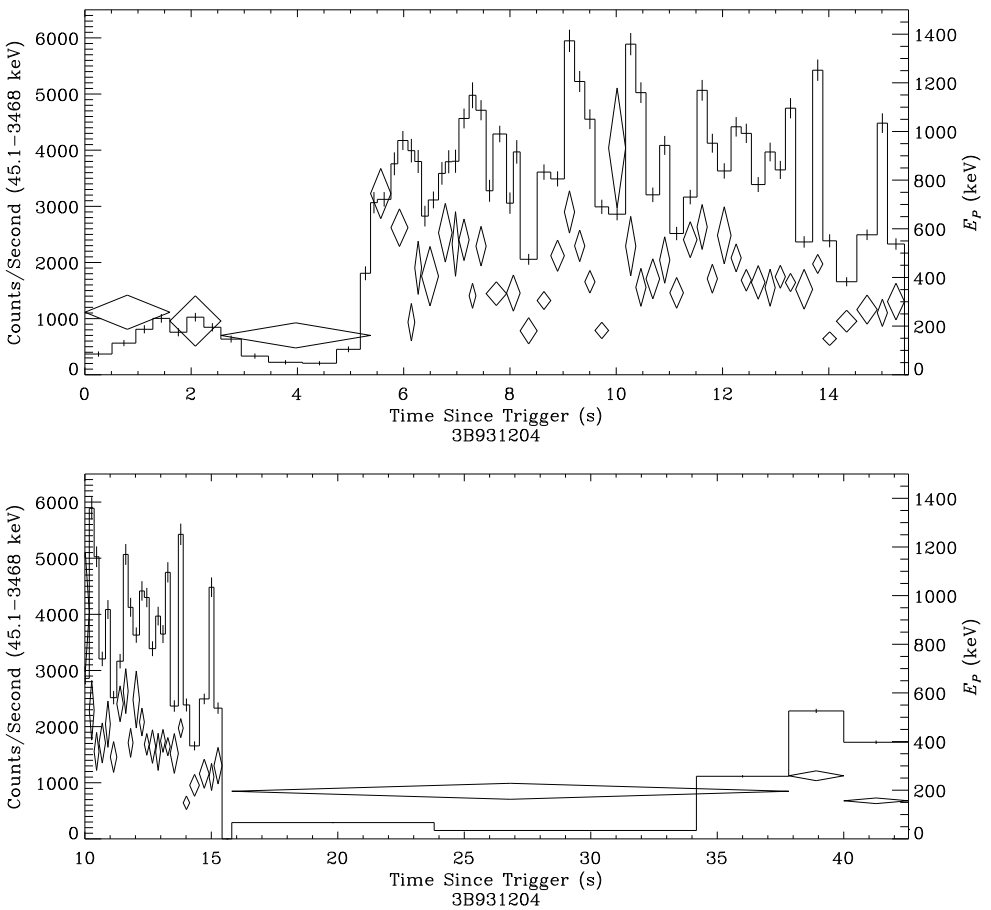

(Figure IV.5 continued)

The plots of Figure IV.5 were used to characterize types of evolution in E_P. The classification categories used were motivated by the work of G83 and N86 in which a spectral characteristic (i.e., OTTB temperature and hardness ratio respectively) was tied to changes in burst intensity. These categories describe both the tendency for variations in E_P to reflect changes in intensity (G83) and hard-to-soft evolution (N86). The categories are:

1. An increase in E_P occurring in proximity to a major intensity increase. E_P and intensity need not be morphologically identical and E_P can lead or lag the intensity increase by a small amount ($\lesssim$ 1 s).

2. General softening of E_P in time outside of intensity pulses over the entire burst. Regions which do not have a spike-like intensity profile are compared for this category. Spikes are considered to be short time intervals (less than a few seconds) in which the count rate was much greater than the rate in nearby intervals. For broader pulses, the first few seconds after the maximum count rate was achieved are considered part of the pulse, the remainder was considered inter-pulse emission.

3. Softening of E_P within intensity pulse structures. E_P should be harder early in the intensity pulse for a burst to fall in this category. It can be measured only if the pulse is temporally resolved.

4. Later intensity pulses have a softer peak in E_P than earlier pulses. This can only be measured if the burst has multiple intensity spikes.

Bursts were judged as showing the property in question, showing an opposite trend, or showing neither trend (+, −, and 0 respectively in Table IV.2). To demonstrate how a burst was categorized, consider 3B921207. This burst satisfies the first category because E_P hardens as the intensity increases at 0.5 and 8 seconds after the trigger. The interpulse region lies between 2.5 and 8 seconds, where E_P clearly softens. Both intensity spikes (0.5-2.5 seconds and 8-10 seconds after trigger) are temporally re-

# Observed	# Possible	Property
23	25	E_P– intensity association
20	30	E_P softens over whole burst
2	30	E_P hardens over whole burst
18	22	E_P softens within intensity spikes
1	22	E_P hardens within intensity spikes
9	17	Later spikes softer than earlier ones
1	17	Later spikes harder than earlier ones

Table IV.3: A summary of GRB spectral evolution observed for this sample.

solved and E_P softens in each. Finally, the peak E_P is softer in the later spike than in the first.

The rating system used here is admittedly simplistic, but is preferable to schemes which allow for finer distinctions within a class (e.g., rating bursts on a scale of 1-10, either discretely or continuously) for two reasons. First, the sample size is small so that the subdivision of bursts into several discrete subcategories reduces the significance of the classification. Second, the mediocre time resolution for some time intervals and sizable errors for some E_P create problems for a continuous classification scheme. Therefore, although the criteria outlined above are subjective, they are the least problematic given the state of the observations.

Individual bursts are detailed in Table IV.2 and characteristics for the sample as a whole are given in Table IV.3. Included in Table IV.2 are the median values of E_P and the range in E_P [$\Delta E_P \equiv \max(E_P)$-$\min(E_P)$] for each burst. Not all bursts could be classified because of large errors in E_P, unresolved structure, lack of structure, poor time resolution, etc. Bursts in which β was fit consistently at the upper constraint are noted in Table IV.2 as are bursts which were simultaneously observed in the 1-30 MeV range with the COMPTEL instrument on *CGRO* (Hanlon *et al.* 1994). In all four cases, the fitted β was consistent with power law fits to the COMPTEL data in that for bursts in which COMPTEL reported a power law of index > -2, β was consistently fit to the upper constraint. It can be seen from Figure IV.5 that there are several instances in which E_P was poorly fit resulting in a large error (σ_{E_P})

for this quantity. Spectra for which $\sigma_{E_P} \gtrsim 0.5 E_P$ were ignored when characterizing bursts and calculating ΔE_P.

Table IV.3 clearly demonstrates that increases in E_P are associated with rises in intensity and examination of Figure IV.5 shows that in many cases, the peak in E_P leads the intensity peak. A quantitative analysis of E_P leading intensity was not performed since Kouveliotou *et al.* (1992) found the typical lead time is shorter then the resolution of this sample. In addition, the time profile is extremely complex on short time scales so that a detailed study would best be performed using data with better time resolution. This data can be obtained from the LADs and the analysis is currently being performed (Preece *et al.* 1996b). Table IV.3 shows that many bursts undergo hard-to-soft evolution both within and outside of intensity spikes as well as between successive pulses. Softening of successive spikes is explicitly demonstrated in Figure IV.6, where the peak in E_P for early intensity spikes is compared to the same quantity in later spikes in multi-spike bursts. It can be seen that late pulses are more likely to be softer than those which occurred previously, suggesting that the maximum possible value for E_P is bounded by an envelope decaying in time. The trends noted above suggest that spectral hardness leads the intensity modulated by a decay envelope.

It should be mentioned that there are bursts in the sample which do not share the traits outlined above. This shows that while typical burst characteristics may have been identified, they are not universal on the time scale at which this sample was studied. However, it is not unreasonable to expect that E_P leading intensity and the softening trends noted above will be found in most bursts when observed at finer time resolution.

The general softening trends in E_P imply that the time at which emission occurs relative to the beginning of the burst is an important factor in spectral evolution. This raises an interesting question: assuming that the maximum values of E_P are bounded by an envelope decaying in time, then if a burst has a precursor several seconds before most of the emission occurs, does this envelope begin to decay

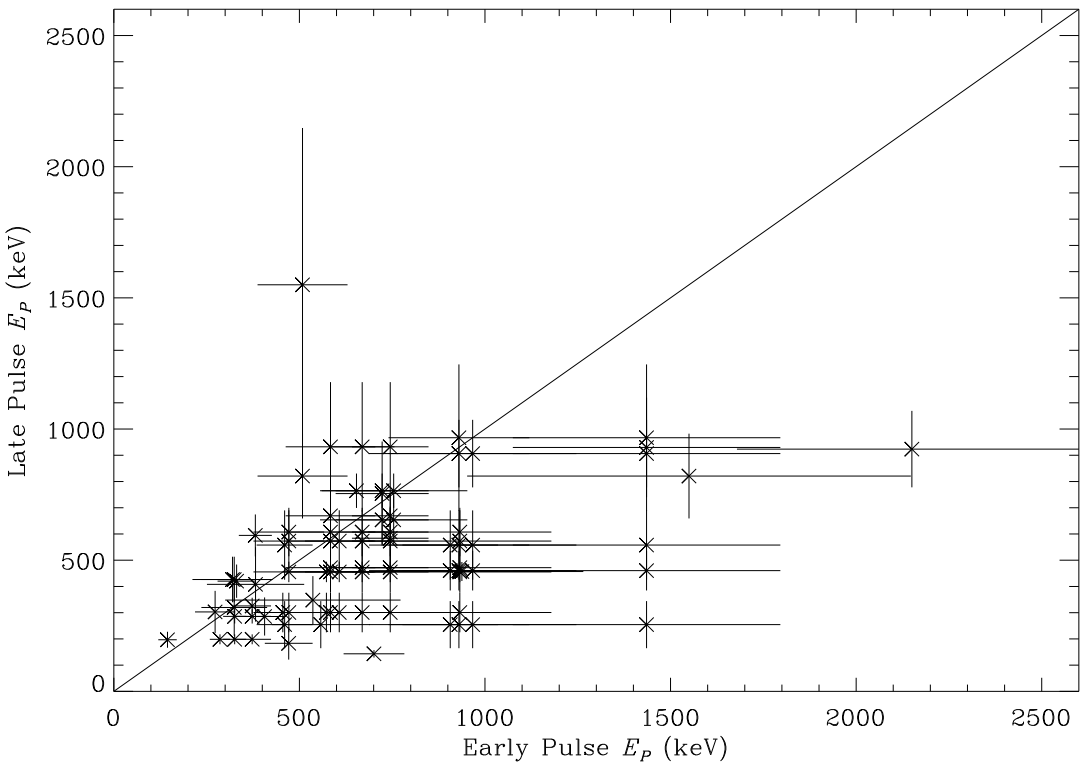

Figure IV.6: A comparison of the peak in E_P between intensity pulses within the same burst. The diagonal line indicates equality. Harder early pulses lie below this line and harder late pulses above it. The bursts used are those for which a +, −, or 0 answer could be determined for column 4 in Table IV.2. Several points line up vertically and horizontally since early pulses were individually compared to all those which followed.

	$\Delta E_P < 400$ keV	$\Delta E_P \geq 400$ keV
$t_d \neq 0$	10	7
$t_d = 0$	8	12

Table IV.4: This table shows little evidence that bursts in which emission is delayed evolve differently than those which emit promptly. However, although the criteria used to divide the sample is unbiased, it may not be appropriate since most bursts emit very soon after the trigger.

when the precursor happens or is the precursor irrelevant with respect to spectral evolution? To examine this question, the range in E_P and the time at which significant emission occurred relative to the BATSE trigger were compared (Figure IV.7). Significant emission was defined as emission capable of producing spectra which met the S/N criterion. In Figure IV.7 the horizontal bar indicates the period of significant emission. It begins at t_d, the time delay between the instrument trigger and the beginning of significant emission, and has length equal to the duration of significant emission (ΔT). A large value of t_d results when a long period of time passes between the trigger (a burst precursor) and the brightest emission. The data in Figure IV.7 occupy a triangular region indicating the sample was devoid of bursts with hard, highly evolving spectra which began emitting significantly well after the BATSE trigger: the few bursts with large t_d have small values of E_P and ΔE_P. To determine the importance of these bursts, the sample was divided into four groups based on the values of t_d and ΔE_P. Since there are no clear groupings in Figure IV.7, the divisions were $t_d = 0$ (significant emission at trigger) and ΔE_P=400 keV, which each divide the sample in half, producing an unbiased division. As shown by Table IV.4, bursts with $t_d \neq 0$ do tend to evolve less, but the significance of this result is small ($\sim 1\sigma$), implying that the apparent $t_d - \Delta E_P$ association may be a statistical aberration which will vanish when more bursts with large t_d are observed.

For several bursts, the nonzero time delay was short compared to the duration of significant emission. This suggests that the measure of time delay should be the ratio of t_d and Δt. This definition is preferable to the absolute measure since

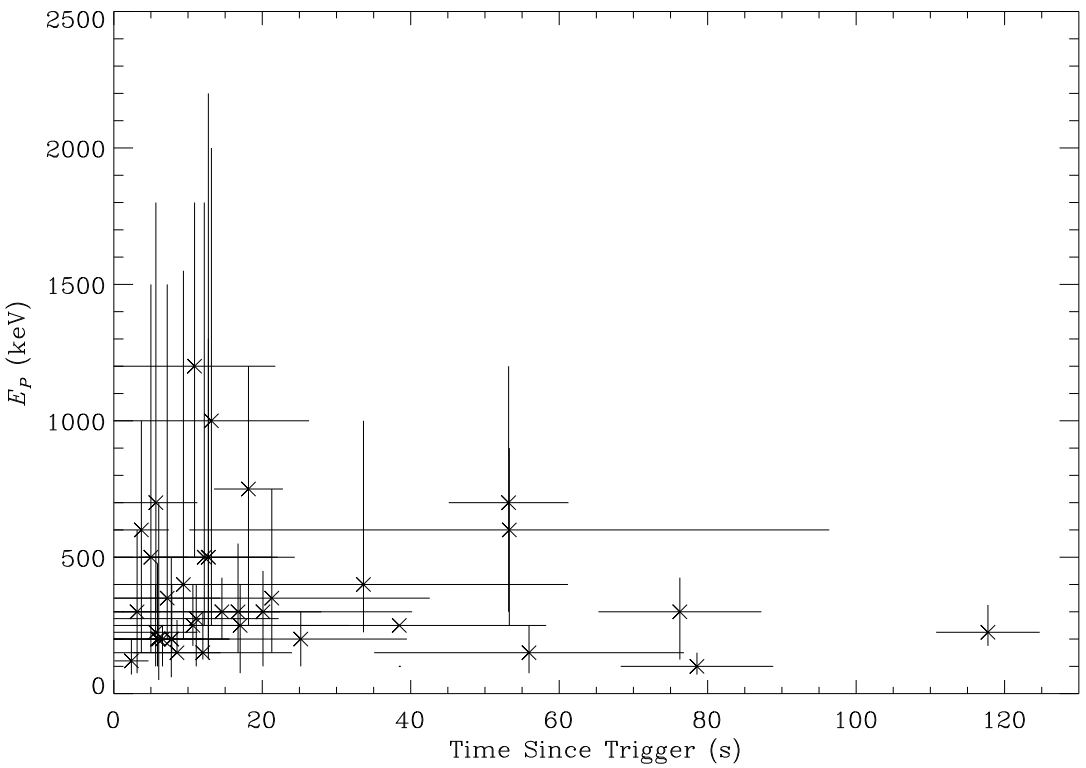

Figure IV.7: The range in E_P for a given emission time for all bursts in the sample. The vertical bars give the range in E_P (max-min) and the horizontal bars show the period during which significant emission occurred relative to trigger. The crosses mark median values.

$\frac{t_d}{\Delta T}$	Number	Min(ΔE_P) (keV)	Med(ΔE_P) (keV)	Max(ΔE_P) (keV)
> 0.25	10	80	300	950
≤ 0.25	27	120	525	2075
> 0.5	8	80	300	950
≤ 0.5	29	120	525	2075
> 0.9	7	80	300	950
≤ 0.9	30	120	525	2075
> 1	5	80	300	950
≤ 1	32	120	440	2075

Table IV.5: This table summarizes the differences in evolution of E_P for bursts grouped according to the time at which they emit.

it incorporates the time scale of the event from the trigger to the end of significant emission, allowing comparisons based on the time the burst began its most active stages and the total length of the burst. Bursts were divided into two groups based on the value of $t_d/\Delta t$. Table IV.5 shows the number of bursts in each group for several values of this ratio as well as the median and extreme values of ΔE_P for each group. The table shows that late emitters tend to show less E_P variability than bursts which emit promptly after the trigger. Although this is very suggestive, there is sizable overlap between the groups. Considering the small size of the sample, this result is not too significant and therefore the possibility of a dependence of ΔE_P on t_d should be treated with some caution.

IV.D Discussion

In this work it was shown that for most gamma-ray bursts, the energy of the peak of νF_ν is associated with and sometimes leads the intensity of the burst modulated by an envelope decaying in time. Indications that bursts whose main emission occurs at relatively long times after the trigger are generally soft and tend to evolve less in E_P were also found. In this section the phenomenological implications of these results are discussed. Some recently proposed burst models are also examined

in light of the observations reported here and no qualitative conflicts between the models considered and observations are found.

IV.D.1 Phenomenological Implications

While it has been known for some time that burst spectra tend to evolve from hard to soft (N86), the observations presented here show that the time of emission relative to the beginning of the burst may also determine how the spectral hardness evolves. For optically thin burst models (in which particles radiate on time scales much shorter than the resolution of SHERB spectra), these results imply that as the burst transpires, the emission region 'remembers' previous emission suggesting that either emission comes from only one region or that different emission regions must be physically connected. The softening of successive intensity pulses could be caused by significant change in the emitting region during intense episodes (such as an expansion or an increase in the number density of particles). The softness of delayed emission implies that the emission region can evolve without observable radiation. For optically thick models, a burst could be the result of a single energy input since the radiation does not escape the region on short time scales. If the region cools by adiabatic expansion and the surface of last scattering does not propagate inward to higher temperature regions too quickly, then observable radiation would be expected to evolve from hard-to-soft. The softness of delayed emission could also be explained in this way if the region was not able to emit significantly during the initial stages of expansion.

The hard-to-soft spectral evolution within pulse structures indicates that intensity spikes are not symmetric in time. Nemiroff *et al.* (1994b) reached a similar conclusion by examining the time structure of intensity profiles. These observations clearly show that time symmetric models of spectra formation as well as overall intensity profiles cannot be correct. An example of the kind of model eliminated by these observations is symmetric beam models in which the beam sweeps by much faster than the time scale over which the beam changes.

Another implication of this work relates to burst duration classes. The distribution of gamma-ray burst durations observed by BATSE is bimodal and short bursts (duration $\lesssim$ 2 s) tend to have larger hardness ratios than longer ones (Koveliotou *et al.* 1993b; Lamb, Graziani, & Smith 1993) where the hardness ratios were averaged over the whole burst. Based on the large values of ΔE_P reported here and the fact that the hardest emission tends to come early in a burst, short bursts are expected to be harder than long ones since they do not have softer tails, not necessarily because of an inherent difference in the radiation mechanism. An example of the effect of time averaging is burst 3B920525. If spectra from 4.16-6.72 s (the first spike) are used E_P=650$\pm$70 keV but falls to 421$\pm$25 keV if the entire burst is integrated into one spectrum. As Norris *et al.* (1994) also suggested, if hardnesses are measured over the same absolute time interval (e.g., compare short bursts to the first few seconds of long bursts), the hardness distribution may be the same for both classes.

In B93 it was shown that E_P varied considerably from burst to burst indicating that there is no universal characteristic energy of burst emission. One conclusion which was drawn from this was that pair processes could be directly observed only if burst sources had a broad range of redshifts. Such processes would produce spectra with an annihilation feature at 511 keV and would cut off above this energy because of pair opacity. The observed energy of these features depends on the redshift of the source region. The argument against observable pair processes can be extended by noting the large changes in ΔE_P observed within many bursts in this sample (Table IV.3). Unless the emission process involves large and rapid changes in redshift, pair processes cannot be directly observed in burst spectra.

The data in Figure IV.7 include several bursts in which the emission was prompt but had small ΔE_P. An interesting possibility is that these prompt emitting, relatively non-evolving bursts were preceded by a precursor too faint to trigger BATSE. In this case, bursts which occupy the lower left-hand corner of the figure are late emitters for which BATSE did not trigger on the initial event. A less exciting

possibility is that bursts which emit late but evolve considerably exist and there is no relation between emission time and ΔE_P. Although this type of behavior is not seen, it cannot be ruled out because of the small sample size and rarity of late emitters (about one strong burst per year with t_d >60s). Therefore, this may remain an open question even if BATSE detects many bursts over the next few years.

IV.D.2 Implications for Burst Models

A plethora of gamma-ray burst scenarios have been proposed (Nemiroff 1994a). However, most attempt to explain only general spectral characteristics and energetics with little or no mention of how spectra are expected to evolve. Therefore, several models are examined to find those which can accommodate the observations presented here. Because BATSE observations of burst isotropy and inhomogeneity have cast serious doubt on older models, only those proposed after 1991 (the year BATSE was launched) are considered. Discussion is further restricted to models which purport to explain all or most gamma-ray bursts. Although arguments have been made for two population distributions (Lingenfelter & Higdon 1992; Smith & Lamb 1993), the inability to separate bursts into two uncontroversial classes makes such discussion premature. Jet models are also avoided (c.f. Brainerd 1992; Dermer & Schlickeiser 1994) since the phenomenon is poorly understood and the models are incomplete. 'Exotic' sources such as cosmic strings (Paczyński 1988), strange stars (Haensel, Paczyński, & Amsterdamski 1991), or primordial black holes (Cline & Ho 1992) are also omitted since the existence of such sources is highly speculative.

The distribution of bursts seen by BATSE has forced bursts out to extended halo or cosmological distances if they arise from a single source population. Since source regions are inferred to be small from the fast rise times of bursts, the energy density at the source must be enormous, particularly if the burst radiates isotropically. Therefore, many models incorporate optically thick relativistic electron-positron fireballs. As originally proposed (Goodman 1986; Paczyński 1986), fireballs cannot explain the observed nonthermal emission and will not be relativistic if the fireball is

contaminated by baryons (Cavallo & Rees 1978; Paczyński 1990). Many different scenarios have been proposed recently (c.f. Narayan, Paczyński & Piran 1992; Usov 1992; Woosley 1992) which can essentially be reduced to a fireball which must either form in a region free of baryons or break through a cloud of baryons to be observed. In these cases, the observed nonthermal spectra are produced either by several thermal black bodies at different temperatures (corresponding to different fireballs) or through interactions with a strong or turbulent magnetic field. If a number of fireballs occur, then hard-to-soft spectral evolution could be explained by the creation of low temperature fireballs or rapid cooling as the burst transpires. For magnetic interaction models, the general softening of E_P may reflect a gradual decline in available energy as the field evolves into a stable configuration.

Mészáros & Rees (1992) have proposed a model involving a baryon contaminated fireball from any source, galactic or cosmological. The baryons in the fireball interact with the interstellar medium (ISM) to form a relativistic shock where gamma-rays are radiated. Hard-to-soft evolution could be explained either by the most energetic baryons reaching the shock first or the gradual decline of average energy as more particles encounter the shock. The softness of late emission could be a consequence of the baryon front losing energy to the ISM before the shock is fully formed or could arise from the shock losing energy as it propagates through the ISM.

In a different type of model suggested by Melia & Fatuzzo (1992), a gamma-ray burst is generated by sheared Alfvén waves from a radio pulsar. The waves are created by crustal disturbances at the polar cap which flood the magnetosphere with charged particles. These charges upscatter ambient radio photons to gamma-ray energies which are beamed outward. Hard-to-soft evolution may result from the most energetic charges scattering first and successive spikes soften if subsequent disturbances are less energetic than the original disturbance. Since the emission is beamed, the hard emission might occur when the beam was not pointed in our direction. Delayed emission might be soft because the early hard emission was not beamed in our direction.

IV.E Summary

In this work, the evolution of the energy of the maximum flux per logarithmic energy band (E_P) in long, bright gamma-ray bursts was studied using high energy resolution spectra from the BATSE SDs. I found that E_P is coupled with the intensity of a burst (either leading or accompanying intensity increases). These results are consistent with previous studies by N86 and Bhat *et al.* (1994a) and show that the work of G83 and K94 did not have sufficient temporal resolution to accurately describe spectral evolution. In addition to resolving the disparity between previous studies, I found that the maximum values of E_P are modulated by and envelope decaying in time so that late spikes are softer than early spikes in a given burst. Indications were also found that bursts in which significant emission is substantially delayed relative to the instrument trigger tend to be soft and evolve less in E_P although the significance of this result is low. Several burst models were examined in light of these results and it was found that none of those discussed could be ruled out on the basis of these results alone. However, as the models mature to the point of more precise spectral predictions, the observations presented here may prove to be a useful constraint or suggest directions for further effort.

Chapter V

Extrapolations to the Optical–UV

V.A Introduction

Perhaps the greatest impediment to theoretical progress in studies of GRBs is that the sources of of these events are unknown. Although it is widely thought that neutron stars are involved, at present there is no consensus on even the broadest details of the physical processes involved. The main reason for this is that the distance to GRBs is not known. Many have interpreted Burst and Transient Source Experiment (BATSE) observations of GRB isotropy and boundedness in space (Fishman *et al.* 1994) as an indication that bursts are at cosmological distances. Attempts have been made to verify this conclusion with BATSE data (Davis *et al.* 1994; Norris *et al.* 1994) but the claims are controversial (Band 1994; Brainerd 1994) and the possibility of a Galactic origin has not been ruled out (c.f., Podsiadlowski, Rees, & Ruderman 1995). Uncertainty in the distance to GRBs leads to uncertainty in the energy required to generate observed GRBs and hence, confusion about the source physics. If the distance scale to GRBs can be determined, it could be the greatest step yet taken toward understanding these enigmatic events.

An excellent way to establish the GRB distance scale is to discover counterparts at other wavelengths. Counterparts could also reveal valuable information about burst sources and environments which would have an enormous impact on our

physical understanding of these events. For example, if GRBs were found only in a particular environment, properties unique to that environment would likely be responsible for the burst. Many groups (see Schaefer 1994; Greiner 1995) have attempted to find counterparts which flare along with the burst, are observable in quiescence, or appear as afterglows. To date, convincing counterparts have been found only for soft gamma repeaters, which many believe to be unrelated to GRBs (though this opinion is not universal, see Rothschild & Lingenfelter 1996). Several theories have been been suggested which predict emission at wavelengths other than gamma-rays (a number of them are listed in Schaefer 1994) although the guidance they provide is slim considering that many were advanced at a time when bursts were thought to originate at distances $\lesssim 1$ kpc, much closer than is now believed.

A GRB model which predicts simultaneous optical emission and assumes a distant burst source has recently been proposed by Katz (1994). In this scenario, ejecta from a violent event (such as the collision of two neutron stars) interact with the interstellar medium creating a relativistic shocked plasma. Particles in the plasma radiate a synchrotron spectrum at optical energies. Although this model takes into account BATSE observations, it has not yet achieved universal acceptance.

Since there are no clear expectations as to how a burst source will appear in quiescence or just after the gamma-ray event, in this work all optical emission is assumed to occur at the same time as the high energy emission and is linked to the gamma-ray emission. Several models predict this kind of concurrent low energy emission based on the reprocessing of gamma-rays in a neutron star magnetosphere (Hartmann, Woosley, & Arons 1988), an accretion disk (Epstein 1985) or a stellar companion (London & Cominsky 1983). These models all assume nearby (~ 100 pc) sources and consequently much smaller source energies ($\lesssim 10^{38}$ ergs) than is implied for bursts in the Galactic halo or at cosmological distances ($\gg 10^{41}$ ergs). Since it is unclear what effect such a large energy release will have on the reprocessing region, the utility of these theories is questionable.

Lacking compelling theoretical expectations, an empirical approach is taken

to determine how bright simultaneous counterpart emission may be by extrapolating spectra observed by BATSE to optical and ultraviolet energies. Several experiments capable of detecting simultaneous optical emission from a GRB are described and the implications of these results for these experiments are discussed.

V.B Analysis

Extrapolated fluxes are based on spectral fits to 54 bright GRBs from the first 13 months of BATSE operation (Band *et al.* 1993). The bursts were selected with a brightness criterion based on the peak count rate in the $50-300$ keV energy band. Most bursts which met the intensity requirement were included in the sample, but there were a few exceptions. Bright bursts shorter than one second were left out of the sample while some dim bursts with interesting time structure were included; the number in both cases was small. Although the sample is not statistically complete, it is representative of bright bursts.

In this work, interstellar absorption is ignored. While this effect will render sources which must be observed through the Galactic plane invisible in the optical-UV band, it is far less important above the plane. Near the Galactic poles, absorption typically dims sources by $\Delta m_V \sim 0.3$ (Mihalas & Binney 1981, p.181). The exact amount of absorption depends on the amount of interstellar matter along the line of sight, something which is not a simple function of elevation angle above the plane because of the clumpy nature of the interstellar medium. Given the large range of magnitudes which results from extrapolation of the spectrum over four energy decades, the additional complexity of modeling interstellar absorption of order $\Delta m_V \sim 0.3-1$ off the Galactic plane is not warranted.

Band et al. (1993) fitted spectra averaged over the entire burst to a four parameter function of the form

$$N_E(E)\left(\frac{\text{photons}}{\text{keV-s-cm}^2}\right) = \begin{cases} A\left(\frac{E}{100\text{ keV}}\right)^{\alpha} e^{-E/E_0}, & E \le (\alpha-\beta)E_0 \\ A'\left(\frac{E}{100\text{ keV}}\right)^{\beta}, & E > (\alpha-\beta)E_0 \end{cases} \tag{V.1}$$

where A, α, β, and E_0 were fit to observed spectra and A' was chosen to make the function continuously differentiable everywhere. The energy range covered by the fit varied, with typical low energy values of $10 - 30$ keV and upper cutoffs of $1 - 3$ MeV. This is a differential photon number spectrum which must be multiplied by energy, $F_E(E) = N_E(E)E$, to get the energy flux. Note that the spectral indices in equation V.1 do not have an explicit minus sign.

The fitted spectra were extrapolated down to 1 keV where they connected to a power law with a different energy index which describes the lower energy spectra. The index of the low energy extrapolation was varied from -4 to 4 in integer steps. In addition, a low energy power law spectrum of index $\alpha + 1$ was extrapolated. This last extrapolation is just an unmodified continuation of the high energy spectrum.

Discussions of counterpart emission are conventionally based on burst fluence; expected magnitudes are presented as if all the emission occurred in one second (Schaefer 1981). Although this is not consistent with the assumption of strictly simultaneous optical emission, it is a useful exposure-time independent standardization. Fluence based magnitudes were calculated in the energy bands of the U, B, and V filters and the $5 - 7$ eV bandpass of the UV camera array on the High Energy Transient Explorer (HETE, discussed below). For the first three bands, spectra were convolved with the filter response functions (Budding 1993, p. 46) and fluxes were converted to magnitudes. The HETE bandpass is not a standard wavelength band so the entire flux in the $5 - 7$ eV band was calculated. Expected magnitudes for a one second exposure are given in Table V.1 and distributions for the $\alpha + 1$ extrapolation are shown in Figure V.1 (the distributions for other indices have similar, but not identical shapes). This differential distribution peaks because only bright bursts were selected. If all BATSE bursts had been included, the distribution would continue to rise as a function of magnitude.

Although fluence-based measures of brightness are the standard, flux-based measures are more meaningful when detector exposure durations are comparable to the burst duration (optical emission is assumed to have the same duration as the

Index	min(m_V)	median(m_V)	min(m_B)	median(m_B)
$\alpha+1$	7.8	15.3	8.0	15.4
-4	-17.3	-12.3	-16.1	-11.1
-3	-10.7	-5.7	-9.7	-4.7
-2	-4.1	0.9	-3.4	1.6
-1	2.5	7.5	3.0	8.0
0	9.1	14.1	9.3	14.3
1	15.7	20.7	15.6	20.6
2	22.3	27.3	22.0	27.0
3	28.9	33.9	28.3	33.3
4	35.5	40.4	34.6	49.6
Index	min(m_U)	median(m_U)	min(flux)†	median(flux)†
$\alpha+1$	7.2	14.4	1.03×10^{-11}	1.72×10^{-14}
-4	-16.0	-11.1	3.13×10^{-3}	3.57×10^{-5}
-3	-10.0	-5.0	1.81×10^{-5}	2.06×10^{-7}
-2	-3.8	1.2	1.05×10^{-7}	1.20×10^{-9}
-1	2.3	7.3	6.22×10^{-10}	7.08×10^{-12}
0	8.4	13.4	3.70×10^{-12}	4.21×10^{-14}
1	14.5	19.5	2.22×10^{-14}	2.53×10^{-16}
2	20.6	25.6	1.34×10^{-16}	1.52×10^{-18}
3	26.7	31.7	8.21×10^{-19}	9.34×10^{-21}
4	32.8	37.8	5.06×10^{-21}	5.76×10^{-23}

†Values for HETE are in terms of ergs/cm^2-s in the $5-7$ eV band.

Table V.1: The expected brightness for a fluence based extrapolation of GRB spectra to optical wavelengths. All values assume the entire burst occurred in 1 s.

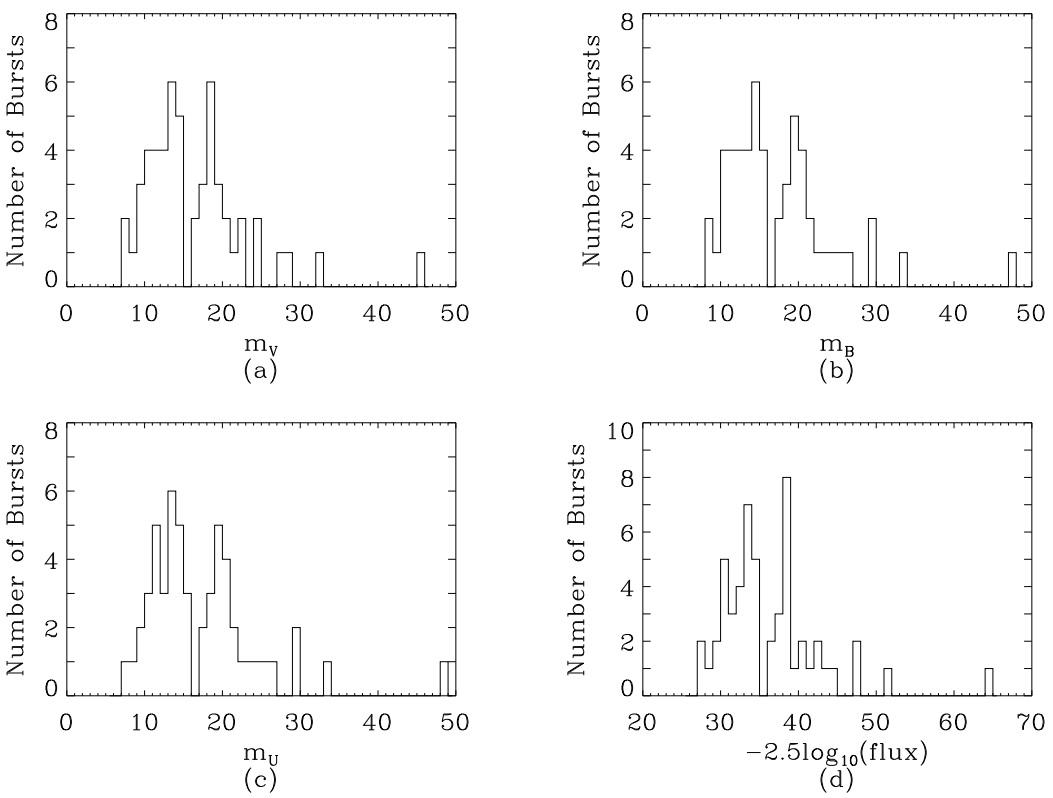

Figure V.1: The number of bursts at a given fluence-based magnitude (entire burst occurs in one second) assuming the flux extrapolates as a power law of index $\alpha + 1$ from the gamma-rays and a one second exposure. Panels (a)-(d) are the V, B, U, and $5 - 7$ eV (HETE) bands respectively. Note: Only bright bursts included. If all BATSE bursts had been included in the sample, this differential distribution would continue to rise as the magnitude increased, not peak as indicated here.

gamma-ray emission). This distinction is unimportant when the exposure time is longer than the burst since the entire burst fluence will be observed. If, however, the exposure time is shorter than the burst, then only a fraction of the total flux is observed and fluence-based measures will overestimate the brightness of a burst.

Another concern when dealing with real experiments is spectral response. All the instruments considered except HETE are ground based and sensitive between $\sim 4000 - 7000$Å. Although this energy band is very wide, the convention is to define sensitivities in terms of V magnitudes. Therefore, spectra were convolved with the response function of the V-filter and the flux converted to magnitude. This introduced slight errors in the comparison of observability because the GRB spectra were assumed to be power laws while the sensitivities of the instruments were determined using stars, which have black body continua. These errors are not large however and a proper treatment would require detailed knowledge of the complicated response functions of the various experiments.

For each instrument the expected observed flux was calculated within each experiment's exposure time. In all cases, the detector response was assumed to be linear (no saturation). If a burst was shorter than the exposure time, the entire flux of the burst was averaged over the exposure time (equivalent to the fluence-based magnitude with dilution for exposure times > 1 s). If the burst was longer, the average flux over the exposure time was used. This process can be expressed mathematically as

$$m_V = 2.5 \log(T f_V / f_0), \tag{V.2}$$

where f_V is the V band extrapolated flux and f_0 is the V band flux of a magnitude zero object (3.08×10^{-9} ergs/cm^2-s, Budding 1993, p. 46). T is defined as

$$T = \begin{cases} 1 & t_{exp} < t_{dur} \\ t_{dur}/t_{exp} & t_{exp} > t_{dur}, \end{cases} \tag{V.3}$$

where t_{exp} is the instrument exposure time and t_{dur} is the burst duration. The case where $t_{exp} < t_{dur}$ is an approximation to the true instantaneous flux because intensity and spectra vary within a burst (Ford *et al.* 1995). Although the spectral changes are

not as radical as intensity fluctuations, spectral variations are amplified by the four decade extrapolation to the optical from the lowest energy gamma-rays included in the original spectral fits.

Better sensitivity can be obtained for the short exposure instruments by adding subsequent images together. This effect was not considered since approximately one magnitude is gained for a typical burst. This boost in sensitivity is likely to be more than compensated by the neglect of slew times for telescopes which respond to a burst trigger since typically the brightest emission occurs early in the burst.

V.C Instrumentation

Instruments which can detect simultaneous optical emission from GRBs can be grouped into two categories. The first has large fields-of-view and long exposure times ($>$ 30 min). These telescopes were designed for meteor patrols but their large fields-of-view make them well suited for GRB detection. Many of these instruments are outlined in Greiner *et al.* (1994). Those most likely to image a field containing a GRB because of their large fields-of-view are sky patrols from Sonneberg, Ondřejov, Odessa, and Dushanbe. Although the patrol plates have a variety of sensitivities and exposure times, the sky patrol plates from Ondřejov are of particular interest because its field-of-view is particularly wide and it has three coincidences with bursts in the Band *et al.* (1993) sample (Greiner *et al.* 1994).

The second class of instruments considered is characterized by short exposure times. These instruments are much more sensitive to GRBs, which seldom last more than a few minutes (the longest burst in our sample is 130s). Four experiments are considered here: the Explosive Transient Camera (ETC, Vanderspek *et al.* 1992), the Gamma-Ray Optical Counterpart Search Experiment (GROCSE, Akerlof *et al.* 1994), the Gamma-ray To Optical Transient Experiment (GTOTE, S. Barthelmy 1995, private communication), and the Ultraviolet Transient Camera Array on the

Observatory or Instrument	Field of View (sr)	Exposure Time	Sensitivity
Sonneberg[c]	0.15	40 m	$6(m_B)$[a]
Ondřejov[c]	4.36	4 hr	$3(m_V)$[a]
Odessa[c]	1.10	30 m	$6(m_B)$[a]
Dushanbe[c]	0.49	1 hr	$6(m_V)$[a]
ETC[d]	0.75	5 s	$11(m_V)$[b]
GROCSE[e]	0.621	0.4 s	$13(m_V)$[b]
GTOTE[f]	$0.06 - 0.12$	$3.3 - 4$ s	$12 - 14$ (m_V)[b]
HETE[g]	1.7	4 s	8×10^{-9} ergs/cm^2-s$(5 - 7$ eV$)$[b]

[a]Limiting magnitude for 1s flash.
[b]Sensitivity to field stars.
[c]Greiner *et al.* (1994).
[d]Vanderspek *et al.* (1994).
[e]Akerlof *et al.* (1994), values for the second generation camera are used here.
[f]S. Barthelmy (1995), private communication (preliminary).
[g]Ricker *et al.* (1992); R. Vanderspek (1995), private communication.

Table V.2: A summary of the characteristics of optical counterpart search experiments.

HETE spacecraft (Ricker *et al.* 1992; Vanderspek *et al.* 1995). All of these instruments monitor a portion of the sky but the ETC, GROCSE, and GTOTE can slew to preliminary BATSE positions distributed on the BACODINE network (Barthelmy *et al.* 1994). BACODINE requires up to five seconds to localize a GRB and another few seconds to distribute the coordinates on the network. After that, the telescope must slew to the proper position. These delays will often result in bright portions of the burst being missed by the telescope. These concerns are ignored here so the extrapolated brightness may be somewhat optimistic. Characteristics of all the instruments mentioned here are presented in Table V.2.

	ETC, GTOTE & GROCSE		Ondřejov[1]		HETE[2]	
Index	min (m_V)	median (m_V)	min (m_V)	median (m_V)	max ($flux$)	median ($flux$)
$\alpha+1$	9.9	19.2	18.2	25.7	1.57×10^{-12}	5.12×10^{-16}
-4	-15.2	-8.8	-6.9	-1.9	4.75×10^{-4}	1.52×10^{-6}
-3	-8.6	-2.2	-0.3	4.7	2.75×10^{-6}	8.82×10^{-9}
-2	-2.0	4.4	6.3	11.3	1.60×10^{-8}	5.14×10^{-11}
-1	4.6	11.0	12.9	17.9	9.44×10^{-11}	3.03×10^{-13}
0	11.2	17.6	19.5	24.5	5.61×10^{-13}	1.80×10^{-15}
1	17.8	24.2	26.1	31.1	3.37×10^{-15}	1.08×10^{-17}
2	24.4	30.8	32.7	37.7	2.04×10^{-17}	6.54×10^{-20}
3	30.9	37.4	39.3	44.3	1.25×10^{-19}	4.00×10^{-22}
4	37.5	44.0	45.9	50.9	7.68×10^{-22}	2.46×10^{-24}

[1]Values for Sonneberg, Odessa, and Dushanbe are typically 2 magnitudes brighter than for Ondřejov.
[2]Values for HETE are in terms of ergs/cm^2-s in the $5-7$ eV band.

Table V.3: The expected brightness of GRBs using a flux based extrapolation of the gamma-ray spectrum.

V.D Discussion

The flux-based magnitudes of bursts expected are given in Table V.3. Figure V.2 shows the V-band brightness distribution of the sample for the $\alpha+1$ extrapolation (the simple extrapolation from the gamma-ray fits) for the ETC. The other extrapolations have similar shapes with the magnitude scale shifted. Although the ETC, GROCSE, and GTOTE have varying integration times, only six of the 54 bursts in the sample were shorter than five seconds (the exposure time of the ETC). These bursts are slightly brighter in GROCSE and GTOTE. The difference is only a few tenths of a magnitude though and the resulting distributions have the same maximum and median brightness. The overall distributions are almost identical as well so that Figure V.2 applies to all three of these experiments.

An interesting case with an immediate physical interpretation is a power

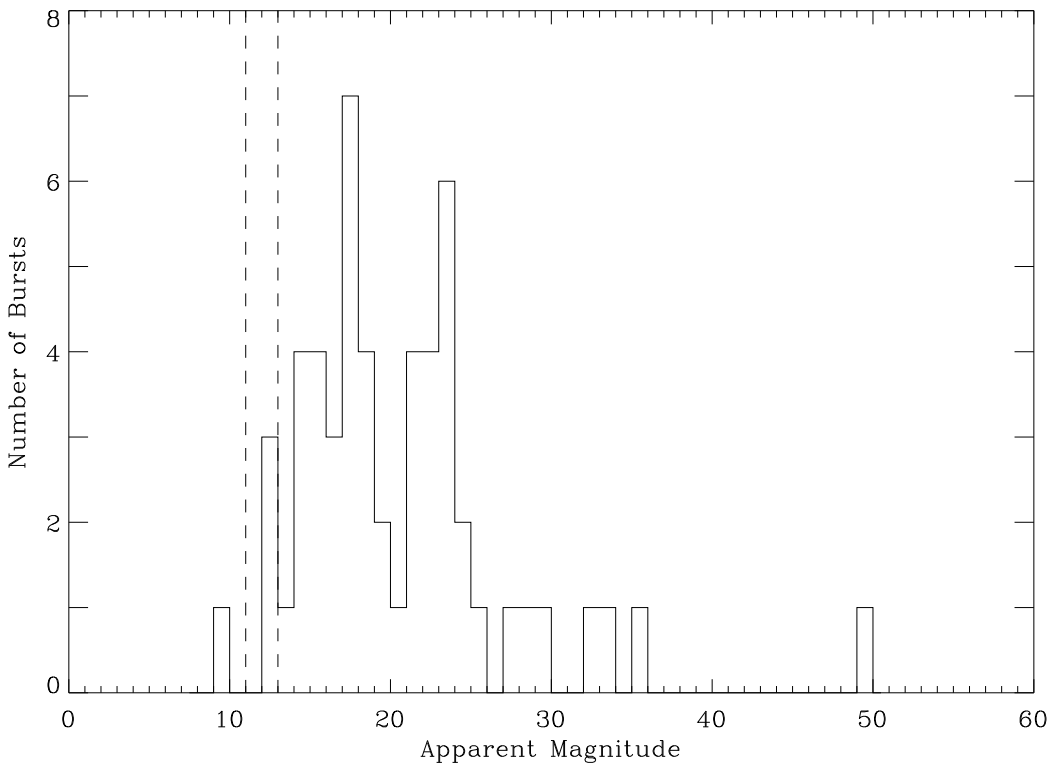

Figure V.2: The number of bursts at a given flux-based magnitude for a five second exposure assuming the flux extrapolates as a power law of index $\alpha + 1$ from the gamma-rays. The dashed lines indicate the sensitivities of the ETC ($m_V = 11$) and GTOTE and GROCSE ($m_V = 13$) experiments. Note: Only bright bursts included. If all BATSE bursts had been included in the sample, this differential distribution would continue to rise as the magnitude increased, not peak as indicated here.

law of index 2. This spectral form would result from a thermal distribution of particles with temperature greater than 1 keV, which is certainly possible in a burst environment. Table V.3 shows that if this is the only component of concurrent GRB emission at lower energies, GRBs will not be observable at optical or UV wavelengths (assuming no afterglow).

These calculations can also be applied to the synchrotron emission model of Katz (1994). This model predicts a low energy flux $F_E \propto E^{1/3}$. If this type of emission occurs, then the brightest burst in this sample would have appeared as a $m_V \sim 13$ transient, just at the sensitivity limit of GROCSE. Therefore, it is doubtful current instruments can effectively test this model of counterpart emission.

The results of previous optical searches can be used to rule out some of the spectral indices considered in this simple model. In particular, Greiner *et al.* (1994) examined sky patrol plates from several sites which were coincident with GRBs. Three plates from the Ondřejov patrol were coincident with bursts in the sample. These plates had four-hour exposures with sensitivity to events brighter than $m_V \sim 3$. The three bursts which overlap with the sample (2B911127, 2B920525, and 2B920530) would have produced optical images at least this bright if the spectrum was a power law of index less than -3 below 1 keV. This rules out more steeply falling power laws in the empirical model which is not a severe constraint.

Lacking compelling physical guidance for any expectations, the simplest hypothesis is that spectra in the optical band have the same index as at higher energies (the $\alpha + 1$ case). If this is true, then the ETC, GROCSE, and GTOTE have a chance of detecting the very brightest bursts which trigger BATSE and are distributed by the BACODINE network. The ETC would see only the brightest burst in the sample while GROCSE and GTOTE would see about five. HETE would not fare as well, being unable to detect any GRBs in the UV if the $\alpha + 1$ extrapolations hold.

Being able to detect a GRB does not imply it will be observed. Assuming that each site can image half the sky half the time (night only), then there is a 25%

chance a telescope can slew to a BATSE GRB. Therefore, GROCSE and GTOTE might be able to detect one burst per year for the $\alpha + 1$ extrapolation and the ETC might record a positive detection every four years. All of these detectors have a monitor mode which could catch a burst BATSE does not see. BATSE has about 33% sky coverage, so the number of potentially detectable GRBs is tripled assuming a site can view all the sky all the time. 75% of these are lost to a given ground based site when earth blockage and daytime are figured in. Most of the rest are inaccessible because the fields-of-view of these instruments is small. The ETC has the largest field-of-view and it covers only 10% of the sky accessible to it. Therefore, it appears detection in the monitor mode of any of these instruments is unlikely for this extrapolation.

The instruments discussed here would have difficulty observing simultaneous optical emission from a GRB if optical photons are generated as part of the same spectrum as the gamma-rays. This implies that if concurrent emission is observed more than about once a year, the energy flux must follow a power law of index $> \alpha+1$, indicative of another spectral component. Above 10 keV, GRB spectra are concave down. However, there are indications of emission in excess of simple extrapolations at ~ 4 keV in 10% of GRBs (Preece *et al.* 1996a). Therefore, aside from the discovery of a GRB counterpart, the observation of simultaneous optical emission would indicate a multifaceted emission process, providing new and important information about the burst environment.

Chapter VI

Short Time Scale Emission

VI.A Introduction

BATSE has observed that GRBs are distributed isotropically on the sky but are bounded in space. This fact has led most astrophysicists to speculate that GRBs arise from sources either in a very extended Galactic Halo (radius $\sim$150 kpc) or at the edge of the Universe (distances of order Gpc). While either distance scale can explain the spatial distribution of GRBs, the enormous energy densities implied by such large distances and small emission regions from which GRBs are believed to originate suggests an optical thickness to $\gamma\gamma \rightarrow e^+e^-$ which effectively removes photons with energy $\gtrsim 0.5$ MeV from the spectrum (Schmidt 1978). In addition, a definite spectral form is expected from such a hot, optically thick pair plasma (known as a 'fireball'). Goodman (1986) and Paczyński (1986) have demonstrated that if there is a single optically thick, relativistically expanding emission region, then the spectrum should appear morphologically similar to a black body spectrum. If this type of spectrum was a correct description of GRBs, then the observed flux would only extend over one or two decades in energy (depending on intensity relative to background) as opposed to the six decades that have been observed. Figure VI.1 illustrates the difference between a black body spectrum and a typical GRB spectrum. Another problem with fireballs is if there is even small amount of baryonic matter in the fireball, the main

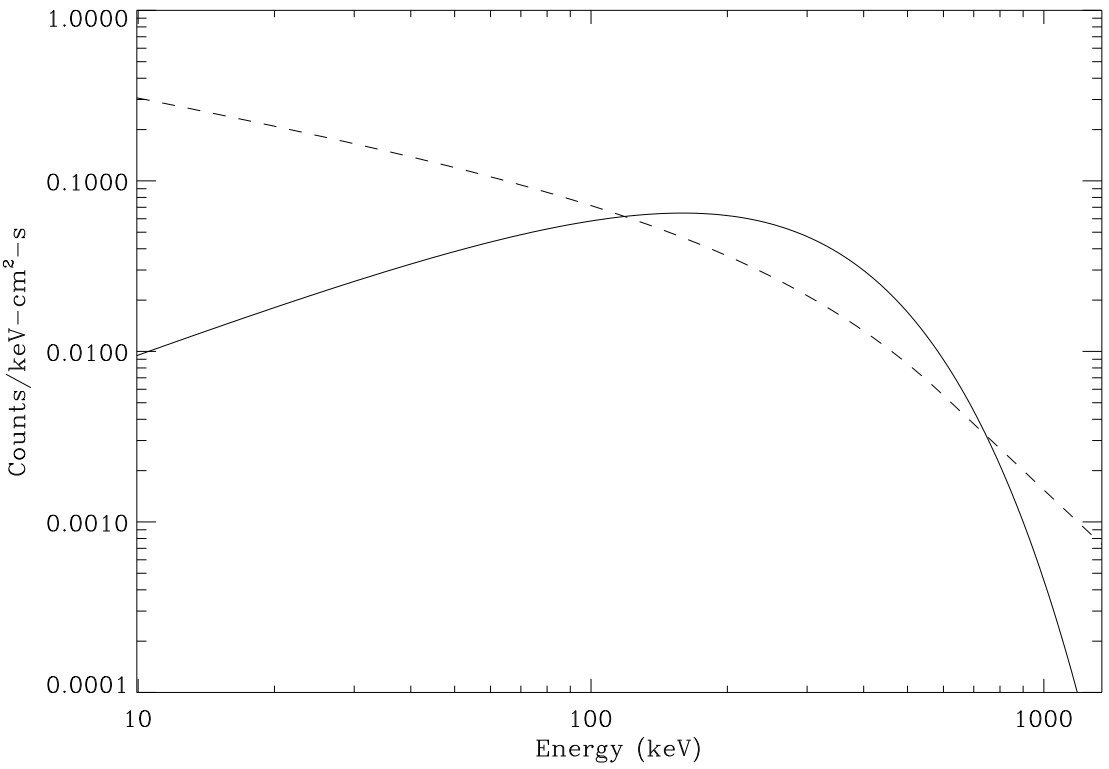

Figure VI.1: A comparison between a 100 keV black body (solid curve) and a typical GRB spectrum (dashed curve). The GRB spectrum is the empirical model of equation I.6 with parameters A=0.1 photons/keV-cm^2-s, $\alpha = -0.5$, $\beta = -2.5$, and $E_0 = 300$ keV. Note the very different low and high energy flux between the two spectra.

energy loss mechanism is acceleration of the baryons and not radiation so that no gamma-ray burst occurs. Therefore, simple fireball models can not explain GRBs.

At the time simple fireball models were suggested, GRBs were not thought to have energy densities large enough to worry about fireballs. However, the BATSE results have forced fireballs on the community because they seem to be a natural phase of GRBs at large distances. Since simple fireballs do not describe GRBs, Narayan, Paczyński, & Piran (1992) suggested two general solutions which can be applied to nearly any type of source. First, a GRB could be composed of a number of flare-like

energy releases which are individually black body but when taken together, produce the observed broad band spectrum. The second possibility is that the fireball has sufficient baryon contamination that the energy of the fireball goes into producing ultrarelativistic ejecta instead of gamma-rays. These ejecta produce a nonthermal burst of gamma-rays through collisions with the interstellar medium at large radii and small optical depths. The former idea has received little theoretical attention while the latter has been extensively developed (cf. the series of Rees & Mészáros (1992), Mészáros & Rees (1993a), and Mészáros, Laguna, & Rees (1993b)).

The reason for this disparity of attention is not difficult to understand. Current conceptions of GRBs are that they are extremely violent events in which a large amount of baryonic matter from the source object (*e.g.,* a merging pair of neutron stars or disrupted star) is likely to be present in the fireball. Since only $\sim 10^{-9} M_{\odot}$ is required to stifle direct gamma-ray emission (Mészáros & Rees 1993a), a clean fireball is very difficult to produce. In addition, bursts are known to be broad-band on time scales as short as 0.1 s, which forces numerous black bodies to be either short-lived or emit cooperatively. Thus, ultrarelativistic ejecta appears more natural in the context of a fireball. However, the multiple black body hypothesis has not been ruled out by the data and even if the baryon contaminated fireballs are correct, they may produce occasional narrow band flares.

An obvious question is whether it is possible to distinguish between the two types of fireballs. One possibility is that spectra are indeed composed of many black bodies (or black bodies in addition to a weaker nonthermal spectrum) and individual thermal regions may produce observable radiation at different times. If this is the case, then at any given instant only a small number of regions may be emitting, resulting in a narrow energy band spectrum. If this idea is to explain all GRBs, then the lifetime of the individual radiating regions should be short enough to account for the shortest observed GRBs ($\sim$ 30 ms for the BATSE bursts [Meegan *et al.* 1996]). Such short duration, narrow energy band emission could be impossible to detect with standard spectral analysis techniques since there would be very few counts to work

with. Fortunately, analytical tools do exist which will find this type of emission if it does occur in GRBs.

VI.B Statistical Background

VI.B.1 The Problem with Traditional Analysis

Spectral analysis in high-energy astrophysics has traditionally involved a trade-off between time resolution and energy resolution, a consequence of the typically low signal-to-noise ratio of high-energy observations and the methods used to analyze data. To understand how low counting rates and traditional analysis conspire against the high-energy astrophysicist, consider the problem of fitting a model to data. By far, the most common way to perform this task is to apply a least-squares minimization algorithm (Bevington 1969, p. 204; Press *et al.* 1992, p. 665). This algorithm adjusts the model parameters until the smallest value of the χ^2 statistic is found. χ^2 is defined as

$$\chi^2 \equiv \sum_{i=1}^{n} \frac{(y_m(x_i;\Theta) - y_d(x_i))^2}{\sigma_i}, \qquad \text{(VI.1)}$$

where the sum is over all data points, $y_m(x_i;\Theta)$ are the model values as a function of independent variables x_i and parameters Θ, $y_d(x_i)$ are the data values, and σ_i are the errors associated with the data points. The value of χ^2 is the negative logarithm of the likelihood that the model explains the data assuming the data are distributed as a Gaussian around the model values.

The primary difficulty with applying least-squares fitting to counting data from high-energy sources is that data are not distributed around 'true' values as a Gaussian, but rather according to a Poisson distribution. When a data point is composed of a large number of counts, the two distributions are effectively indistinguishable but this is not true for data composed of very few counts. Therefore, one must choose to give up time or energy resolution in order to accumulate enough counts to ensure a Gaussian distribution or choose to abandon least-squares methods

altogether and along with it all forms of model testing which have been developed for traditional (also known as Gaussian) methods.

To search for millisecond black bodies in GRB spectra, a combination of high time and high energy resolution is required. BATSE provides such data in the form of Spectroscopy Detector Time Tagged Event (STTE) data (see Chapter II). This data type is a list of individual counts detected by the SDs. During the intial portions of a burst, individual events are both accumulated into spectra and stored as individual counts. Up to 65,536 individual counts can be stored, timed to an accuracy of 128 μs providing extremely high time resolution. While the STTE data provide good time and energy resolution, to exploit both properties, non-Gaussian methods must be used because of the small number of counts accumulated on millisecond time scales. An additional constraint imposed by high time and energy resolution is that the analysis must be practical. As discussed later on, simply fitting numerous millisecond spectra using a Poisson likelihood function instead of the Gaussian is extremely time consuming. Therefore, an entirely different approach to the problem must be taken. In the method developed here, pairs of counts are compared to find if there is any tendency toward clustering in energy and time. Such a signal would characterize short-lived black body emission because of the relatively narrow energy range of emission compared to the broad spectrum observed on long time scales. The method is statistical and to understand the results, the statistics used to describe the data must be well understood. To accomplish this understanding, a Bayesian approach is used because it allows a simple derivation of the probability theory underlying any statistical method from first principles.

VI.B.2 Bayesian Probability Theory

Before describing the method used to analyze the STTE data, it is useful to briefly summarize Bayesian probability theory. The concept of probability that is most often used is based on idea of relative frequencies of occurrence. In this approach, statistics calculated from the data are used to determine how likely a given

observation is based on the expected results of a large number of observations of an identical system. The statistic is expected to have a certain distribution and the observed value is compared to the expected distribution. The Bayesian approach to probability theory is a way of quantitatively expressing confidence in a proposition in which ignorance or previous experience must be factored into the calculation. The difference in concepts is important because each GRB is unique and repeated observations of the same event are impossible. Thus, the Bayesian formalism is more general and in a sense, more realistic than the 'frequentist' approach since any *a priori* knowledge is factored into the analysis. Several arguments on the superiority of Bayesian inference are advanced by Loredo (1990) but it is sufficient to note here that the theory is more rigorous than the frequentist approach used by many scientists and forces one to explicitly acknowledge all prejudices about the expected results.

Bayesian probability theory is based on two axioms (Loredo 1990): the sum rule,

$$p(A|C) + p(\overline{A}|C) = 1, \tag{VI.2}$$

and the product rule,

$$p(AB|C) = p(A|BC)p(B|C), \tag{VI.3}$$

where A, B, and C are propositions which are either true or false, $\overline{A}$ is the negation of A, and AB is true only if A and B are true. The notation of conditional probabilities is used so $p(A|C)$ is the probability that A is true given C. Obviously, $AB = BA$ so that equation VI.3 could also read

$$p(AB|C) = p(B|AC)p(A|C). \tag{VI.4}$$

Equations VI.3 and VI.4 can be solved for $p(A|BC)$ yielding

$$p(A|BC) = p(A|C)\frac{p(B|AC)}{p(B|C)}, \tag{VI.5}$$

a relation known as Bayes' Theorem.

To demonstrate the utility of Bayes' Theorem for any type of data analysis, consider the case where $A = M$, a model in question, $B = D$, the data collected, and

$C = I$, any other information about the hypothesis and system which is available. With these substitutions, Bayes Theorem becomes

$$p(M|DI) = p(M|I)\frac{p(D|MI)}{p(D|I)}. \tag{VI.6}$$

The terms on the right-hand side of this expression can be understood as follows. $p(M|I)$ (the prior probability) is the probability that the model is correct before the observation is made. This is a term which quantitatively incorporates bias and previous experience into the probability calculation. For example, if the acceleration of gravity at the Earth's surface was measured to be 9.8 m/s^2 for 100 consecutive days, then the prior for the 101st measurement would be near unity for a model which specified the acceleration to be 9.8 m/s^2 and near zero for other models. $p(D|MI)$ is the probability of observing the data given the model. In the acceleration of gravity measurement, if the measured values have a Gaussian distribution of width σ about 9.8 m/s^2, then

$$p(D|MI) = \frac{1}{\sigma\sqrt{2\pi}} \exp\left[-\frac{1}{2}\left(\frac{D - 9.8 \text{ m/s}^2}{\sigma}\right)^2\right]. \tag{VI.7}$$

It should be noted that $p(D|MI)$ is not restricted to Gaussian distributions but can be any likelihood function. The last term in equation VI.6 is $p(D|I)$, the probability of observing the data independent of the chosen model. This term can be shown to be a normalization constant, ensuring $0 \leq p(M|DI) \leq 1$ (Loredo 1990).

The use of equation VI.6 for fitting models to data is clear. The best fit to the data is obtained when the model parameters are chosen to maximize $p(M|I)p(D|MI)$. However, this only finds the most likely set of parameters for a given model, it does not allow one to choose the more probable of two competing models. Fortunately, the Bayesian formalism provides a clear prescription for finding the more likely hypothesis.

The key to understanding Bayesian model comparison is the realization that Bayes' Theorem applies not only to parameters within a model, but to the models themselves (which will be called hypotheses). In other words, the probability that a hypothesis is correct (regardless of the actual values of the parameters) can be

discussed. Using Bayes' Theorem, the probability of hypothesis H is

$$p(H|DI) = p(H|I)\frac{p(D|HI)}{p(D|I)}. \tag{VI.8}$$

The meaning of the terms on the right-hand side of this expression are similar to the model fitting case. $p(H|I)$ is the prior probability that the hypothesis is correct. If there is no reason to favor a particular hypothesis, this term is the same for all hypotheses. $p(D|HI)$ is the likelihood that the observed data would have been produced assuming H is correct. Often, one is interested in deciding whether a class of models is superior to another without regard to the particular parameterization of the model. In this case, the values of the parameters of H are not important, just the likelihood the H explains the observation. This likelihood is found by 'marginalizing' the parameters, integrating the likelihood function over the allowed parameter space of the model. Mathematically, this is expressed as

$$p(D|HI) = \int d\Theta p(\Theta|I)p(D|\Theta I), \tag{VI.9}$$

where Θ represents the model parameters, $p(\Theta|I)$ are priors for the parameters, and $p(D|\Theta I)$ is the likelihood that the data is explained by a given set of parameters. Returning to equation VI.8, $p(D|I)$ is a normalizing term found by adding together the probabilities for all possible hypotheses.

For model comparison, it is not necessary to calculate the value of $p(D|I)$ because only the relative likelihoods of two models are needed in order to to judge one superior to another. Suppose there are two competing hypotheses H_0 and H_1. Since the probability of each hypothesis can be quantified, the ratio of these values can be formed, $p(H_1|DI)/p(H_0|DI)$. If the resulting 'odds ratio' is much larger than unity, then H_1 is favored. If the ratio is much less than unity, then H_0 is a better description of the system. The ratio itself is

$$\frac{p(H_1|DI)}{p(H_0|DI)} = O_{10} = \left[\frac{p(H_1|I)}{p(H_0|I)}\right]\frac{\int d\Theta_1 p(\Theta_1|I_1)p(D|\Theta_1 I_1)}{\int d\Theta_0 p(\Theta_0|I_0)p(D|\Theta_0 I_0)}, \tag{VI.10}$$

where the factor in brackets is called the prior odds. To declare one hypothesis superior to the other, the odds ratio must favor a hypothesis by at least an order of

magnitude (a matter of judgement). Specifically, $O_{10} > 10$ selects H_1 and $O_{10} < 0.1$ favors H_0. If neither hypothesis is preferred by the odds ratio, then both hypotheses should be considered viable until better observations become available.

This subsection demonstrates the attractiveness of the Bayesian approach to probability theory. Parameter estimation and model comparison are derived from first principles and the meaning of the resulting probabilities is clear. There are no uncertainties involving the appropriate statistic or test for these procedures, a problem in traditional analysis in which the statistical tools seem far removed from the experiment. A significant problem with Bayesian statistics is the determination of priors, which is often a subjective quantification of one's expectations. However, these same problems can occur in the frequentist formalism, for example, the F-test significance level at which one accepts a observation. Other practical and philosophical benefits of Bayesian probability theory are discussed by Loredo (1990).

VI.B.3 Application to Count Data

Although the Bayesian approach provides a well-defined prescription for analyzing any type of data, an important question is whether it can be applied practically. If one were interested in simply analyzing a number of spectra with very short accumulation times, the answer is no. Loredo & Lamb (1989; 1996) performed a likelihood analysis similar to the Bayesian method outlined above on 24 neutrino events from Supernova 1987a to investigate neutron star cooling and the mass of the electron antineutrino. Essentially, their problem was identical to the problem of examining short time scale emission from GRBs since both are cases in which a Gaussian approximation to the Poisson distribution is unrealistic. The likelihood function used by Loredo & Lamb was derived as follows. If $N(E,t)$ is a model of the number of neutrinos detected with energy less than E and arrival times earlier than t, then $d^2N/dEdt$ is the expected neutrino detection rate per unit time per unit energy. The number of neutrinos detected in a time interval Δt and energy range ΔE is just the detection rate times $\Delta E \Delta t$. Given that the data is described by a Poisson distribution, then

the probability that no neutrinos are detected in the interval is

$$P_0(E,t) = \exp\left[-\frac{d^2N(E,t)}{dEdt}\Delta E\Delta t\right], \tag{VI.11}$$

and for one neutrino

$$P_1(E,t) = \frac{d^2N(E,t)}{dEdt}\Delta E\Delta t \exp\left[-\frac{d^2N(E,t)}{dEdt}\Delta E\Delta t\right]. \tag{VI.12}$$

The intervals chosen were small enough that the probability of detecting more than one neutrino was negligible compared to P_0 and P_1.

The likelihood of an observation is just the product of the probabilities of detection of each of the observed neutrinos times the probability of the all intervals which did not contain a neutrino, which is

$$\Lambda = \left[\prod_{i=1}^{N_{obs}} P_1(E_i,t_i)\right]\left[\prod_j P_0(E_j,t_j)\right], \tag{VI.13}$$

where N_{obs} are the observed neutrinos and j refers to all intervals in which no neutrinos were observed which is essentially all of the $E-t$ space. Since it is computationally more convenient to minimize $\ln(\Lambda)$ than maximize Λ (the extrema are at the same values of E and t), the quantity of interest is

$$L = \ln(\Lambda) = \sum_{i=1}^{N_{obs}} \ln\left[\frac{d^2N(E,t)}{dEdt}\Delta E\Delta t\right] - \sum_j \frac{d^2N(E,t)}{dEdt}\Delta E\Delta t, \tag{VI.14}$$

where j runs over all intervals (the exponentials from P_0 and P_1 were combined to form the send term). In the limit of small ΔE and Δt, the second term becomes the integral of the rate function over all intervals which is the total number of events expected in the observation N_{det}. Therefore, the likelihood function is just

$$L = \sum_{i=1}^{N_{obs}} \ln\left[\frac{d^2N(E,t)}{dEdt}\right] - N_{det}, \tag{VI.15}$$

where the ΔE and Δt intervals were omitted because they are constant and do not affect the functional dependence of L on N_{det}.

While Loredo & Lamb were able to obtain interesting results, a supercomputer was required for their work. While computing capabilities have advanced considerably in the years since Loredo & Lamb's work, it remains impractical to process

the STTE data in this way. Loredo & Lamb had 24 events to work with in a single spectrum as compared to hundreds of counts in a single short time scale GRB spectrum. Therefore, the assumption that the detection of one event in an energy and time interval is negligible is invalid even for the highest time and energy resolution available for BATSE and L becomes much more complicated. In addition, thousands of millisecond spectra can be extracted from a single GRB, each of which must be individually examined for short-lived black bodies because the long duration spectrum is known to be broad band. The impracticality of this approach was confirmed when in an attempt to determine whether a simple power law or black body spectrum was preferred by equation VI.10, an answer could not be obtained for a single spectrum after one week of computer time.

It is apparent that simply performing spectral fits to a set of high time resolution spectra from a GRB in order to find millisecond, black body flares is not feasible with Bayesian methods using the likelihood function of Loredo & Lamb. However, this does not imply that such behavior is undiscoverable in the BATSE data. All that is required is a new approach to the problem, one in which individual counts are used to ferret out any potential signal. If GRBs are composed of a number of millisecond duration black bodies, then it is expected that counts that are separated by a small time interval ($\sim$ 1 ms) are more likely to have been caused by photons which had similar energies than counts separated by long time intervals. In the following section, a method is developed which determines the likelihood that the energies of photons are more correlated when the counts they create in the detector have small time separations, a strong indication that GRBs are composed of numerous, short lived black bodies.

VI.C Pair Correlations

VI.C.1 Comparing Counts

The method of pair correlations considers the probability that a pair of counts came from a pair of photons in a specified energy range. When an event is recorded by the SDs, the energy loss channel to which it is assigned is related in a complicated way to the energy of the incident photon (see Chapters II & III) which prevents the direct comparison of counts. The detection process is modeled with a detector response function. For BATSE, this function is quantified in terms of a detector response matrix and calibration algorithm. In conventional spectral analysis, an assumed model spectrum is folded through the response and the result compared to observed spectra. Mathematically, the folding process is expressed as

$$C(E') = \int R(E, E') f(E) dE, \tag{VI.16}$$

where $C(E')$ is the observed spectrum, $f(E)$ is the incident spectrum, and $R(E, E')$ is a model of the detector response which quantifies the probability that a photon of incident energy E is assigned by the detector to energy-loss bin E'.

The quantity of interest is the probability distribution of incident energies given that a count was observed in channel E', which is denoted as $p(E|E'I)$ (I represents any information in addition to energy). From Bayes' Theorem,

$$p(E|E'I) = p(E|I)\frac{p(E'|EI)}{p(E'|I)}. \tag{VI.17}$$

The terms on the right-hand side of this equation are easy to understand. The prior $p(E|I)$ is the probability that a photon had incident energy E. Since black body emission is being searched for, a black body spectrum should be used for $p(E|I)$. However, there is no way of knowing what temperature is appropriate. Further, the model being tested assumes the black body temperature is highly variable within the burst, making the prior a complicated function of time. Even if the correct temperatures and time dependance of the black bodies could be known, recalculating

$p(E|E'I)$ (and everything which depends on it) for every time bin would require enormous computational resources. Therefore, the spectrum observed on long time scales is used for the prior, $p(E|I) = f(E)$. Aside from the benefit that this quantity is easy to determine, this prior is conservative in the sense that the search is biased against detecting short time scale black bodies. Any positive detections will be more reliable because the black bodies are harder to find.

As for the other terms in equation VI.17, $p(E'|EI)$ is the likelihood that a photon of incident energy E will end up in bin E', which is exactly $R(E', E)$ in equation VI.16. $p(E'|I)$ is the probability anything at all will fall in bin E'. This term is necessary to normalize $p(E|E'I)$ because neither $f(E)$ nor $R(E, E')$ is normalized to unity. Putting everything together yields

$$p(E|E'I) = \frac{f(E)R(E', E)}{\int f(E)R(E', E)dE}. \tag{VI.18}$$

With the probability distribution of equation VI.18, the degree of correlation of incident energies between any pair of observed counts can be defined. If the incident GRB spectrum was composed of a set of monoenergetic pulses (with a different energy for each individual pulse), then the quantity of interest would be

$$\begin{aligned} L(E'_1, E'_2) &= \int p(E_1 = E_2|E'_1E'_2I)dE_1 \\ &= \int p(E|E'_1I)p(E|E'_2I)dE. \end{aligned} \tag{VI.19}$$

Although black body pulses are being searched for, I hoped that the sensitivity of this likelihood function would be sufficient to see non-monochromatic (but narrow band) spectra since equation VI.19 is easy to calculate. Unfortunately, tests with simulated data composed of short time scale black bodies did not reveal a short time scale black body signal.

When working with narrow band spectra, the probability two photons had incident energy $a(E) < E < b(E)$ is desired. For this case, the likelihood is

$$L(E'_1, E'_2) = \int dE \int_{a(E)}^{b(E)} d(\Delta E)p(E|E'_1I)p(E + \Delta E|E'_2I), \tag{VI.20}$$

where the substitutions $E_1 = E$ and $E_2 = E + \Delta E$ have been made. The values of $a(E)$ and $b(E)$ depend on the allowed energy difference between photons. Since black bodies are the object of the search, $a(E)$ and $b(E)$ are defined as the energies at which the flux from a black body of temperature $T = E$ is a specified fraction of the peak black body flux. The sensitivity of this method to the peak flux fraction fraction chosen has been determined using a simulated GRB composed of many short-lived black bodies. The sensitivity as a function of peak flux fraction used to determine $a(E)$ and $b(E)$ is shown in Figure VI.2. This figure shows that the sensitivity does not depend strongly on the values of $a(E)$ and $b(E)$ except when an extremely large or small amount of black body flux is included. Therefore, the exact choice of $a(E)$ and $b(E)$ is not crucial so long as the extremes are avoided.

With the measure of correlation between counts defined by equation VI.20, short time scale black bodies can be searched for. This is done by comparing all pairs of counts separated by some interval Δt and finding the average value of $L(E'_1, E'_2)$. The time intervals are effectively time bins since the STTE data are timed in 128 μs increments. Therefore, at a given Δt the quantity

$$A(\Delta t) = \frac{1}{N_{pairs}} \sum_i L_i(E'_i, E'_{i+\Delta t}) \qquad \text{(VI.21)}$$

is calculated, where $L_i(E'_i, E'_{i+\Delta t})$ is the correlation between a given count and a count which occurred Δt seconds later, N_{pairs} is the total number of pairs separated by Δt, and the sum is over all counts. Although the assumption is that black bodies have finite duration and all counts less than some lifetime Δt_0 could be correlated together, $A(\Delta t)$ is calculated only for pairs separated by exactly Δt so that the values of A in adjacent time bins are nearly independent of one another. This makes statistical analysis of $A(\Delta t)$ much simpler. Note that a single count may correlate to more than one count if there is more than one count in the $t_i + \Delta t$ time bin. If a count has no future counts to correlate with, L_i is not computed and does not affect the average. Since a count is only correlated with future counts, double counting is not a concern. If burst spectra are narrow band for short periods, $A(\Delta t)$ will fall from a maximum value at $\Delta t = 0$ to some lower constant value as Δt becomes larger and the counts

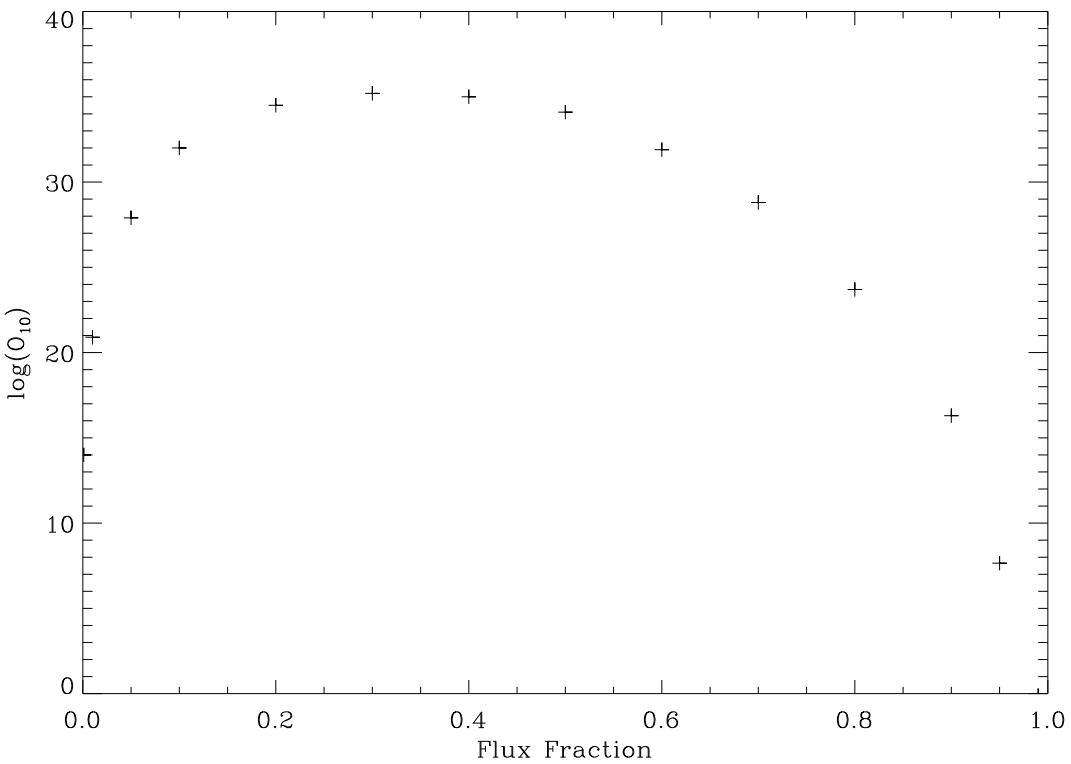

Figure VI.2: The significance of detection as a function of peak flux fraction used to determine $a(E)$ and $b(E)$. Test data from the fourth test described below were used. O_{10} is the odds ratio favoring short-lived black bodies over a broad band spectrum. This ratio is discussed in section IV.C.2.

become uncorrelated. This constant value is just be the average correlation of all channels with each other weighted by the spectral distribution of the total emission (source plus background). If this pattern is seen, then the decay time of $A(\Delta t)$ will give the time scale of the narrow band emission and the fraction of total emission which is narrow band can be found from the slope of this decay.

VI.C.2 Significance

Once $A(\Delta t)$ has been calculated, the reality of any potential signal must be evaluated quantitatively. Note that although $A(\Delta t)$ is a statistical description of the count data, $A(\Delta t)$ is now being used as data which can be modeled. Essentially, it must be determined whether the hypothesis of short time scale, narrow energy band emission describes the observations better than a broad band spectrum. Each type of emission has clear consequences for $A(\Delta t)$. If the broad band spectrum description is correct (the null hypothesis, denoted H_0), $A(\Delta t)$ should be a constant. If short time scale black bodies exist (the test hypothesis, H_1), $A(\Delta t)$ should have larger values for small Δt. For each hypothesis, parameterized models can be constructed which are used in equation VI.10 to determine the more likely hypothesis.

The odds ratio analysis requires a choice of not only hypotheses, but a likelihood function that describes the data, $p(D|\Theta I)$, and priors for the model parameters, $p(\Theta|I)$). For this analysis, the values of $A(\Delta t)$ are assumed to be distributed as a Gaussian around the model values. Therefore, the likelihood function is

$$p(D|\Theta_i, I_i) = \exp\left[-\sum_{\Delta t} \frac{(m(\Delta t;\Theta_i) - A(\Delta t))^2}{\sigma^2_{\Delta t}}\right], \qquad \text{(VI.22)}$$

where m refers to the model values of $A(\Delta t)$ and σ is the error in the average correlation. This assumption is based on the fact that a large number of pairs is used to determine each $A(\Delta t)$. The Central Limit Theorem states that if a model is correct and the number of data points is large, then the sample mean will be distributed as a Gaussian around the model value (Martin 1971, p.47). The accuracy of this assumption can be demonstrated with simulated data. A set of counts was generated using a

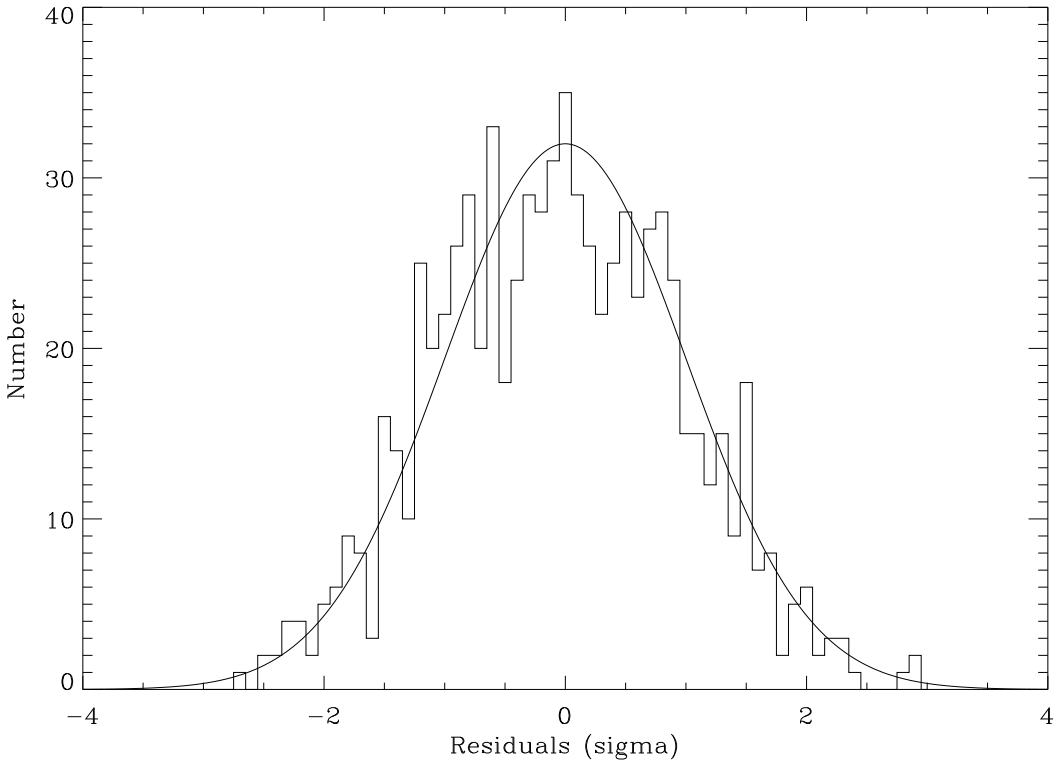

Figure VI.3: The distribution of residuals from the average value of the average correlations from the third test. The associated Gaussian is not a fit.

power law spectrum and $A(\Delta t)$ was calculated. Figure VI.3 shows the distribution of residuals when the median of $A(\Delta t)$ is assumed to be the true value. It is clear that the overplotted Gaussian (which is not a fit) is an excellent match to the residuals.

The errors for all average correlations are assumed to be equal (*i.e.*, $\sigma_{\Delta t}$ is constant). This is not likely to be strictly true since the number of pairs in each $A(\Delta t)$ is different. However, the individual errors should be similar since the number of pairs does not vary radically from one Δt to the next. It is also assumed that the errors on the data points can be empirically determined from the average number of pairs in each $A(\Delta t)$. Figure VI.4 shows the ratio of the calculated variance to the inverse square root of the mean number of pairs ($1/\sqrt{\overline{N}}$, recall $A(\Delta t) \propto 1/\overline{N}$) for many sets of test data. This ratio falls around 0.4 so $\sigma = 0.4/\sqrt{\overline{N}}$ is used.

As for the hypothesis themselves, the null hypothesis (H_0) states that $A(\Delta t)$

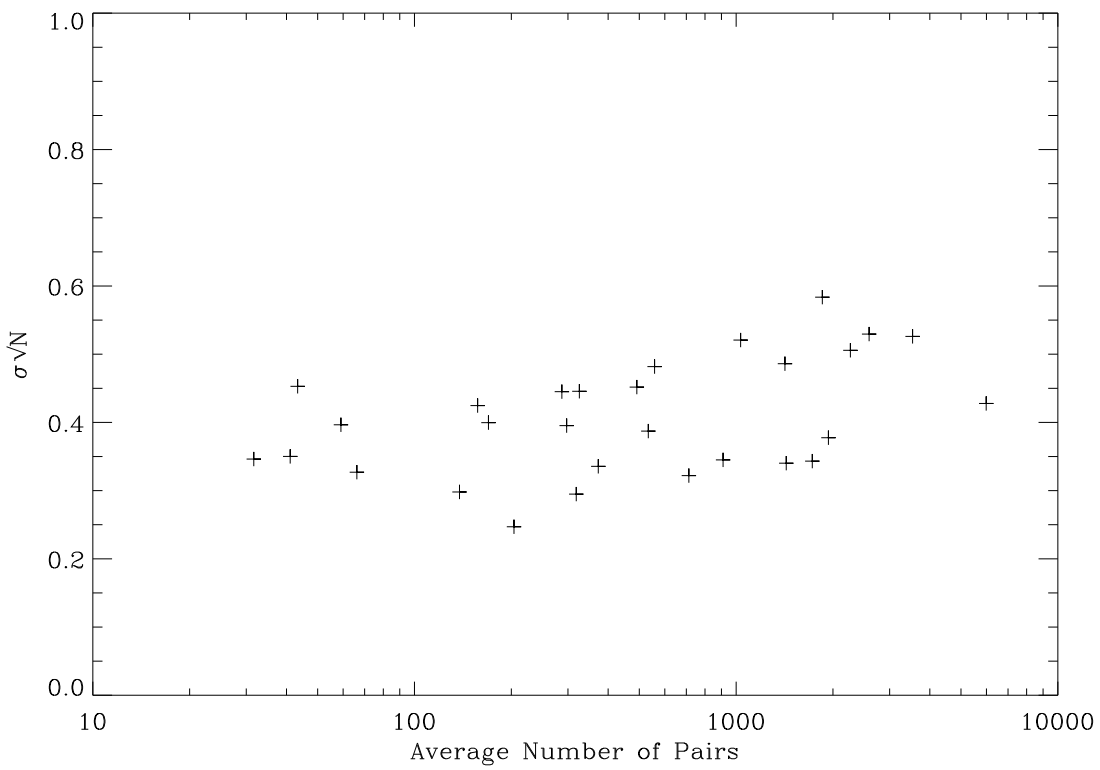

Figure VI.4: The ratio of calculated variance to mean number of pairs for a large number of simulated bursts.

is constant as a function of time separation,

$$m_0(\Delta t; \Theta_0) = \theta_0, \tag{VI.23}$$

where θ_0 is the only parameter. A three parameter model is used for the hypothesis that GRB spectra are composed of short time scale black bodies (H_1),

$$m_1(\Delta t; \Theta_1) = \begin{cases} \theta_1(1 - \Delta t/\theta_2) + \theta_3, & \Delta t \leq \theta_2; \\ \theta_3, & \Delta t > \theta_2. \end{cases} \tag{VI.24}$$

In this model, $A(\Delta t)$ has a maximum value at $\Delta t = 0$ and linearly declines until it reaches the long term average θ_3. Since there are no expectations for the likely values of the parameters for either model, uniform priors are used for the $p(\Theta_i|I)$ in equation VI.10. This means θ_0 and θ_3 are between 0 and 1, the largest and smallest possible values for $A(\Delta t)$. θ_1 must be larger than zero since $A(\Delta t)$ is not expected to increase as a function of Δt so $0 \leq \theta_1 \leq 1 - \theta_3$. Finally, θ_2 is fixed by the boundaries of Δt on which short time scale correlations are searched for. The allowed range of θ_2 can be freely chosen and all values of θ_2 are assumed equally likely within that range. In all the analysis described below, lower boundary for θ_2 was set to 0 and the upper to one tenth the time span covered by the STTE data. The upper limit was chosen to minimize any effects due to finite duration of the data but provide a significant range in θ_2. Expressing these priors explicitly,

$$p(\theta_0|I_0) = p(\theta_3|I_1) = 1, \tag{VI.25}$$

$$p(\theta_1|I_1) = \frac{1}{1 - \theta_3}, \tag{VI.26}$$

$$p(\theta_2|I_1) = \frac{1}{\theta_{2,max} - \theta_{2,min}}. \tag{VI.27}$$

The last element of equation VI.10 is the prior odds. Since there is no reason to prefer one model over another, the prior odds ratio is set to unity.

VI.C.3 Black Body Characteristics and Upper Limits

If short time scale black body emission is observed in GRBs, the typical duration of the black bodies and the fraction of the total emission which is black

body are important quantities. Conversely, if a short time scale spectral signature is not found, upper limits on such emission should be determined. If these limits are stringent enough, an entire class of GRB models can be ruled out.

For the case of a detection, the $A(\Delta t)$ curve can be fit with the model of equation VI.24 and the parameters used to determine the duration and strength of the black bodies. The effective duration is defined as the smallest time Δt where the constant term θ_3 alone can account for the observed $A(\Delta t)$. This is where $\Delta t = \theta_2$. The strength calculation is more involved. Assume that a pure black body would produce an average correlation z. Adding a broad band background with average correlation y would reduce the observed correlation to $fz + (1-f)y$ where f is the fraction of total emission that is black body. This is not strictly correct since the average correlations are products of sums. However, this quantity is much simpler to work with than the true expression which has of order 100 terms. The situation of a constant black body with background is similar to the case of short time scale black bodies except the black bodies turn off so that as Δt increases, $A(\Delta t)$ decreases. At $\Delta t = 0$ though, $A(\Delta t)$ should behave as in the idealized picture above. In this case, any broad band emission and black bodies of different temperature produce the long term correlations described by θ_3. The combination of single black body and background emission produce the $\Delta t = 0$ correlation,

$$A(\Delta t = 0) = \theta_1 + \theta_3 = zf + (1-f)\theta_3, \tag{VI.28}$$

where again, z is the average correlation produced by a pure black body, an independently determined quantity. Simplifying this equation for the fraction of black body emission f,

$$f = \frac{\theta_1}{z - \theta_3}. \tag{VI.29}$$

Although a prescription for determining f has been specified, the value of z must be found. This is done by comparing a pure, noiseless black body to itself. The resulting z depends on the temperature of black body. Figure VI.5 shows the dependence of z on temperature for the correlation matrix used for the tests.

Although this variation is only about 10%, it cannot be ignored since values of θ_3 are close to z. The best way to proceed would be to average z over the distribution of black body temperatures. However, this distribution cannot be known though the long time scale distribution of photons can be found. The distribution of photons will not equal the temperature distribution but it does provide some measure of guidance. Therefore, a value of z is weighted by the energy distribution of all the photons used in the correlation analysis is calculated. A more problematic concern is that the resulting value of f is strictly valid only for emission which consists of a series of single black bodies. When more black bodies are active at a given instant, the value of z will be lower than the value used and the quoted strength will be an underestimate of the true fraction of black body emission. This underestimate should not be too serious if the number of active black bodies at a given instant is small. No attempt is made to calculate z assuming more than one active black body distribution of temperatures since the appropriate number of active black bodies to include or their distribution of temperatures cannot be known. Therefore, only the single black body strength is determined.

Upper limits on the fraction of short time scale black body emission depend on the duration assumed for the individual black bodies. Short duration black bodies are more difficult to restrict since their $A(\Delta t)$ does not extend to large Δt so that a large average correlation (above the average value) is needed to produce a convincing rise at low Δt. Upper limits are calculated for three time scales, $\theta_2 = 1, 5, 10$ ms. The average of the large Δt correlations (θ_3) is assumed to be correct and is held constant. This leaves one free parameter in the model, θ_1, for which a 90% upper limit is found. This value is used to find a limit for single black body strength as described for the positive detection case.

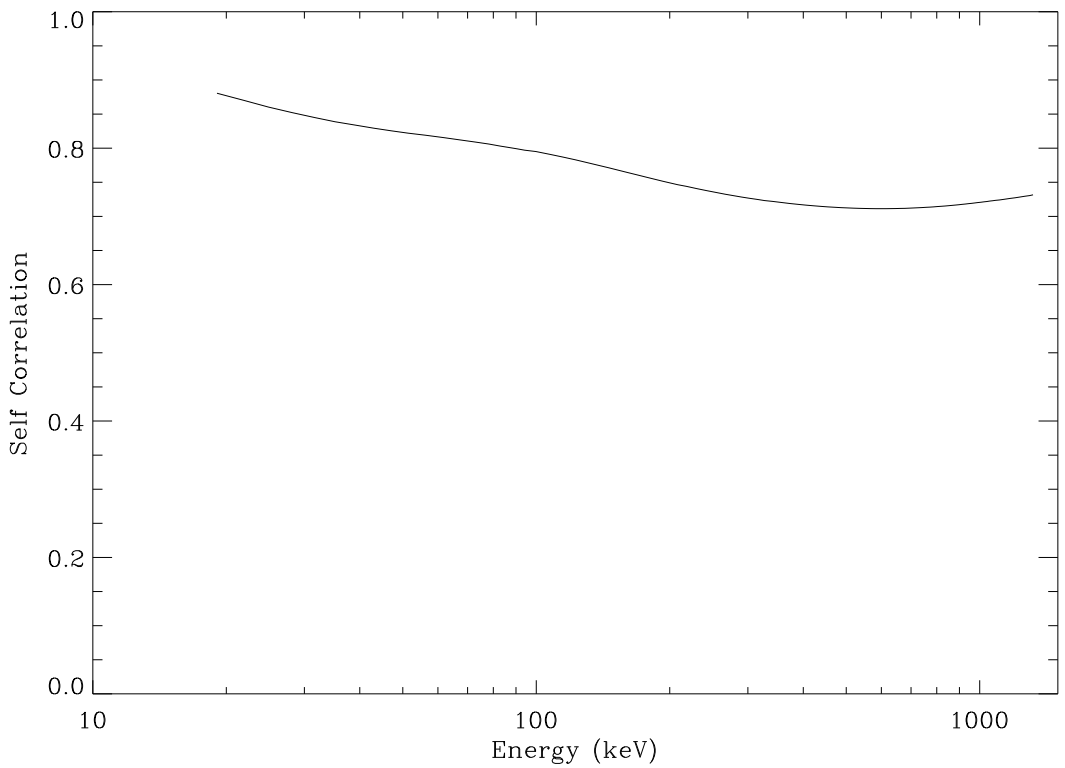

Figure VI.5: The dependance of black body self-correlation on temperature.

VI.D Tests

Several tests of this method have been performed with simulated data and the results prove that short time scale black body emission is detectable. In all the tests (summarized in Table VI.1), a series of black bodies was generated with temperatures distributed as a power law of index -2 below 200 keV and index -3 above with allowed temperatures between 10 keV and 10 MeV. The break in the distribution was required to keep the number of high energy black bodies small and avoid overproduction of high energy counts. For the first test, the duration of a single black body was randomly determined to be between $1 - 5$ ms and only one black body was on at a given time. A typical background was included which contributed ~ 1200 counts/s in the $15-1400$ keV observation region. The length of the burst was 1 s and the total number of counts (source and background) was 3670, a moderately strong burst. The resulting spectrum with a power law fit is shown in Figure VI.6. The fit is not perfect (χ^2 per degree of freedom of 1.31) but does show the total emission is broad band. Correlations were calculated in bins of 128 μs, the resolution of the STTE data. $A(\Delta t)$ is shown in Figure VI.7, the drop in $A(\Delta t)$ with increasing Δt is quite clear. The signal also has systematic deviations from a constant value at large Δt. This behavior is caused by unrelated black bodies of similar energy producing similar counts though separated by a large Δt.

The second test was similar to the first except two black bodies were on at a given time (though not necessarily of the same duration). Figure VI.8 shows that the expected signal is again quite strong, which indicates the method works even if the signal is complicated by simultaneous narrow band emission processes. Note that systematic variations in $A(\Delta t)$ are not as severe as those from the first test. This is because deviations caused by spurious alignments of black bodies separated by large Δt are diluted by other sets of black bodies which are not similarly correlated.

To ensure that these results are not produced by broad band emission, counts generated with a power law of index -2 were created and the results are shown in

Test	Duration (s)	Spectrum	Counts
1	1	One Black Body	3670
2	1	Two Black Bodies	4231
3	1	Power Law	4072
4	0.128	Two Black Bodies	596
5	0.128	Many Black Bodies	442

Table VI.1: A summary of the test data sets. All black body data sets were created with black bodies of randomly determined temperature. A typical 1200 counts/s background was used and the temperature distribution was the same for all black body data sets (described in the text). Test 2 has a larger power law index than tests 1 and 4 because of the chance generation of a larger number of high temperature black bodies. Test 5 was composed of black bodies which turned on at $1 - 5$ ms intervals and remained on throughout the burst.

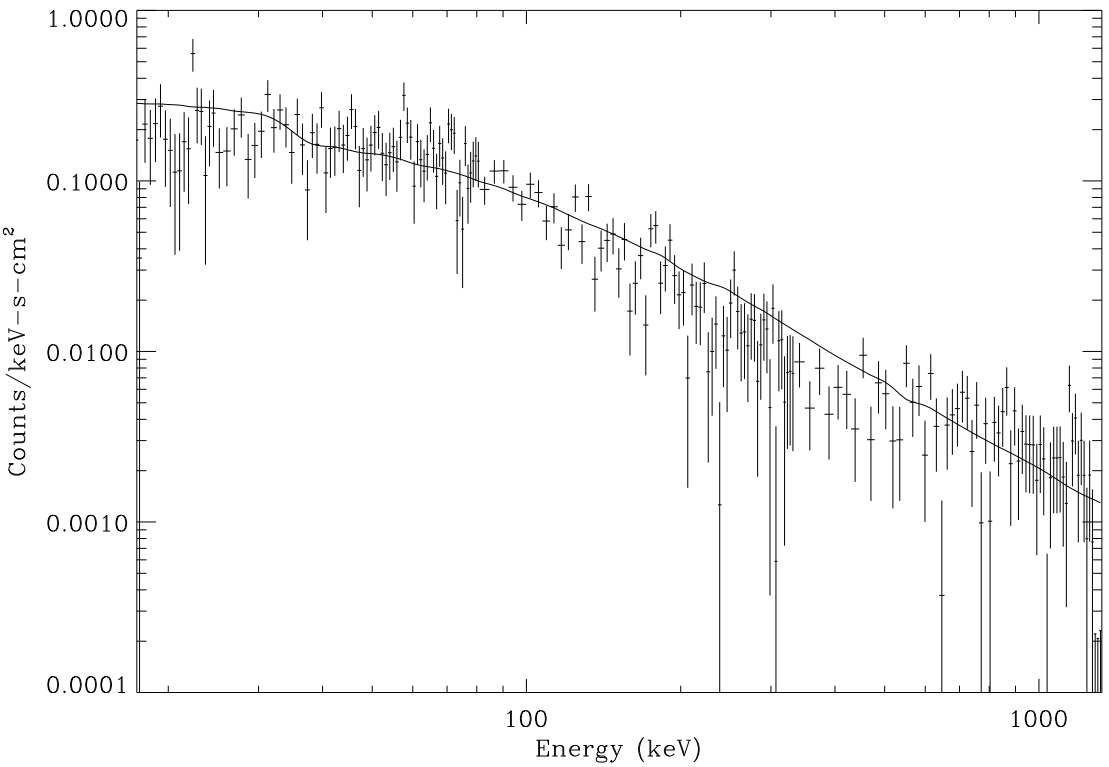

Figure VI.6: The count spectrum from the first test. The line is a power law fit to the data.

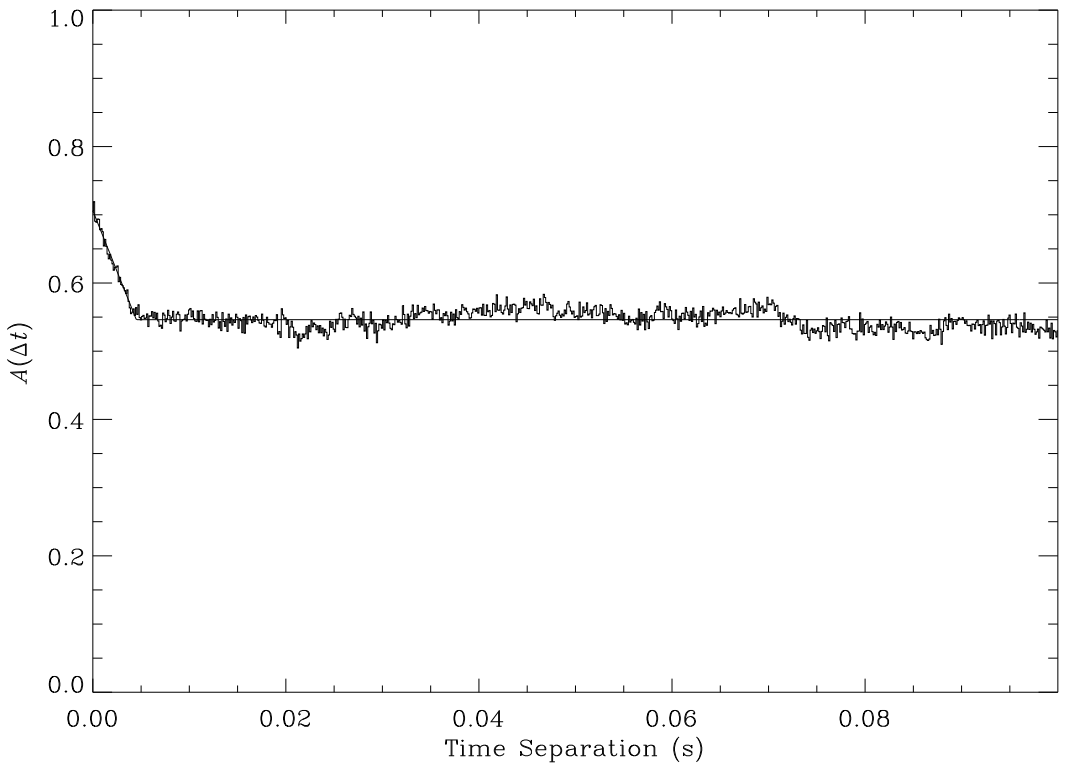

Figure VI.7: $A(\Delta t)$ for the first set of test data. The solid line is the best fit model value.

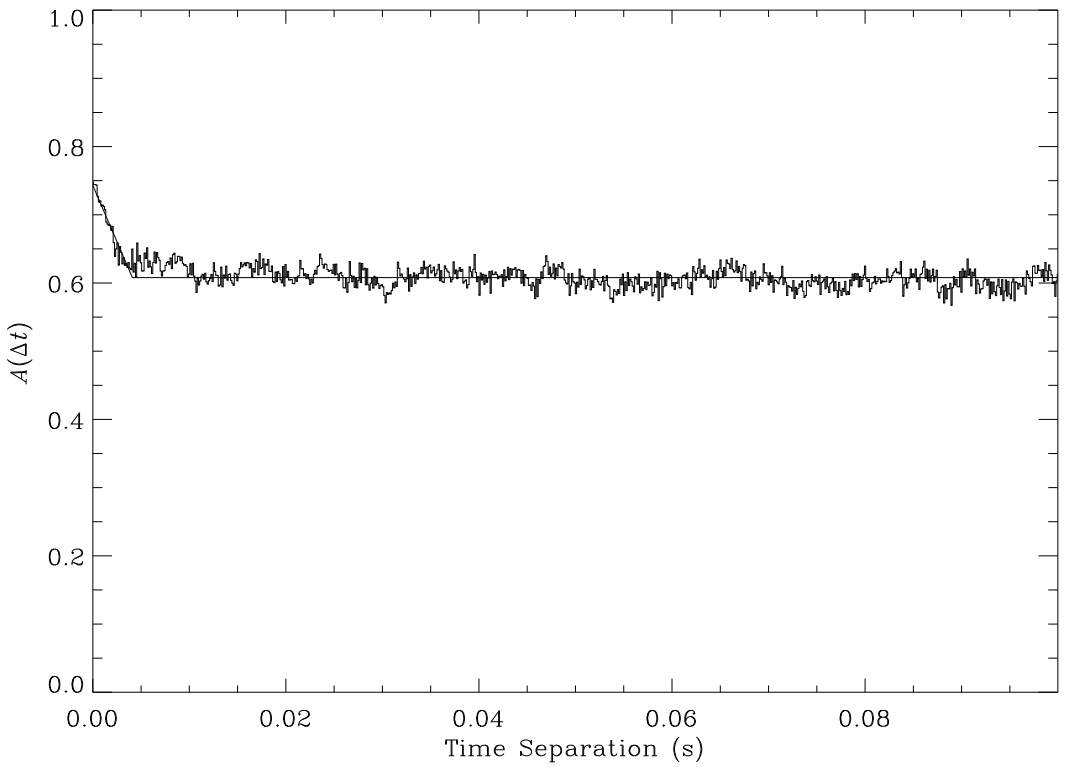

Figure VI.8: $A(\Delta t)$ for the second set of test data. The solid line is the best fit model value.

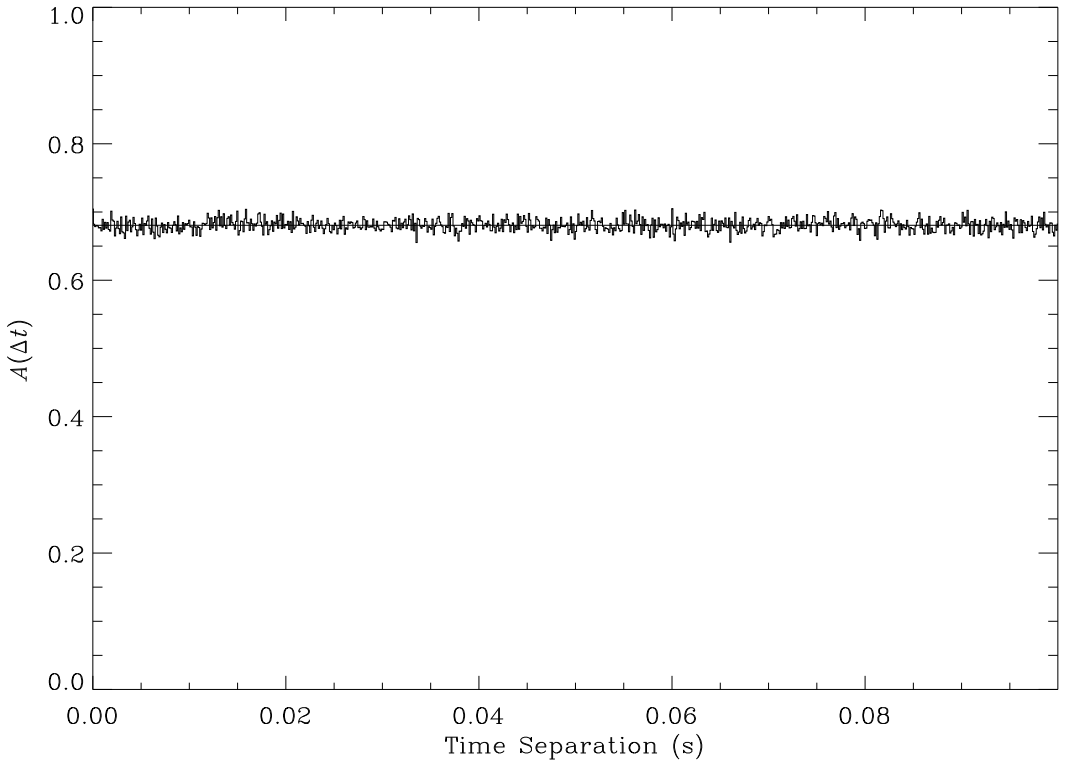

Figure VI.9: $A(\Delta t)$ for the third set of test data. The solid line is the best fit model value.

Figure VI.9. $A(\Delta t)$ is remarkably flat, indicating the expected result of no significant correlations on small time scales.

Since short time scales are of particular interest, another test was performed with a smaller data set. Test 2 was repeated but the length of the burst was reduced to 0.128 s. Although the results are noisier, Figure VI.10 clearly shows a correlation on small time scales.

The tests outlined above are successful if the individual black bodies last only a short time. An obvious question is if the method will detect black bodies which turn on at random but stay on for the remainder of the burst. Although being able to detect this kind of emission would be extremely useful, the method outlined here is not expected to be sensitive to this behavior because the emission rapidly becomes broad band. A test was performed which was similar to test 4 except that

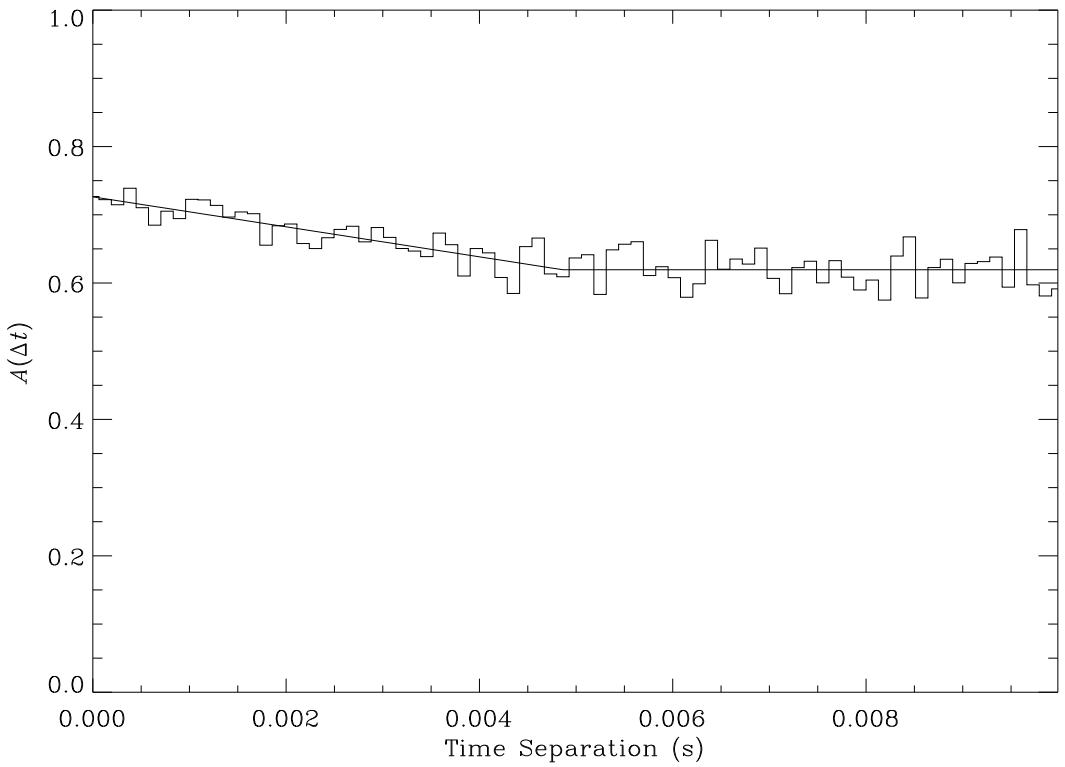

Figure VI.10: $A(\Delta t)$ for the fourth set of test data. The solid line is the best fit model value.

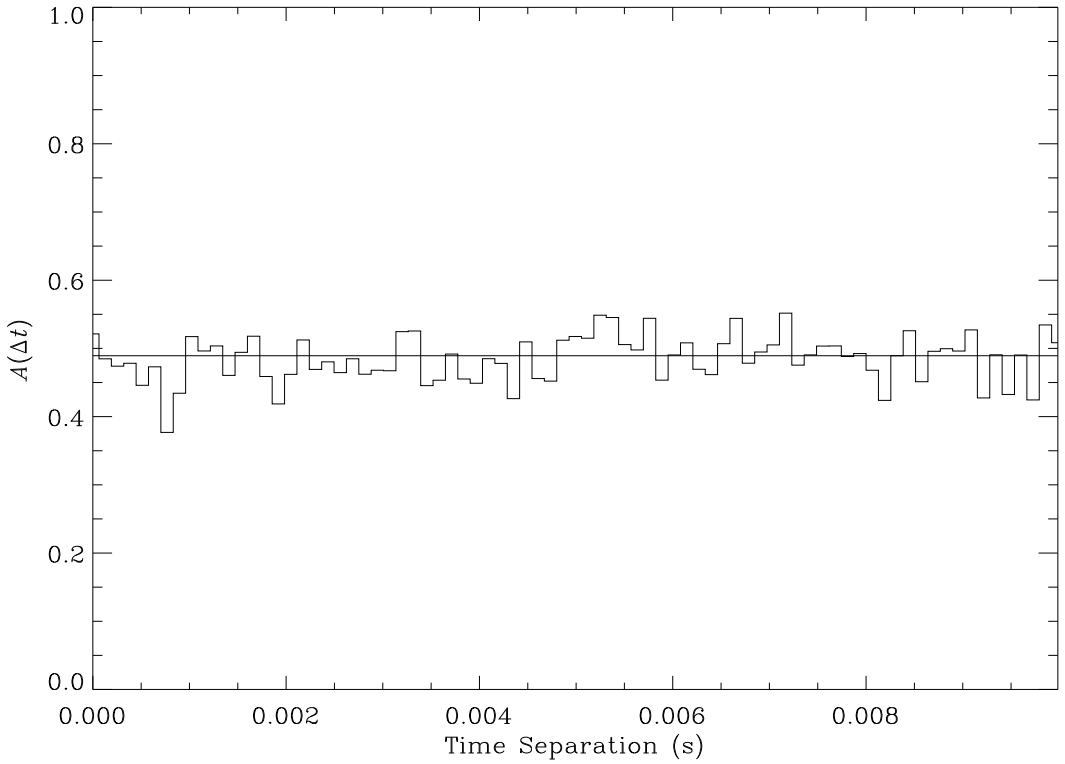

Figure VI.11: $A(\Delta t)$ for the fifth set of test data. The solid line is the best fit model value.

once a black body began, it radiated throughout the remainder of the burst. The results (Figure VI.11) show no sign of a short time scale correlation.

The tests qualitatively verify the potential of the method. However, the real issue is whether the quantitative measures of sensitivity and black body fraction are useful. Odds ratios, effective durations, and black body fraction or upper limits for all the tests are given in Table VI.2. In every case, the odds ratios confirm qualitative expectations, indicating a viable detection measure. The effective durations are shorter than the maximum allowed black body duration of 5 ms but this is to be expected since the actual durations were distributed uniformly between $1 - 5$ ms. The measurements of black body fraction are in slight error. For the first test, the measured black body flux is about 10% less than the expected value. While this inaccuracy is disappointing, the fact that it is reasonably close is encouraging given

Test	O_{10}	t_{eff} (ms)	f_{exp}	f_{obs}	$f_{1\text{ms}}$	$f_{5\text{ms}}$	$f_{10\text{ms}}$
1	$> 10^{100}$	4.1	1.00	0.92	···	···	···
2	$> 10^{100}$	4.5	1.00	0.85	···	···	···
3	0.012	···	···	···	0.014	0.0069	0.0054
4	1.3×10^{35}	4.9	1.00	0.70	···	···	···
5	0.012	···	···	···	0.032	0.0032	···

Table VI.2: Odds ratios, black body durations, black body fractions, and upper limits. f_{exp} is the fraction of total source emission (total minus background) which is black body and f_{obs} is the observed fraction. $f_{n,ms}$ is the 90% upper limit for black bodies of n ms duration.

the approximation on which the calculations are based. Tests 2 and 4 are expected to be accurate since they are bursts in which two black bodies are active at a given instant, diluting a 'pure' signal. In the cases in which a signal was not detected, the methods outlined here show that even with a 10% underestimate of f, strong upper limits can be placed on models in which a few simultaneous short time scale black bodies account for a significant fraction of burst emission.

These tests show that the method developed here is promising. In principle, it could be applied to any burst. However, some bursts will provide more information than others. An obvious selection criterion is burst intensity. Since the background counts cannot be removed from the data (there is no way of knowing whether a given count is signal or noise), intense bursts are preferred because $A(\Delta t)$ will be broad band background dominated for weak bursts. Such intense bursts will allow easier signal detection or provide more meaningful upper limits.

Another consideration is the overall spectrum of the burst. If a burst spectrum is particularly soft (little flux above 100 keV), this method will not be able to reveal a short time scale black body signal. Because there is significant overlap in black bodies which have a small temperature distribution so that $A(\Delta t)$ will be constant. This was tested using simulated data from black bodies which had a power law distribution of temperatures in the $10 - 30$ keV and $10 - 50$ kev ranges. No short time scale signal was found. Therefore, in addition to concentrating on brighter

bursts, only bursts which have significant flux over the full range of the SDs should be analyzed.

VI.E Results

The method outlined above can be applied to any GRB for which STTE data exists. However, there is a great deal of freedom in the way the method can be applied. For example, individual intensity spikes can be analyzed independently or and entire burst measured at once. At the moment, the issue is whether short-lived black bodies exist at all in GRBs. Therefore, to keep the analysis as straightforward as possible, a sample of 20 GRBs was studied which had short durations ($\lesssim 2$ s) and were very bright. Characteristics of the sample are given in Table VI.3. Note that the sample of bursts used here is different than the long duration bursts ($\gtrsim 2$ s) used for the spectral evolution study of Chapter IV.

GRB	S	B	$t_{start}(s)$	$t_{stop}(s)$
3B910718	148	114	-0.1	0.25
3B910725	150	535	-0.17	0.45
3B911210	1068	2797	-0.6	2.0
3B920227	940	2531	-0.5	2.2
3B920229	317	263	-0.06	0.2
3B921022	767	215	-0.1	0.19
3B930116	1300	2114	-0.25	1.5
3B930131	1326	62	0.0	0.1
3B930905	808	188	-0.02	0.18
3B931017	2401	2198	-0.05	2.15
3B931205	830	534	-0.12	0.4
3B931229	841	357	-0.06	0.42
3B940206B	1229	2122	-0.1	1.8
3B940428	242	512	-0.1	0.27
3B940512	261	550	-0.1	0.27
3B940717	1372	829	-0.6	0.7
3B940902	950	2191	-0.2	1.7
3B940918	351	303	-0.125	0.14
941003	350	299	-0.1	0.2
941016	265	190	0.07	0.13

Table VI.3: Characteristics of the GRBs searched for short-lived black body emission. The last two GRBs were observed just after the end of the BATSE 3B catalog set of GRBs (Meegan *et al.* 1996). The S and B columns refer to the expected number of source and background counts respectively based on backgrounds fitted to data taken before and after the GRBs. Errors in S and B are on the order of 5%.

Figure VI.12: LAD time histories and $A(\Delta t)$ curves for all bursts in the sample. The time histories are a sum of all four discriminators. The horizontal line in the $A(\Delta t)$ curves is the median value of $A(\Delta t)$. GRBs 3B930116, 3B940512, and 941016 have incomplete time histories because of telemetry problems. The time history for 3B931017 is from the SDs because no LAD discriminator data was available for this burst.

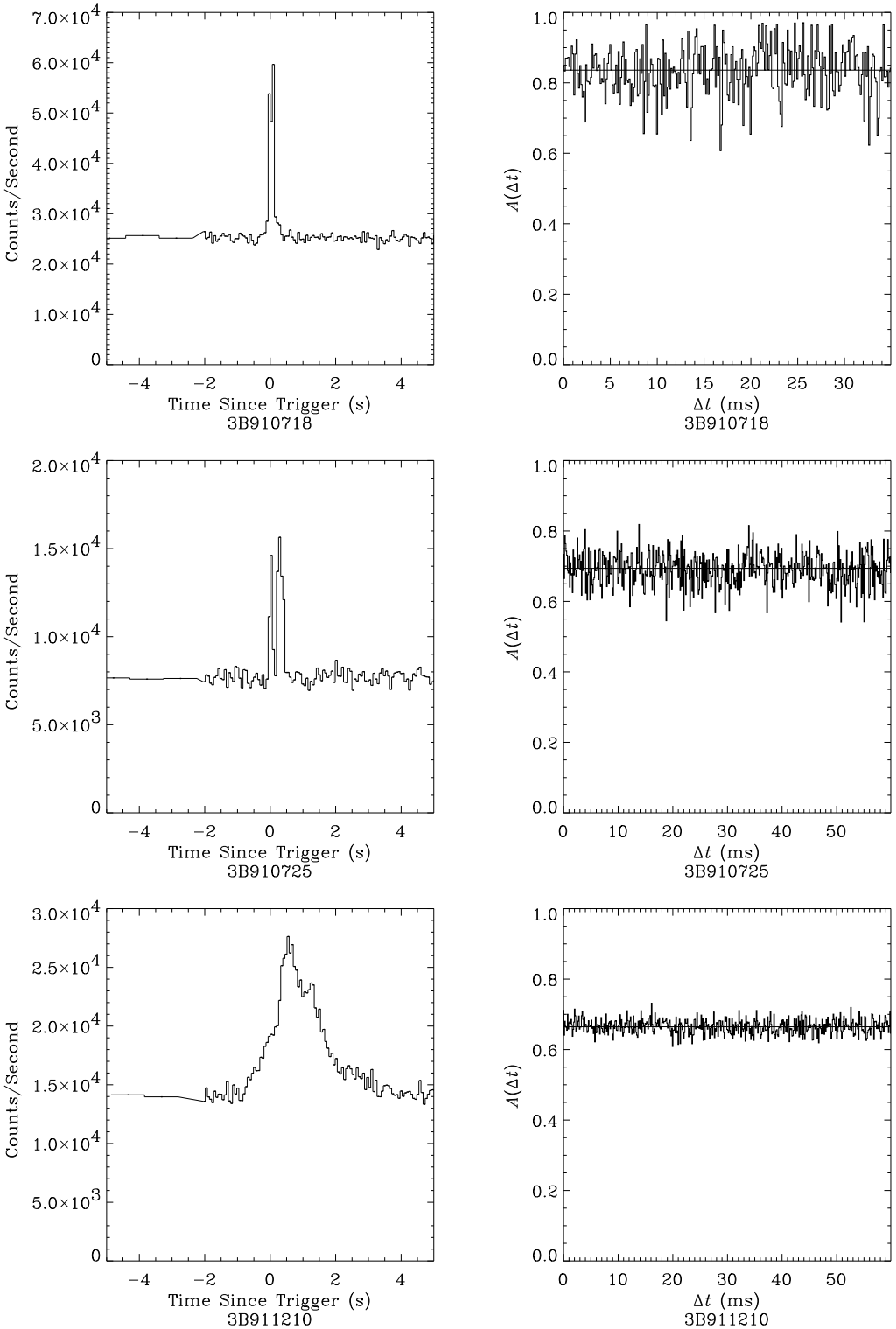
Counts/Second
Time Since Trigger (s)
3B910718
$A(\Delta t)$
Δt (ms)
3B910718
Counts/Second
Time Since Trigger (s)
3B910725
$A(\Delta t)$
Δt (ms)
3B910725
Counts/Second
Time Since Trigger (s)
3B911210
$A(\Delta t)$
Δt (ms)
3B911210

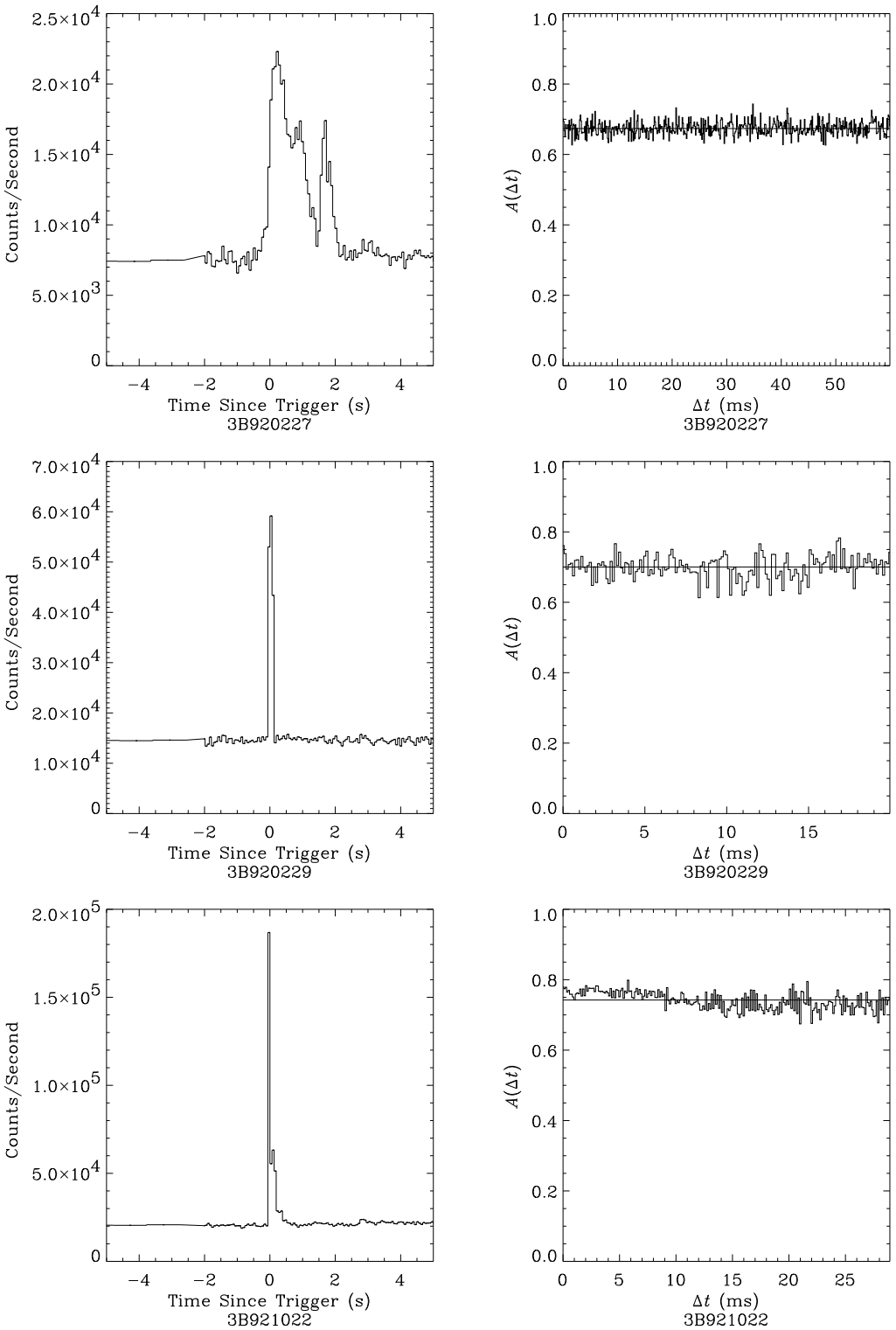

(Figure VI.12 continued)

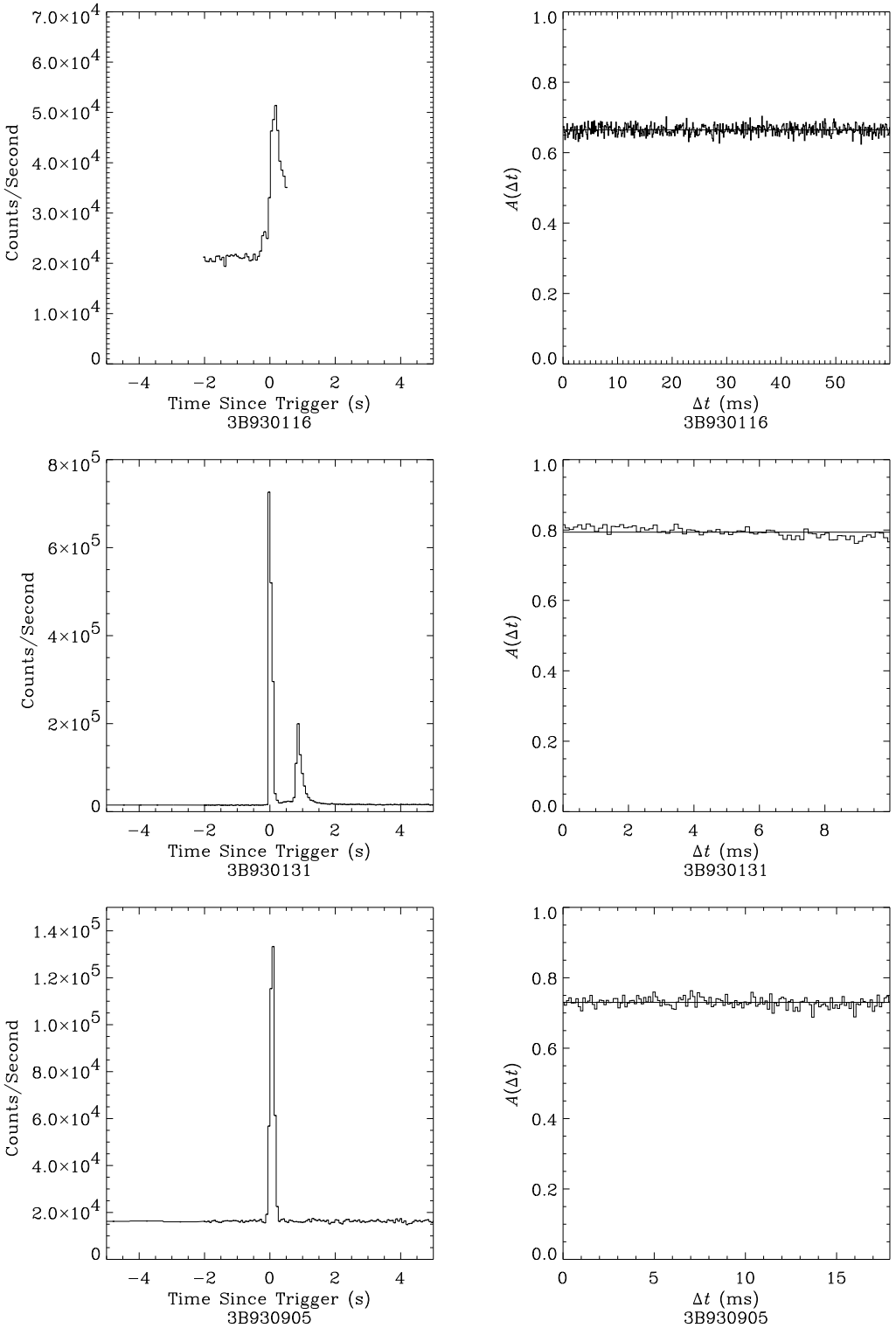

(Figure VI.12 continued)

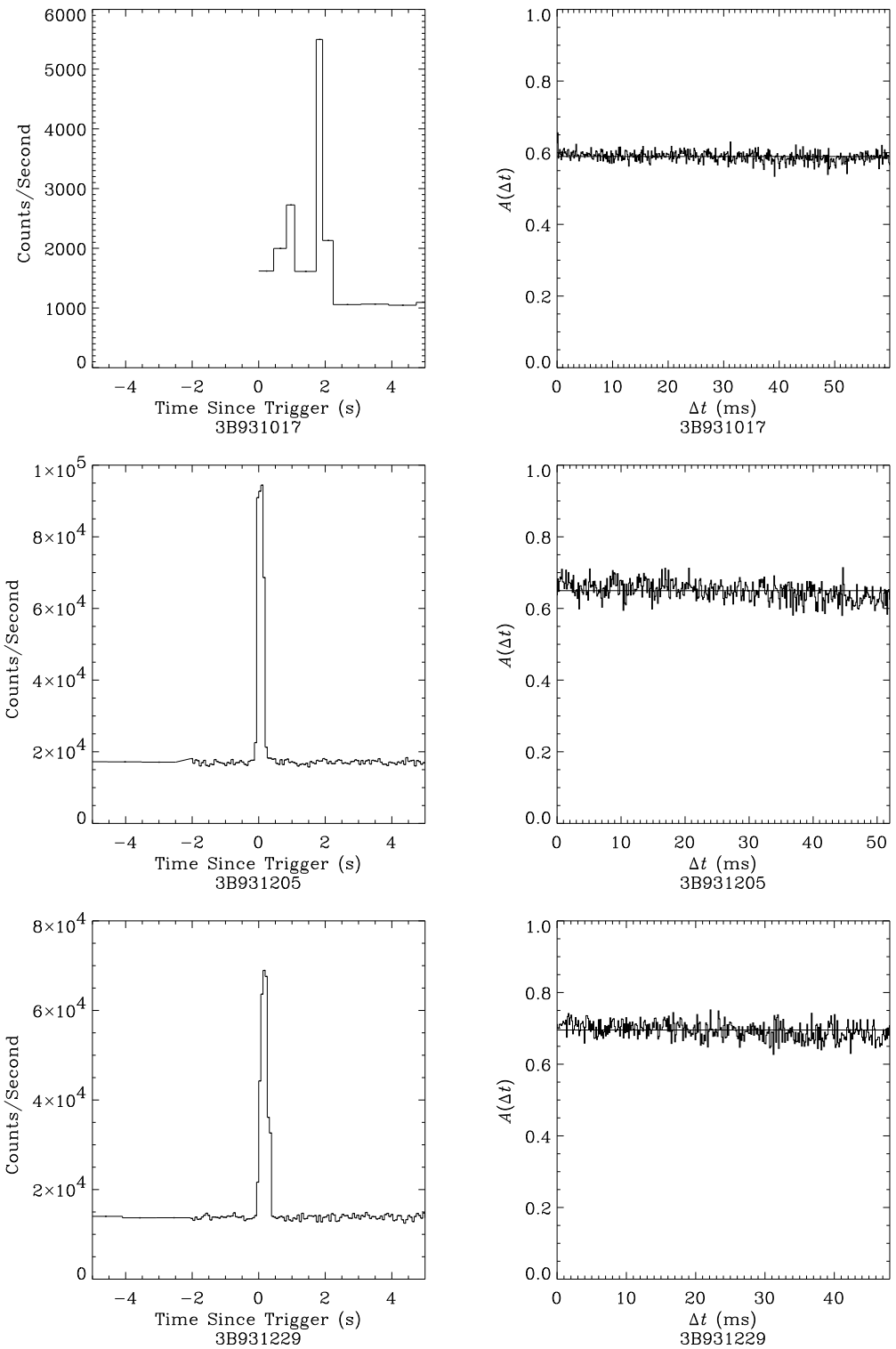

(Figure VI.12 continued)

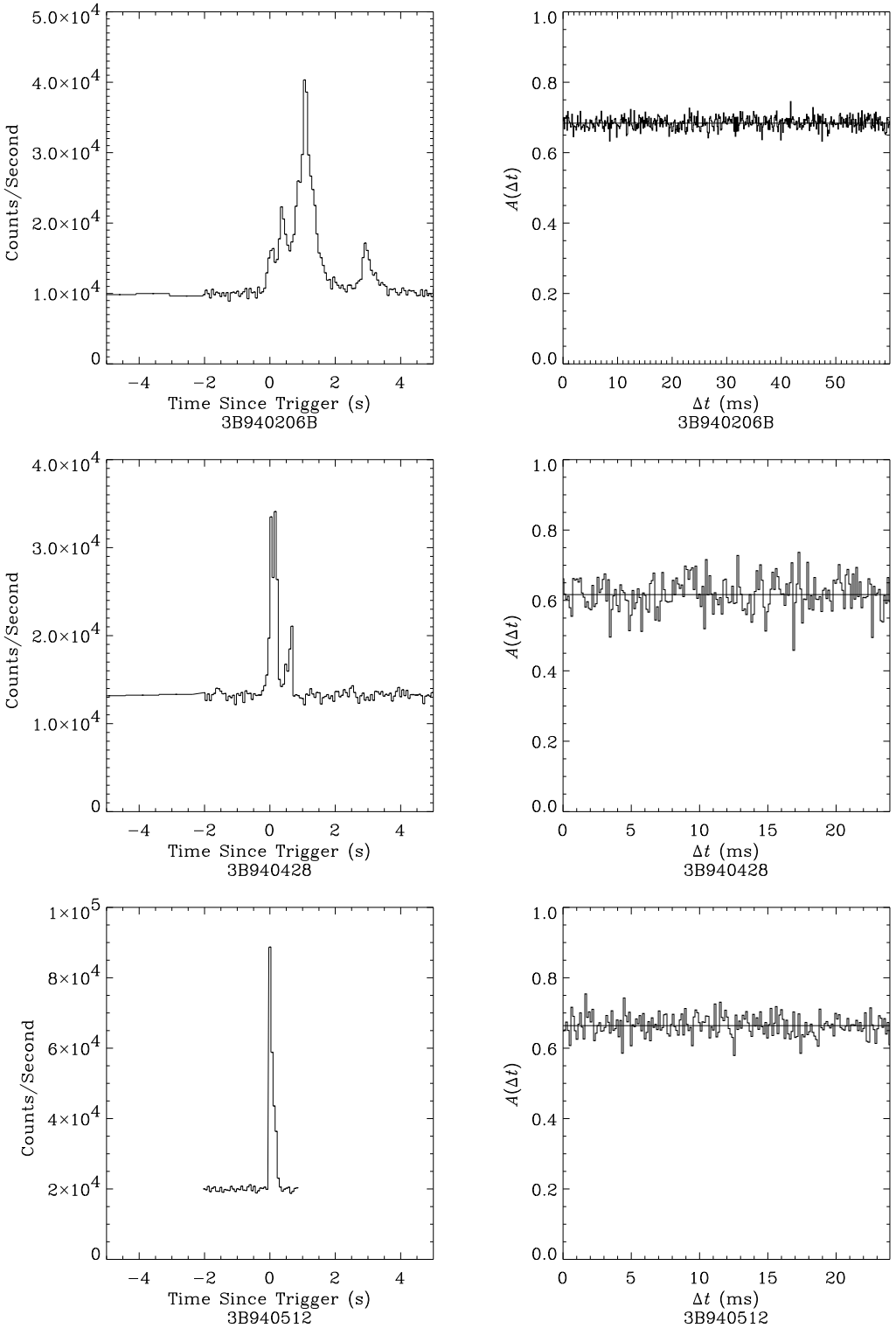

(Figure VI.12 continued)

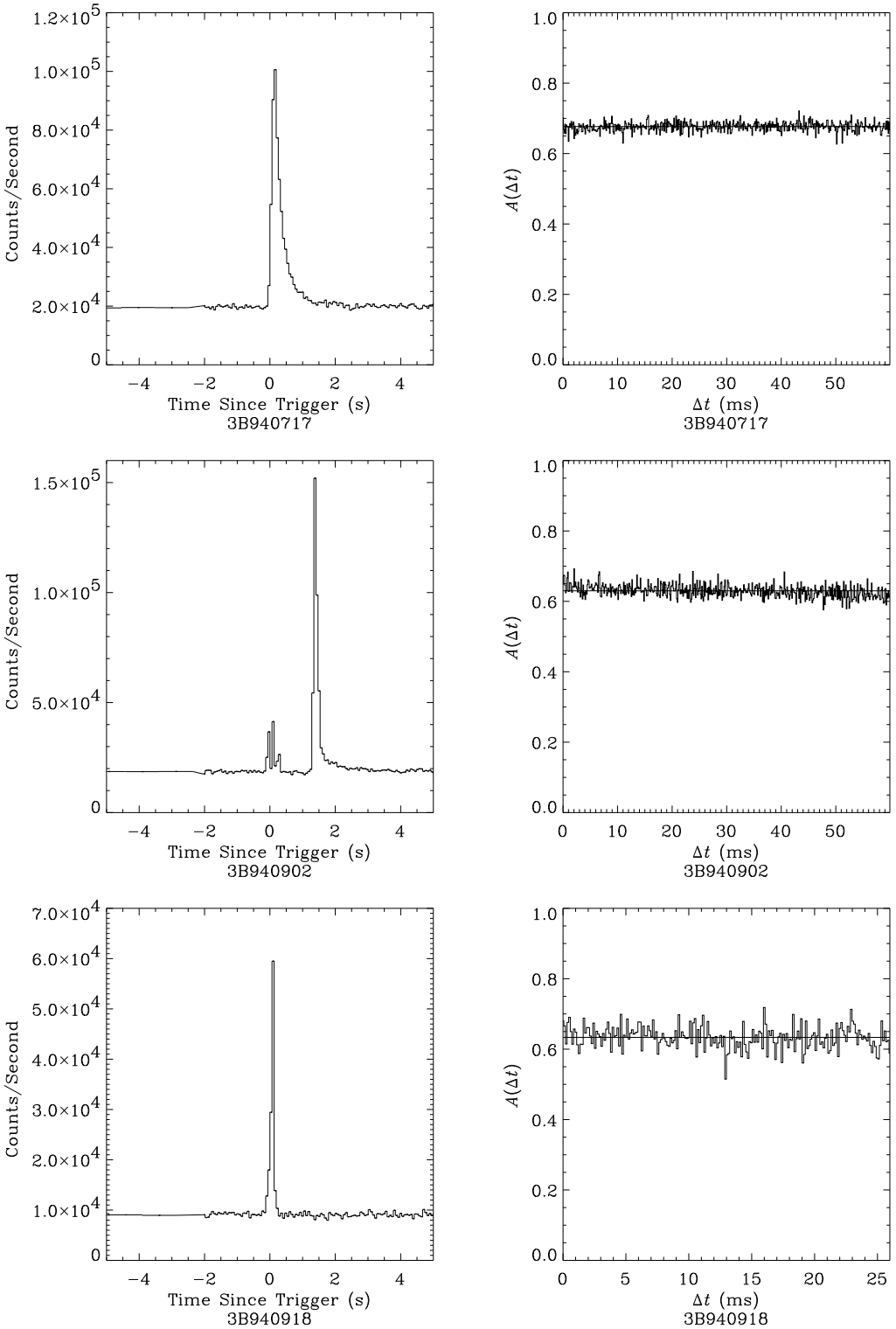

(Figure VI.12 continued)

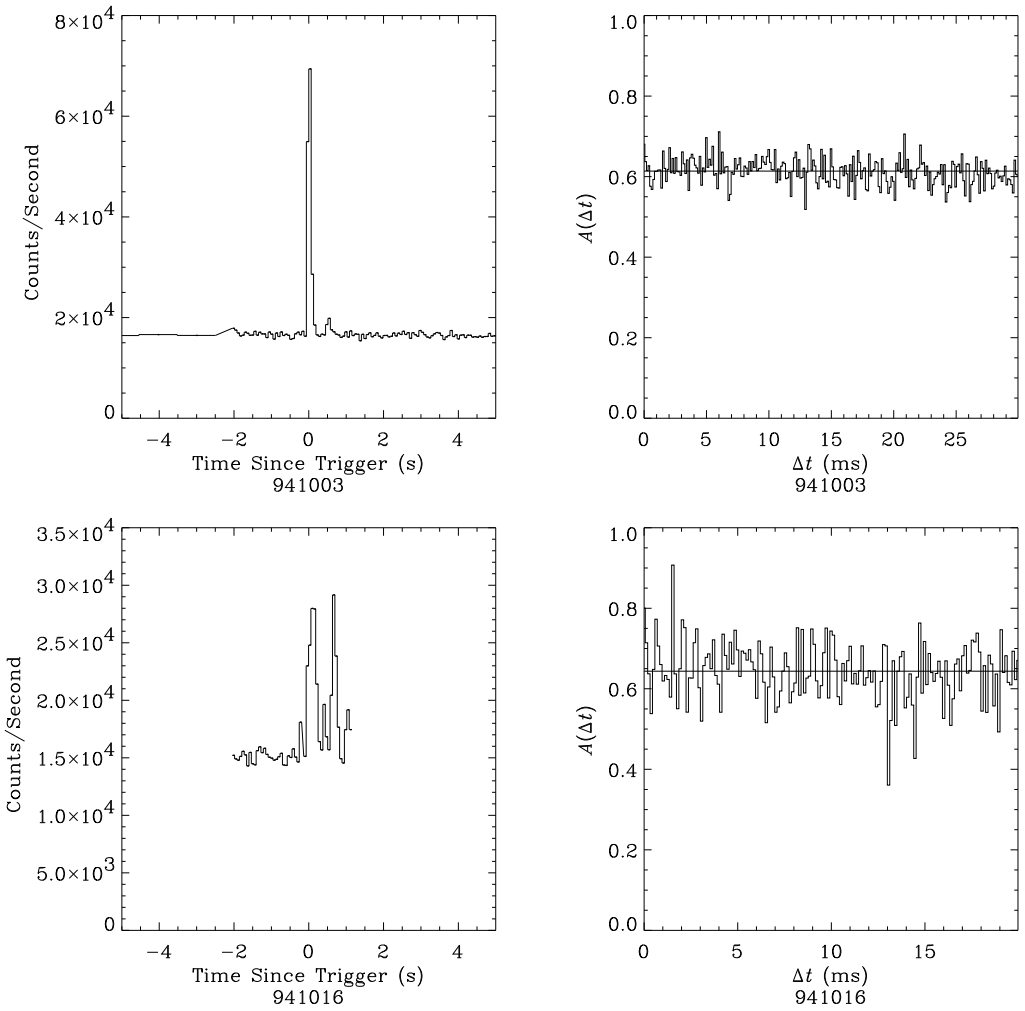

(Figure VI.12 continued)

Correlations were calculated over the main intensity spike (t_{start} and t_{stop} in Table VI.3). Time profiles and correlation histories for the entire sample are shown in Figure VI.12 and numerical results presented in Table VI.4. For the most part, short-lived black bodies are rejected by the odds ratio analysis. However, there are 5 GRBs in which the odds ratio favors the black body hypothesis but the behavior of the $A(\Delta t)$ curves do not match expectations based on the test data. Instead, $A(\Delta t)$ appears to decline very slightly with increasing Δt for the entire range of Δt rather than drop to a constant. In the context of the black body hypothesis, the duration of the black bodies is longer than the largest Δt for which correlations were calculated. Therefore, only a lower limit to the black body duration and upper limit to black body fraction can be set. The upper limit on black body fraction though is not a detection upper limit (the odds ratio claims a detection) but a value which reflects the uncertainty in black body duration.

Although there appears to be a positive detection of short time scale black body emission in several GRBs, the fact that the $A(\Delta t)$ curves for these bursts do not show the behavior expected from the simulated bursts suggests that these observations can be explained another way. The most likely cause of the false signal is spectral evolution. Burst spectra are known to evolve significantly (Bhat *et al.* 1994a; Ford *et al.* 1995; Chapter IV) and changes in the photon spectral distribution will change the value of the average correlation. The most common form of spectral evolution for the simple intensity spikes considered here is from hard to soft, a gradual steepening of the spectrum. To determine whether this type of spectral evolution can produce an $A(\Delta t)$ curve which has a small and persistent negative slope, a burst was simulated with a power law distribution of photons. The burst lasted 0.128 s and the power law index was gradually reduced from -2 to -3. The resulting $A(\Delta t)$ was flat and the odds ratio was $O_{10} = 0.13$.

While simple spectral evolution cannot explain the positive results, more complicated evolution can. In particular, one of the bursts in which the odds ratio favored the black body hypothesis (3B930131) does not show a simple hard-to-soft

GRB	O_{10}	$f_{1\mathrm{ms}}$	$f_{5\mathrm{ms}}$	$f_{10\mathrm{ms}}$	f_{obs}
3B910718	0.37	1.00	1.00	1.00	···
3B910725	0.014	0.13	0.050	0.035	···
3B911210	0.029	0.054	0.013	0.0091	···
3B920227	9.3×10^{-4}	0.091	0.063	0.037	···
3B920229	0.28	0.11	0.066	0.044	···
3B921022	2.7×10^{5}	···	···	···	0.69
3B930116	0.011	0.092	0.050	0.014	···
3B930131	1.1×10^{13}	···	···	···	0.39
3B930905	0.064	0.016	0.0038	···	···
3B931017	2.2×10^{5}	···	···	···	0.16
3B931205	1.9×10^{3}	···	···	···	0.31
3B931229	7.8	0.031	0.0061	0.0037	···
3B940206B	0.033	0.044	0.020	0.015	···
3B940428	0.22	0.20	0.056	0.047	···
3B940512	0.033	0.22	0.037	0.019	···
3B940717	1.7×10^{-4}	0.045	0.032	0.019	···
3B940902	1.3×10^{3}	···	···	···	0.40
3B940918	0.74	0.043	0.016	0.0086	···
941003	0.12	0.056	0.016	0.0076	···
941016	2.1	0.058	0.020	0.013	···

Table VI.4: The results of the correlation analysis. In the cases with $O_{10} > 10$, the black body duration was assumed to be equal to the largest Δt for which an average correlation was calculated.

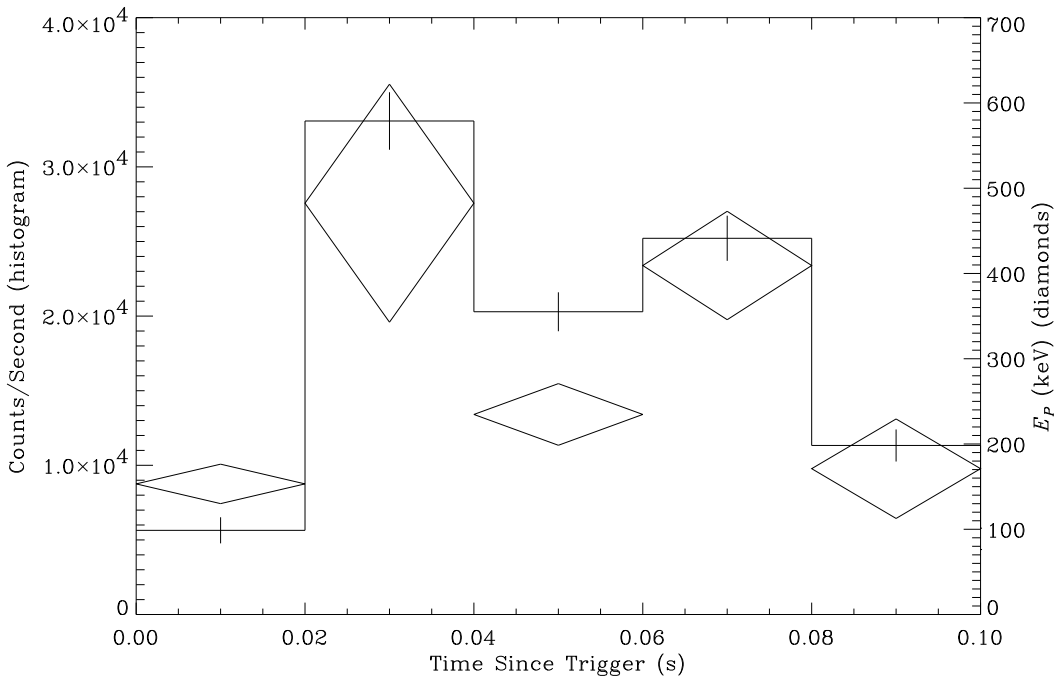

Figure VI.13: The evolution of the peak in νF_ν for GRB 3B930131. The histogram is the count rate observed by the SDs and the diamonds are the peak in νF_ν. The height of the diamonds reflects 1σ errors.

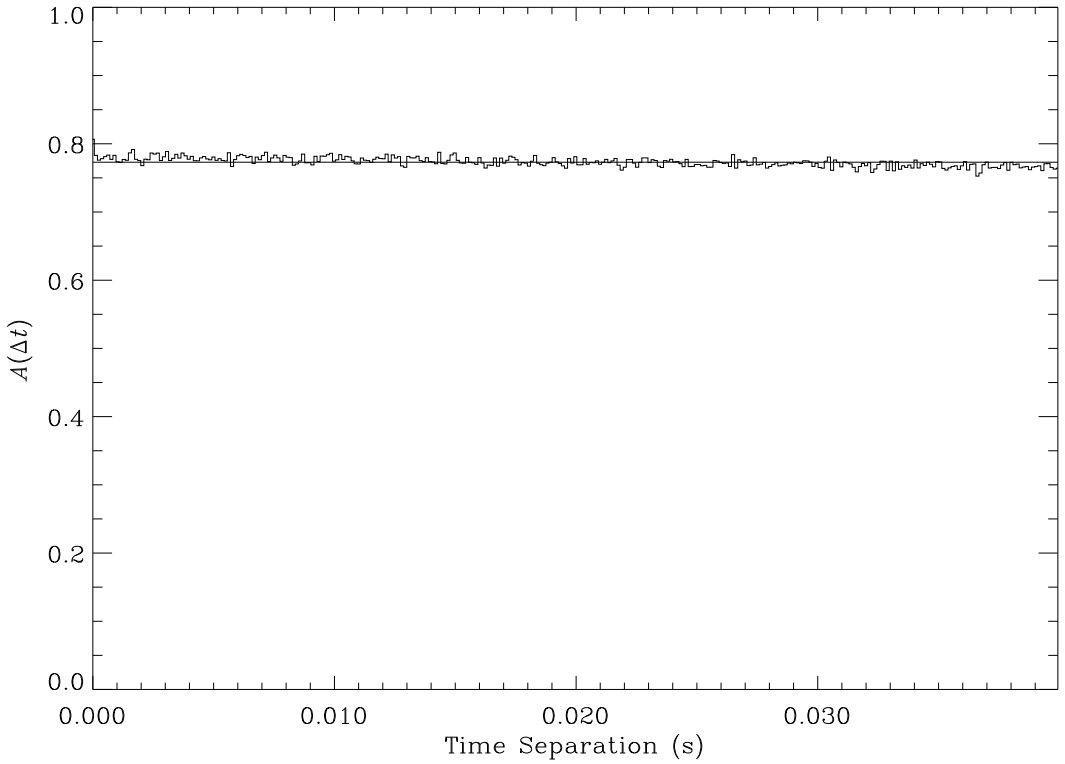

Figure VI.14: The $A(\Delta t)$ curve for a simulated GRB in which the index was allowed to fluctuate randomly. The dotted line is a constant value.

spectral evolution throughout the spike. Figure VI.13 shows the evolution of the peak in νF_ν (a tracer of the spectral hardness, see Chapter IV) in time. This evolution is not surprising since the intensity variation on the 0.02 s time scale is more complicated than it appears in the 0.064 s time scale of Figure VI.12. With this example in mind, another 0.128 s burst was simulated with a power law whose index was allowed to take on random values between -2 and -3 at 0.01 s intervals. The resulting $A(\Delta t)$ curve (Figure VI.14) shows a slight negative slope, similar to that seen in GRB 3B930131. The odds ratio favoring short time scale black bodies is $O_{10} = 3.1 \times 10^{13}$, suggesting a possible non-black body origin for a small deviation in $A(\Delta t)$ from a constant.

VI.F Discussion

Strictly speaking, the results of this work could be used to argue that at least some GRBs have short time scale black body emission. However, although possible black body signatures were detected in several GRBs, the behavior of the average correlations could also be explained if the bursts in question had extremely chaotic spectral evolution. Such evolution is seen in one of these GRBs (3B930131) but the others were not bright enough to perform a similar evolution analysis. If the short lived black body hypothesis is correct, then it is unclear why some bursts would have clearly discernible black bodies while other bursts do not behave similarly and place strong limits on this form of emission. Since there is no other apparent difference between the bursts in the sample (they are all short, bright, and have broad band spectra on long time scales), the more likely conclusion is that complex spectral evolution is responsible for $O_{10} > 10$ in the exceptional cases.

The results of this analysis agree with the work of Schaefer *et al.* (1993), who examined 20 bright bursts (not the same set analysed here) for clustering of events in time without regard to energy. They found no evidence for significant intensity pulses on time scales of the order of microseconds. Although the work presented here does not have microsecond time resolution, it does retain energy information which rules out black body emission which is short duration but the intensity is somehow regulated to inhibit flashes which are much brighter than other contemporaneous emission.

This analysis severely constrains the entire class of GRB models which involve black bodies in the emission process. It is found that if short time scale black bodies exist, then they can supply no more than $\sim 10\%$ of the overall emission if they have lifetimes of 1 ms and account for less than $\sim 4\%$ of the emission if their lifetimes are 10 ms. While this will not surprise anyone, the fact that the general prejudice of the field against these models has been experimentally confirmed is important. In addition, these results limit all models which have even minor emission in the form

of short duration black bodies. Such emission could be expected from any optically thick model of GRBs. At present, most models of GRBs are not developed to the point of predicting the detailed characteristics of weaker emission so the consequences of these results are not immediately apparent in those cases.

Another significant result of this work is that it appears to indicate that in some very short GRBs, complex spectral evolution is occurring. In other studies of spectral evolution, GRBs with simple time profiles tended to show a simple hard-to-soft evolution (c.f. Bhat *et al.* 1994a). However, GRB 3B930131 shows complex evolution of the kind noted in bursts with more complex time profiles (Ford *et al.* 1995). Thus, while this work did not reveal short time scale, narrow energy band emission, it has found suggestions of rapid and complex broad band behavior in at least some GRBs which may indicate similarly complex intensity variability on time scales shorter than 64 ms, the finest time scale on which most comprehensive studies of GRBs have been conducted. It therefore seems possible that the most fundamental GRB time scale (the smallest time at which global changes in the source can occur) can only be probed using the extremely high time resolution TTE or STTE data, data which have traditionally been ignored in favor of other, far more accessible, data types.

To summarize, this work has not found millisecond, black body emission, and it has limited such emission to a small fraction of the observed radiation from GRBs. In addition, the possibility of complex spectral evolution on millisecond time scales suggests that global changes occur in the GRB environment that can only be effectively probed using data of finer time resolution than has been traditionally used. It therefore appears likely that clues of vital importance to the GRB problem are buried in BATSE data which exist but have received little attention.

Chapter VII

Conclusion

Observations from the Burst And Transient Source Experiment (BATSE) on the *Compton Gamma-Ray Observatory* have profoundly affected our understanding of the phenomenon of Gamma-Ray Bursts (GRBs). BATSE's comprehensive study of the GRB spatial distribution destroyed the old paradigm that GRBs arose from nearby ($\lesssim$1 kpc) neutron stars. This conclusion caught nearly everyone who studies GRBs by surprise and as yet, a clear consensus has not formed in support a new source model or even a likely source distance. The scientific ideal is to form a hypothesis which can be tested by observations. Unfortunately the diversity of ideas is so large that the elimination of a few specific source models by rigorous analysis would not significantly alleviate the current confusion in the field.

In an effort to reduce the uncertainty surrounding GRBs and suggest promising avenues for future development, this thesis studied GRB spectra in detail. In the past, most spectral analysis was centered on absorption and emission features in GRB spectra. While a great deal can be learned from such features, their apparent absence in BATSE GRBs removes a powerful diagnostic of the GRB environment. Fortunately, useful physical information can be derived from the continuum, which was the focus of the thesis. The work was necessarily phenomenological but important physical conclusions were drawn from the data that any burst model must accommodate.

Three aspects of the GRB continuum were studied: possibilities for observ-

able optical emission, spectral evolution within a burst, and a search for short-lived black body type emission within bursts. I showed that if optical emission accompanies GRBs and the spectrum is just a simple extrapolation from higher energies, the brightest flaring optical counterpart will only have $m_V \sim 10$, only slightly brighter than the sensitivity of systems built to detect such emission. The discovery of a counterpart could set the distance scale to GRBs but it appears unwise to depend on such an easy solution to the distance scale problem at this time.

The spectral evolution study confirmed earlier observations that GRB spectra tend to evolve from hard to soft though I found the hardness of the spectrum is tied in a complicated way to the intensity of the emission. This suggests that the emission region may have an constant influx of radiating particles or may cool rapidly during the burst. The behavior of the peak in energy per logarithmic energy band (the peak in νF_ν or E_P) places an additional important observational constraint on GRBs. E_P could mark the energy where electron-positron pair processes render the source region optically thick to high-energy gamma-rays. This energy would be expected to lie at 511 keV but relativistic flow or cosmological effects may cause this energy to be redshifted or blueshifted. E_P was shown to vary on time scales of seconds between 100–1000 keV within several GRBs which cannot be accounted for with cosmological effects and is very difficult to explain with highly variable relativistic motion. Therefore, pair processes are not directly observable in GRBs, a significant result since pair processes would be expected to occur in what is believed to be an extremely energy dense source region.

Finally, I found that if short time scale black body emission occurs in GRBs, it can account for no more than 10% of the emission if the black body lifetime is of order 1 ms. While few consider short time scale black body emission likely because GRB spectra appear non-thermal on all time scales investigated so far, thermal emission does appear to be a natural consequence of a popular class of GRB models known as fireballs. Although most fireball models avoid thermal emission by assuming the energy of the burst is carried away by relativistic ejecta which then radiates after

encountering a shock, it is still possible that thermal emission is observable at some point during the evolution of the fireball. If so, then these results will provide important constraints on those models, or indeed any model in which the emission region is optically thick to gamma-rays.

This thesis has concentrated on the phenomenology of GRB spectra and found several properties which provide important insights into the GRB source region, such as the lack of thermal emission on any time scale and absence of directly observable electron-positron pair processes. While it would be much more satisfying to discuss these results in the context of the physics of a particular GRB model, most models have not progressed to the point where spectral observations can can be interpreted in terms of the details of the GRB environment. Therefore, observational properties of the continuum were discovered which can limit any model. Eventually, enough models and even classes of models will be eliminated by this type of phenomenological analysis that it will be fruitful to consider the remaining ideas in greater detail.

While phenomenological analyses such as those performed in this thesis do extend our knowledge, progress is painfully slow. Therefore, it is important to consider what should be done in the near future to ensure significant successes. With regard to BATSE, the most important question which can be resolved concerns the existence of absorption features in GRB spectra. Everyone who studies GRBs is waiting for a definitive statement from BATSE as to whether spectral features do or do not exist in the data. As discussed in Chapter III, the computational infrastructure necessary to carry out a comprehensive search took considerable time to develop and we have only recently begun to analyze many GRBs in detail. If spectral features are found in BATSE data, they may provide some powerful diagnostics of the GRB environment.

Considering the GRB problem as a whole, perhaps the greatest impediment to progress is that we do not know the distance to GRBs. That such a fundamental quantity is uncertain severely limits meaningful work because it is unclear how much energy is required to produce the outbursts we see. As discussed in Chapter V, I am

pessimistic about prospects for finding flaring optical counterparts to GRBs. I find a much more promising approach to be the attempt to locate many GRBs to sub-arcminute error boxes. An example of this approach is the Burst Locations with an Arc Second Telescope (BLAST, Johnson *et al.* 1996) which is a proposed high-energy (7–150 keV) astrophysics satellite with arcminute to arcsecond imaging capabilities. Restricting the size of errors boxes to GRBs will allow meaningful searches for quiescent counterparts. If GRB locations are consistently correlated with a particular object, then the distance scale problem would be solved and the exact energy requirements for GRB sources known. Identification with known objects would also permit the utilization of a much broader base of astronomical knowledge than that available from gamma-ray observations alone.

Appendix A

Model Weights for χ^2

The Levenberg-Marquardt algorithm (Bevington 1969, p. 237; Press *et al.* 1992, p. 678) is a prescription to efficiently minimize goodness-of-fit statistics. The most common statistic used is

$$\chi^2 = \sum_{i=1}^{N} \left[\frac{y_i - y(x_i; \mathbf{a})}{\sigma_i} \right]^2, \tag{A.1}$$

where: x is the independent variable (here energy); y is an observed variable (count rate in this case); $y(x_i; \mathbf{a})$ is the value of the model at x_i for parameters $\mathbf{a}$; N is the number of measurements (here, channels in a spectrum); $\mathbf{a}$ represents the parameters to be fit; and σ_i are the errors associated with y_i. χ^2 is minimized using an iterative gradient procedure for which the first and second partial derivatives of χ^2 with respect to $\mathbf{a}$ are needed. In its usual implementation, the algorithm assumes that the σ_i are taken directly from the data and are constant.

The problem with using data variances (σ_i) in equation A.1 is that σ_i weights downward fluctuations in the data too strongly, a result of the Poisson nature of count data in which $\sigma_i^2 \propto n_i$, the number of observed counts. In this case, a small number of counts create a smaller than average σ_i which causes the associated data points to be more important in the calculation of χ^2. Wheaton *et al.* (1995, hereafter W95) examined this problem in detail using a Monte Carlo simulation of 24,000 one-parameter data sets and found that the mean of fitted values deviated from the true

value by -170σ (note the downward shift). The solution to this problem is to use σ_i generated from the model under consideration rather than the data, replacing $\sigma_i^2 \propto n_i$ with $\sigma_i^2(x_i;\mathbf{a}) \propto n_i(x_i;\mathbf{a})$ (model variance). When W95 performed the simulation with this new scheme, the bias was -0.34σ.

Although W95 demonstrated the importance of using weights derived from the model, they do not mention a necessary change in the standard Levenberg-Marquardt prescription to accommodate the new weighting. The algorithm assumes that σ_i is taken from the data so that changes in the χ^2 surface are contained in only the $y(x_i;\mathbf{a})$ term in equation A.1. However, by making σ_i model dependent without changing the partial derivatives, assumed changes in the χ^2 surface caused by variation in $\mathbf{a}$ will be incorrect, resulting in slightly off-course iterations and an incorrect minimum since $\partial\chi^2/\partial\mathbf{a}$=0 can be at the wrong value of $\mathbf{a}$. It was found that when this effect is not accounted for, the true minimum of the χ^2 surface is not reached and the values of the fitted parameters differ from the true best fit by roughly the quoted error in the fitted parameters though it is not biased toward higher or lower values making it difficult to detect in large collections of fits.

Alterations in the second derivative terms only affect the route used to find the minimum of χ^2 and therefore need not be corrected for the new weighting scheme (Press *et al.* 1992, p. 678). On the other hand, the first partial derivatives need to reflect any changes which might occur in the χ^2 surface and must be corrected. The corrected version is

$$\frac{\partial\chi^2}{\partial a_j} = -2\sum_{i=1}^{N}\left[\frac{y_i - y_i(x_i;\mathbf{a})}{\sigma_i^2(x_i;\mathbf{a})}\right]\left(\frac{\partial y_i(x_i;\mathbf{a})}{\partial a_j} - \frac{[y_i - y_i(x_i;\mathbf{a})]}{\sigma_i(x_i;\mathbf{a})}\frac{\partial\sigma_i(x_i;\mathbf{a})}{\partial a_j}\right). \qquad \text{(A.2)}$$

The first partial derivative term in this equation is equal to the partial derivative specified by the Levenberg-Marquardt algorithm with model variances replacing data variances but the second term is new. For this work, equation (A2) can be expressed in a simpler form since background subtracted count rates are used ($y_i = n_i/f_i - b_i$ where f_i is a term which converts counts to a count rate and b_i is the background

counting rate). In this case, $\sigma_i^2(x_i;\mathbf{a})$ becomes

$$\sigma_i^2(x_i;\mathbf{a}) = \frac{y_i(x_i;\mathbf{a})}{f_i} + \sigma_{b_i}^2, \tag{A.3}$$

where $\sigma_{b_i}^2$ is the error in the determination of the background rate in channel i. Differentiating A.3 with respect to $\mathbf{a}$ and substituting into equation A.2, it is found that

$$\frac{\partial \chi^2}{\partial a_j} = -\sum_{i=1}^{N}[y_i - y_i(x_i;\mathbf{a})]\frac{\sigma_i^2 + \sigma_i^2(x_i;\mathbf{a})}{\sigma_i^4(x_i;\mathbf{a})}\frac{\partial y_i(x_i;\mathbf{a})}{\partial a_j}. \tag{A.4}$$

This expression is equal to the uncorrected expression when $\sigma_i(x_i;\mathbf{a})$ is replaced by σ_i which allows the standard algorithms (e.g. Bevington 1969, p. 237; Press *et al.* 1992, p. 678) to be modified easily. When this expression is substituted into the algorithm, the true minimum of the χ^2 surface with model variances is found.

References

Akerlof, C., Fatuzzo, M., Lee, B., Bionta, R., Ledebuhr, A., Park, H-S., Barthelmy, S., Cline, T., & Gehrels, N. 1994, *Gamma-Ray Bursts—Second Workshop*, eds. G. J. Fishman, J. J. Brainerd, & K. Hurley (New York: American Institute of Physics), 633.

Atteia, J.-L., Barat, C., Hurley, K., Niel, M., Vedrenne, G., Evans, W. D., Fenimore, E. E., Klebesadel, R. W., Laros, J. G., Cline, T., Desai, U., Teegarden, B., Estulin, I. V., Zenchenko, V. M., Kuznetsov, A. V., & Kurt, V. G. 1987, *The Astrophysical Journal Supplement*, **64**, 305.

Band, D., Ford, L., Matteson, J., Lestrade, J. P., Teearden, B., Schaefer, B., Cline, T., Briggs, M., Paciesas, W., Pendleton, G., Austin, R., Fishman, G., Meegan, C, & Wilson, R. 1992a, *Experimental Astronomy*, **2**, 307.

Band, D., Matteson, J., Ford, L., Schaefer, B., Teegarden, B., Cline, T., Paciesas, W., Pendleton, G., Fishman, G., Meegan, C., Wilson, R., & Lestrade, P. 1992b, *Gamma-Ray Bursts*, eds. W. S. Paciesas, & G. J. Fishman (New York: American Institute of Physics), 169.

Band, D., Matteson, J., Ford, L., Schaefer, B., Palmer, D., Teegarden, B., Cline, T., Briggs, M., Paciesas, W., Pendleton, G., Fishman, G., Kouveliotou, C., Meegan, C., Wilson, R., & Lestrade, P. 1993, *The Astrophysical Journal*, **413**, 281.

Band, D. L. 1994a, *The Astrophysical Journal*, **432**, L23.

Band, D. L., Ford, L. A., Matteson, J. L., Briggs, M., Paciesas, W., Pendleton, G., Preece, R., Palmer, D., Teegarden, B., & Schaefer, B. 1994b, *The Astrophysical Journal*, **434**, 560.

Band, D. L., Ford, L. A., Matteson, J. L., Briggs, M., Paciesas, W., Pendleton, G., Preece, R., Palmer, D., Teegarden, B., & Schaefer, B. 1995, *The Astrophysical*

Journal, **447**, 289.

Band, D. L., Ryder, S., Ford, L. A., Matteson, J. L., Palmer, D. M., Teegarden, B. J., Briggs, M. S., Paciesas, W. S., Pendleton, G. N., & Preece, R. D. 1996, *The Astrophysical Journal*, **458**, 746.

Barat, C., Hurley, K., Niel, M., Vedrenne, G., Mitrofanov, I. G., Estulin, I. V., Zenchenko, V. M., & Dolidze, V. S. 1984, *The Astrophysical Journal*, **286**, L11.

Barthelmy, S. D., Cline, T. L., Gehrels, N., Bialas, T. G., Robbins, M. A., Kuyper, J. R., Fishman, G. J., Kouveliotou, C., & Meegan, C. A. 1994, *Gamma-Ray Bursts—Second Workshop*, eds. G. J. Fishman, J. J. Brainerd, & K. Hurley (New York: American Institute of Physics), 643.

Beurle, K., Bewick, A., Mills, J. S., & Quenby, J. J. 1981, *Astrophysics & Space Science*, **77**, 201.

Bhat, P. N., Fishman, G. J., Meegan, C. A., Wilson, R. B, Kouveliotou, C., Paciesas, W. S., Pendleton, G. N., & Schaefer, B. E. 1994a, *The Astrophysical Journal*, **426**, 604.

Bhat, P. N., Fishman, G. J., Meegan, C. A., Wilson, R. B, Paciesas, W. S. 1994b, *Gamma-Ray Bursts—Second Workshop*, eds. G. J. Fishman, J. J. Brainerd, & K. Hurley (New York: American Institute of Physics), 197.

Bevington, P. R. 1969, *Data Reduction and Error Analysis for the Physical Sciences*, (New York: McGraw-Hill).

Blissett, R. J., & Cruise, A. M. 1979, *Monthly Notices of the Royal Astronomical Society*, **186**, 45.

Brainerd, J. J. 1992, *The Astrophysical Journal*, **394**, L33.

Brainerd, J. J. 1994, *The Astrophysical Journal*, **428**, L1.

Brainerd, J. J., Meegan, C. A., Briggs, M. S., Pendleton, G. N., & Brock, M. N. 1995, *The Astrophysical Journal*, **441**, L39.

Briggs, M. S. 1993, *The Astrophysical Journal*, **407**, 126.

Briggs, M. S., Paciesas, W. S., Pendleton, G. N., Meegan, C. A., Fishman, G. J., Horack, J. M., Brock, M. N., Kouveliotou, C., Hartmann, D. H., & Hakkila, J. 1996a, *The Astrophysical Journal*, **459**, 40.

Briggs, M. S., Preece, R. D., Pendleton, G. N., Paciesas, W. S., Band, D. L., Ford, L., & Matteson, J. L. 1996b, *Proceedings of the Third Huntsville Gamma-Ray Burst Symposium*, eds. M. S. Briggs, C. Kouveliotou, & G. J. Fishman, in press.

Brock, M. N., Meegan, C. A., Fishman, G. J., Wilson, R. B., Paciesas, W. S., & Pendleton, G. N. *Gamma-Ray Bursts*, eds. W. S. Paciesas, & G. J. Fishman (New York: American Institute of Physics), 399.

Budding, E. 1993, *Astronomical Photometry*, (Cambridge: New York).

Carter, B. 1992, *The Astrophysical Journal*, **391**, L67.

Cavallo, G. & Rees, M. J. 1978, *Monthly Notices of the Royal Astronomical Society*, **183**, 359.

Chakrabarty, D., Koh, T., Bildsten, L., Prince, T. A., Finger, M. H., Wilson, R. B., Pendleton, G. N., & Rubin, B. C. 1995, *The Astrophysical Journal*, **446**, 826.

Cline, D. B. & Hong, W. 1992, *The Astrophysical Journal*, **401**, L57.

Cline, T. L., Desai, U. D., Klebesadel, R. W., & Strong, I. B. 1973, *The Astrophysical Journal*, **185**, L1.

Colgate, S. A., & Leonard, P. J. T. 1994, *Gamma-Ray Bursts—Second Workshop*, eds. G. J. Fishman, J. J. Brainerd, & K. Hurley (New York: American Institute of Physics), 581.

Craig, I. J. D., & Brown, J. C. 1986, *Inverse Problems in Astronomy*, (Boston: Adam Hilger).

Davis, S. P., Norris, J. P., Kouveliotou, C., Fishman, G. J., Meegan, C. A., & Paciesas, W. S. 1994, *Gamma-Ray Bursts—Second Workshop*, eds. G. J. Fishman, J. J. Brainerd, & K. Hurley (New York: American Institute of Physics), 182.

Dermer, C. D. & Schlickeiser, R. 1994, *Gamma-Ray Bursts—Second Workshop*, eds. G. J. Fishman, J. J. Brainerd, & K. Hurley (New York: American Institute of Physics), 510.

Eichler, D., Livio, M., Piran, T., & Schramm, D. N. 1989, *Nature*, **340**, 126.

Epstein, R. I. 1985, *The Astrophysical Journal*, **291**, 822.

Evans, W. D., Klebesadel, R. W., Laros, J. G., Cline, T. L., Desai, U. D., Pizzichini, G., Teegarden, B. J., Hurley, K., Niel, M., Vedrenne, G., Estoolin, I. V., Kouznetsov, A. V., Zenchenko, V. M., & Kurt, V. G. 1980, *The Astrophysical Journal*, **237**, L7.

Fenimore, E. E., Klebesadel, R. W., & Laros, J. G. 1983, *Advances in Space Research*, **3**(4), 207.

Fenimore, E. E., Conner, J. P., Epstein, R., Klebesadel, R. W., Laros, J. G., Yoshida, A., Fujii, M., Hayashida, K., Itoh, M., Murakami, T., Nishimura, J., Yamagami, Kondo, I., & Kawai, N. 1988, *The Astrophysical Journal*, **335**, L71.

Fishman, G. J., Meegan, C. A., Wilson, R. B., Paciesas, W. S., Parnell, T. A., Austin R. W., Rehage, J. R., Matteson, J. L., Teegarden, B. J., Cline, T. L., Schaefer, B. E., Pendleton, G. N., Berry, F. A., Horack, J. M., Storey, S. D., Brock, M. N., & Lestrade, J. P. 1989, *Proceedings of the Gamma Ray Observatory Science Workshop*, ed. W. N. Johnson, (Greenbelt, MD: Goddard Space Flight Center), 2–39.

Fishman, G. J., Meegan, C. A., Wilson, R. B., Kouveliotou, C., Howard, S., Paciesas, W. S., Briggs, M. S., Pendleton, G. N., Koshut, T. M., Mallozzi, R. S., Stollberg, M., & Lestrade, J. P. 1994, *The Astrophysical Journal Supplement*, **92**, 229.

Fishman, G. J., Bhat, P. N., Mallozzi, R., Horack, J. M., Koshut, T., Kouveliotou, C., Pendleton, G. N., Meegan, C. A., Wilson, R. B., Paciesas, W. S., Goodman, S. J., & Christian, H. J. 1994, *Science*, **264**, 1313.

Freeman, P. E., Lamb, D. Q., Wilson, R. B., Briggs, M., Paciesas, W., Preece, R., & Band, D. 1996, *Proceedings of the Third Huntsville Gamma-Ray Burst Symposium*, eds. M. S. Briggs, C. Kouveliotou, & G. J. Fishman, in press.

Ford, L., Band, D., Matteson, J., Palmer, D., Teegarden, B., Schaefer, B., Preece, R., Briggs, M., Paciesas, W., & Pendleton, G. 1994, *Gamma-Ray Bursts—Second Workshop*, eds. G. J. Fishman, J. J. Brainerd, & K. Hurley (New York:

American Institute of Physics), 261.

Ford, L. A., Band, D. L., Matteson, J. L., Briggs, M. S., Pendleton, G. N., Preece, R. D., Paciesas, W. S., Teegarden, B. J., Palmer, D. M., Schaefer, B. E., Cline, T. J., Fishman, G. J., Kouveliotou, C., Meegan, C., Wilson, R. B., & Lestrade, J. P. 1995, *The Astrophysical Journal*, **439**, 307.

Ford, L. A., & Band, D. L. 1996, *The Astrophysical Journal*, in press.

Fujimoto, M. Y. 1985, *The Astrophysical Journal*, **293**, L19.

Golenetskii, S. V., Mazets, E. P., Aptekar, R. L., & Ilyinskii, V. N. 1983, Nature, **306**, 451.

Golenetskii S. V. 1988, *Advances in Space Research*, **8**(2-3), 653.

Goodman, J. 1986, *The Astrophysical Journal*, **308**, L47.

Graziani, C., Fenimore, E. E., Murakami, T., Yoshida, A., Lamb, D. Q., Wang, J. C. L., & Loredo, T. J. 1992, *Gamma Ray Bursts*, eds. C. Ho, R. I. Epstein, & E. E. Fenimore (Cambridge: Cambridge University Press), 407.

Greiner, J., Wenzel, W., Hudec, R., Moskalenko, E. I., Metlov, V., Chernych, N. S., Getman, V. S., Ziener, R., Birkle, K., Bade, N., Tritton, S. B., Fishman, G. J., Kouveliotou, C., Meegan, C. A., Paciesas, W. S., & Wilson, R. B. 1994, *Gamma-Ray Bursts—Second Workshop*, eds. G. J. Fishman, J. J. Brainerd, & K. Hurley (New York: American Institute of Physics), 408.

Greiner, J. 1995, *The 17th Texas Symposium on Relativistic Astrophysics*, (New York: New York Academy of Sciences) 749, 429.

Gruber, D. E., Jung, G. V., & Matteson, J. L. 1989, *High-Energy Radiation Background in Space*, eds. A. C. Rester, Jr., & J. I. Trombka, (New York: American Institute of Physics), 232.

Haensel, P., Paczyński, B., & Amsterdamski, P. 1991, *The Astrophysical Journal*, **375**, 209.

Hakkila, J., Meegan, C. A., Pendleton, G. N., Fishman, G. J., Wilson, R. B., Paciesas, W. S., Brock, M. N., & Horack, J. M. 1994, *The Astrophysical Journal*, **422**, 659.

Hameury, J. M., Bonazzola, S., Heyvaerts, J., & Ventura, J. 1982, *Astronomy & Astrophysics*, **111**, 242.

Hanlon, L. O., Bennett, K., Collmar, W., Conners, A., Diehl, R., van Dijk, R., Greiner, J., den Herder, J. W., Hermson, W., Kippen, R. M., Kuiper, L., McConnell, M., Ryan, J., Schönfelder, V., Steinle, H., Strong, A., Varendorff, M., Williams, O. R., & Winkler, C. 1994, *Astronomy & Astrophysics*, **285**, 161.

Harding, A. K. 1991, *Physics Reports*, **206**, 327.

Harmon, B. A., Wilson, C. A., Paciasas, W. S., Pendleton, G. N., Briggs, M. S., Rubin, B. C., Finger, M. H., Fishman, G. J., Brock, M. N., Wilson, R. B., & Meegan, C. A. 1994, *The Astrophysical Journal*, **425**, L17.

Hartmann, D., Woosley, S. E., & Arons, J. 1988, *The Astrophysical Journal*, **332**, 777.

Harwit, M., & Salpeter, E. E. 1973, *The Astrophysical Journal*, **186**, L37.

Higdon, J. C., & Lingenfelter, R. E. 1986, *The Astrophysical Journal*, **307**, 197.

Higdon, J. C., & Lingenfelter, R. E. 1990, *Annual Reviews of Astronomy and Astrophysics*, **28**, 401.

Higdon, J. C., & Lingenfelter, R. E. 1994, *The Astrophysical Journal*, **434**, 552.

Horack, J. M. 1991, *Development of the Burst and Transient Source Experiment*, NASA Reference Publication 1268.

Hueter, G. J. 1987, Ph.D. Thesis, University of California, San Diego, La Jolla.

Hurley, K. 1992, *Gamma-Ray Bursts*, eds. W. S. Paciesas, & G. J. Fishman (New York: American Institute of Physics), 3.

Hurley, K., Dingus, B. L., Mukherjee, R., Sreckumar, P., Kouveliotou, C., Meegan, C., Fishman, G. J., Band, D., Ford, L., Bertsch, D., Cline, T., Fictel, C., Hartman, R., Hunter, S., Thompson, D. J., Kanbach, G., Mayer-Hasselwander, H., von Montigny, C., Sommer, M., Lin, Y., Nolan, P., Michelson, P., Kniffen, D., Mattox, J., Schneid, E., Boer, M., & Niel, M. 1994a, *Nature*, **372**, 652.

Hurley, K., Sommer, M., Kouveliotou, C., Fishman, G., Meegan, C., Cline, T., Boer, M., & Niel, M. 1994b, *The Astrophysical Journal*, **431**, L31.

Jennings, M. C. 1988, *The Astrophysical Journal*, **333**, 700.

Johnson, W. N., Kinzer, R. L., Kurfess, J. D., Strickman, M. S., Purcell, W. R., Grabelsky, D. A., Ulmer, M. P., Hillis, D. A., Jung, G. V., & Cameron, R. A. 1993, *The Astrophysical Journal Supplement*, **86**, 693.

Johnson, W. N., Dermer, C. D., Grove, J. E., Hertz, P. L., Kinzer, R. L., Kroeger, R. A., Kurfess, J. D., Lovellette, M., Strickman, M. S., Wood, K. S., Inderhees, S. E., Phlips, B. F., Hartmann, D., & Leising, M. D. 1996, *Proceedings of the Third Huntsville Gamma-Ray Burst Symposium*, eds. M. S. Briggs, C. Kouveliotou, & G. J. Fishman, in press

Kargatis, V. E., Liang, E. P., Hurley, K. C., Barat, C., Eveno, E., & Niel, M. 1994, *The Astrophysical Journal*, **422**, 260.

Katz, J. I. 1994, *The Astrophysical Journal*, **432**, L107.

Klebesadel, R. W., Strong, I. B., & Olson, R. A. 1973, *The Astrophysical Journal*, **182**, L85.

Klebesadel, R. W. 1992, *Gamma Ray Bursts*, eds. C. Ho, R. I. Epstein, & E. E. Fenimore (Cambridge: Cambridge University Press), 161.

Knoll, G. F. 1989, *Radiation Detection and Measurement*, (New York: Wiley).

Kouveliotou, C., Norris, J. P., Cline, T. L., Dennis, B. R., Desai, U. D., Orwig, L. E., Fenimore, E. E., Klebesadel, R. W., Laros, J. G., Atteia, J.-L., Boer, M., Hurley, K., Niel, M., Vedrenne, G., Kuznetsov, A. V., Sunyaev, R. A., & Terekhof, O. V. 1987 *The Astrophysical Journal*, **322**, L21.

Kouveliotou, C., Norris, J. P., Fishman, G. J., Meegan, C. A., Wilson, R. B., & Paciesas, W. S. 1992, *Gamma-Ray Bursts—Second Workshop*, eds. G. J. Fishman, J. J. Brainerd, & K. Hurley (New York: American Institute of Physics), 299.

Kouveliotou, C., Fishman, G. J., Meegan, C. A., Paciesas, W. S., Wilson, R. B., van Paradijs, J., Preece, R. D., Briggs, M. S., Pendleton, G. N., Brock, M. N., Koshut, T. M., & Horack, J. M. 1993a, *Nature*, **362**, 728.

Kouveliotou, C., Meegan, C. A., Fishman, G. J., Bhat, N. P., Briggs, M. S., Koshut,

T. M., Paciesas, W. S., & Pendleton, G. N. 1993b, *The Astrophysical Journal*, **413**, L101.

Kouveliotou, C., Fishman, G. J., Meegan, C. A., Paciesas, W. S., van Paradijs, J., Norris, J. P., Preece, R. D., Briggs, M. S., Horack, J. M., Pendleton, G. N., & Green, D. A. 1994a, *Nature*, **368**, 125.

Kouveliotou, C., Preece, R., Bhat, N, Fishman, G. J., Meegan, C. A., Horack, J. M., Briggs, M. S., Paciesas, W. S., Pendleton, G. N., Band, D., Matteson, J., Palmer, D., Teegarden, B., & Schaefer, B. 1994b, *The Astrophysical Journal*, **422**, L59.

Kouveliotou, C., van Paradijs, J., Fishman, G. J., Briggs, M. S., Kommers, J., Harmon, B. A., Meegan, C. A., & Lewin, W. H. G. 1996, *Nature*, **379**, 799.

Kulkarni, S. R., Frail, D. A., Kassim, N. E., Murakami, T., & Vasisht, G. 1994, *Nature*, **368**, 129.

Lamb, D. Q., Graziani, C., & Smith, I. A. 1993, *The Astrophysical Journal*, **413**, L11.

Laros, J. G., Evans, W. D., Fenimore, E. E., Klebesadel, R. W., Middleditch, J., Barat, C., Hurley, K., Niel, M., Vedrenne, G., Nakano, G. H., Imhof, W. L., Cline, T. L., Desai, U. D., Schaefer, B. E., Teegarden, B. J., Estulin, I. V., Kurt, V. G., Mersov, G. A., & Zenchenko, V. M. 1985, *The Astrophysical Journal*, **290**, 728.

Larson, S. B., McLean, I. S., & Becklin, E. E. 1996, *The Astrophysical Journal*, **460**, L95.

Lestrade, J. P. 1991, "Energy-Channel Calibration of the Burst and Transient Source Experiment", BATSE internal memo, September 9, 1991.

Lestrade, J. P. 1994, *The Astrophysical Journal*, **429**, L5.

Leventhal, M., MacCallum, C., & Watts, A. 1977, *The Astrophysical Journal*, **216**, 491.

Lingenfelter, R. E. & Higdon, J. C. 1992, *Nature*, **356**, 132.

London, R. A., & Cominsky, L. R. 1983, *The Astrophysical Journal*, **275**, L59.

Loredo, T. J., & Epstein, R. I. 1989, *The Astrophysical Journal*, **336**, 896.

Loredo, T. J., & Lamb, D. Q. 1989, *Fourteenth Texas Symposium on Relativistic Astrophysics*, ed. E. J. Fenyves, (New York: New York Academy of Sciences), 601.

Loredo, T. J. 1990, *Maximum Entropy and Bayesian Methods*, ed. P. F. Fougère (Dordrecht: Kluwer Academic), 81.

Loredo, T. J. & Lamb, D. Q., 1996, *Physical Review D*, submitted.

Martin, B. R. 1971, *Statistics for Physicists*, (London: Academic Press).

Matz, S. M., Forrest, D. J., Vestrand, W. T., Chupp, E. L., Share, G. H., & Rieger, E. 1985, *The Astrophysical Journal*, **288**, L37.

Mazets, E. P., Golenetskii, S. V., Aptekar, R. L., Guryan, Y. A., & Ilyinskii, V. N. 1981, *Nature*, **290**, 378.

Mazets, E. P., Golnetskii, V. P., Ilyinskii, V. N., Guryan, Y. A., Aptekar, R. L., Panov, V. N., Sokolov, I. A., Sokolova, Z. Y., & Kharitonova, T. V. 1982, *Astrophysics & Space Science*, **82**, 261.

Meegan, C. A., Fishman, G. J., & Wilson, R. B. 1985, *The Astrophysical Journal*, **291**, 479.

Meegan, C. A., Pendleton, G. N., Briggs, M. S., Kouveliotou, C., Koshut, T. M., Lestrade, J. P., Paciesas, W. S., McCollough, M. L., Brainerd, J. J., Horack, J. M., Hakkila, J., Henze, W., Preece, R. D., Mallozzi, R. S., & Fishman, G. J. 1996, *The Astrophysical Journal Supplement*, in press.

Melia, F., & Fatuzzo, M. 1992, *The Astrophysical Journal*, **398**, L85.

Mészáros, P. 1992, *High Energy Radiation from Magnetized Neutron Stars*, (Chicago: University of Chicago).

Mészáros, P., & Rees, M. J. 1993a, *The Astrophysical Journal*, **405**, 278.

Mézáros, P., Laguna, P., & Rees, M. J. 1993b, *The Astrophysical Journal*, **415**, 181.

Mihalas, D, & Binney, J. 1981, *Galactic Astronomy*, (New York: Freeman).

Mitrofanov, I. G., Chernenko, A. M., Pozanenko, A. S., Paciesas, W. S., Kouveliotou, C., Meegan, C. A., Fishman, G. J., Sagdeev, & R. Z. 1994, *Gamma-Ray Bursts—Second Workshop*, eds. G. J. Fishman, J. J. Brainerd, & K. Hurley

(New York: American Institute of Physics), 187.

Mitrofanov, I. G., Chernenko, A. M., Pozanenko, A. S., Briggs, M. S., Paciesas, W. S., Fishman, G. J., Meegan, C. A., Sagdeev, R. Z. 1996, *The Astrophysical Journal*, **459**, 570.

Murakami, T., Fujii, M., Hayashida, K., Itoh, M., Nishimura, J., Yamagami, T., Conner, J. P., Evans, W. D., Fenimore, E. E., Klebesadel, R. W., Yoshida, A., Kondo, I., & Kawai, N. 1988, *Nature*, **335**, 234.

Murakami, T., Tanaka, Y., Kulkarni., S. R., Ogasaka, Y., Sonobe, T., Ogowara, Y., Aoki, T., & Yoshida, A. 1994, *Nature*, **368**, 127.

Narayan, R., Paczyński, B., & Piran, T. 1992, *The Astrophysical Journal*, **395**, L83.

Narayan, R., & Piran, T. 1993, *Monthly Notices of the Royal Astronomical Society*, **265**, L65.

Nemiroff, R. J. 1994, *Comments on Astrophysics*, **17**, 4, 189.

Nemiroff, R. J., Norris, J. P., Kouveliotou, C., Fishman, G. J., Meegan, C. A., & Paciesas, W. S. 1994, *The Astrophysical Journal*, **423**, 432.

Norris, J. P., Cline, T. L., Desai, U. D., & Teegarden, B. J. 1984, *Nature*, **308**, 434.

Norris, J. P., Share, G. H., Messina, D. C., Dennis, B. R., Desai, U. I., Cline, T. L., Matz, S. M., & Chupp, E. L. 1986, *The Astrophysical Journal*, **301**, 213.

Norris, J. P., Nemiroff, R. J., Davis, S. P., Kouveliotou, C., Fishman, G. J., Meegan, C. A., & Paciesas, W. S. 1994a, *Gamma-Ray Bursts—Second Workshop*, eds. G. J. Fishman, J. J. Brainerd, & K. Hurley (New York: American Institute of Physics), 172.

Norris, J. P., Nemiroff, R. J., Scargle, J. D., Koveliotou, C., Fishman, G. J., Meegan, C. A., Paciesas, W. S., & Bonnell, J. T. 1994b, *The Astrophysical Journal*, **424**, 540.

Pacini, F., & Ruderman, M. 1974, *Nature*, **251**, 399.

Paczyński, B. 1986, *The Astrophysical Journal*, **308**, L43.

Paczyński, B. 1988a, *The Astrophysical Journal*, **335**, 525.

Paczyński, B. & Long, K., 1988b, *The Astrophysical Journal*, **333**, 694.

Paczyński, B. 1990, *The Astrophysical Journal*, **363**, 218.

Palmer, D. M., Teegarden, B., Schaefer, B., Cline, T., Fishman, G., Meegan, C., Wilson, R., Paciesas, W., Pendleton, G., Briggs, M., Band, D., Ford, L.., Matteson, J., & Lestrade, J. P. 1993, *Compton Gamma-Ray Observatory*, eds. M. Friedlander, N. Gehrels, & D. J. Macomb (New York: American Institute of Physics), 892.

Palmer, D. M., Teegarden, B. J., Schaefer, B. E., Cline, T. L., Band, D. L., Ford, L. A., Matteson, Paciesas, W. S., Pendleton, G. N., Briggs, M. S., Preece, R. D., Fishman, G. J., Meegan, C. A., Wilson, R. B., & Lestrade, J. P. 1994, *The Astrophysical Journal*, **433**, L77.

Pendleton, G. N., Paciesas, W. S., Lestrade, J. P., Fishman, G. J., Wilson, R. B., & Meegan, C. A. 1989, *Proc. Gamma Ray Observatory Science Workshop* (Washington: NASA), 4-547.

Pendleton, G. N., Paciesas, W. S., Fishman, G. N., Wilson, R. B., Meegan, C. A., Roberts, F. E., Lestrade, J. P., Horack, J. M., Brock, M. N., & Flickinger, M. D. 1992, *The Compton Observatory Science Workshop* (Washington:NASA), 47.

Pendleton, G. N., Paciesas, W. S., Mallozzi, R. S., Koshut, T. M., Fishman, G. J., Meegan, C. A., Wilson, R. B., Horack, J. M., Lestrade, J. P. 1995, *Nuclear Instruments & Methods in Physics Research A*, **364**, 567.

Petrosian, V., & Efron, B. 1995, *The Astrophysical Journal*, **441**, L37.

Podsiadlowski, P., Rees, M. J., & Ruderman, M. 1995, *Monthly Notices of the Royal Astronomical Society*, 273, 755.

Preece, R., Briggs, M., Paciesas, W., Pendleton, G., Ford, L., Band, D., Matteson, J., Palmer, D., Teegarden, B., Schaefer, B., & Brock M. 1994, *Gamma-Ray Bursts—Second Workshop*, eds. G. J. Fishman, J. J. Brainerd, & K. Hurley (New York: American Institute of Physics), 266.

Preece, R. *et al.* , 1996a, *The Astrophysical Journal*, submitted.

Preece, R. *et al.* , 1996b, in preparation.

Press, W. H., Flannery, B. P., Teukolsky, S. A., Vetterling, W. T. 1992, *Numerical*

Recipes (New York: Cambridge)

Quashnock, J. M., & Lamb, D. Q. 1993, *Monthly Notices of the Royal Astronomical Society*, **265**, L59.

Rees, M. J., & Mézáros, P. 1992, *Monthly Notices of the Royal Astronomical Society*, **258**, 41P.

Ricker, G. R., Doty, J. P., Rappaport, S. A., Vanderspek, R. K., Matsuoka, M., Kawai, N., Yoshida, A., Fenimore, E. E., Ho., C., Roussel-Dupre, D., Atteia, J-L., Niel, M. J., Vedrenne, G., Hurley, K., Lamb, D. K., & Woosley, S. E. 1992, *Gamma Ray Bursts*, eds. C. Ho, R. I. Epstein, & E. E. Fenimore (Cambridge: Cambridge University Press), 288.

Rothschild, R. E., Kulkarni, S. R., & Lingenfelter, R. E. 1994, *Nature*, **368**, 432.

Rothschild, R. E. 1996, *High Velocity Neutron Stars and Gamma-Ray Bursts*, eds. R. E. Rothschild & R. E. Lingenfelter (New York: American Institute of Physics), 51.

Rothschild, R. E., & Lingenfelter, R. E. 1996, *High Velocity Neutron Stars and Gamma-Ray Bursts*, (New York: American Institute of Physics).

Ruderman, M. A., & Cheng, K. S. 1988, *The Astrophysical Journal*, **335**, 306.

Rybicki, G. B., & Lightman, A. P. 1979, *Radiative Processes in Astrophysics*, (New York: Wiley).

Schaefer, B. E. 1981, *Nature*, **294**, 722.

Schaefer, B. E., Cohen, J., Teegarden, B. J., Cline, T. L., Fishman, G. J., Meegan, C. A., Wilson, R. B., Paciesas, W. S., Pendleton, G. N., Matteson, J. L., Band, D. L., & Lestrade, J. P. 1993, *The Astrophysical Journal*, **404**, 673.

Schaefer, B. E. 1994a, *Gamma-Ray Bursts—Second Workshop*, eds. G. J. Fishman, J. J. Brainerd, & K. Hurley (New York: American Institute of Physics), 382.

Scheafer, B. E., Teegarden, B. J., Palmer, D. M., Ford, L. A., Band, D. L., Matteson, J. L., Briggs, M. S., Paciesas, W. S., Pendleton, G. N., & Preece, R. D. 1994b, *Gamma-Ray Bursts—Second Workshop*, eds. G. J. Fishman, J. J. Brainerd, & K. Hurley (New York: American Institute of Physics), 271.

Schmidt, M. 1968, *The Astrophysical Journal*, **151**, 393.

Schmidt, M., Higdon, J. C., & Hueter, G. 1988, *The Astrophysical Journal*, **329**, L85.

Schmidt, W. K. H. 1978, *Nature*, **271**, 525.

Schneid, E. J., Bertsch, D. L., Fichtel, C. E., Hartman, R. C., Hunter, S. D., Kanbach, G., Kniffen, D. A., Kwok, P. W., Lin, Y. C., Mattox, J. R., Mayer-Hasselwander, H. A., Michelson, P. F., von Montigny, C., Nolan, P. L., Pinkau, K., Rothermel, H., Sommer, M., Sreekumar, P., & Thompson, D. J. 1992, *Astronomy & Astrophysics*, **255**, L13.

Schönfelder, V., Aarts, H., Bennett, K., de Boer, H., Clear, J., Collmar, W., Conners, A., Deerenberg, A., Diehl, R., von Dordrecht, A., den Herder, J. W., Hermsen, W., Kippen, M., Kuiper, L., Lichti, G., Lockwood, J., Macri, J., McConnell, M., Morris, D., Much, R., Ryan, J., Simpson, G., Snelling, M., Stacy, G., Steinle, H., Strong, A., Swanenburg, B. N., Taylor, B., de Vries, C., & Winkler, C. 1993, *The Astrophysical Journal Supplement*, **86**, 657.

Smith, I. A., & Lamb, D. Q. 1993a, *The Astrophysical Journal*, 410, L23.

Smith, I. A., & Lamb, D. Q. 1993, *Compton Gamma-Ray Observatory*, eds. M. Friedlander, N. Gehrels, & D. J. Macomb (New York: American Institute of Physics), 1020.

Stanek, K. Z., Paczyński, B., & Goodman, J. 1993, *The Astrophysical Journal*, **413**, L7.

Strong, A. W., & Diehl, R. 1989, *Data Analysis in Astronomy III*, eds. Di Gesù, V., Scarsi, L., Crane, P., Friedman, J. H., Levialdi, S., & Maccarone, M. C., (New York: Plenum), 55.

Sturrock, P. A., Harding, A. K., & Daugherty, J. K. 1989, *The Astrophysical Journal*, **346**, 950.

Teegarden, B. J., & Cline, T. L. 1980, *The Astrophysical Journal*, **236**, L67.

Teegarden, B. J. 1984, *High Energy Transients in Astrophysics*, ed. S. E. Woosley, (New York: American Institute of Physics), 352.

Thompson, D. J., Bertsch, D. L., Fichtel, C. E., Hartman, R. C., Hofstadter, R., Hughes, E. B., Hunter, S. D., Hughlock, B. W., Kanbach, G., Kniffen, D. A., Lin, Y. C., Mattox, J. R., Mayer-Hasselwander, H. A., von Montigny, C., Nolan, P. L., Nel, H. I., Pinkau, K., Rothermel, H., Schneid, E. J., Sommer, M., Sreekumar, P., Tieger, D., & Walker, A. H. 1993, *The Astrophysical Journal Supplement*, **86**, 629.

Trimble, V. 1994, *Gamma-Ray Bursts—Second Workshop*, eds. G. J. Fishman, J. J. Brainerd, & K. Hurley (New York: American Institute of Physics), 717.

Ulmer, M. P., Lomatch, S., Matz, S. M., Grabelsky, D. A., Purcell, W. R., Grove, J. E., Johnson, W. N., Kinzer, R. L., Kurfess, J. D., Strickman, M. S., Cameron, R. A., & Jung, G. V. 1994, *The Astrophysical Journal*, **432**, 228.

Usov, V. V. 1992, *Nature*, **357**, 472.

Vanderspek, R., Krimm, H. A., & Ricker, G. R. 1994, huntii, 438.

Vanderspek, R., Atlas, A., Brady, T. M., Crew, G. B., Doty, J. P., Kissle, S. E., Ricker, G. R., Tappian, P. C., Martel, F., & Jones, M. T. 1995, *Astrophysics & Space Science*, **231**, 479.

Vasisht, G., Kulkarni, S. R., Frail, D. A., & Greiner, J. 1994, *The Astrophysical Journal*, **431**, L35.

Wang, J. C. L., Lamb, D. Q., Loredo, T. J., Wasserman, I. M., Salpeter, E. E., Fenimore, E. E., Cannor, J. P., Epstain, R. I., Klebesadel, R. W., Laros, J. G., Murakami, T., Nishimura, J., Yoshida, A., & Kondo, I. 1989, *Physical Review Letters*, **63**, 1550.

Wang, V. C., & Lingenfelter, R. E. 1993, *The Astrophysical Journal*, **416**, L13.

Wheaton, W. A., Dunklee, A. L., Jacobson, A. S., Ling, J. C., Mahoney, W. A., & Radocinski, R. G. 1995, *The Astrophysical Journal*, **438**, 322.

Wilson, R. B., Fishman, G. J., Finger, M. H., Pendleton, G. N., Prince, T. A., & Chakrabarty, D. *Compton Gamma-Ray Observatory*, eds. M. Friedlander, N. Gehrels, & D. J. Macomb (New York: American Institute of Physics), 291.

Woosley, S. E., & Wallace, R. K. 1982, *The Astrophysical Journal*, **258**, 716.

Woosley, S. E. 1993, *The Astrophysical Journal*, **405**, 273.

Yamagami, T., & Nishimura, J. 1986, *Astrophysics & Space Science*, **121**, 241.

Yoshida, A., Murakami, T., Nishimura, J., Kondo, I., & Fenimore, E. E. 1991, *Publications of the Astronomical Society of Japan*, **43**, L69.

Zaritsky, D., Smith, R., Frenk, C., & White, S. D. M. 1993, *The Astrophysical Journal*, **405**, 464.

Zerby, C. D., Meyer, A., & Murray, R. B. 1961, *Nuclear Instruments & Methods*, **12**, 115.

Zhang, S. N., Fishman, G. J., Harmon, B. A., & Paciesas, W. S. 1993, *Nature*, *366*, 245.